ACOUSTIC TRANSDUCTION – MATERIALS AND DEVICES

Period 31 July 1996 to 31 December 1997

Annual Report

VOLUME I

OFFICE OF NAVAL RESEARCH
Contract No: N00014-96-1-1173

APPROVED FOR PUBLIC RELEASE – DISTRIBUTION UNLIMITED

Kenji Uchino

PENNSTATE

THE MATERIALS RESEARCH LABORATORY
UNIVERSITY PARK, PA

REPORT DOCUMENTATION PAGE

Form Approved
OMB No. 0704-0188

1. AGENCY USE ONLY (Leave blank)	2. REPORT DATE	3. REPORT TYPE AND DATES COVERED
	05/01/98	ANNUAL REPORT 07/31/96-12/31/97

4. TITLE AND SUBTITLE
ACOUSTIC TRANSDUCTION -- MATERIALS AND DEVICES

5. FUNDING NUMBERS
ONR CONTRACT NO:
N00014-96-1-1173

6. AUTHOR(S)
KENJI UCHINO

7. PERFORMING ORGANIZATION NAME(S) AND ADDRESS(ES)
Materials Research Laboratory
The Pennsylvania State University
University Park, PA 16802

8. PERFORMING ORGANIZATION REPORT NUMBER

9. SPONSORING / MONITORING AGENCY NAME(S) AND ADDRESS(ES)
Office of Naval Research
ONR 321SS
Ballston Centre Tower One
800 N Quincy Street
Arlington, VA 22217-5660

Office of Naval Research
Regional Office Chicago
536 S Clark Str., Rm 208
Chicago IL 60605-1588

10. SPONSORING / MONITORING AGENCY REPORT NUMBER

11. SUPPLEMENTARY NOTES

12a. DISTRIBUTION / AVAILABILITY STATEMENT

12b. DISTRIBUTION CODE

13. ABSTRACT *(Maximum 200 words)*

SEE FOLLOW PAGE

14. SUBJECT TERMS

15. NUMBER OF PAGES

16. PRICE CODE

17. SECURITY CLASSIFICATION OF REPORT	18. SECURITY CLASSIFICATION OF THIS PAGE	19. SECURITY CLASSIFICATION OF ABSTRACT	20. LIMITATION OF ABSTRACT

GENERAL INSTRUCTIONS FOR COMPLETING SF 298

The Report Documentation Page (RDP) is used in announcing and cataloging reports. It is important that this information be consistent with the rest of the report, particularly the cover and title page. Instructions for filling in each block of the form follow. It is important to ***stay within the lines*** to meet ***optical scanning requirements***.

Block 1. Agency Use Only *(Leave blank)*.

Block 2. Report Date. Full publication date including day, month, and year, if available (e.g. 1 Jan 88). Must cite at least the year.

Block 3. Type of Report and Dates Covered. State whether report is interim, final, etc. If applicable, enter inclusive report dates (e.g. 10 Jun 87 - 30 Jun 88).

Block 4. Title and Subtitle. A title is taken from the part of the report that provides the most meaningful and complete information. When a report is prepared in more than one volume, repeat the primary title, add volume number, and include subtitle for the specific volume. On classified documents enter the title classification in parentheses.

Block 5. Funding Numbers. To include contract and grant numbers; may include program element number(s), project number(s), task number(s), and work unit number(s). Use the following labels:

C	- Contract	PR	- Project
G	- Grant	TA	- Task
PE	- Program Element	WU	- Work Unit Accession No.

Block 6. Author(s). Name(s) of person(s) responsible for writing the report, performing the research, or credited with the content of the report. If editor or compiler, this should follow the name(s).

Block 7. Performing Organization Name(s) and Address(es). Self-explanatory

Block 8. Performing Organization Report Number. Enter the unique alphanumeric report number(s) assigned by the organization performing the report.

Block 9. Sponsoring/Monitoring Agency Name(s) and Address(es). Self-explanatory.

Block 10. Sponsoring/Monitoring Agency Report Number. *(If known)*

Block 11. Supplementary Notes. Enter information not included elsewhere such as: Prepared in cooperation with....; Trans. of....; To be published in.... When a report is revised, include a statement whether the new report supersedes or supplements the older report.

Block 12a. Distribution/Availability Statement. Denotes public availability or limitations. Cite any availability to the public. Enter additional limitations or special markings in all capitals (e.g. NOFORN, REL, ITAR).

DOD	-	See DoDD 5230.24, "Distribution Statements on Technical Documents."
DOE	-	See authorities.
NASA	-	See Handbook NHB 2200.2.
NTIS	-	Leave blank.

Block 12b. Distribution Code.

DOD	-	Leave blank.
DOE	-	Enter DOE distribution categories from the Standard Distribution for Unclassified Scientific and Technical Reports.
NASA	-	Leave blank.
NTIS	-	Leave blank.

Block 13. Abstract. Include a brief *(Maximum 200 words)* factual summary of the most significant information contained in the report.

Block 14. Subject Terms. Keywords or phrases identifying major subjects in the report.

Block 15. Number of Pages. Enter the total number of pages.

Block 16. Price Code. Enter appropriate price code *(NTIS only)*.

Blocks 17. - 19. Security Classifications. Self-explanatory. Enter U.S. Security Classification in accordance with U.S. Security Regulations (i.e., UNCLASSIFIED). If form contains classified information, stamp classification on the top and bottom of the page.

Block 20. Limitation of Abstract. This block must be completed to assign a limitation to the abstract. Enter either UL (unlimited) or SAR (same as report). An entry in this block is necessary if the abstract is to be limited. If blank, the abstract is assumed to be unlimited.

ABSTRACT

The report documents work carried out over the period 31 July 1996 to 31 December 1997 on a Multi-University Research Initiative (MURI) program under Office of Naval Research (ONR) sponsorship. The program couples transducer materials research in the Materials Research Laboratory (MRL), design and testing studies in the Applied Research Laboratory (ARL) and vibration and flow noise control in the Center for Acoustics and Vibration (CAV) at Penn State.

The overarching project objective is the development of acoustic transduction materials and devices of direct relevance to Navy needs and with application in commercial products. The initial focus of studies is upon high performance sensors and high authority high strain actuators. This objective also carries the need for new materials, new device designs, improved drive and control strategies and a continuing emphasis upon reliability under a wide range of operating conditions.

In *Material Studies*, undoubtedly major breakthroughs have occurred in the ultra-high strain relaxor ferroelectric systems. Earlier reports of unusual piezoelectric activity in single crystal perovskite relaxors have been amply confirmed in the lead zinc niobate : lead titanate, and lead magnesium niobate : lead titanate systems for compositions of rhombohedral symmetry close to the Morphotropic Phase Boundary (MPB) in these solid solutions. Analysis of the unique properties of 001 field poled rhombohedral ferroelectric crystals suggests new intrinsic mechanisms for high strain and carries the first hints of how to move from lead based compositions. A major discovery of comparable importance is a new mode of processing to convert PVDF:TrFE copolymer piezoelectric into a relaxor ferroelectric in which electrostrictive strains of 4% have been demonstrated at high fields. Both single crystal and polymer relaxors appear to offer energy densities almost order of magnitude larger than in earlier polycrystal ceramic actuators.

Transducer Studies have continued to exploit the excellent sensitivity and remarkable versatility of the cymbal type flextensional element. Initial studies of a small cymbal arrays show excellent promise in both send and receive modes, and larger arrays are now under construction for tests at ARL. New studies in constrained layer vibration damping and in flow noise reduction are yielding exciting new results.

In *Actuator Studies*, an important advance in piezoelectric generated noise control now permits wider use of acoustic emission as a reliability diagnostic technique. Joint studies with NRL, Washington have developed a completely new d_{15} driven torsional actuator and the CAV program element has designed an exciting high strain high force inchworm.

Finite element analysis continues to be an important tool for understanding the more complex composite structures and their beam forming capability in water. *Thin and Thick Thin Film Studies* are gearing up to provide the material base for micro-tonpilz arrays. New exploitation of ultra sensitive strain and permittivity measurements is providing the first reliable data of electrostriction in simple solids, and suggesting new modes for separating the polarizability contributors in dielectrics and electrostrictors.

TABLE OF CONTENTS

APPENDICES

VOLUME I

GENERAL SUMMARY PAPERS

1. Ito, Y. and K. Uchino, Wiley Encyclopedia of Electrical and Electronics Engineering, J. G. Webster, Edit., (Partial Charge "Piezoelectricity"), John Wiley & Sons (1998). [in press].
2. Newnham, R.E., "Molecular Mechanisms in Smart Materials," MRS Bulletin (May 1997).
3. Swartz, S.L., T.R. Shrout, and T. Takenaka, "Electronic Ceramics R&D in the U.S., Japan, Part I: Patent History," The American Ceramic Society Bulletin **76** (8) (1997).

2.0 MATERIALS STUDIES

2.1 Polycrystal Perovskite Ceramics

4. Alberta, E.F., and A.S. Bhalla, "Piezoelectric Properties of $Pb(InNb)_{1/2}O_3$-$PbTiO_3$ Solid Solution Ceramics," J. Korean Phys. Soc. **32**, S1265-S1267 (February 1998).
5. Alberta, E.F. and A.S. Bhalla, "High Strain and Low Mechanical Quality Factor Piezoelectric $Pb[Sc_{1/2}Nb_{1/2})_{0.575}Ti_{0.425}]O_3$ Ceramics" (1997).
6. Zhang, Q.M. and J. Zhao, "Polarization Responses in Lead Magnesium Niobate Based Relaxor Ferroelectrics," Appl. Phys. Lett. **71** (12, 1649-1651 (1997).
7. Glazounov, A.E., J. Zhao, and Q.M. Zhang, "Effect of Nanopolar Regions on Electrostrictive Coefficients of a Relaxor Ferroelectric," Proceedings Williamsburg Meeting, Williamsburg, Virginia (1998).
8. Zhao, J. A.E. Glazounov, Q.M. Zhang, and B. Toby, "Neutron Diffraction Study of Electrostrictive Coefficients of Prototype Cubic Phase of Relaxor Ferroelectric $PbMg_{1/3}Nb_{2/3}O_3$," Appl. Phys. Lett. **72** (9), 1-3 (1998).
9. Park, S.-E., T.R. Shrout, P. Bridenbaugh, J. Rottenberg, and G.M. Loiacono, "Electric Field Induced Anisotropy in Electrostrictive $Pb(Mg_{1/3}Nb_{2/3})O_3$ - $PbTiO_3$ Crystals," Ferroelectrics (1997).
10. You, H. and Q.M. Zhang, "Diffuse X-Ray Scattering Study of Lead Magnesium Niobate Single Crystals," Phys. Rev. Lett. **79** (20), 3950-3953 (1997).
11. Zhao, J., V. Mueller, and Q.M. Zhang, "The Influence of the External Stress on the Electromechanical Response of Electrostrictive $0.9Pb(Mg_{1/3}Nb_{2/3})O_3$–$0.1PbTiO_3$ in the DC Electrical Field Biased State," J. Mat. Res. (1998).

VOLUME II

12. Yoon, S.-J., A. Joshi, and K. Uchino, "Effect of Additives on the Electromechanical Properties of $Pb(Zr,Ti)O_3$–$Pb(Y_{2/3}W_{1/3})O_3$ Ceramics," J. Am. Ceram. Soc **80** (4), 1035-39 (1997).
13. Hackenberger, W., M.-J. Pan, V. Vedula, P. Pertsch, W. Cao, C. Randall, and T. Shrout, "Effect of Grain Size on Actuator Properties of Piezoelectric Ceramics," Proceedings of the SPIE's 5th International Symposium on Smart Structures and Materials, San Diego, CA (March 1-5, 1998).

Materials Studies–continued

14. Mueller, V. and Q.M. Zhang, "Shear Response of Lead Zirconate Titanate Piezoceramics," J. Appl. Phys. (1998).
15. Park, S.-E., M.-J. Pan, K. Markowski, S. Yoshikawa, and L.E. Cross, "Electric Field Induced Phase Transition of Antiferroelectric Lead Lanthanum Zirconate Titanate Stannate Ceramics," J. Appl. Phys. **82** (4), 1798-1803 (1997).
16. Yoshikawa, S., K. Markowski, S.-E. Park, M.-J. Pan, and L.E. Cross, "Antiferroelectric-to-Ferroelectric Phase Switching Lead Lanthanum Zirconate Stannate Titanate (PLZST) Ceramics)," Proceedings of SPIE's 4th Annual Symposium on Smart Structures and Materials, San Diego, CA (March 3-6, 1997).
17. Pan, M.-J., S.-E. Park, K.A. Markowski, W.S. Hackenberger, S. Yoshikawa, and L.E. Cross, "Electric Field Induced Phase Transition in Lead Lanthanum Stannate Zirconate Titanate (PLSnZT) Antiferroelectrics: Tailoring Properties through Compositional Modification" (1997).
18. Pan, M.-J., P. Pertsch, S. Yoshikawa, T.R. Shrout, and V. Vedula, "Electroactive Actuator Materials: Investigations on Stress and Temperature Characteristics," Proceedings of the SPIE's 5th International Symposium on Smart Structures and Materials, San Diego, CA (March 1-5, 1998).
19. Pan, M.-J. and S. Yoshikawa, "Effect of Grain Size on the Electromechanical Properties of Antiferroelectric-to-Ferroelectric Phase Switching PLSnZT Ceramics" (1997).

2.2 *Relaxor Ferroelectric Single Crystal Systems*

20. Service, R.F., "Shape-Changing Crystals Get Shiftier," Science **275**, 1878 (28 March 1997).
21. Shrout, T.R., S.-E. Park, C.A. Randall, J.P. Shepard, L.B. Hackenberger, "Recent Advances in Piezoelectric Materials" (1997).
22. Park, S.-E. and T.R. Shrout, "Ultrahigh Strain and Piezoelectric Behavior in Relaxor Based Ferroelectric Single Crystals," J. Appl. Phys. **82** (4), 1804-1811 (1997).
23. Park, S.-E. and T. R. Shrout, "Characteristics of Relaxor-Based Piezoelectric Single Crystals for Ultrasonic Transducers," IEEE Transactions, Ferroelectrics, and Frequency Control **44** (5), 1140-1147 (1997).
24. Park, S.-E. and T.R. Shrout, "Relaxor Based Ferroelectric Single Crystals for Electro-Mechanical Actuators," Mat. Res. Innov. **1**, 20-25 (1997).
25. Park, S.-E., M.L. Mulvihill, G. Risch, and T.R. Shrout, "The Effect of Growth Conditions on the Dielectric Properties of $Pb(Zn_{1/3}Nb_{2/3})O_3$ Single Crystals," Jpn. J. Appl. Phys. **36**, 1154-1158 (1997).
26. Mulvihill, M.L., L.E. Cross, W. Cao, and K. Uchino, "Domain-Related Phase Transionlike Behavior in Lead Zinc Niobate Relaxor Ferroelectric Single Crystals," J. Am. Ceram. Soc. **80** (6), 1462-68 (1997).
27. Park, S.-E., P.D. Lopath, K.K. Shung, and T.R. Shrout, "Relaxor-Based Single Crystal materials for Ultrasonic Transducer Applications" (1997).
28. Lopath, P.D., S.-E. Park, K.K. Shung, and T.R. Shrout, "$Pb(Zn_{1/3}Nb_{2/3})O_3/PbTiO_3$ Single Crystal Piezoelectrics for Ultrasonic Transducers" (1997).
29. Lopath, P.D., S-E. Park, K.K. Shung, and T.R. Shrout, "Single Crystal $Pb(Zn_{1/3}Nb_{2/3})O_3/PbTiO_3$ (PZN/PT) in Medical Ultrasonic Transducers" (1997).

Materials Studies–continued

2.3 New High Strain Polymer Materials

30. Su. J., Q.M. Zhang, C.H. Kim, R.Y. Ting, and R. Capps, "Effect of Transitional Phenomena on the Electric Field Induced Strain–Electrostrictive Response of a Segmented Polyurethane Elastomer" (1997).
31. Su, J., Q.M. Zhang, and R.Y. Ting, "Space-Charge-Enhanced Electromechanical Response in Thin-Film Polyurethane Elastomers," Appl. Phys. Lett **71** (3), 386-388 (1997).

VOLUME III

32, Su, J., Q.M. Zhang, P.-C. Wang, A.G. MacDiarmid, K.J. Wynne, "Preparation and Characterization of an Electrostrictive Polyurethane Elastomer with Conductive Polymer Electrodes," Polymers for Adv. Tech. (1998).
33. Zhang, Q.M., V. Bharti, and X. Zhao, "Giant Electrostriction and Relaxor Ferroelectric Behavior in Electron Irradiated Poly(vinylidene Fluoride-Trifluoroethylene) Copolymer," Science (1998).

3.0 TRANSDUCER STUDIES

3.1 Cymbal : Moonie : BB Composites

34. Newnham, R.E., "Composite Sensors and Actuators" (1997).
35. Steele, B.CH., R.E. Newnham, and A.G. Evans, "Ceramics, Composites, and Intergrowth," Current Opinion in Solid State & Materials Science **2**, 563-565 (1997).
36. Tressler, J.F. S. Alkoy, and R.E. Newnham, "Piezoelectric Sensors and Sensor Materials" (1997).
37. Tressler, J.F., S. Alko, A. Dogan, and R.E. Newnham, "Functional Composites for Sensors, Actuators, and Transducers" (1997).
38. Dogan, A., K. Uchino, R.E. Newnham, "Composite Piezoelectric Transducer with Truncated Conical Endcaps 'Cymbal'," IEEE Transactions on Ultrasonics, Ferroelectrics, and Frequency Control **44** (3), 597-605 (1997).
39. Dogan, A., J.F. Fernandez, K. Uchino, and R.E. Newnham, "The 'Cymbal' Electromechanical Actuator" (1997).
40. Tressler, J.F., W. Cao, K. Uchino, and R.E. Newnham, "Ceramic-Metal Composite Transducers for Underwater Acoustic Applications" (1997).
41. Tressler, J.F. and R.E. Newnham, "Doubly Resonant Cymbal-Type Transducers," IEEE Transactions on Ultrasonics, Ferroelectrics, and Frequency Control **44** (5), 1175-1177 (1997).
42. Tressler, J.F., W. Cao, K. Uchino, and R.E. Newnham, "Finite Element Analysis of The Cymbal-Type Transducer" (1997).
43. Tressler, J.F., W.J. Hughes, W. Cao, K. Uchino, and R.E. Newnham, "Capped Ceramic Underwater Sound Projector" (1997).

Transducer Studies–continued

VOLUME IV

44. Alkoy, S., P.D. Lopath, R.E. Newnham, A.-C. Hladky-Hennion, and J.K. Cochran, "Focused Spherical Transducers for Ultrasonic Imaging" (1997).
45. Alkoy, S., A. Dogan, A.-C. Hladky, P. Langlet, J.K. Cochran, and R.E. Newnham, "Miniature Piezoelectric Hollow Sphere Transducers (BBs)" (1997).
46. Zipparo, M.J., K.K. Shung, and T.R. Shrout, "Piezoceramics for High-Frequency (20 to 100 MHz) Single-Element Imaging Transducers," IEEE Transactions on Ultrasonics, Ferroelectrics, and Frequency Control **44** (5), 1038-1048 (1997).

3.2 Frequency Agile Transducers

47. Davis, C. and G.A. Lesieutre, "An Actively-Tuned Solid State Piezoelectric Vibration Absorber" (1997).
48. Davis, C.L., G.A. Lesieutre, and J. Dosch, "A Tunable Electrically Shunted Piezoceramic Vibration Absorber" (1997).
49. Lesieutre, G.A. and U. Lee, "A Finite Element for Beams Having Segmented Active Constrained Layers with Frequency-Dependent Viscoelastic Material Properties" (1997).
50. Hebert, C.A. and G.A. Lesieutre, "Rotocraft Blade Lag Damping Using Highly Distributed Tuned Vibration Absorbers," American Institute of Aeronautics and Astronautics (AIAA 98-2001).
51. Lesieutre, G.A. and C.L. Davis, "Can a Coupling Coefficient of a Piezoelectric Device be Higher than Those of its Active Material?," SPIE 4th Annual Symposium on Smart Structures and Materials, San Diego, CA (March 1997).

3.3 3-D Acoustic Intensity Probes

52. Lauchle, G.C., J.R. MacGillivray, and D.C. Swanson, "Active Control of Axial-flow Fan Noise," J. Acoust. Soc. Am 101 (1), 341-349 (1997).
53. McGuinn, R.S., G.C. Lauchle, and D.C. Swanson, "Low Flow-Noise Microphone for Active Noise Control Applications," AIAA Journal **35** (1), 29-34 (1997).
54. McGuinn, R.S., G.C. Lauchle, and D.C. Swanson, "Low Flow-Noise Pressure Measurements Using a "Hot-Mic," AIAA -97-1665-CP.
55. Capone, D.E., and G.C. Lauchle, "Designing a Virtual Sound-Level Meter in LabVIEW," Education/Acoustics, LabVIEW, National Instruments.

VOLUME V

4.0 ACTUATOR STUDIES

4.1 Materials : Designs : Reliability

56. Uchino, K., "Piezoelectric Actuators" (1997).
57. Uchino, K., "Overview: Materials Issues in Design and Performance of Piezoelectric Actuators," SPIE Mtg. (1997).
58. Uchino, K., "Shape Memory Ceramics," Chapter 8 (1997).

Actuator Studies–continued

59. Aburatani, H., S. Yoshikawa, K. Uchino, and J.W.C. deVries, "A Study of Acoustic Emission in Piezoelectric Multilayer Ceramic Actuator," Jpn. J. Appl. Phys. **37**, 204-209 (1998).
60. Aburatani, H. and K. Uchino, "Acoustic Emission (AE) Measurement in Piezoelectric Ceramics" (1997).
61. Aburatani, H. and K. Uchino, "The Application of Acoustic Emission (AE) Method for Ferroelectric Devices and Materials," 8th US-Japan Seminar (1997).
62. Uchino, K., "Reliability of Ceramic Actuators" (1997).

4.2 Photostrictive Actuators

63. Tonooka, K. P. Poosanaas, and K. Uchino, "Mechanism of the Bulk Photovoltaic Effect in Ferroelectrics," Proceedings of the 5th SPIE Mtg., San Diego, CA (1998).
64. Poosanass, P. A. Dogan, S. Thakoor, and K. Uchino, "Dependence of Photostriction on Sample Thickness and Surface Roughness for PLZT Ceramics," Proceedings of the 1997 IEEE Ultrasonics Symposium, Toronto, Ontario, Canada (October 1997).
65. Poosanaas, P. A. Dogan, A.V. Prasadarao, S. Komarneni, and K. Uchino, "Photostriction of Sol-Gel Processed PLZT Ceramics," J. Electroceramics **1** (1), 105-111 (1997).

VOLUME VI

66. Poosanaas, P., A. Dogan, A.V. Prasadarao, S. Komarneni, and K. Uchino, "Effect of Ceramic Processing Methods on Photostrictive Ceramics," J. Adv. Perf. Mat. (1997).
67. Thakoor, S., P. Poosanaas, J.M. Morookian, A. Yavrovian, L. Lowry, N. Marzwell, J. Nelson, R.R. Neurgaonkar, and K. Uchino, "Optical Microactuation in Piezoceramics" (1997).

4.3 New Torsional Amplifier/Actuators

68. Glazounov, A.E., Q.M. Zhang, and C. Kim, "Piezoelectric Actuator Generating Torsional Displacement from Piezoelectric d_{15} Shear Response," Appl Phys. Lett. (1997).
69. Glazounov, A.E., Q.M. Zhang, and C. Kim, "A New Torsional Actuator Based on Shear Piezoelectric Response," Proceedings of SPIE Smart Materials, San Diego, CA (March 1998).

4.4 High Force Amplifiers and Inchworms

70. Uchino, K., J. Zheng, A. Joshi, S. Yoshikawa, S. Hirose, S. Takahashi, and J.W.C. deVries, "High Power Characterization of Piezoelectric Materials" (1997).
71. Uchino, K., "High Electromechanical Coupling Piezoelectrics - How High Energy Conversion Rate is Possible," Mat. Res. Soc. Symp. Proc. **459**, 3-14 (1997).
72. Park, S.-E., V. Vedula, M.-J. Pan, W.S. Hackenberger, P. Pertsch, and T.R. Shrout, "Relaxor Based Ferroelectric Single Crystals for Electromechanical Actuators," Proceedings of the SPIE's 5th International Symposium on Smart Structures and Materials, San Diego, CA (March 1998).

Actuator Studies–continued

73. Koopmann, G.H. G.A. Lesieutre, B.R. Dershem, W. Chen, and S. Yoshikawa, "Embeddable Induced Strain Actuators Using Framed 3-3 Piezoceramic Stacks: Modeling and Characterization," Proceedings of the SPIE's 4th Annual International Symposium on Smart Structures and Materials, San Diego, CA (March 1997).
74. Driesch, P.L., G.H. Koopmann, J. Dosch, and H. Iwata, "Development of a Surface Intensity Probe for Active Control Applications," IMECE, Dallas, Texas (November 1997).
75. Galante, T., J. Frank, J. Bernard, W. Chen, G.A. Lesieutre, and G.H. Koopmann, "Design, Modeling, and Performance of a High Force Piezoelectric Inchworm Motor" (1997).
76. Galante, T.P., "Design and Fabrication of a High Authority Linear Piezoceramic Actuator: The PSU H3 Inchworm," Master of Science Thesis, The Pennsylvania State University (August 1997).
77. Lesyna, M.W., "Shape Optimization of a Mechanical Amplifier for Use in a Piezoceramic Actuator," Master of Science Thesis, The Pennsylvania State University (May 1998).

VOLUME VII

78, Uchino, K., "Piezoelectric Ultrasonic Motors: Overview," J. Smart Materials and Structures–Special Issue (1997).
79. Uchino, K., "Compact Piezoelectric Ultrasonic Motors," J. Medical Ultrasonics 24 (9), 1191-92 (1997).

5.0 MODELING and CHARACTERIZATION

5.1 Finite Element Methods

80. Qi, W. and W. Cao, "Finite Element Analysis and Experimental Studies on the Thickness Resonance of Piezocomposite Transducer," Ultrasonic Imaging **18**, 1-9 (1996).
81. Qi, W. and W. Cao, "Finite Element Study on Random Design of 2-2 Composite Transducer," SPIE **3037**, 176-180 (1997).
82. Geng, X. and Q.M. Zhang, "Evaluation of Piezocomposites of Ultrasonic Transducer Applications–Influence of the Unit Cell Dimensions and the Properties of Constituents on the Performance of 2-2 Piezocomposites," IEEE Transactions on Ultrasonics, Ferroelectrics, and Frequency Control **44** (4), 857-872 (1997).
83. Zhang, Q. and X. Geng, "Acoustic Properties of the Interface of a Uniform Medium-2-2 Piezocomposite and the Field Distributions in the Composite," Jpn. J. Appl. Phys. **36**, 6853-6861 (1997).
84. Geng, X. and Q.M. Zhang, "Analysis of the Resonance Modes and Losses in 1-3 Composites for Ultrasonic Transducer Applications," IEEE UFFC (1997).

Modeling and Characterization–continued

5.2 Relaxor Ferroelectrics

85. Li, S., J.A. Eastman, R.E. Newnham, and L.E. Cross, "Diffuse Phase Transition in Ferroelectrics with Mesoscopic Heterogeneity: Mean-field Theory," Phys. Rev. B **55** (18), 12067-12078 (1997).
86. Li, S., J.A. Eastman, J.M. Vetrone, R.E. Newnham, and L.E. Cross, "Dielectric Response in Ferroelectric Superlattices," Philosophical Magazine B **76** (1), 47-57 (1997).

VOLUME VIII

87. Du, X-H., U. Belegundu, and K. Uchino, "Crystal Orientation Dependence of Piezoelectric Properties in Lead Zirconate Titanate: Theoretical Expectation for Thin Films," Jpn. J. Appl. Phys. **36**, 5580-5587 (1997).

5.3 Thin and Thick Thin Films

88. Cross, L.E. and S. Trolier-McKinstry, "Thin-Film Integrated Ferroelectrics," Encyclopedia of Applied Physics **21**, 429-451 (1997).
89. Xu, B., P. Moses, N.G. Pai, and L.E. Cross, "Charge Release of Lanthanum-Doped Lead Zirconate Titanate Stannate Antiferroelectric Thin Films," Appl. Phys. Lett. **72** (5), 593-595 (1998).
90. Xu. B., N.G. Pai, and L.E. Cross, "Lanthanum Doped Lead Zirconate Titanate Stannate Antiferroelectric Thin Films From Acetic Acid-Based Sol-Gel Method," Materials Letters **34** (3 & 4) (March 1998).
91. Xu, B., N.G. Pai, P. Moses, and L.E. Cross, "Antiferroelectric Thin Films for Decoupling Capacitor and Microactuator Applications," Materials Research Society Symposium **493**, Ferroelectric Thin Films VI.

5.4 Domain Studies

92. Zhu, S. and W. Cao, "Direct Observation of Ferroelectric Domains in LiTaO3 Using Environmental Scanning Electron Microscopy," Phys. Rev. Lett. 79 (13), 2558-1561 (1997).
93. Cao, W. and C.A. Randall, "Grain Size and Domain Size Relations in Bulk Ceramic Ferroelectric Materials," J. Phys. Chem. Solids **57** (10), 1499-1505 (1996).
94. Zavala, G., J.H. Fendler, and S. Trolier-McKinstry "Characterization of Ferroelectric Lead Zirconate Titanate Films by Scanning Force Microscopy," J. Appl. Phys. 81 (11), 7480-7491 (1997).

5.5 Electrostriction

95. Newnham, R.E., V. Sundar, R. Yimnirun, J. Su, and Q.M. Zhang, "Electrostriction-Nonlinear Electromechanical Coupling in Solid Dielectrics" (1997).
96. Newnham, R.E., V. Sundar, R. Yimnirun, J.H. Su, and Q.M. Zhang, "Electrostriction in Dielectric Materials" (1997).

Modeling and Characterization–continued

97. Sundar, V., R. Yimnirun, B.T. Aitken, and R.E. Newnham, "Structure-Property Relationships in the Electrostriction Response of Low Permittivity Silicate Glasses" (1997).

ABSTRACT

The report documents work carried out over the period 31 July 1996 to 31 December 1997 on a Multi-University Research Initiative (MURI) program under Office of Naval Research (ONR) sponsorship. The program couples transducer materials research in the Materials Research Laboratory (MRL), design and testing studies in the Applied Research Laboratory (ARL) and vibration and flow noise control in the Center for Acoustics and Vibration (CAV) at Penn State.

The overarching project objective is the development of acoustic transduction materials and devices of direct relevance to Navy needs and with application in commercial products. The initial focus of studies is upon high performance sensors and high authority high strain actuators. This objective also carries the need for new materials, new device designs, improved drive and control strategies and a continuing emphasis upon reliability under a wide range of operating conditions.

In *Material Studies*, undoubtedly major breakthroughs have occurred in the ultra-high strain relaxor ferroelectric systems. Earlier reports of unusual piezoelectric activity in single crystal perovskite relaxors have been amply confirmed in the lead zinc niobate : lead titanate, and lead magnesium niobate : lead titanate systems for compositions of rhombohedral symmetry close to the Morphotropic Phase Boundary (MPB) in these solid solutions. Analysis of the unique properties of 001 field poled rhombohedral ferroelectric crystals suggests new intrinsic mechanisms for high strain and carries the first hints of how to move from lead based compositions. A major discovery of comparable importance is a new mode of processing to convert PVDF:TrFE copolymer piezoelectric into a relaxor ferroelectric in which electrostrictive strains of 4% have been demonstrated at high fields. Both single crystal and polymer relaxors appear to offer energy densities almost order of magnitude larger than in earlier polycrystal ceramic actuators.

Transducer Studies have continued to exploit the excellent sensitivity and remarkable versatility of the cymbal type flextensional element. Initial studies of a small cymbal arrays show excellent promise in both send and receive modes, and larger arrays are now under construction for tests at ARL. New studies in constrained layer vibration damping and in flow noise reduction are yielding exciting new results.

In *Actuator Studies*, an important advance in piezoelectric generated noise control now permits wider use of acoustic emission as a reliability diagnostic technique. Joint studies with NRL, Washington have developed a completely new d_{15} driven torsional actuator and the CAV program element has designed an exciting high strain high force inchworm.

Finite element analysis continues to be an important tool for understanding the more complex composite structures and their beam forming capability in water. *Thin and Thick Thin Film Studies* are gearing up to provide the material base for micro-tonpilz arrays. New exploitation of ultra sensitive strain and permittivity measurements is providing the first reliable data of electrostriction in simple solids, and suggesting new modes for separating the polarizability contributors in dielectrics and electrostrictors.

INTRODUCTION

This report delineates the research performed over the period of 31 July 1996 to 31 December 1997 on an MURI under Office of Naval Research contract N00014-96-1-1173 on the topic "Acoustic Transduction: Materials and Devices." The program brings together activities in the Materials Research Laboratory (MRL), the Applied Research Laboratory (ARL), and the Center for Acoustic and Vibration (CAV) at Penn State. Principal Investigator on the program is Professor Kenji Uchino, Professor of Electrical Engineering at Penn State and the Program Officer in ONR is Dr. Scott Littlefield.

The overarching project objective is the development of acoustic transduction materials and devices of direct relevance to Navy needs and with application in commercial products. The initial focus is upon high performance sensors and high authority high strain actuators. This however also carries the need for new materials, new device designs, improved drive and control strategies and a continuing emphasis upon reliability under a wide range of use conditions.

In the original proposal, the topics to be studied were divided into:

MATERIAL STUDIES	A.S. Bhalla
COMPOSITE SYSTEMS	R.E. Newnham
DEVICE STRUCTURES	T.R. Shrout
MODELLING	W. Cao
DEVICE FABRICATION and TESTING	W.J. Hughes
AIR ACOUSTICS and STEP and REPEAT SYSTEMS	G. Lesieutre

Following long established precedent, the report will draw upon published results which will be connected by a brief narrative summary to highlight the major achievements. For convenience the work will be presented under:

1.0 GENERAL SUMMARY PAPERS
2.0 MATERIALS STUDIES
- 2.1 Polycrystal Perovskite Ceramics
- 2.2 Relaxor Ferroelectric Single Crystal Systems
- 2.3 New High Strain Polymer Materials

3.0 TRANSDUCER STUDIES
- 3.1 Cymbal : Moonie : BB Composites
- 3.2 Frequency Agile Transducers
- 3.3 3-D Acoustic Intensity Probes

4.0 ACTUATOR STUDIES
- 4.1 Materials : Designs : Reliability
- 4.2 Photostrictive Actuators
- 4.3 New Torsional Amplifier/Actuators
- 4.4 High Force Amplifiers and Inchworms

5.0 MODELING and CHARACTERIZATION
- 5.1 Finite Element Methods
- 5.2 Relaxor Ferroelectrics
- 5.3 Thin and Thick Thin Films
- 5.4 Domain Studies
- 5.5 Electrostriction

In the *General Summary Papers*, the senior faculty continue to discharge their responsibility as educators updating and explaining the general background topics piezoelectricity, smart material systems, and the status of electroceramic R&D in the US vs Japan.

Materials Studies in polycrystal perovskite ceramics have focused upon ultra soft systems, where the whole poling strain may be utilized at low frequency, and upon antiferroelectric : ferroelectric switching compositions. Undoubtedly however the major breakthroughs have occurred in ultra-high strain relaxor ferroelectric systems. Current studies have amply confirmed the massive strain, blocking force, and exceptional energy density in the relaxor perovskite single crystals. A major new discovery of comparable importance has been a new mode of processing to convert PVDF:TrFE copolymer piezoelectric into a relaxor ferroelectric in which electrostrictive strains up to 4% can be induced at high fields. Both single crystal and polymer relaxors appear to offer energy densities almost order of magnitude higher than in earlier actuator materials.

Transducer Studies have continued to underscore the excellent sensitivity and remarkable versatility of the cymbal type flextensional elements. Initial testing of a 3 × 3 cymbal array shows excellent promise is both send and receive modes in water, and a larger array is under construction.

New work in vibration absorption has demonstrated the advantage of agile, lightly damped resonant absorbers. Segmented active constrained layer damping is shown to be more robust than a single active layer, and studies of an axially constrained beam raise interesting questions in the definition of piezoelectric coupling coefficient.

Noise control studies demonstrate a significant advantage for a hot wire anemometer : microphone combination with suitable feedback to quiet flow noise. Continuing the educational role, a software generated virtual sound level meter is discussed for hands on student analysis of acoustic signals.

Actuator Studies explore acoustic emission as a tool in reliability assessment, photostriction in both bulk and thin films. In single crystals a possible model for the very high coupling is proposed. Joint studies with NRL have evolved a completely new type of d_{15} driven torsional amplifier/actuator. A new design of high force piezoelectric inchworm is presented and rotary motors are discussed for a very wide range of scales down to 3 mm diameter.

Finite element models are developed for 1:3 and 2:2 composites and beam forming characteristics explored. Thick and thin film systems are discussed, and very rapid change release documented for backswitching square loop antiferroelectrics. Electrostriction is the basic driving force in all perovskite piezoelectrics. Using new ultra-sensitive measuring techniques it has been possible for the first time to determine quantitatively the electrostriction constants for simple low permittivity glasses and ceramics.

1.0 GENERAL SUMMARY PAPERS

"Piezoelectricity" by Yukio Ito and Kenji Uchino is an encyclopedia article covering the History Properties and Applications of Ceramic Piezoelectrics (1). A very useful discussion of molecular mechanisms in smart materials is presented by R.E. Newnham, which

is an edited version of his David Turnbull Lecture in MRS (2). Electroceramics research and development in the US and Japan (3) gives a very clear summary of patent history, ongoing interests and future prospects across this whole field.

2.0 MATERIALS STUDIES

2.1 Polycrystal Ceramics

Lead indium niobate : lead titanate (PIN:PT) is a solid solution system embracing a morphotropic boundary at the 62 mole% PIN composition. MPB composition yield soft piezoelectrics with d_{33} ~ 395 pC/N, d_{31} - 175 pC/N and P_r ~ 35 $\mu c/cm^2$ (4). In the lead scandium niobate : lead titanate system it is possible to develop ultra-soft compositions with S_3 ~ 0.4% and narrow hysteresis (5). A very interesting family of papers (6,7,8,9,10,11) follow the polarization and strain generating mechanisms in the lead magnesium niobate system in detail. The role of the heterogeneous structure of nano-polar regions is clearly expounded, the changing volume of the polar phase is quantified for the first time, and the very strong influence of the volume conserving polarization changes in this heterogeneous structure properly expounded.

The effects of 'donor' and 'acceptor' dopants in the PZT:$Pb(Y_{2/3}W_{1/3})O_3$ ceramics at the 0.02 $Pb(Y_{2/3}W_{1/3})O_3$ composition have been examined (12) showing a beneficial effect from donor dopants without significant degradation of Q. Exploration of grain size effects in soft PZT show that ceramics with average grain size down to 1 μm can be produced (13) with negligible degradation of piezoelectric properties, but much enhanced mechanical properties. For the torsional mode actuator discussed later, it is important to know the behavior of d_{15} at higher E fields and the compositions which will permit maximum induced strain (14). Papers (15, 16, 17, 18, 19) deal with aspects of the behavior of phase switching antiferroelectric : ferroelectric lead zirconate titanate stannate compositions. The behaviors are most interesting and unusual in that both antiferroelectric and ferroelectric phases have different ferroelastic domain structures which respond to elastic stress fields. This lead to an uncoupling of polarization and strain switching (15) and the "strange" effect that the field induced uniaxial strain is larger under compressive stress than in the unstressed state (18). Dopants can be used to control the temperature dependence of the switching (16) and isovalent substituents used to modify the hysteresis between forward (AF $\rightarrow$ F) and backward (F $\rightarrow$ AF) switching.(17) Grain size reduction enhances mechanical strength (19) without degrading of electrical properties, provided final sintering is carried out above 1000°C.

2.2 Relaxor Ferroelectric Single Crystal Systems

The first 'popular' announcement of the massive piezoelectric response in the relaxor single crystals of the lead zinc niobate : lead titanate system was in Science (20) composed by that magazine's science writers. A more balanced account (21) gives a proper comparison with earlier polycrystal systems, emphasizing the unique character of the 001 field poled rhombohedral state for compositions close to the morphotropic phase boundary (MPB). The behavior is confirmed (22) with coupling coefficients k_{33} up to 0.94 and maximum S_3 strain of order 1.7%. A simple model is also proposed to account for the unusual anhysteritic strain

behavior. A wider range of possible relaxor based MPB compositions are proposed (23) with higher Curie temperatures, and the large property values further confirmed (24).

Effects of flux growth conditions on realized properties are discussed (25) which highlights the difficulty of annealing the crystals which are in the metastable perovskite form. Relaxor type behavior is confirmed by domain studies (26) which reveal the expected micro-to-macro domain induction by electric field in zero field cooled crystals and reveals the persistent static domain structure in 001 poled sections of the rhombohedral symmetry. Probably the first area of application for the single crystal will be in medical ultrasound (27). The possible major advantages associated with the large permittivity and exceptional coupling coefficient k_{33} are discussed (28) and an intercomparison with soft PZT given (29).

2.3 High Strain Polymer Electrostrictors

Here-to-fore the Ferroelectrics group at Penn State has been focused on inorganic ceramic piezoelectrics, with polymers treated as a passive phase for composites. Reports of very large (5%) field induced strains in polyurethane elastomers and our major interests in electrostriction kindled a new interest. In cooperation with NRL Orlando, work was initiated to sort out "true" electrostriction from the compressive effects of Maxwell Stress in soft segmented polyurethane elastomers (30). Below the glass transition temperature, only 10% of strain is from Maxwell stress, however at 40°C between 35 and 50% of strain in these soft polymers is Maxwell stress. Enhanced response in thin film urethanes is measured (31) and explained on the basis of a charge injection/space charge model. A novel conductive polymer (poly pyrrole) electrode is developed in (32) and shown to have excellent compatibility with the urethane and electrical properties at low frequency equivalent to metal electrodes.

A major breakthrough in current work has been an electron irradiation treatment for the polyvinylidene fluoride-trifluoroethylene copolymer (33) which converts the system to a relaxor ferroelectric. Properties achieved are startlingly similar to lead magnesium niobate, with strong dispersion of the dielectric permittivity following Vogel Fulcher Law, anhysteretic response, recovering hysteresis at low temperature and massive electrostriction with strains up to 4% at high field levels. Clearly a most exciting development for sensor and actuator systems

3.0 TRANSDUCER STUDIES

3.1 Cymbal, Moonie, and BB Composites

Composite Studies at the MRL are reviewed (34) and the more general composite scene reviewed.(35) The focus is narrowed to piezoelectric systems (36) and specifically to the flextensional systems (37). Significantly more detail for the cymbal geometry is given in (38) which used finite element analysis and experimental verification to demonstrate the advantage of this geometry. The advantages are further underscored in (39) which compares the salient characteristics of multilayers, bimorphs, rainbows, cymbals, and moonies. The resonant characteristics of the cymbal are analyzed by finite element methods (40) and compare well with experiment. The versatility of the system is highlighted by experiments with two different end cap metals, and different end cap geometries, which clearly demonstrate the capability to sustain two largely uncoupled resonance frequencies.(41)

Cymbal resonant mode analysis by FEM is further delineated in (42) which calculates mode shapes resonant frequencies and admittance spectra in excellent agreement with measured properties.

Characteristics for a simple 3 × 3 cymbal array as a shallow water larger area transducer are discussed (43) and shown to be competitive with the more widely used tonpilz. Preliminary examination of the hollow mini-sphere PZT BBs as a focused ultrasound transducer are presented in (44) showing center frequency at 48 MHz, bandwidth 22% and insertion loss- 44 dB. A detailed discussion of the preparation, characterization, electroding and performance of the hollow sphere Bbs is given in (45). Piezoceramics for high frequency single element imaging transducers are discussed in (46) using both PZT and modified lead titanate. In each case except where cable impedance is dominant there is performance benefit from electrical matching.

3.2 Frequency Agile Transducers

In piezoelectric resonant vibration damping, maximum effect at a single frequency can be achieved by a lightly damped piezoelectric resonator. An interesting scheme for active tuning using parallel shunt capacitance has been demonstrated (47) with an average improvement of 10 dB across the tuning range as compared to a simple passive system. Both capacitative and resistive shunting methods are discussed in (48). A new model treatment has been developed for segmented constrained layer damping using frequency dependent viscoelastic media, and shown to be more robust then a single continuous active constrained layer (49). Damping of rotocraft blades is considered in (50) which makes a strong case for distributed discrete tuned absorbers. The influence of destabilizing mechanical pre-loads on flexural beam resonance are considered in (51) and the question posed as to whether the effective coupling coefficient of such a system may exceed that of a driving piezoelectric.

3.3 3-D Acoustic Intensity Probes

For active noise control on intriguing approach for reducing axial flow fan noise uses the fan blades as the coupling diaphragm for the noise canceling loudspeaker (52). To explore sound fields in low flow noise environments, a hot wire anemometer: microphone combination (hot-mic) with suitable feedback is considered (53) and shown to permit of order 20 dB reduction in flow noise at frequencies below 100 Hz, without perturbing the measured sound field. Verification of the performance of such a combination is given in (54) using adaptive filtering of the hot-wire signal in subtraction from the microphone output. The educational role is taken up in (55) where a software generated virtual sound-level meter is described which can have broad application for "hands-on" student analysis of acoustic signals.

4.0 ACTUATOR STUDIES

4.1 Materials : Designs : Reliability Issues

Trends in piezoelectric ceramic actuator materials, actuator designs, drive and control techniques, device design and application are discussed in (56). Materials issues are further reviewed in (57) but now from the perspective of device design and driving methods. Shape

memory possibilities in ceramic systems are discussed in (58) based on the antiferroelectric : ferroelectric phase switching materials. Acoustic emission as a diagnostic technique for actuator reliability has taken a great leap forward with the discovery and isolation of spurious power supply induced 'vibrational' noise (59). It now begins to be possible to explore the role of domain switching in acoustic emission (60), and the possible use of AE for damage assessment is now realized (61). The complex of reliability issues for multilayer systems is discussed in (62) for both actuators and motors.

4.2 Photostrictive Actuation

Optical driving of displacement using the photovoltaic effect in ferroelectrics is examined in (63) showing nonlinear behavior as a function of sample thickness and illumination intensity. Corresponding photostriction driven by the photovoltage is reviewed in (64) for WO_3 doped PZTs. Studies of the effect of sample thickness for this ceramic suggest an optimum at ~32 mm. The advantage of sol-gel synthesized ceramics in the same WO_3 doped system is demonstrated in (65) and further examined in (66) which considers grain size, homogeneity and high density as the critical parameters. Optical actuation of unimorph structures is discussed in (67) and potential advantages of a highly flexible polymeric substrate hypothesized.

4.3 New Torsional Amplifier/Actuator

In cooperation with NRL, a completely new concept has been developed for a torsional actuator/amplifier driven by the piezoelectric d_{15} (68). Amplification is developed by using the shear mode actuator as a segment in a cylinder forcing the shear to rotate the tube and giving an amplification l/r where r is the radius and l the length of the tube. Unlike most amplifiers, because increased length encompasses more drive ceramic the gain is not at the expense of torque.

Study of d_{15} at higher drive levels reveals a strong positive nonlinearity, which is of fundamental interest (14) but also vastly beneficial to the torque capability (69).

4.4 High Force Amplifiers and Inchworms

High power level characterization of piezoceramics is discussed in (70) which explores the limitations and advantages of constant voltage , constant current and pulsed excitation of resonance. Ultra high coupling in the lead zinc niobate: lead titante single crystal is examined in (71) and possible explanations for the unusual properties of 001 poled rhombohedral compositions explored. The potentiality of the single crystal materials for actuator application is emphasized in (72) which show energy densities 5× that available in PZT or PMN polycrystals.

Design and testing of a high authority PZT cofired multilayer actuator and frame structures is discussed in (73) the system permits direct measurement of both electrical input and mechanical output power. The system is as expected most efficient when the mechanical impedance is matched to the corresponding mechanical load. The design, calibration and performance of a new type of surface probe to measure acceleration and acoustic pressure is discussed in (74). The device uses commercial accelerometer and microphone components,

chosen for low mass and low phase shifts. A most interesting high strain, high force inchworm, is described in (75, 76, 77) which permits speeds of order 1 cm/sec dynamic force in excess of 50N and a clamped holding force greater than 200 N.

Piezoelectric Ultrasonic motors are reviewed in (78). Both standing wave and traveling wave rotary and linear motors are considered and characteristics compared to electromagnetic motors. Very compact ultrasonic motors are described in (79).

5.0 MODELING and CHARACTERIZATION STUDIES

5.1 Finite Element and Modeling Methods

The finite element methods have proven most useful in the analysis of complex composite structures. Resonant modes in moonies and cymbals (38) thickness mode resonances in 2-2 connected piezoceramic/polymer systems (80) where both mode structures and beam pattern in water can be traced (81). The FEM is always in competition with direct analysis which can be applied to the regular 2:2 geometry (82) and can even calculate the interactions with a matching layer for a water load (83). Model methods have also been applied to the resonant modes and losses in 1:3 composites where the mechanical Q of the ceramic plays the major role (84).

5.2 Relaxor Ferroelectrics

The diffuse phase transition and relaxor character is discussed on the basis of Landau theory for the local polar regions (85). In (86) a similar treatment is applied to a ferroelectric multilayer of ultra-thin layers indicating the possibility of enhanced dielectric response over a broadened temperature range. For the PZT system (87) Landau Devonshire theory has been applied to explore orientation dependence of the intrinsic dielectric and piezoelectric response. Interestingly the maximum response in the rhombohedral phase is for fields 57° to the polar axis suggesting that in thin films, the 001 orientation in the rhombohedral phase may be most effective.

5.3 Thin and Thick Thin Films

Current status of research on integrated ferroelectric thin films is summarized in (88) which discusses perovskite, bismuth oxide layer structure and 'relaxor' ferroelectrics. It has often been postulated that thin film antiferroelectric could make excellent capacitors and transducers if bulk type switching could be preserved. For lead lanthanum zirconate titanate stannate (89) demonstrates that square loop character is preserved in films down to 0.4 μm thick, and that rapid charge release ~10 n sec is possible from the F → AF transition. Techniques for sol-gel deposition of the PLSnZT films are discussed in (90). Both "square" are "slanted loop" compositions have been developed and shown to produce switchable S_3 strain up to 0.4% (91).

5.4 Domain Studies

Direct observation of 180° domain structures in $LiTaO_3$ single crystals, without etching or surface coating has been demonstrated using an environmental scanning electron microscope, which avoids surface charging effects (92). Detailed observation of ferroelastic

domains in hard and soft PZT ceramics suggest that the bulk domain configuration can be 'frozen' in thin section. It is shown that the accepted parabolic law for ferroelastic domain wall separation is only valid for grain size in the range 1-10 μm, and that at lower sizes below 1 μm the exponent is smaller than 1/2 (93). Scanning force microscopy using both contact and noncontact modes has been used to study dielectric ferroelectric and piezoelectric properties of ferroelectric films (94). The technique appears to offer scope for identifying small inclusion of second phase, polarization hysteresis from nano scale regions, with both piezoelectric and dielectric permittivity information.

5.5 Electrostriction

Electrostriction is probably the most important elasto-electric coupling parameter, yet until the measurements at Penn State no reliable data were available in the literature for simple low permittivity solids. Recent measurements (95) using both ultradilatometry (direct) and precision compressometry (converse) effects have filled the gap with completely reliable data.

It is surprising to see the enormous range of the polarization related hydrostatic electrostriction constants, ranging from 0.006 m^4/c^2 in relaxor ferroelectrics, to over 850 m^4/c^2 in elastomeric polymers almost six orders of magnitude (96). For glass systems the behavior is frequency dependent in the alkali silicates, but almost frequency independent in pure silica glass (97). Preliminary data suggest that electrostriction (as we have shown in the relaxors) may be a very effective tool for probing the different polarizability mechanisms in dielectric systems.

6.0 GRADUATE STUDENTS IN THE PROGRAM

Student	**Supervisor**
E. Alberta	A.S. Bhalla
D. Van Tol	W.J. Hughes
P. Bednarchik	W.J. Hughes
N.W. Lesyna	G. Koopmann
E.W. Constans	G. Koopmann
M. Yang	G. Koopmann
J. McConnell	G.C. Lauchle
J. Wang	G.C. Lauchle
D.E. Capone	G.C. Lauchle
K. Bastyr	G.C. Lauchle
J. Tressler (Graduated, PhD, Nov. 1997).	R.E. Newnham
J. Zhang	R.E. Newnham
Y.-H. Chen	K. Uchino
X. Dong	Q.M. Zhang

7.0 HONORS and AWARDS

Bhalla, A., *Editor*, J. Ferroelectric Review (1998).
Cross, L.E., *Dow Lecture*, Northwest University (November 1997).
Lauchle, G.C., *elected* to *Board of Directors*, Inst. for Noise Control Engineers (1997-2000).
Koopmann, G., *Distinguished Professor of Mechanical Engineering* (January 1998).
Koopmann, G., *Senior Member* of AIAA (April 1998).
Newnham, R.E., *1997 Buessem Award*, Center for Dielectrics Studies, Penn State (November 19, 1997).
Newnham, R.E., *Materials Science and Engineering Service Award*, Penn State University (December 11, 1997).
Newnham, R.E., *Distinguished Life Member*, American Ceramic Society (May 6, 1997).
Uchino, K., *Fellow*, American Ceramic Society (December 1997).

8.0 PAPERS PUBLISHED IN REFEREED JOURNALS

1. Alberta, A. and A. Bhalla, "Piezoelectric Properties of Lead Indium Niobate:Lead Titanate Solid Solution Ceramics," J. Korean Phys. Soc. **32**, 1265-1267 (1998).
2. Jin, B.M., R. Guo, and A.S. Bhalla, "Piezoelectric Properties and Equivalent Circuits of Ferroelectric Relaxor Single Crystals, "Ferroelectrics **195** (1-4), 73-76 (1997).
3. Guo, R., H.T. Evans, Jr., and A.S. Bhalla, "Crystal Structure Analysis and Polarization Mechanisms of Ferroelectric Tetragonal Tungsten Bronze Lead Barium Niobate," Ferroelectrics **206-207**, 123-132 (1998).
4. Siny, I.G., R. Tao, R.S. Katiyar, R. Guo, and A.S. Bhalla, "Raman Spectroscopy of Mg-Ta Order-Disorder in $BaMg_{1/3}Ta_{2/3}O_3$," J. Phys. Chem. Solids **59**, 181-195 (1998).
5. Giniewicz, J.R., A.S. Bhalla, and L.E. Cross, "Identification of the Morphotropic Phase Boundary in the Lead Scandium Tantalate: Lead Titanate Solid Solution System," J. Mater. Sci. **32**, 2249-2253 (1997).
6. Jin, B.M., R. Guo, A.S. Bhalla, and S.C. Kim, "Piezoelectric Properties and Equivalent circuits of Ferroelectric Relaxor Single Crystals," J. Materials Science **32**(8), 2055-2058 (1997).
7. Jin, B.M., R. Guo, and A.S. Bhalla, "Piezoelectric Properties and Equivalent Circuits of Ferroelectroc Relaxor Single Crystals," Ferroelectrics **195**(1-4), 73-76 (1997).
8. Yoon, S.J., A. Joshi and K. Uchino, "Effect of Additives on the Electromechanical Properties of $Pb(Zr,Ti)O_3$-$Pb(Y_{2/3}W_{1/3})O_3$," J. Amer. Ceram. Soc. **80**(4), 1035-39 (1997).
9. Dogan, A., K. Uchino and R.E. Newnham, "Composite Piezoelectric Transducer with Truncated Conical Endcaps 'Cymbal'," IEEE Trans. UFFC **44**(3), 597-605 (1997).
10. Poosanaas, P., A. Dogan, A.V. Prasadarao, S. Komarneni, and K. Uchino, "Photostriction of Sol-Gel Processed PLZT Ceramics," J. Electroceramics **1**, 105-111 (1997).
11. Mulvihill, M.L., L.E. Cross, W. Cao, and K. Uchino, "Domain-Related Phase Transition like Behavior in Lead Zinc Niobate Relaxor Ferroelectric Single Crystals," J. Amer. Ceram. Soc. **80**(6), 1462-68 (1997).
12. Du, X.H., U. Belegundu, and K. Uchino, " Crystal Orientation Dependence of Piezoelectric Properties in Lead Zirconate Titanate: Theoretical Expectation for Thin Films," Jpn. J. Appl. Phys. **36**(9A), 5580-5587 (1997).

13. Aburatani, H., J.P. Witham, and K. Uchino, "Acoustic Emission in Lead Zirconate Titanate PLZT(18/40/60) Ceramics with Small Electrostriction," Jpn. J. Appl. Phys. **36**(pt. 1, No.11), 6829-6831 (1998).
14. Aburatani, H. and K. Uchino, "A Study of Acoustic Emission in Piezoelectric Multilayer Ceramic Actuator," Jpn. J. Appl. Phys. **37**(pt. 1, No. 1), 204-209 (1998).
15. Uchino, K., "High Electromechanical Coupling Piezoelectrics - How High Energy Conversion Rate is Possible?-," Mat. Res. Soc. Symp. Proc. **459**, p.3-14 (1997).
16. Aburatani, H. and K. Uchino, "The Application of Acoustic Emission (AE) Method for Ferroelectric Devices and Materials," Proc. 8th US-Japan Seminar on Dielectrics, Boston, p.28-31 (1997).
17. Uchino, K., "Compact Piezoelectric Ultrasonic Motors," J. Med. Ultrasonics **24**(9), 1191-92 (1997).
18. Zhang, Q.M., J. Zhao, K. Uchino, and J. Zheng, "Change of Weak Field Properties of $Pb(ZrTi)O_3$ Piezoceramics with Compressive Uniaxial Stresses and Its Links to the Effect of Dopants on the Stability of the Polarization in the Materials," J. Mater. Res. **12**, 226 (1997).
19. Zhang, Q.M., J. Zhao, and T.R. Shrout, "The Effect of Ferroelastic Coupling in Controlling the Abnormal Aging Behavior in Lead Magnesium Niobate-Lead Titante Relaxor Ferroelectrics," J. Mater. Res. **12**, 1777 (1997).
20. Zhang, Q.M. J. Su, C. Kim, R. Ting, and R. Cappas, "An Experimental Investigation of Electromechanical Responses in a Polyurethane Elastomer," J. Appl. Phys. **81**, 2770 (1997).
21. Geng, X., and Q.M. Zhang, "Evaluation of Piezocomposites for Ultrasonic Transducer Applications–Influence of the Unit Cell Dimensions and the Properties of Constituents on the Performance of 2-2 Piezocomposites," IEEE Trans. **44**, 857 (1997).
22. Su, J., Q.M. Zhang, C.H. Kim, R. Ting, and R. Capps, "Effects of Transitional Phenomena on the Electric Field Induced Strain Response of a Segmented Polyurethane Elastomer," J. Appl. Polym. Sci. **65**, 1363 (1997).
23. Mueller, V. and Q.M. Zhang, "Threshold of Irreversible Domain Wall Motion in Soft PZT-Piezoceramic," Ferroelectrics (1997).
24. Su, J., Q.M. Zhang, and R.Y. Ting, "Space Charge Enhanced Electromechanical Response in Thin Film Polyurethane Elastomers," Appl. Phys. Lett. **71**, 386 (1997).
25. Zhang, Q.M. and J. Zhao, "Polarization Responses of Lead Magnesium Niobate Based Relaxor Ferroelectrics," Appl. Phys. Lett. **71**, 1649 (1997).
26. Zhang, Q.M. and X. Geng, "Acoustic Properties of the Interface of a Uniform Medium 2-2 Piezocomposite and the Field Distributions in the Composite," Jpn. J. Appl. Phys. **36**, 65 (1997).
27. You, H. and Q.M. Zhang, "A Diffuse X-ray Scattering Study of Lead-Magnesium-Niobate Single Crystals," Phys. Rev. Lett. **79**, 3950 (1997).
28. Park, S.-E. and T.R. Shrout, "Ultrahigh Strain and Piezoelectric Behavior in Relaxor Based Ferroelectric Single Crystals," J. Appl. Phys. **82**(4), 1804-1811 (1997).
29. Park, S.-E. and M.-J. Pan, K. Markowski, S. Yoshikawa, and L.E. Cross, "E-Field Induced Phase Transition of Antiferroelectric Lead Lanthanum Zirconate Titanate Stannate (PLZTS) Ceramics," J. Appl. Phys. **82**(4), 17980-1803 (1997).

30. Park, S.-E. and T.R. Shrout, "Characteristics of Relaxor-Based Piezoelectric Single Crystals for Ultrasonic Transducers," IEEE Trans. on Ultrasonics, Ferroelectric and Frequency Control Special Issue on Ultrasonic Transducers **44**(5), 1140-1147 (1997).
31. Park, S.-E. and T.R. Shrout, "Relaxor Based Ferroelectric Single Crystals for Electro-Mechanical Actuators," Materials Research Innovations **1**, 20-25 (1997).
32. Park, S.-E., M.L. Mulvihill, G. Risch, and T.R. Shrout, "The Effect of Growth Condition on Dielectric Properties of $Pb(Zn_{1/3}Nb_{2/3})O_3$ Crystal," Jpn. J. Appl. Phys. **36**(pt. 1, No. 3), 1154-1158 (1997).
33. Zavala, G., J.H. Fendler, and S. Trolier-McKinstry, "Characterization of Ferroelectric Lead Zirconate Titanate Films by Scanning Force Microscopy," J. Appl. Phys. **81**(11), 7480-7491 (1997).
34. Cross, L.E. and S. Trolier-McKinstry, "Thin Film Integrated Ferroelectrics," Encycl. Appl. Phys. **21**, 429-451 (1997).
35. Trolier-McKinstry, S., G.R. Fox, A. Kholkin, C.A.P. Muller, and N. Setter, "Optical Fibers with Patterned ZnO/Electrode Coatings for Flexural Actuators," MRS Proc. 459: Materials for Smart Systems, 189-194 (1997).
36. Shepard, Jr., J.F., P.J. Moses, and S. Trolier-McKinstry, "A Technique for the Measurement of d_{31} Coefficient of Piezoelectric Thin Films," MRS Proc. 459: Materials for Smart Systems II, 225-230 (1997).
37. Shepard, Jr., J.F., S. Trolier-McKinstry, M. Hendrickson, and R. Zeto, "The Effects of Biaxial Stress on the Ferroelectric Characteristics of PZT Thin Films," MRS Proc. 459: Materials for Smart Systems II, 47-52 (1997).
38. Lacey, J.L. and S. Trolier-McKinstry, "Hard and Soft Composition Lead Zirconate Titanate Thin Films Deposited by Pulsed Laser Deposition," MRS Proc. 459: Materials for Smart Systems II, 207-212 (1997).
39. Li, S., J.A. Eastman, R.E. Newnham ,and L.E. Cross, "Diffuse Phase Transition in Ferroelectrics with Mesoscopic Heterogeneity: Mean Field Theory," Phys. Rev. B **55**(18), 1-12 (1997).
40. Li, S., J.A. Eastman, J.M. Vertrone, R.E. Newnham, and L.E. Cross, "Dielectric Response in Ferroelectric Superlattices, Philosophical Mag. B **76**(1), 47-57 (1997).
41. Dogan, A., K. Uchino, and R.E. Newnham, "Composite Piezoelectric Transducer with Truncated Conical Endcaps 'Cymbal'," IEEE Trans. on Ultrasonics, Ferroelectrics, and Frequency Control **44**(3), 597-605 (1997).
42. Tressler, J.F., and R.E. Newnham. "Doubly Resonant Cymbal-Type Transducers," IEEE Transactions on Ultrasonics, Ferroelectrics, and Frequency Control **44**(5), 1175-77 (September, 1997).
43. Alkoy, S., A. Dogan, A-C. Hladky, P. Langlet, J.K. Cochran, and R.E. Newnham, "Miniature Piezoelectric Hollow Sphere Transducers (BBs)," IEEE Transactions on Ultrasonics, Ferroelectrics, and Frequency Control **44**(5), 1067-76 (September, 1997).
44. Newnham, R.E., "Composite Sensors and Actuators" in Neue Werkstoffkonzepte, edited by H. Schmidt and R.F. Singer. DGM-Informations Gesellschaft Verlag, Frankfurt, Germany, 27-34 (1997).
45. Newnham, R.E., "Molecular Mechanisms in Smart Materials", Mat. Res. Bulletin, **22**(5) 20-34 (May, 1997).

46. Muller, R.S., M. Albin, P.W. Barth, S.B. Crary, D.D. Denton, K.W. Markus, P.J. McWhorter, R.E. Newnham, and R.S. Payne, "Microelectromechanical Systems: Advanced Materials and Fabrication Methods,", NMAB-483, National Academy Press, Washington, DC, 61 (1997).
47. B.C.H. Steele, R.E. Newnham, and A.G. Evans, "Ceramics, Composites and Intergrowths," Editorial Review, Current Opinion in Solid State & Materials Science **1**,563-565 (1997).
48. Newnham, R.E., V. Sundar, R. Yimnirun, J. Su, and Q.M. Zhang, "Electrostriction—Nonlinear Electromechanical Coupling in Solid Dielectrics," J. Phys. Chem. B **101**(48), 10141-10150 (November, 1997).
49. "Shape-Changing Crystals Get Shifter," Science **275**, 1878 (28 March 1997).
50. Zipparo, M.J., K.K. Shung, and T.R. Shrout, "Piezoceramics for High Frequency (20-100 Mhz) Single-Element Transducers," IEEE Transactions on Ultrasonics, Ferroelectric, and Frequency Control **44** (5) (September 1997).
51. Swartz, S.L., T.R. Shrout, and T. Takenaka, "Electronic Ceramics R&D in the U.S., Japan Part I. Patent History. Part II: Japanese View," Amer. Cer. Soc. Bull **76** (8) (August 1997).
52. McGuinn, R.S., G.C. Lauchle, D.C Swanson, Low Flow Noise Microphone for Active Noise Control Applications," AIAA J. **35**, 29-34 (1997).
53. Lauchle, G.C., J.R. MacGillivray, D.C. Swanson, "Active Control of Axial-Flow Fan Noise," J. Acoust. Soc. Am. **101**, 341-349, 1997).
54. McGuinn, R.S., G.C. Lauchle, D.C. Swanson, "Low Flow-Noise Pressure Measurements Using a 'Hot-Mic'," Proc. 3rd AIAA/CEAS Aeroacoust. Conf., Paper No. 97-1665-CP (1997).
55. Salagame, R.R. and A.D. Belegundu, " A Simple p-Adaptive Refinement Procedure for Structural Shape Optimization," Finite Elements in Analysis and Design, **24**(3),133-155 (1997).
56. Constans, E.W., Belegundu, A.D. and G.H. Koopmann, "Design Approach for Minimizing Sound Power from Vibrating Shell Structures," AIAA Journal **36** (2), 134-139 (1998).
58. Naghshineh, K. W. Chen, and G.H. Koopmann, "Use of Acoustic Basis Functions for Active Control of Sound Power Radiated from a Cylindrical Shell," J. Acoust. Soc. Am. **103** (4) (1998).
59. Lesieutre, G.A. and C.L. Davis, "Can a Coupling Coefficient of a Piezoelectric Actuator be Higher than those of its Active Material?," J. Intel. Mat. Syst. & Struct. (accepted 1998).
60. Zhao, J., A. Glazanouv, Q.M. Zhang, and B. Toby, "Neutron Diffraction Study of Electrostrictive Coefficients of Prototype Cubic Phase of Relaxor Ferroelectric $PbMg_{1/3}Nb_{2/3}O_3$," *Appl. Phys. Lett.* **72** (1998).

9.0. PAPERS SUBMITTED FOR PUBLICATIONS

1. Nair, N., R. Guo, Y. Jiang, and A.S. Bhalla, "Ferroelectric Properties and Phase Relations in $2(Sr,Ba)Nb_2O_6$:$(K,Na)NbO_3$ Solid Solutions Family," Ceramic Transactions, ACerS, Westerville, OH (in print 1997).
2. Pandya, K., R. Guo, and A. Bhalla, "Structure and Properties of Near MPB Compositions of Tungsten Bronze Ferroelectric Ceramics in $Pb_2KNb_5O_{15}$ (PKN)-$SrNaNb_5O_{15}$ (SNN) System," Ceramic Transactions, ACerS, Westerville, OH (in print 1997).
3. Guo, R., N. Nair, Y. Jiang, and A. Bhalla, "A-Site Filled Ferroelectric tungsten Bronze $(Ba,Sr,K.Na)Nb_2O_6$: Dielectric, Thermal Expansion Properties and Phase Relation," J. Phys. & Chem, Solids (accepted 1998).

4. Pandya, K. R. Guo, and A. Bhalla, "Morphotropic Phase Boundary Compositions of Tungsten Bronze Ferroelectric Ceramics in $Pb_2KNb_5O_{15}$ (PKN)-$SrNaNb_5O_{15}$ (SNN) System," Ferroelectrics (accepted 1998).
5. Meng, J.F., R. Katiyar, E. Alberta, R. Guo, and A.S. Bhalla, "Optical and Raman Spectroscopic Studies of PIN:PST Solid Solutions," Ferroelectrics (accepted 1997).
6. Jiang, Y., R. Guo, and A.S. Bhalla, "Single Crystal Growth and Ferroelectric Properties of a $(Ba_{1-x}Sr_x)Nb_2O_6$:b$(Na_{1-y}K_y)NbO_3$ Solid Solutions," J. Appl. Phys. (submitted 1998).
7. Cheng, Z.Y., R.S. Katiyar, X. Yao, and A.S. Bhalla, "Temperature Dependence of the Dielectric Constant of Relaxor Ferroelectrics," Phys. Rev. B (accepted 1998).
8. Uchino, K., "Recent Developments in Ceramic Actuators," Proc. SPIE's Symp. (in press, 1996).
9. Uchino, K., "Piezoelectric Actuators," (Partial Contribution) Encyclopedia of Electrical and Electronics Engineering, John Wiley & Sons (in press, 1997).
10. Uchino, K., "Shape Memory Ceramics," (Partial Contribution) Shape Memory Materials, Press of Univ. Cambridge (in press, 1997).
11. Poosanaas, P., A. Dogan, S. Thakoor, and K. Uchino, "Dependence of Photostriction on Sample Thickness and Surface Roughness for PLZT Ceramics," Proc. 1997 IEEE Ultrasonics Symposium, Toronto Marriott Eaton Centre, Toronto, Ontario, Canada, (October 5-8 1997)[in press].
12. Tonooka, K., P. Poosanaas, and K. Uchino, "Mechanism of the Bulk Photovoltaic Effect in Ferroelectrics," Proc. 5th SPIE Mtg., San Diego (1998).[in press].
13. Thakoor S., P. Poosanaas, J.M. Morookian, A. Yavrovian, L. Lowry, N. Marzwell, J. Nelson, R.R. Neurgaonkar, and K. Uchino, "Optical Microactuation in Piezoceramics," Proc. 5th SPIE Mtg., San Diego (1998).[in press].
14. Ito, Y. and K. Uchino, Wiley Encyclopedia of Electrical and Electronics Engineering, J. G. Webster, Edit., (Partial Charge "Piezoelectricity"), John Wiley & Sons (1998). [in press]
15. Uchino, K., "Ferroelectric Devices," Marcel Dekker, NY (1998). [in press]
16. Poosanaas, P., A. Dogan, A.V. Prasadarao, S. Komarneni, and K. Uchino, "Effect of Ceramic Processing Methods on Photostrictive Ceramics," J. Advanced Performance Mater. (accepted, 1997).
17. Uchino, K., "High Power Characterization of Piezoelectric Materials," J. Electroceramics (accepted, 1998).
18. Uchino, K., "Piezoelectric Ultrasonic Motors: Overview," J. Smart Mater. & Structures (accepted, 1998).
19. Su, J. Q.M. Zhang, P.C. Wang, A.G. MacDiarmid, and K.J. Wynne, "Preparation and Characterization of Electrostrictive Polyurethane Films with Conductive Polymer Electrodes," *Polymers of Advanced Technologies* (in press, 1998).
20. Mueller, V. and Q.M. Zhang, "Shear Response of Lead Zirconate Titanate Piezoceramics," *J. Appl. Phys.* (in press, 1998).
21. Mueller, V. and Q.M. Zhang, "Nonlinearity and Scaling Behavior in Donor Doped Lead Zirconate Titanate Piezoceramic," *Appl. Phys. Lett.* (in press, 1998).
22. Geng, X. and Q.M. Zhang, "Analysis of the Resonance Modes and Losses in 1-3 Composites for Ultrasonic Transducer Applications," Submitted to *IEEE Trans. UFFC* (1997).
23. Zhang, Q.M., V. Bharti, and X. Zhao, "Giant Electrostrictive Response and Ferroelectric Relaxor Behavior in Electron Irradiated Polyvinylidene Fluoride-Trifluoroethylene Polymer," Submitted to *Science* (1998).

24. Glazounov, A.E., Q.M. Zhang, and C. Kim, "Piezoelectric Actuator Generating Torsional Displacement from the Shear Strain," Submitted to *Appl. Phys. Lett.* (1998).
25. Kugel, V.D., B. Xu, Q.M. Zhang, and L.E. Cross, "Bimorph-Based Piezoelectric Air Acoustic Transducer: Model," Submitted to *Sensors and Actuators* (1997).
26. Su, J., P. Moses, and Q.M. Zhang, "A Piezoelectric Bimorph Based Dilatometer for Field Induced Strain Measurement in Soft and Thin Free Standing Polymer Films," Submitted to *Rev. Sci. Instruments* (1997).
27. Zhao, J., V. Mueller, and Q.M. Zhang, "The Influence of External Stress on the Electromechanical Response of Electrostrictive 0.9PMN-0.1PT in the DC Field Biased State," Submitted to *J. Mater. Res.* (1998).
28. Park, S.-E. and T.R. Shrout, "Electric-Field Induced Anisotrophy in Electrostrictive $Pb(Mg_{1/3}Nb_{2/3})O_3$ - $PbTiO_3$ Crystals," Ferroelectrics.
29. Pan, M.-J., S.-E. Park, K.A. Markowski, S. Yoshikawa, and L.E. Cross, "Electric field Induced Phase Transition in Lead Lanthanum Stannate Zirconate Titanate (PLSnZT) Antiferroelectrics: Tailoring Properties through Compositional Modification," Submitted to *Ferroelectrics*.
30. Pan, M.-J., P. Pertsch, S. Yoshikawa, T.R. Shrout, and V. Vendula, "Electroactive Actuator Materials: Investigations on Stress and Temperature Characteristics," Submitted to the SPIE's 5th International Symposium on Smart Structures and Materials, San Diego, California (March 1-5, 1998).
31. Park, S.-E., V. Vedula, M.-J. Pan, W.S. Hackenberger, P. Pertsch, and T.R. Shrout, "Relaxor Based Ferroelectric Single Crystals for Electomechanical Actuators," submitted to the SPIE's 5th International Symposium on Smart Structures and Materials, San Diego, California (March 1-5, 1998).
32. Hackenberger, W.S., M.-J. Pan, V. Vedula, P. Pertsch, W.W. Cao, C.A. Randall, and T.R. Shrout, "Effect of Grain Size on Actuator Properties of Piezoelectric Ceramics," submitted to the SPIE's 5th International Symposium on Smart Structures and Materials, San Diego, California (March 1-5, 1998).
33. Trolier-McKinstry, S., J.F. Shepard, Jr., J.L. Lacey, T. Su, G. Zavala, and J. Fendler, "Piezoelectricity in Ferroelectric thin Films: Domain and Stress Issues," to be published in *Ferroelectrics* (1997).
34. Cross, L.E. and S. Trolier-McKinstry, "Ferroelectrics," to be published in *The Era of Materials*, ed. S.K. Majumdar, R.E. Tressler, and E.W. Miller, PA Academy of Science (1996).
35. Su, T., S. Trolier-McKinstry, M. Hendrickson, and R.J. Zeto, "Grazing Angle X-Ray Diffraction Analysis of $Pb(Zr,Ti)O_3$ Films," to be published in ACerS Proc. *Integrated Thin Films and Applications*.
36. McKinstry, H.A., C.Y. Huang, and S. Trolier-McKinstry, "Thermal Expansion by X-Ray Diffraction," to be published in *Thermal Expansion in Solids*.
37. Maria, J.-P., S. Trolier-McKinstry, and D.G. Schlom, "Structure-Property Relationships in $SrRuO_3$ Epitaxial Films," to be published in MRS Proc. *Epitaxial Oxide Thin Films* (1997).
38. Shepard, Jr., J.F., S. Trolier-McKinstry, and J.-P. Maria, "The Effects of Applied Biaxial Stress on the Low and High-Field Characteristics of Thin Film PZT," submitted to *J. Mat. Res.*
39. Trolier-McKinstry, S., G.R. Fox, A. Kholkin, C. Muller, and N. Setter, "Optical Fibers Patterned with ZnO/Electrode Coatings for Flexural Actuators," submitted to *Sensors and Actuators A*.

40. Trolier-McKinstry, S. and J. Koh, "Composition Profiling of Graded Dielectric Function Materials by Spectroscopic Ellipsometry," submitted to *Thin Solid Films*.
41. Shepard, Jr., J.F., P.J. Moses, and S. Trolier-McKinstry, "The Wafer Flexure Technique for the Determination of the Transverse Piezoelectric Coefficient (d_{31}) of PZT Thin Films," submitted to *Sensors and Actuators A*.
42. Tressler, J.F., Ph.D. Thesis, "Capped Ceramic Underwater Sound Projector, 'the cymbal'," Ph.D. Thesis in Ceramic Science (August 1997).
43. Tressler, J.F. and R.E. Newnham. "Capped Ceramic Underwater Sound Projector: the 'cymbal' transducer", *Proc. US-Japan Seminar* (October, 1997).
44. Tressler, J.F., S. Alkoy, and R.E. Newnham. "Piezoelectric Sensors and Sensor Materials," submitted to *Journal of Electroceramics* (October, 1997).
45. Tressler, J.F., S. Alkoy, A. Dogan and R.E. Newnham. "Functional Composites for Sensors, Actuators, and Transducers," Proceedings of the 6th International Symposium on Ceramic Materials & Components for Engines, Arita, Japan (October, 1997).
46. Tressler, J.F., S. Alkoy, A. Dogan and R.E. Newnham. "Functional Composites for Sensors, Actuators, and Transducers," Composites Part A: Applied Science and Manufacturing (accepted December, 1997).
47. Alkoy, S., P.D. Lopath, R.E. Newnham, Anne-Christine Hladky-Hennion and J.K. Cochran. "Focused Spherical Transducers for Ultrasonic Imaging," Proceedings of the IEEE Intl. Ultrasonics Symposium '97, Toronto, Canada (October, 1997).
48. Newnham, R.E., V. Sundar, R. Yimnirun, J. Su and Q.M. Zhang. "Electrostriction in Dielectric Materials," (invited), Symposium on Dielectric Materials, American Ceramic Society Annual Mtg., Cincinnati, OH (1997).
49. Sundar, V., R. Yimnirun, B.T. Aitken, and R.E. Newnham. "Structure-property Relationships in the Electrostriction Response of Low Permittivity Silicate Glasses," submitted to *Mat. Res. Bull.* (1997).
50. Tressler, J.F., W. Cao, K. Uchino, and R.E. Newnham. "Finite Element Analysis of the Cymbal-Type Flextensional Transducer", *IEEE Transactions on Ultrasonics, Ferroelectrics, and Frequency Control* (accepted January, 1998).
51. Randall, C.A., N. Kim, J.-P. Kucera, W. Cao, and T.R. Shrout, "Intrinsic and Extrinsic Size Effects in Fine-Grained Morphotropic Phase Boundary Lead Zirconate Titanate Ceramics," J. Amer. Cer. Soc. **81** (3) (1998).
52. Lauchle, G.C. and A.R. Jones, "Unsteady Lift Force on a Towed Sphere," submitted to *J. Fluids and Structures* (January 1998).
53. Brungart, T.A., G.C. Lauchle, S. Deutsch, and E. Riggs, "Outer Flow Modifications on Turbulent Boundary Layer Wall Pressure Flectuations," submitted to *J. Acoust. Soc. Am.* (November 1997).
54. Brungart, T.A., G.C. Lauchle, S. Deutsch, and E. Riggs, "Wall Pressure Fluctuations Induced by Non-Equilibrium Turbulent Boundary Layer Flow," submitted to *J. Acoust. Soc. Am.* (December 1997).
55. Brungart, T.A., G.C. Lauchle, and R.K. Ramanujam, "Installation Effects of Fan Acoustic and Aerodynamic Performance," submitted to *Noise Control Eng. J.* (January 1998).
56. Brungart, T.A., G.C. Lauchle, S. Deutsch, and E. Riggs, "Effect of a Moving Wall Boundary Condition on a Fully-Developed, Equilibrium Turbulent Boundary Layer," submitted to *Phys. Fluids* (February 1998).
57. Fahnline, J.B. and G.H. Koopmann, "Numerical Implementation of the Lumped Parameter Model for the Acoustic Power Output of a Vibrating Structure," J. Acoust. Soc. Am, in print.

58. Lesieutre, G.A., and C.L. Davis, "A Solid-State Tunable Piezoelectric Vibration Absorber" (1998).
59. Koopmann, G.H., G.A. Lesieutre, W. Chen, T. Galante, and J. Bernard, "Design, Modeling, and Performance of a High Force Piezoelectric Inchworm Motor" (1998).

10.0 PAPERS APPEARING IN NON REFEREED PUBLICATIONS

1. Xu, B., Q.M. Zhang, V.D. Kugel, and L.E. Cross, "Piezoelectric Air Transducer for Active Noise Control," Proceeding SPIE, Smart Structures and Integrated Systems **271** (7), 388 (1996).
2. Xu, B., Q.M. Zhang, V.D. Kugel, Q. Wang, and L.E. Cross, "Optimization of Bimorph Based Double Amplifier Transducer under Quasistatic Conditions," Proceedings of IEEE International Symposium on the Applications of Ferroelectrics, Rutgers University, East Brunswick, New Jersey (August 1996).
3. Kugel, V.D., Q.M. Zhang, B.M. Xu, Q.-M. Wang, S. Chandran, and L.E. Cross, "Behavior of Piezoelectric Actuators under High Electric Field," Proceedings of IEEE International Symposium on the Applications of Ferroelectrics, Rutgers University, East Brunswick, New Jersey (August 1996).
4. Wang, Q.M., B. Xu, V.D. Kugel, and L.E. Cross, "Characteristics of Shear Mode Piezoelectric Actuators," Proceedings of IEEE International Symposium on the Applications of Ferroelectrics, Rutgers University, East Brunswick, New Jersey (August 1996).
5. Chandran, S., V.D. Kugel, and L.E. Cross, "CRESCENT: A Novel Piezoelectric Bending Actuators," Proceedings SPIE's 4th Annual Symposium on Smart Structures and Materials: Smart Materials Technologies, San Diego, CA (March 3-6, 1997).
6. Kugel, V.D., S. Chandran, and L.E. Cross, "A Comparative Analysis of Piezoelectric Bending-Mode Actuators," Proceedings SPIE's 4th Annual Symposium on Smart Structures and Materials: Smart Materials Technologies, San Diego, CA (March 3-6, 1997).
7. Mulvihill, M.L., L.E. Cross, K. Uchino, and W. Cao, "Domain Related Phase Transitions in Lead Zinc Magnesium Niobate Relaxor Ferroelectric Single Crystals," Proc. 10th Int'l Symp. Appl. Ferroelectrics, P2-51, East Brunswick, NJ (1997).
8. Dogan, A., J.F. Fernandez, K. Uchino, and R. E. Newnham, "The 'Cymbal' Electromechanical Actuator," Proc. 10th Int'l Symp. Appl. Ferroelectrics, P2-73, East Brunswick, NJ (1997).
9. Tressler, J.F., W. Cao, K. Uchino, and R.E. Newnham, "Ceramic-Metal Composite Transducers for Underwater Acoustic Applications," Proc. 10th Int'l Symp. Appl. Ferroelectrics, p.561-564, East Brunswick, NJ (1997).
10. Dogan, A., J.F. Fernandez, K. Uchino, and R.E. Newnham, "The 'Cymbal' Electromechanical Actuator," Proc. 10th Int'l Symp. Appl. Ferroelectrics, p.213-216, East Brunswick, NJ (1997).
11. Uchino, K., "Reliability of Ceramic Actuators," Proc. 10th Int'l Symp. Appl. Ferroelectrics, p.763-766, East Brunswick, NJ (1997).
12. Aburatani, H. and K. Uchino, "Acoustic Emission (AE) Measurement in Piezoelectric Ceramics," Proc. 10th Int'l Symp. Appl. Ferroelectrics, p.871-873, East Brunswick, NJ (1997).

13. Zhang, Q.M. and X. Geng, "Acoustic and Electromechanical Behavior of 1-3 Piezocomposites for Ultrasonic Transducer Applications," Proc. IEEE Ultrasonic Symp. Toronto, Canada (1997).
14. Glazounov, A.E., Q.M. Zhang, and C. Kim, "A New Torsional Actuator Based on Shear Piezoelectric Response," Proc. 1998 SPIE Conference on Smart Structures and Materials, San Diego, California (1998).
15. Glazounov, A.E., J. Zhao, and Q.M. Zhang, "Effect of Nonpolar Regions in Electrostrictive Coefficients of a Relaxor Ferroelectric," Proc. Williamsburg Mtg. on Ferroelectrics (1998).
16. Park. S.-E., P.D. Lopath, K.K. Shung, and T.R. Shrout, "Relaxor-Based Single Crystal Materials for Ultrasonic Transducer Applications," Proceedings on SPIE's International Symposium on Medical Imaging, Newport Beach, California (February 1997).
17. Lopath, P.D., S.-E. Park, K.K. Shung, and T.R. Shrout, "$Pb(Zn_{1/3}Nb_{2/3})O_3/PbTiO_3$ Single Crystal Piezoelectrics for Ultrasonic Transducers," Proceedings on SPIE's International Symposium on Medical Imaging, Newport Beach, California (February 1997).
18. Yoshikawa, S., K. Markowski, S.-E. Park, M.-J. Pan, and L.E. Cross, "Antiferroelectric-to-Ferroelectric Phase Switching Lead Lanthanum Zirconate Stannate Titante (PLZST) Ceramics," Proceedings on SPIE's 4th Annual Symposium on Smart Structures and Materials, San Diego, California (March 1997).
19. Wada, S., S.-E. Park, L.E. Cross, and T.R. Shrout, "Domain Configuration and Ferroelectric Related Properties of Relaxor-Based Single Crystals," Proceedings on 9th International Meeting on Ferroelectrics '97, Seoul, Korea (August 1997).
20. Park, S.-E. and T.R. Shrout, "Relaxor-Based Ferroelectric Single Crystals with High Piezoelectric Performance," Proceedings on 8th US-Japan Seminar on Dielectric and Piezoelectric Ceramic Thin Films, Plymouth, MA (October 1997).
21. Wada, S., S.-E. Park, L.E. Cross, and T.R. Shrout, "Domain Configuration and Ferroelectric Related Properties of Relaxor Based Single Crystals," Proceedings on 8th US-Japan Seminar on Dielectric and Piezoelectric Ceramic Thin Films, Plymouth, MA (October 1997).
22. Lopath, P.D., S.-E. Park, K.K. Shung, and T.R. Shrout, "Single Crystal $Pb(Zn_{1/3}Nb_{2/3})O_3/PbTiO_3$ (PZN/PT) in Medical Ultrasonic Transducers," Proceedings on IEEE on Ultrasonics, Ferroelectric and Frequency Control, Toronto, Ontario (October 1997).
23. Shrout, T.R., S.-E. Park, J. Shepard, and W.S. Hackenberger, "Recent Advances in Piezoelectric Materials," Proceedings on SPIE's Far East and Pacific Rim Symposium on Smart Materials, Structures, and MEMS, Adalaide, Australia (December 1997).
24. Yoshikawa, S., K.A. Markowski, S.-E. Park, M.-J. Pan, and L.E. Cross, "Antiferroelectric-to-Ferroelectric Phase Switching Lead Lanthanum Zirconate Stannate titanate (PLZST) Ceramics," Proceedings of the SPIE's 4th Annual Symposium on Smart Structures and Materials, San Diego, California (March 3-6, 1997).
25. Pan, M.-J. and S. Yoshikawa, "Effect of Grain Size on the Electromechanical Properties of Antiferroelectric-to-Ferroelectric Phase Switching PLSnZT Ceramics," Proceedings of the 8th US-Japan Seminar on Dielectric and Piezoelectric Ceramics, pp. 288-91, Plymouth, MA (October 15-18, 1997).

26. Ritter, T.A., K.K. Shung, S.E. Park, X. Geng, and T.R. Shrout, "1-3 Single Crystal Composites for Ultrasonic Transducer Arrays," SPIE: International Symposium Medical Imaging 1998, San Diego, CA (February 21-27, 1998).
27. Shrout, T.R., S.E. Park, P. Lopath, R. Meyer, T. Ritter, and K. Shung, "Innovationa in Piezoelectric Materials for Ultrasonic Transducers," SPIE: International Symposium Medical Imaging 1998, San Diego, CA (February 21-27, 1998).
28. Lopath, P.D., S.-E. Park, K.K. Shung, and T.R. Shrout, "Single Crystal PZN/PT Transducer," SPIE: International Symposium Medical Imaging 1998, San Diego, CA (February 21-27, 1998).
29. wa Gachigi, K., P.M. Pruna, C.A. Randall, T.R. Shrout, S.J. Jang, and J.P. Dougherty, "Phase Transitions with Respect to Temperature in La^{+3} and Ca^{+2} Modified $PbZrO_3$," 9th International Meeting on Ferroelectrics 97, Seoul, Korea (August 1997).
30. Pan, M.-J., P. Pertsch, S. Yoshikawa, T.R. Shrout, and V. Vedula, "Electroactive Acuator Materials: Investigations on Stress and Temperature Characteristics," Proc. SPIE's 5th International Symposium on Smart Structures and Materials, San Diego, CA (March 1-5, 1998).
31. Hackenberger, W., M.-J. Pan, V. Vedula, P. Pertsch, W. Cao, C.Randall, and T.Shrout, "Effect of Grain Size on Actuator Properties of Piezoelectric Ceramics," Proc. SPIE's 5th International Symposium on Smart Structures and Materials, San Diego, CA (March 1-5, 1998).
32. Park, S.-E., V. Vedula, M.-J. Pan, W. Hackenberger, P. Pertsch, and T.R. Shrout, "Relaxor Based Ferroelectric Single Crystals fo Electromechanical Actuators," Proc. SPIE's 5th International Symposium on Smart Structures and Materials, San Diego, CA (March 1-5, 1998).
33. Park, S.-E., P.D. Lopath, K.K. Shung, and T.R. Shrout, "Relaxor-Based Single Crystal Materials for Ultrasonic Transducer Applications," Proceedings of SPIE's International Symposium on Medical Imaging, Newport Beach, California (February 1997).
34. Lopath, P.D., S.-E. Park, K.K. Shung, and T.R. Shrout, "Pb(Zn1/3Nb2/3)O3/PbTiO3 Single Crystal Piezoelectrics for Ultrasonic Transducers," Proceedings on SPIE's International Symposium on Medical Imaging, Newport Beach, California (February 1997).
35. Wada, S., S.-E. Park, L.E. Cross, and T.R. Shrout, "Domain Configuration and Ferroelectric Related Properties of Relaxor-Based Single Crystals," Proceedings on 9th International Meeting on Ferroelectrics, Seoul, Korea (August 1997).
36. Park, S.-E. and T.R. Shrout, "Relaxor Based Piezoelectric Single Crystals with High Piezoelectric Performance," The 8th US-Japan Seminar on Dielectric & Piezoelectric Ceramics, (October 15-18, 1997).
37. Hackenberger, W., J. Helgeland, M. Zipparo, C.A. Randall, and T.R. Shrout, "Fine Grain Piezoelectric Ceramics for Transducer and Actuator Applications," The 8th US-Japan Seminar on Dielectric & Piezoelectric Ceramics (October 15-18, 1997).
38. Meyer, R.J., T.R. Shrout, and S. Yoshikawa, "Preparation of Fine Scale PZT Fibers and Their 1-3 Composite Properties," The 8th US-Japan Seminar on Dielectric & Piezoelectric Ceramics (October 15-18, 1997).
39. Wada, S., S.E. Park, L.E. Cross, and T.R. Shrout, "Domain Configurations and Ferroelectric Related Properties of Relaxor Based Single Crystals," The 8th US-Japan Seminar on Dielectric & Piezoelectric Ceramics (October 15-18, 1997).

40. Hitomi, A., X. Lium T.R. Shrout, and C.A. Randall, "Hypothesis on Rare Earth Doping of $BaTiO_3$ Ceramic Capacitors," The 8th US-Japan Seminar on Dielectric Piezoelectric Ceramics (October 15-18, 1997).
41. Swartz, S., T. Takenaka, and T.R. Shrout, "Comparative Assessment of Electronic Ceramics R&D in the U.S. and Japan," The 8th US-Japan Seminar on Dielectric & Piezoelectric Ceramnics (October 15-18, 1997).
42. Capone, D.E. and G.C. Lauchle, "Designing a Virtual Sound-Level Meter in LabVIEW," National Instruments Newsletter **A-3** (Summer 1997).
43. Ho, Y.R., I.S.Kim, W. Chen, and G.H. Koopmann, "Active Control of Broadband Sound Transmission Using Feedback and Feedforward Techniques,"Noise-Con 97, Penn State, PA (June 1997).
44. Sharp, S. G.H. Koopmann, and W. Chen, "Transmission Loss Characteristics of an Active Trim Panel," Noise-Con 97, Penn State, PA (June 1997).
45. Lesieutre, G.A., and C.L. Davis, "A Solid-State Tunable Piezoelectric Vibration Absorber," proceedings of the SPIE Smart Structures and Materials Conference: Smart Structures and Integrated Systems, San Diego, CA (March 1-5, 1998).
46. Koopmann, G.H., G.A. Lesieutre, W. Chen, T. Galante, and J. Bernard, "Design, Modeling, and Performance of a High Force Piezoelectric Inchworm Motor," proceedings of the SPIE Smart Structures and Materials Conference: Passive Damping and Isolation, San Diego, CA (March 1-5, 1998).
47. Hebert, C.A., and G.A. Lesieutre, "Rotorcraft Lag Damping using Highly-Distributed Tuned Vibration Absorbers," proceedings of the 7th ARO International Workshop on Dynamics and Aeroelastic Stability Modeling of Rotorcraft Systems, St. Louis, MO (October, 14-16, 1997).
48. Lesieutre, G.A. and C.L. Davis, "A Semi-Actively Tuned Piezoceramic Vibration Absorber," proceedings of the 3rd ARO Smart Structures Workshop, Blacksburg, VA (August 27, 1997).
49. Galante, T., G.H. Koopmann, and G.A. Lesieutre, "A High-Force Piezoelectric Inchworm Actuator," at the 1997 ONR Transducer Materials and Transducers Workshop, State College, PA (April, 1997).
50. Lee, U. and G.A. Lesieutre, "Design Concerns for Active Constrained Layer Damping Treatments," proceedings of the 38th AIAA/ASME/ASCE/AHS/ASC Structures, Structural Dynamics and Materials Conference, Kissimee, FL (April 7-10, 1997).
51. Lesieutre, G.A., and C.L. Davis, "A Tunable Piezoelectric Inertial Actuator," proceedings of the SPIE Smart Structures and Materials Conference: Smart Structures and Integrated Systems, San Diego, CA (March 4, 1997).
52. Lesieutre, G.A., and C.L. Davis, "Can the Coupling Coefficient of a Piezoelectric Device be Higher Than Those of the Basic Material?," proceedings of the SPIE Smart Structures and Materials Conference: Smart Structures and Integrated Systems, San Diego, CA (March 4, 1997).
53. Lesieutre, G.A., and U. Lee, "A Finite Element Model for Beams Having Segmented Active Constrained Layers with Frequency-Dependent Viscoelastic Material Properties," proceedings of the SPIE Smart Structures and Materials Conference: Passive Damping and Isolation, San Diego, CA (March 4, 1997).

11.0 INVITED PAPERS PRESENTATIONS AT NATIONAL AND INTERNATIONAL MEETINGS

1. Cross, L.E., "Relaxor Ferroelectrics," 1997 Williamsburg Workshop on Ferroelectrics, Williamsburg, Virginia (February 2-5, 1997).
2. Zhao, X.Z., S.J. Jang, J.P. Dougherty, and L.E. Cross, "Dielectric and Electrical Polyimide Properties of LARC-Si: A Self Bonding Polyivide Material," MRS Spring Mtg., San Francisco California (March 31-April 4, 1997).
3. Cross, L.E., "Relaxor Ferroelectrics," Indo:US Project Mtgs., New Delhi, India (March 11, 1997).
4. Cross, L.E., "Smart Materials and Adaptive Structures," Rippon Lecture: Indian Institute of Science, Calcutta, India (March 4, 1997).
5. Cross, L.E., "Piezoelectric and Electrostrictive Sensors and Actuators," School of Materials Science, Institute of Technology, Banares Hindu University, Varanasi, India (March 7, 1997).
6. Cross, L.E., "Ferroic Group Activities at MRL," 21st ICAT Smart Actuator Symposium, Penn State (April 23, 1997).
7. Cross, L.E., "Transducer Studies in MRL," 1997 ONR Transducer Materials and Transducers Workshop (April 29-May 1, 1997).
8. Cross, L.E., "Fundamental Concepts in Dielectrics," Am. Ceram. Soc. 99th Annual Mtg., Cincinnati, Ohio (May 4-7, 1997).
9. Cross, L.E., "Electric Field Tuning in Monolithic Materials," Frequency Agile Materials for Electronics (FAME) Workshop, Washington, DC (May 15-16, 1997).
10. Cross, L.E., "Exploiting Ferroelectric Phase Transitions for Practical Applications," 3rd US/CIS. Baltic Ferroelectric Seminar, Bozeman, Montana (June 1-7, 1997).
11. Cross, L.E., "Recent Developments in Composite Transducers and Actuators," ICCE 4, Big Island of Hawaii (July 6-12, 1997).
12. Cross, L.E. and J. Fousek, "The History of the International Meeting of Ferroelectrics (IMF)," Plenary Lecture, IMF9, Seoul, Korea (August 25-29, 1997).
13. Cross, L.E., "Relaxor Ferroelectrics," Invited Tutorial, IMF9, Seoul, Korea (August 25-29, 1997).
14. Cross, L.E., "Bimorph and Pseudo-Shear Mode Actuation," 8th US-Japan Seminar on Dielectric and Piezoelectric Ceramics, Plymouth, MA (October 15-18, 1997).
15. Cross, L.E., "Recent Development in Piezoelectric Ferroelectric Materials and Composites," Dow Lecture, Northwest University (November 4, 1997).
16. Cross, L.E., A.S. Bhalla, and R. Guo, "Frequency Agile Materials of Electronics (FAME)," Center for Dielectric Studies (Fall Mtg.), Penn State (November 19-20, 1997).
17. Uchino, K., "Ferroelectric Devices," Symp. Ferroelectric Mater. & Appl., Mat. Tech. Center, Chiangmai, Thailand (June 1997).
18. Uchino, K., "How to Design the Ceramic Actuators for Bestseller Devices," 2nd Symp. Adv. R & D, Jpn. Steel Soc., Tokyo, Japan, (June 1997).
19. Uchino, K., "High Electromechanical Coupling Piezoelectrics: Relaxor and Normal Ferroelectric Solid Solutions," 4th IUMRS Int'l Conf. in Asia, Mater. Res. Soc. Jpn., Tokyo, Japan (September 16-18, 1997).
20. Uchino, K., "Compact Piezoelectric Ultrasonic Motors," 70th Mtg. of Jpn. Med. Ultrasonics, Sendai, Japan (November 2-4, 1997).

21. Shrout, T.R., S.-E. Park, J. Shepard, and W.S. Hackenberger, "Recent Advances in Piezoelectric Materials," SPIE's Far East and Pacific Rim Symposium on Smart Materials, Structures, and MEMS, Adelaide, Australia (December 1997)
22. Trolier-McKinstry, S., J.F. Shepard, Jr., J.L. Lacey, T. Su, G. Zavala, and J. Fendler, "Piezoelectricity in Ferroelectric Thin Films: Domain and Stress Issues," Williamsburg Workshop on Ferroelectrics, Williamsburg, Virginia (1997).
23. Trolier-McKinstry, S. J.F. Shepard, Jr., J.L. Lacey, T. Su, G. Zavala, and J. Fendler, "Piezoelectricity in Ferroelectric Thin Films" Domain and Stress Issues," Acta Materialia.Scripta Materialia Meeting on Coupled Property Issues in Integrated Microstructures (1997).
24. Newnham, R.E., "Molecular Mechanisms in Smart Materials," Mardi Gras Conference on Multiscale Phenomena in Science and Engineering, Baton Rouge, LA (February 6-9, 1997).
25. Newnham, R.E., "Molecular Mechanisms in Smart Materials," The American Physical Society March Meeting, Kansas City, MO (March 17-21, 1997).
26. Newnham, R.E., "Biomimetic Ferroelectric Sensors and Actuators, 21st International Center for Transducers and Actuators Meeting, Penn State University (April 23-24, 1997).
27. Tressler, J., W. Cao, K. Uchino, and R.E. Newnham, "Ceramic-Metal Composite Transducers for Underwater Acoustic Application," 21st International Center for Transducers and Actuators Meeting, Penn State University (April 23-24, 1997).
28. Tressler, J. and R.E. Newnham, "Capped Ceramic Underwater Sound Projector," Annual Meeting of the Acoustical Society of America, Penn State University (June 16-20, 1997).
29. Newnham, R.E., "Biomimetic Ferroelectric Sensors and Actuators," The Ninth International Meeting on Ferroelectricity, Seoul, Korea (August 24-29, 1997).
30. Newnham, R.E., "Ferroelectric Hollow Spheres," 3rd US/CIS/Baltic Ferroelectrics Seminar, Montana State University, Bozeman, MT (June 1-7, 1997).
31. Newnham, R.E., "Size Effects in Ferroic Solids," 214th Americal Chemical Society National Meeeting, Las Vegas, NV (September 7-10, 1997).
32. Newnham, R.E., "Smart Materials: Molecular Mechanisms and Industrial Applications," Adaptronic Congress Berlin Conference, Berlin, Germany (September 29-October 3, 1997).
33. Newnham, R.E., "Functional Composite Sensors, Actuators and Transducers," 6th International Symposium on Ceramic Materials and Components for Engines, Arita, Japan (October 19-24, 1997).
34. Newnham, R.E., "Piezoelectric Crystals and Composites," NGK Insulators Company, Nagoya, Japan (October 27, 1997).
35. Newnham, R.E., "Molecular Mechanisms in Smart Materials," Asian Meeting of the International Center for Actuators and Transducers (ICAT), Tokyo, Japan (October 27, 1997).
36. Newnham, R.E., "Composite Piezoelectric Sensors and Actuators," Fifth Japan International SAMPE Symposium and Exhibition, Tokyo, Japan (October 28-31, 1997).
37. Park, S.-E. and T.R. Shrout, "Characteristics of Relaxor-Based Materials for Transducers," 1996 IEEE International Ultrasonics Symposium, San Antonio, TX (November 1996).
38. Park, S.-E. and T.R. Shrout, "Relaxor-Based Single Crystals," Williamsburg Workshop on Ferroelectrics, Williamsburg, VA (February 2-5, 1997).
39. Shrout, T.R., S.E. Park, C.A. Randall, J. Shepard, L.B. Hackenberger, D. Pickrell, and W.S. Hackenberger, "Recent Advances in Piezoelectric Materials," SPIE Far East and Pacific Rim Symposium on Smart Materials, Structures, and MEMS, Adelaide, Australia (December 10-13, 1997).

40. Shrout, T. S.E. Park, P. Lopath, T. Ritter, and K. Shung, "Single Crystal Perovskites with High Piezoelectric Performances," DARPA/ONR Workshop on Medical Ultrasound Imaging Technology Development for Combat Casualty Care, Lansdowne, VA (February 11-13, 1998).
41. Shrout, T.R., S.-E. Park, P. D. Lopath, and K.K. Shung, "Relaxor-Based Single Crystal Materials for Ultrasonic Transducer Applications," 133rd Acoustical Society of America, The Pennsylvania State University (June 19, 1997).
42. Maria, J.-P., T.R. Shrout, and S. Trolier-McKinstry, "Deposition and Electrical Characterization of Epitaxial $Pb(Mg_{1/3}Nb_{2/3})O_3$-$PbTiO_3$ Relaxor Thin Films," MRS 1997 Fall Meeting, Boston, MA.
43. G.H. Koopmann,E. Constans, and A. Belegundu, "The Use of Tuned Absorbers in Minimizing Sound Power From Vibrating Structures - Manfred Heckl Memorial Session," Acoustical Society of America, Seattle, WA (1998).
44. Belegundu, A.D., G.H. Koopmann and E.W. Constans, "Minimization of Radiated Sound Power from Vibrating Shells by Optimal Placement of Lumped Masses," Paper DETC97/VIB-3798, 16th Biennial Conference on Mechanical Vibration and Noise, Sacramento, CA (1997).
45. Koopmann, G. H., G.A. Lesieutre, B.R. Dershem, and W. Chen, "Embeddable Induced Strain Actuators Using Framed 3-3 Stacks, Modeling and Characterization," SPIE's 4 the Annual International Symposium on Smart Structures and Materials, San Diego, CA (1997).
46. Driesch, P., G.H. Koopmann, W. Chen, J. Dosch, and H. Iwata, "Development of a Surface Intensity Probe for Active Control Applications," IMECE, Dallas, TX (1997).
47. Cao, W., "Characterization of Ferroelectric Domains in LiTaO3 using Environmental Electron Microscopy," The 3rd US/CIS/Baltic Ferroelectric Seminar, Bozeman, Montana (June 1997).
48. Cao, W., "Design Simulation of Composite," The 133rd Meeting of Transducers," Acoust. Soc. of America, State College (June 1997).
49. Cao, W., "Computer Simulation of Piezocomposite Transducers," Eighth US:Japan Seminar on Dielectric and Piezoelectric Ceramics, Plymouth, MA (October 1997).
50. Lesieutre, G.A. and G.H. Koopmann, "PSU Piezoelectric Actuators: Induced Strain, Proof-Mass, Inchworm," at the Engineering Foundation Workshop on Engineered Adaptive Composite Structures for Noise and Vibration Control, Banff, Albert, Canada (July 13-18, 1997).
51. Lesieutre, G.A., "Can a Coupling Coefficient of a Piezoelectric Device Be Higher Than Those of Its Active Material?,", 21st International Smart Actuator Symposium (ICAT), State College, PA (April 23-24, 1997).

12.0 INVITED PAPERS PRESENTED AT UNIVERSITY, INDUSTRY, AND GOVERNMENT LABORATORIES

1. Park, S.-E. and T.R. Shrout, "Relaxor-Based Single Crystals," Williamsburg Workshop on Ferroelectrics, Williamsburg, Virginia (February 2-5, 1997).
2. Trolier-McKinstry, S., "Piezoelectricity in Ferroelectric Thin Films: Domain and Stress Issues," Chemistry Department, Syracuse University (April 1997).
3. Trolier-McKinstry, S., "Piezoelectricity in Ferroelectic Thin Films: Domain and Stress Issues," NIST, Gaithersburg, Maryland (July 1997).
4. Newnham, R.E., "Molecular Mechanisms in Smart Materials," Harvard University, Boston, MA (February 26, 1997).
5. Newnham, R.E., "Molecular Mechanisms in Smart Materials," Princeton University (April 16, 1997).

6. Tressler, J., W.J. Hughes, W. Cao, K. Uchino, and R.E. Newnham, "Capped Ceramic Underwater Sound Projector, 'the cymbal'," Naval Research Laboratory, Washington, DC (August 1997).
7. Tressler, J., R.E. Newnham, and J. Hughes, "Cymbal Transducers," MURI Review Meeting, Penn State University (November 1997).
8. Newnham, R.E., "Predicting Electrostriction in High and Low Permittivity Dielectrics," CDS Fall Meeting, Penn State University (November 1997).
9. Newnham, R.E., "Molecular Mechanisms in Smart Materials," Raychem Corporation, Menlo Park, CA (January 1998).
10. Newnham, R.E., "Molecular Mechanisms in Smart Materials," Materials Science Department Seminar, University of California at Berkeley (January 1998).
11. Newnham, R.E., "Molecular Mechanisms in Smart Materials," Physics Department Seminar, Indiana University of Pennsylvania (February 1998).
12. Cao, W., "Interdisciplinary Research: The Need, the Challeng and the Fun," Department of Physics and Astronomy, Brigham Young University (July 1997).
13. Cao, W., "New Characterization Techniques for Piezoelectric Materials," TDK Inc, Narita Research Center, Chiba, Japan (September 1997).
14. Cao, W., "Finite Element Study of Piezoelectric and Dielectric Devices," Murata Manufacturing Co., Ltd, Kyoto, Japan (September 1997).
15. Cao, W., "Virtual Design of Piezoelectric Devices," Shonan Institute of Technology, Fujisawa, Japan (October 1997).
16. Cao, W., "Observation of Ferroelectric Domains," University of Tsukuba, Tsukuba, Japan (September 1997).
17. Lesieutre, G.A., "A Solid-State Tunable Piezoelectric Vibration Absorber," UCLA (November 1997).
18. Lesieutre, G.A., "Can a Coupling Coefficient of a Piezoelectric Device Be Higher Than Those of Its Active Material?," UCLA (February 1998).
19. Hughes, W.J., "MURI: Micro Tonpilz Transducers," DARPA/ONR Workshop on Medical Ultrasonic Imaging, Lansdowne, Virginia (February 1997).
20. Hughes, W.J., "MURI: Acoustic Transduction," ARL Advisory Board (ARLAB), State College, PA (October 1997.
21. Hughes, W.J., "MURI Review," MURI: Acoustics Transduction," ONR sponsors, State College, PA (November 1997).
22. Hughes, W.J., "MURI and Portable Sonar Project," Penn State NIH Transducer Resource Center Advisory Board, State College, PA (April 1998).
23. Hughes, W.J., "Ultrasonic Transducer Efforts at Penn State: MURI: Micro Tonpilz Transducer and DARPA/ONR: Sonolelectronics," DARPA/ONR Workshop on Medical Ultrasonic Imaging, Lansdowne, Virginia (February 1998).

13.0 CONTRIBUTED PAPERS AT NATIONAL AND INTERNATIONAL MEETINGS

1. Xu, B., Q.M. Zhang, V.D. Kugel, and L.E. Cross, "Piezoelectric Air Transducer for Active Noise Control," Proceeding SPIE, Smart Structures and Integrated Systems **271** (7), 388 (1996).
2. Xu, B., Q.M. Zhang, V.D. Kugel, Q. Wang, and L.E. Cross, "Optimization of Bimorph Based Double Amplifier Transducer under Quasistatic Conditions," Proceedings of IEEE International Symposium on the Applications of Ferroelectrics, Rutgers University, East Brunswick, New Jersey (August 1996).

3. Kugel, V.D., Q.M. Zhang, B.M. Xu, Q.-M. Wang, S. Chandran, and L.E. Cross, "Behavior of Piezoelectric Actuators under High Electric Field," Proceedings of IEEE International Symposium on the Applications of Ferroelectrics, Rutgers University, East Brunswick, New Jersey (August 1996).
4. Wang, Q.M., B. Xu, V.D. Kugel, and L.E. Cross, "Characteristics of Shear Mode Piezoelectric Actuators," Proceedings of IEEE International Symposium on the Applications of Ferroelectrics, Rutgers University, East Brunswick, New Jersey (August 1996).
5. Chandran, S., V.D. Kugel, and L.E. Cross, "CRESCENT: A Novel Piezoelectric Bending Actuators," Proceedings SPIE's 4th Annual Symposium on Smart Structures and Materials: Smart Materials Technologies, San Diego, CA (March 3-6, 1997).
6. Kugel, V.D., S. Chandran, and L.E. Cross, "A Comparative Analysis of Piezoelectric Bending-Mode Actuators," Proceedings SPIE's 4th Annual Symposium on Smart Structures and Materials: Smart Materials Technologies, San Diego, CA (March 3-6, 1997).
7. Kugel, V.D., S. Chandran, R. Liu, and L.E. Cross, "PANEL: A Novel Piezoelectric Air Acoustic Transducer," 1997 ONR Transducer Materials and Transducers Workshop, Penn State Scanticon Conference Center (April 29-May 1, 1997).
8. Wang, Q.-M. and L.E. Cross, "Analysis of Bending Displacement and Force of PZT-based Cantilever RAINBOW Actuator," 1997 ONR Transducer Materials and Transducers Workshop, Penn State Scanticon Conference Center (April 29-May 1, 1997).
9. Liu, R.B., B.M. Xu, Q.M. Zhang, V.D. Kugel, Q.-M. Wang, and L.E. Cross, "Multilayer Bimorph Based Double Amplifier Air Transducer," 1997 ONR Transducer Materials and Transducers Workshop, Penn State Scanticon Conference Center (April 29-May 1, 1997).
10. Guo, R., H.T. Evans, and A.S. Bhalla, "Crystal Structure Analysis of Ferroelectric Tetragonal Tungsten Bronze $Pb_{0.596}Ba_{0.404}Nb_{2.037}O_6$," Proceedings of the Tenth IEEE International Symposium on Applications of Ferroelectrics (ISAF 10), East Brunswick, NJ, pp. 241-244 (1996).
11. Uchino, K. and H. Aburatani, "Acoustic Emission in Actuator Ceramic Materials," 1997 ONR Transducer Materials and Transducers Workshop, State College, Pennsylvania (March 1997).
12. Tressler, J.F., W.J. Hughes, W. Cao, K. Uchino, and R.E. Newnham, "Capped Ceramic Underwater Sound Projector," 1997 ONR Transducer Materials and Transducers Workshop, State College, Pennsylvania (March 1997).
13. Witham, J.P. and K. Uchino, "Optical Study of Domains in PLZT Ceramics," 1997 ONR Transducer Materials and Transducers Workshop, State College, Pennsylvania (March 1997).
14. Chen, Y.H. and K. Uchino, "High Power Piezoelectric Characteristics and Loss Mechanisms of PMN-PT Based Ceramics," 1997 ONR Transducer Material and Transducers Workshop, State College, PA (March 1997).
15. Uchino, K., "High Voltage/Power Characterization of Piezoelectric Materials," Amer. Ceram. Soc. Annual Mtg., E-026-97, Cincinnati, Ohio (May 4-7, 1997).
16. Witham, J. P. and K. Uchino, "Optical Study of Domains in PLZT Ceramics: Part I - Experimental Results," Amer. Ceram. Soc. Annual Mtg., E-032-97, Cincinnati, Ohio (May 4-7, 1997).
17. Chen, Y.H., J.S. Kim, and K. Uchino, "High Power Piezoelectric Characteristics and Loss Mechanisms of PMN-PT Based Ceramics," Amer. Ceram. Soc. Annual Mtg., E-033-97, Cincinnati, Ohio (May 4-7, 1997).

18. Koc, B. and K. Uchino, "A New Ultrasonic Motor Design: 'Windmill'," Amer. Ceram. Soc. Annual Mtg., E-034-97, Cincinnati, Ohio (May 4-7, 1997).
19. Zheng, J. and K. Uchino, "Uniaxial Stress Dependence of Piezoelectricity in the Lead Zirconate-Titanate System," Amer. Ceram. Soc. Annual Mtg., EP-020-97, Cincinnati, Ohio (May 4-7, 1997).
20. Kim, J.S., B. Koc, Y.H. Chen and K. Uchino, "Dielectric Properties of the Iron-Doped $Pb(Sc_{1/2}Nb_{1/2})_{0.57}Ti_{0.43}O_3$ Ceramics," Amer. Ceram. Soc. Annual Mtg., EP-021-97, Cincinnati, Ohio (May 4-7, 1997).
21. Aburatani, H. and K. Uchino, "Field-Induced Acoustic Emission (AE) of Piezoelectric, Electrostrictive and Antiferroelectric Ceramics," Amer. Ceram. Soc. Annual Mtg., EP-022-97, Cincinnati, Ohio (May 4-7, 1997).
22. Tressler, J. F., W. J. Hughes, and K. Uchino, "Capped Ceramic Underwater Sound Projector," Amer. Ceram. Soc. Annual Mtg., EP-024-97, Cincinnati, Ohio (May 4-7, 1997).
23. Poosanaas, P., A.V. Prasadarao, S. Komarneni, and K. Uchino, "Coprecipitated PLZT Ceramics for Photostrictive Application," Amer. Ceram. Soc. Annual Mtg., EP-031-97, Cincinnati, Ohio (May 4-7, 1997).
24. Du, X.H., U. Belegundu and K. Uchino, "Elastic, Piezoelectric, and Dielectric Constants of a Single Crystal: $0.91Pb(Zn_{1/3}Nb_{2/3})O_3$-$0.09PbTiO_3$," Amer. Ceram. Soc. 99th Annual Mtg., E-045-97, Cincinnati, Ohio (May 4-7, 1997).
25. Witham, J.P. and K. Uchino, "Optical Study of Domains in PLZT Ceramics," 21th Smart Actuator Symp., University Park, PA (April 1997).
26. Chen, Y.H., J.S. Kim, and K. Uchino, "High Power Piezoelectric Characteristics and Loss Mechanisms of PMN-PT Based Ceramics," 21th Smart Actuator Symp., University Park, PA (April 1997).
27. Koc, B. and K. Uchino, "Transient Response Characteristics of Windmill Ultrasonic Motors," 21th Smart Actuator Symp., University Park, PA (April 21-22, 1997).
28. Zheng, J. and K. Uchino, "Uniaxial Stress Dependence of Piezoelectricity in the Lead Zirconate-Titanate System," 21th Smart Actuator Symp., University Park, PA, (April 1997).
29. Aburatani, H. and K. Uchino, "Field-Induced Acoustic Emission (AE) of Piezoelectric, Electrostrictive and Antiferroelectric Ceramics," 21th Smart Actuator Symp., University Park, PA (April 1997).
30. Tressler, J.F., W.J. Hughes, and K. Uchino, "Capped Ceramic Underwater Sound Projector," 21th Smart Actuator Symp., University Park, PA (April 1997).
31. Poosanaas, P., A. Dogan, and K. Uchino, "Photovoltaic Effect in PLZT Ceramics," 21st ICAT Smart Actuators Symposia, State College, Pennsylvania (April 1997).
32. Koc, B. and K. Uchino, "Miniature Ultrasonic Motor," Graduate Student Exhibition, PSU (March 28, 1997).
33. Uchino, K., "Materials Issues in Design and Performance of Piezoelectric Actuators," Engineering Foundation Conference on Engineered Adaptive Composite Structures for Noise and Vibration Control, Banff, Canada (July 14-18, 1997).
34. Poosanaas, P., A. Dogan, and K. Uchino, "Photostrictive Effects in Lanthanum-Modified Lead Zirconate Titanate Ceramics," The Ninth International Meeting on Ferroelectricity, Seoul, Korea (August 24-29, 1997).
35. Poosanaas, P., A. Dogan, and K. Uchino, "Surface Roughness and Sample Thickness Dependence of Photostrictive Effect," The Pennsylvania Ceramic Association Meeting (52nd Annual Ceramic Forum) (September 11-13, 1997).
36. Chen, Y.H. and K. Uchino, "High Power Piezoelectric Characteristics and Loss Mechanisms of PMN-PT Based Ceramics," 133rd Meeting of the Acoustical Society of America, State College, PA (1997).

37. Poosanaas, P., A. Dogan, and K. Uchino, "Dependence of Photostriction on Thickness and Surface Roughness for PLZT Ceramics," 1997 IEEE on Ultrasonic Symposium, Toronto, Ontario, Canada (October 5-8, 1997).
38. Pertsch, P., M.-J. Pan, F. Chu, and S. Yoshikawa, "The Effects of Uniaxial Stress and Temperature on the Behavior of Electroceramic Actuator Materials," The Ninth International Meeting on Ferroelectricity, Seoul, Korea (August 24-29, 1997).
39. Trolier-McKinstry, S., "Thin Film Technology Comparison, Scientific and Technological Trends in Electroceramics Device Manufacture (1997).
40. Shepard, Jr., J.F., S. Trolier-McKinstry, M. Hendrickson, and R. Zeto, "Characteristics of PZT Thin Films as a Function of Applied Biaxial Stress," Transducers '97 (1997).
41. Trolier-McKinstry and J. Koh, "Composition Profiling of Graded Dielectric Function Materials by Spectros· ɔic Ellipsometry," Second International Conference on Spectroscopic Ellipso: ɛtry (1997).
42. Gibbons, B.J., S. Trolier-McKinstry, D.G. Schlom, and C.B. Hom, "Oxygen Diffusion in $YBa2Cu_3$ Thin Films Studied by Spectroscopic Ellipsometry (1997).
43. Trolier-McKinstry, S., W.J. Hughes, R.L. Tutwiler, R.J. Davis, and W.W. Cao, "Microtonpilz Thin Film Transducer," DARPA/ONR Workshop on Medical Ultrasound Imaging Technology Development for Com. Care.
44. Dogan, A., J. Braidic, G. Lenkner, J.F. Tressler, A.C. Haladky, and R.E. Newnham, "Comparison of Ceramic-Metal Composite Transducers Driver by Different Piezoelctric Modes, ONR Workshop, Penn State University (April 29-May 1, 1997).
45. Tressler, J.F., W. Cao, K. Uchino, R.E. Newnham, and W.J. Hughes, "Capped Ceramic Underwater Sound Projectors," ONR Workshop, Penn State University (April 29-May 1, 1997).
46. Pezanowski, C., R. Natarajan, V. Sundar, J.P. Dougherty, and R.E. Newnham, "Temperature Dependence of Dielectric Properties and Field Induced Strain in Low-Firing PZN-PFW-PFN and PN-PMW-PT Relaxor Ferroelectrics," ONR Workshop, Penn State University (April 29-May 1, 1997).
47. Alkoy, S., R.E. Newnham, A.C. Hladky, and J.K. Cochran, "Size Dependent Properties of Tangentially Poled Sphere Transducers," ONR Workshop, Penn State University (April 29-May 1, 1997).
48. Moses, P, R. Yimnirun, V. Sundar, and R.E. Newnham, " Interferometer and Compressometer Based Methods of Measuring Sensor and Actuator Properties of Materials," ONR Workshop, Penn State University (April 29-May 1, 1997).
49. Streett, S., A. Ling, R. Deering, B. Xu, V. Sundar, and R.E. Newnham, "Photocatalytic Antibacterial Action in Anatase," American Ceramic Society Meeting, Cincinnati, OH (May 4-7, 1997).
50. Newnham, R.E., "Electrostriction in Dielectric Materials," American Ceramic Society Meeting, Cincinnati, OH (May 4-7, 1997).
51. Newnham, R.E., V. Sundar, R. Yimnirun, and Q. Zhang, "Electrostriction in Dielectric Materials," American Ceramic Society Meeting, Cincinnati, OH (May 4-7, 1997).
52. Pezanowski, C., R. Natarajan, V. Sundar, and R.E. Newnham, "Dielectric and Electromechanical Properties of PZN-PFW-PFN and PNN-PMW-PT Relaxor Ferroelectrics," American Ceramic Society Meeting, Cincinnati, OH (May 4-7, 1997).
53. Lopath, P.D., S.-E. Park, K.K. Shung, and T.R. Shrout, "$Pb(Zr_{1/3}Nb_{2/3})O_3$ Single Crystal Piezoelectrics for Ultrasonic Transducers," IEEE Ultrasonic 1997, Toronto, Canada (October 1997).

54. Zipparo, M.J., K.K. Shung, and T.R. Shrout, "Piezoceramics for High Frequency (20-100 Mhz) Transducers and Arrays," IEEE Ultrasonic 1997, Toronto, Canada (October 1997).
55. Randall, C.A., X. Liu, D. McCauley, F.J. Toal, A. Hitomi, J. Van Tassel, and T.R. Shrout, "Scaling and Intefacial Issues in Electroceramic Components," US:Japan Workshop in Electrically Active Ceramic Interface, MIT, Cambridge, MA (March 1998).
56. Maria, J.-P., T.R. Shrout, and S. Trolier-McKinstry, "Deposition and Electrical Characterization of Epitaxial $Pb(Mg_{1/3}Nb_{2/3})O_3$-$PbTiO_3$ Relaxor Thin Films, MRS 1997 Fall Meeting, Boston, MA.
57. Shrout, T.R., S.-E. Park, P.D. Lopath, and K.K. Shung, "Relaxor-Based Single Crystal Materials in Ultrasonic Transducer Applications," SPIE's International Symposium on Medical Imaging, Newport Beach, California (February 1997).
58. Lopath, P.D., S.-E. Park, M.J. Zipparo, W. Hackenberger, and T.R. Shrout, "Piezoelectric Materials for Ultrasonic Transducers," SPIE's International Symposium on Medical Imaging, Newport Beach, California (February 1997).
59. Park, S.-E. and T.R. Shrout, "Relaxor-Based Ferroelectric Single Crystals with High Piezoelectric Performance," 9th International Meeting on Ferroelectrics, Seoul, Korea (August 1997).
60. Wada, S., S.-E. Park, L.E. Cross, and T.R. Shrout, "Domain Configuration and Ferroelectric Related Properties of Relaxor-Based Single Crystals," 9th International Meeting on Ferroelectrics, Seoul, Korea (August 1997).
61. Shrout, T.R. and S.-E. Park, "Single Crystal Perovskites with High Piezoelectric Performance," DARPA/ONR Workshop on Medical Ultrasonic Imaging Techology Development for Combat Casualty Care, Lansdowne, VA (February 1997).
62. Shrout, T.R. and S.-E. Park, "Relaxor Ferroelectric Single Crystals for High Actuators," ONR Transducers Materials and Transducers Workshop, Penn State University, University Park, PA (April 1997).
63. Park, S.-E., S. Wada, P.D. Lopath, L.E. Cross, and T.R. Shrout, "Relaxor Based Ferroelectric Single Crystals-Piezoelectric Properties, Phase Transformations, Electric Field Anisotropy," ONR Transducers Materials and Transducers Workshop, Penn State University, University Park, PA (April 1997).
64. Shrout, T.R. and S.-E. Park, "Relaxor Ferroelectric Crystals for High Strain Actuators," Piezoelectric Crystal Planning Workshop, Washington Dulles Airport Marriott (May 1997).
65. Shrout, T.R. and S.-E. Park, "Single Crystal Perovskite," DARPA Actuator Programs, Technology Interchage Meeting #1 (August 1997).
66. Belegundu, A. D., G.H. Koopmann and T. P. Galante, "Shape Optimization for Mechanical Amplification of PZT Actuator Couplers," ONR Transducer Materials Workshop, The Pennsylvania State University (1997).
67. Ho, Y.R., I.S. Kim, W. Chen, and G.H. Koopmann, "Active Control of Broadband Sound Transmission Using Feedback and Feedforward Techniques," Noise-Con 97, Penn State, PA (1997).
68. Sharp, S., G.H. Koopmann, and W. Chen, "Transmission Loss Characteristics of an Active Trim Panel," Noise-Con 97, Penn State, PA (1997).
69. Lesieutre, G.A., and C.L. Davis, "A Solid-State Tunable Piezoelectric Vibration Absorber", proceedings of the SPIE Smart Structures and Materials Conference: Smart Structures and Integrated Systems, San Diego, CA (March 1-5, 1998).

70. Koopmann, G.H., G.A. Lesieutre, W. Chen, T. Galante, and J. Bernard, "Design, Modeling, and Performance of a High Force Piezoelectric Inchworm Motor," proceedings of the SPIE Smart Structures and Materials Conference: Passive Damping and Isolation, San Diego, CA (March 1-5, 1998).
71. Hebert, C.A., and G.A. Lesieutre, "Rotorcraft Lag Damping using Highly-Distributed Tuned Vibration Absorbers," proceedings of the 7th ARO International Workshop on Dynamics and Aeroelastic Stability Modeling of Rotorcraft Systems, St. Louis, MO (October, 14-16, 1997).
72. Lesieutre, G.A. and C.L. Davis, "A Semi-Actively Tuned Piezoceramic Vibration Absorber," proceedings of the 3rd ARO Smart Structures Workshop, Blacksburg, VA (August 27, 1997).
73. Galante, T., G.H. Koopmann, and G.A. Lesieutre, "A High-Force Piezoelectric Inchworm Actuator," at the 1997 ONR Transducer Materials and Transducers Workshop, State College, PA (April 1997).
74. Lee, U. and G.A. Lesieutre, "Design Concerns for Active Constrained Layer Damping Treatments," proceedings of the 38th AIAA/ASME/ASCE/AHS/ASC Structures, Structural Dynamics and Materials Conference, Kissimee, FL (April 7-10, 1997).
75. Lesieutre, G.A., and C.L. Davis, "A Tunable Piezoelectric Inertial Actuator", proceedings of the SPIE Smart Structures and Materials Conference: Smart Structures and Integrated Systems, San Diego, CA (March 4, 1997).
76. Lesieutre, G.A., and C.L. Davis, "Can the Coupling Coefficient of a Piezoelectric Device be Higher Than Those of the Basic Material?," proceedings of the SPIE Smart Structures and Materials Conference: Smart Structures and Integrated Systems, San Diego, CA (March 4, 1997).
77. Lesieutre, G.A., and U. Lee, "A Finite Element Model for Beams Having Segmented Active Constrained Layers with Frequency-Dependent Viscoelastic Material Properties," proceedings of the SPIE Smart Structures and Materials Conference: Passive Damping and Isolation, San Diego, CA (March 4, 1997).

14.0 BOOKS (AND SECTIONS THERE OF)

1. Bhalla, A.S. and R. Guo, "Pyroelectricity" in Encyclopedia of Electrical and Electronics Engineering, editor, J.G. Webster, John Wiley & Sons, Inc. (in printing 1998).
2. Uchino, K., *Piezoelectric Actuators and Ultrasonic Motors*, Kluwer Academic Publishers, Norwell, MA (1997).
3. Uchino, K., Micro-Optomechatronics Handbook, Sec.5.5 Photostrictive Actuators, Asakura Publishing Co., Tokyo (1997).
4. Belegundu, A., Second Edition, Introduction to Finite Elements In Engineering, Prentice-Hall (1997).
5. Belegundu, A., Text Book in Optimization in Engineering , Prentice-Hall. To Appear (1998).
6. Belegundu, A., Proceedings of the Engineering Foundation Conference, Optimization In Industry, Editor, ASME Publication (To Appear, Dec. 1997).
7. Koopmann, G. H. and J. Fahline, Designing Quiet Structures: A Sound Power Minimization Approach, Academic Press (July 1997).

GENERAL SUMMARY PAPERS

APPENDIX 1

3220MS00.MWM

Piezoelectricity

Yukio Ito and Kenji Uchino

134 Materials Research Laboratory

The Pennsylvania State University

University Park, PA 16802

Introduction

Certain materials produce electric charges on their surfaces as a consequence of applying mechanical stress. The induced charges are proportional to the mechanical stress. This is called the direct piezoelectric effect and was discovered by J. and P. Curie in 1880. Materials showing this phenomenon also conversely have a geometric strain proportional to an applied electric field. This is the converse piezoelectric effect. The root of the word "piezo" means "pressure"; hence the original meaning of the word piezoelectricity implied "pressure electricity". (1)(2)

Piezoelectric materials provide coupling between electrical and mechanical parameters. The material used earliest for its piezoelectric properties was single-crystal quartz. Quartz crystal resonators for frequency control appear today at the heart of clocks and are also used in TVs, computers. Ferroelectric polycrystalline ceramics such as barium titanate and lead zirconate titanate exhibit piezoelectricity when electrically poled. Since these ceramics possess significant and stable piezoelectric effects, i.e., high electromechanical coupling, they are capable of producing large strains / forces and hence are extensively used as transducers. Piezoelectric polymers, notably polyvinyliden difluoride and its copolymers with trifluoroethylene and piezoelectric composites combining a piezoelectric ceramic with a passive polymer have been developed which offer a high potential. Recently, thin films of piezoelectric materials are being paid

attention due to their potential utilization in micro-sensors, micro-transducers and micro-actuators.

Piezoelectricity is being extensively utilized in the fabrication of various devices such as transducers, actuators, surface acoustic wave devices, frequency control and so on. In this chapter we describe the piezoelectric effect, brief history of piezoelectricity followed by present day piezoelectric materials that are used and finally various potential applications of piezoelectric materials.

Piezoelectricity

Relationship between crystal symmetry and properties

All crystals can be classified into 32 point groups according to their crystallographic symmetry. These point groups are divided into two classes; one has a center of symmetry and another lacks it. There are 21 non-centrosymmetric point groups. Crystals belonging 20 of these point groups exhibits piezoelectricity. The cubic class 432, although lacking a center of symmetry, does not permit piezoelectricity. Of these 20 point groups, there are 10 polar crystal classes containing a unique axis, along which an electric dipole moment is oriented in the unstrained condition.

Pyroelectric effect appears in any material that possess a polar symmetry axis. As a result of this the material develops electric charge on the surface owing to change in magnitude of the dipole moment with changing temperature. Among the pyroelectric crystals whose spontaneous polarization are reorientable by application of an electric field of sufficient magnitude (not exceeding the breakdown limit of the crystal) are called ferroelectrics. (3)(4) Table 1 shows the crystallographic classification of the point groups.

Piezoelectric coefficients

Materials are deformed by stresses and the resulting deformations are represented by strains (ΔL/L). When the stress T (force per unit area) causes a proportional strain S,

$$S = sT, \tag{1}$$

where all quantities are tensors; S and T are second rank and s is fourth rank. Piezoelectricity creates additional strains by applied field E. The piezoelectric equation is given by

$$S_{ij} = s_{ijkl}\, T_{kl} + d_{ijk}\, E_k \tag{2}$$

where E is the electric field and d is the piezoelectric constant which is the third rank tensor. This equation can be also expressed in a matrix form such as given for the case in a poled ceramics:

$$\begin{bmatrix} S_1 \\ S_2 \\ S_3 \\ S_4 \\ S_5 \\ S_6 \end{bmatrix} = \begin{bmatrix} s_{11} & s_{12} & s_{13} & & & \\ s_{12} & s_{11} & s_{13} & & 0 & \\ s_{13} & s_{13} & s_{33} & & & \\ & & & s_{44} & & \\ & 0 & & & s_{44} & \\ & & & & & 2(s_{11}-s_{12}) \end{bmatrix} \begin{bmatrix} T_1 \\ T_2 \\ T_3 \\ T_4 \\ T_5 \\ T_6 \end{bmatrix} + \begin{bmatrix} 0 & 0 & d_{31} \\ 0 & 0 & d_{31} \\ 0 & 0 & d_{33} \\ 0 & d_{15} & 0 \\ d_{15} & 0 & 0 \\ 0 & 0 & 0 \end{bmatrix} \begin{bmatrix} E_1 \\ E_2 \\ E_3 \end{bmatrix} \tag{3}$$

Another frequently used piezoelectric constant is 'g' which gives the electric field produced when a stress is applied ($E = gT$). The 'g' constant is related to the 'd'constant through the permitivity ε:

$$g = d / \varepsilon \tag{4}$$

A measure of the effectiveness of the electromechanical energy conversion is the electromechanical coupling factor 'k'. which measures the fraction of the electrical energy converted to mechanical energy when an electric field is applied or vice versa when a material is stressed. (5) The relationship is in terms of k^2.

$$k^2 = \frac{\text{Electrical Energy Converted to Mechanical Energy}}{\text{Input Electrical Energy}} \tag{5}$$

or

$$k^2 = \frac{\text{Mechanical Energy Converted to Electrical Energy}}{\text{Input Mechanical Energy}} \tag{6}$$

which also can be expressed by

$$k^2 = d^2 / (\varepsilon \cdot s). \tag{7}$$

k is always less than 1, because k^2 is below 1. Typical values of k are 0.10 for quartz, 0.4 for $BaTiO_3$ ceramic, 0.5 - 0.7 for PZT ceramic and 0.1 - 0.3 for PVDF polymer. Another

important material parameter is the mechanical quantity factor Q_m which determines the frequency characteristics. The Q_m is given by

$$Q_m = 2\pi \times \frac{\text{Energy stored over one cycle}}{\text{Energy dissipated per cycle}} \quad (8)$$

History of Piezoelectricity

As stated already the discovery of piezoelectricity in quartz (which is not ferroelectric) was done by Piere and Jacques Curie in 1880. Ferroelectricity can provide the creation of useful piezoelectric materials. Rochelle salt was the first ferroelectric discovered in 1921. Till 1940 only two types of ferroelectrics were known, Rochelle salt and potassium dihydrogen phosphate and its isomorph. In 1940 to 1943, unusual dielectric properties like abnormally high dielectric constant of barium titanate $BaTiO_3$ was discovered independently by Wainer and Salmon, Ogawa, and Wul and Golman. After the discovery, compositional modifications for $BaTiO_3$ led to improvement in the temperature stability or the high voltage output. Piezoelectric transducers based on $BaTiO_3$ ceramics were becoming well established in a number of device applications.

In 1950's Jaffe and co-workers established the lead zirconate - lead titanate system (called PZT system) as suitable for inducing strong piezoelectric effects. The maximum piezoelectric response was found for PZT compositions near the morphotropic phase boundary, i.e., the composition-dependent and temperature independent rhombohedral-

tetragonal phase change. Since then, the PZT system with various additives has become the dominant piezoelectric ceramics for potential applications. Other ferroelectric perovskite compounds were also extensively examined. The discovery of PZT solid solution system was rapidly followed by its exploitation in a number of practical piezoelectric applications.

Kawai et al., discovered in 1969 that certain polymers, notably polyvinyliden difluoride, are piezoelectric when stretched during fabrication. Such piezoelectric polymers are also useful for some transducer applications. In 1978 Newnham et al., improved composite piezoelectric materials by combining a piezoelectric ceramic with a passive polymer whose properties can be tailored to the requirements of various piezoelectric devices.

There is another class of ceramic material which recently has become important; relaxor-type electrostrictors such as lead magnesium niobate [PMN], typically doped with 10% lead titanate [PT], which are potentially used for applications in piezoelectric actuator field. Recent breakthrough in the growth of high quality large single crystal relaxor piezoelectric compositions has brought the interest in these materials for wide applications ranging from high strain actuators to high frequency transducers for the medical ultrasound devices due to their superior electromechanical characteristics. More recently, thin films of piezoelectric materials such as zinc oxide [ZnO], or PZT have been extensively investigated and developed for use in micro electromechanical device applications.

Piezoelectric Materials

This section summarizes the current status of piezoelectric materials: single crystal materials, piezoceramics, piezopolymers, piezocomposites and piezofilms. Table 2 shows the material parameters of some representative piezoelectric materials described below. (6)(7)

Single crystals

More recently, the piezoelectric ceramics are widely used for a large number of applications. However, single crystal materials retain their utility, being essential for application field such as frequency stabilized oscillators and surface acoustic devices. The most popular single-crystal piezoelectric materials are quartz, lithium niobate ($LiNbO_3$) and lithium tantalate ($LiTaO_3$). The single crystals are anisotropic, which gives different material properties depending on the cut of the materials and the direction of bulk or surface wave propagation.

Quartz is a well-known piezoelectric material. α-quartz belongs to triclinic crystal system with point group 32 and has a phase transition at 537 °C to β-type which is not a piezoelectric. Quartz has the cut with a zero temperature coefficient. For instance,

quartz oscillators using thickness shear mode of AT-cut are extensively used for clock sources in computers, frequency stabilized ones in TVs and VTRs. On the other hand, an ST-cut quartz substrate with X-propagation has a zero temperature coefficient for surface acoustic wave and so are used for SAW devices with high-stabilized frequencies. The another distinguished characteristic of quartz is that it has a extremely high mechanical quality factor $Q_m > 10^5$.

Lithium niobate and lithium tantalate belong to an isomorphous crystal system and are composed of oxygen octahedron. The Curie temperatures of $LiNbO_3$ and $LiTaO_3$ are 1210 and 660 °C, respectively. The crystal symmetry of the ferroelectric phase of these single crystals is 3m and the polarization direction is along c-axis. These materials have high electromechanical coupling coefficients for surface acoustic wave. In addition, large single crystals can easily be obtained from their melt using the conventional Czochralski technique. Thus both materials occupy very important positions in the SAW device application field.

Ceramics

Perovskite Structure

Most of the piezoelectric ceramics have perovskite structure ABO_3, as shown Fig.1. This ideal structure consists of a simple cubic unit cell with a large cation A on the corner, a smaller cation B in the body center, and oxygens O in the centers of the faces. The structure is a net-work of corner-linked oxygen octahedra surrounding B cations. Piezoelectric properties of perovskite-structure materials can be easily tailored depending on their applications by incorporating various cations in the perovskite structure.

Barium titanate

Barium titanate $BaTiO_3$ is one of the most thoroughly studied and most widely used piezoelectric materials. Figure 2 shows the temperature dependence of dielectric constants in $BaTiO_3$ demonstrating the phase transition in $BaTiO_3$ single crystals. Three anomalies can be observed. The discontinuity at the Curie point (130 °C) is due to a transition from a ferroelectric to a paraelectric phase. The other two discontinuities are accompanied with transitions from one ferroelectric phase to another. Above the Curie point the crystal structure is cubic and has no spontaneous dipole moments. At the Curie point the crystal becomes polar and the structure changes from a cubic to a tetragonal phase. The tetragonal axis is in the direction of the dipole moment and thus along the spontaneous polarization. Just below the Curie temperature, the vector of the spontaneous polarization points in the [001] direction (Tetragonal phase), below 5 °C it reorients in the [011] (Orthrhombic phase) and below - 90 °C in the [111] (Rhombohedral

phase). The dielectric and piezoelectric properties of ferroelectric ceramic $BaTiO_3$ can be affected by its own stoichiometry, microstructure, and by dopants entering into the A or B site solid solution. Modified ceramic $BaTiO_3$ with dopants such as Pb or Ca ions have been used as commercial piezoelectric materials.

Lead zirconate- lead titanate

Piezoelectric $Pb(Ti,Zr)O_3$ solid solutions [PZT] ceramics have been widely used because of their superior piezoelectric properties. The phase diagram of the PZT system ($PbZr_xTi_{1-x}O_3$) is shown in Fig. 3. The crystalline symmetry of this solid-solution system is determined by the Zr content. Lead titanate has also a tetragonal ferroelectric phase of perovskite structure. With increasing Zr content, x, tetragonal distortion decreases and when $x > 0.52$ the structure changes from tetragonal 4mm phase to another ferroelectric phase of rhombohedral 3m symmetry. This transition is rather independent of temperature. The line dividing the two phases is called morphotropic phase boundary, that is, the change of symmetry occurs only as a function of composition. This composition is considered to have both phases. Figure 4 shows the dependence of several d constants on composition near the morphotropic phase boundary. The *d* constants have their highest values near the morphotropic phase boundary. This enhancement in piezoelectric effect is attributed to the increased ease of reorientation of the polarization under electric field. Doping the PZT material with donors or acceptor changes the properties dramatically. Donor doping with ions such as Nb^{5+} or Ta^{5+} provides soft

PZTs like PZT-5, because of the facility of a domain motion due to the resulting Pb-vacancy. On the other hand, acceptor doping such as Fe^{3+} or Sc^{3+} leads to hard PZTs such as PZT-8, because oxygen vacancies will pin the domain wall motion.

Lead titanate

Lead titanate has a large crystal distortion. $PbTiO_3$ has tetragonal structure at room temperature with its tetragonality c/a = 1.063. The Curie temperature is 490 °C. Densely sintered $PbTiO_3$ ceramics can not be obtained easily, because they break up into a powder when cooled through the Curie temperature. This is due to the large spontaneous strain which occurs at the transition. Lead titanate ceramics modified by adding small amount of additives which exhibits a high piezoelectric anisotropy. Either (Pb, Sm)TiO_3 (8) or (Pb, Ca)TiO_3 (9) has extremely low planar coupling, that is, large k_t / k_p ratio. Here, k_t and k_p are thickness-extensional and planar electromechanical coupling factors, respectively. (Pb, Nd)(Ti, Mn, In)O_3 ceramics with a zero temperature coefficient of surface acoustic wave delay have been developed as a superior substrate materials for SAW device applications. (10)

Polymers

Polyvinylidene difluoride, PVDF or PVF2, is piezoelectric when stretched during fabrication. Thin sheets of the cast polymer are then drawn, stretched, in the plane of the sheet in at least one direction, and frequently also in the perpendicular direction, to make the material into its microscopically polar phase. Crystallization from melt forms non-polar α-phase, which can be converted into another polar β-phase by a uniaxial or biaxial drawing operation; these dipoles are then reoriented through electric poling. Large sheets can be manufactured and thermally formed into complex shapes. The copolymerization of vinilydene difluoride with trifluoroethylene (TrFE) results in random copolymer (PVDF-TrFE) with a stable, polar β-phase. This polymer need not be stretched; it can be poled directly as formed. The thickness-mode coupling coefficient of 0.30 has been reported. Such piezoelectric polymers are used for directional microphones and ultrasonic hydrophones.

Composites

Piezocomposites composed of a piezoelectric ceramic and polymer are promising materials because of excellent and tailored properties. The geometry for two-phase composites can be classified according to the connectivity of each phase (1, 2 or 3 dimensionally) into 10 structures; 0-0, 0-1, 0-2, 0-3, 1-1, 1-2, 1-3, 2-2, 2-3 and 3-3. (11) A 1-3 piezocomposite, or PZT-rod / polymer-matrix composite is identified as a most promising candidate. The advantages of this composite are high coupling factors, low

acoustic impedance, good matching to water or human tissue, mechanical flexibility, broad bandwidth in combination with low mechanical quality factor and the possibility of making undiced arrays by only structuring the electrodes. The thickness-mode electromechanical coupling of the composite can exceed the k_t (0.40-0.50) of the constituent ceramic, approaching almost the value of the rod-mode electromechanical coupling, k_{33} (0.70-0.80) of that ceramic. (12) Acoustic impedance is the square root of the product of its density and elastic stiffness. The acoustic match to tissue or water (1.5 Mrayls) of the typical piezoceramics (20-30 Mrayls) is significantly improved by forming a composite structure, that is, by replacing heavy and stiff ceramic by light and soft polymer. Piezoelectric composite materials are especially useful for underwater sonar and medical diagnostic ultrasonic transducer applications.

Thin-films

Both zinc oxide [ZnO] and aluminum nitride [AlN] are simple binary compounds with a Wurtzite-type structure, which can be sputter-deposited in a c-axis oriented thin film on a variety of substrates. ZnO has large piezoelectric coupling and its thin films are widely used in bulk acoustic and surface acoustic wave devices. The fabrication of highly c-axis oriented ZnO films have been extensively studied and developed. The performance of ZnO devices is, however, limited due to their small piezoelectric coupling (20 - 30%). PZT thin films are expected to exhibit higher piezoelectric properties. At present the

growth of PZT thin film is being carried out for use in micro-transducers and micro-actuators.

Relaxor-type ferroelectric materials

Relaxor ferroelectrics differ from normal ferroelectrics in terms of having broad phase transition from paraelectric to ferroelectric state, strong frequency dependence of dielectric constant (i.e. dielectric relaxation) and weak remanent polarization. Lead based relaxor materials have complex disordered perovskite structures with a general formula $Pb(B_1, B_2)O_3$ ($B_1 = Mg^{2+}, Zn^{2+}, Sc^{3+}$, $B_2 = Nb^{5+}, Ta^{5+}, W^{6+}$) The B site cations are distributed randomly in the crystal. The characteristic of relaxors is a broad and frequency dispersive dielectric maximum. Relaxor-type electrostrictive materials such as lead magnesium niobate $Pb(Mg_{1/3}Nb_{2/3})O_3$ - lead titanate $PbTiO_3$ solid solution [PMN-PT] are very suitable for application in actuators. This relaxor ferroelectrics can also provide an induced piezoelectric effect. That is, the electromechanical coupling factor k_t varies with the applied DC bias field. As the DC bias field increases, the coupling increases and saturates. This behavior is reproducible. These materials would be applied for ultrasonic transducers which can be tunable by the bias field. (13)

Recently, single-crystal relaxor ferroelectrics have been developed which show great promising results in ultrasonic transducers and electromechanical actuators. Single crystals of $Pb(Mg_{1/3}Nb_{2/3})O_3$ [PMN], $Pb(Zn_{1/3}Nb_{2/3})O_3$ [PZN] and binary systems of

these materials combined with $PbTiO_3$ [PMN-PT and PZN-PT] exhibit extremely large electromechanical coupling factors. (14)(15) Large coupling coefficients and large piezoelectric constants have been found for these solid-solution crystals with morphotropic phase boundary compositions. PZN-8%PT single crystals were found to possess high k_{33} value of 0.94 for (001) crystal cuts. The k_{33} value of the conventional PZT ceramics is usually 0.70-0.80.

Applications of Piezoelectric Materials

Piezoelectric materials can provide coupling between electrical and mechanical energy and thus have been extensively used in a variety of electro-mechanical device applications. The direct piezoelectric effect is most obviously used in the generation of charge at high voltage such as for the spark ignition of gas in space heaters, cooking stoves and cigarette lighters. Using the converse effect, mechanical small displacements and vibrations can be produced for actuators by applying a field. Acoustic and ultrasonic vibrations can be generated by an alternating field tuned at the mechanical resonance frequency of a piezoelectric device, and can be detected by amplifying the field generated by vibration incident on the material, which is usually used for ultrasonic transducers. The other important application field of piezoelectricity include the control of frequency. The application of piezoelectric materials ranges over many technology fields including ultrasonic transducers, actuators and ultrasonic motors, electronic components such as resonators, wave filters, delay lines, SAW devices and transformers, and high voltage

applications; gas ignitors, ultrasonic cleaning and machining. Piezoelectric-based sensors, for instance, accelerometers, automobile knock sensors, vibration sensors, strain gages and flow meters have been developed, because pressure and vibration can be directly sensed as electric signals through piezoelectric effect. Examples of these applications are given in the following sections.

Ultrasonic Transducers

One of the most important applications of piezoelectric materials is based on ultrasonic echo field. (16)(17) Ultrasonic transducers convert electrical energy into mechanical form when generating an acoustic pulse and convert mechanical energy into an electrical signal when detecting its echo. Now-a-days, piezoelectric transducers are being used in medical ultrasound for clinical applications ranging from diagnosis to therapy and surgery. They are also used for underwater detection, such as sonar and fish finding, and nondestructive testing.

The ultrasonic transducers operate often in a pulse-echo mode. The transducer converts electrical input into acoustic wave output. The transmitted waves propagate into a body and echoes are generated which travel back to be received by the same transducer. These echoes vary in intensity according to the type of tissue or body structure, thereby creating images. An ultrasonic image represents the mechanical properties of the tissue, such as density and elasticity. We can recognize anatomical structures in an ultrasonic

image since the organ boundaries and fluid-to-tissue interfaces are easily discerned. The ultrasonic imaging process can also be done in real time. This means we can follow rapidly moving structures such as heart without motion distortion. In addition, ultrasound is one of the safest diagnostic imaging techniques. It does not use ionizing radiation like X-rays and thus is routinely used for fetal and obstetrical imaging. Useful areas for ultrasonic imaging include cardiac structures, the vascular systems, the fetus and abdominal organs such as liver and kidney. In brief, it is possible to see inside the human body without breaking the skin by using a beam of ultrasound.

There are various types of transducers used in ultrasonic imaging. Mechanical sector transducers consist of single, relatively large resonators and can provide images by its mechanical scanning such as wobbling. Multiple element array transducers permit discrete elements to be individually accessed by the imaging system and enable electronic focusing in the scanning plane to various adjustable penetration depths through the use of phase delays. Two basic types of array transducers are linear and phased (or sector). A linear array is a collection of elements arranged in one direction, producing a rectangular display. A curved linear (or convex) array is a modified linear array whose elements are arranged along an arc to permit an enlarged trapezoidal field of view. The elements of these linear type array transducers are excited sequentially group by group in a sweep of the beam in one direction. These linear array transducers are used for radiological and obstetrical examinations. On the other hand, in a phased array transducer the acoustic beam is steered by signals that are applied to the elements with delays, creating a sector

display. This transducer is useful for cardiology applications where positioning between the ribs is necessary.

Figure 5 shows the basic ultrasonic transducer geometry. The transducer is mainly composed of matching, piezoelectric material and backing layers. (18) One or more matching layers are used to increase sound transmissions into tissues. The backing is added to the rear of the transducer in order to damp the acoustic backwave and to reduce the pulse duration. Piezoelectric materials are used to generate and detect ultrasound. In general, broadband transducers should be used for medical ultrasonic imaging. The broad bandwidth response corresponds to a short pulse length, resulting in better axial resolution. Three factors are important in designing broad bandwidth transducers. The first is acoustic impedance matching, that is, effectively coupling acoustic energy to the body. The second is a high electromechanical coupling coefficient of the transducer. The third is electrical impedance matching, that is, effectively coupling electrical energy from the driving electronics to the transducer across the frequency range of interest. These pulse echo transducers operate based on thickness mode resonance of the piezoelectric thin plate. The thickness mode coupling coefficient, k_t, is related to the efficiency of converting electric energy into acoustic and vice versa. Further, a low planar mode coupling coefficient, k_p, is beneficial for limiting energies being expended in nonproductive lateral mode. A large dielectric constant is necessary to enable a good electrical impedance match to the system, especially with tiny piezoelectric sizes.

Table 3 compares the properties of ultrasonic transducer materials. (7)(19) Ferroelectric ceramics, such as lead zirconate titanate and modified lead titanate, are now-a-days almost universally used as ultrasonic transducers. The success of ceramics is due to their very high electromechanical coupling coefficients. In particular, soft PZT ceramics such as PZT-5A and 5H type compositions are most widely used because of their exceedingly high coupling properties and because they can be relatively easily tailored, for instance, in the wide dielectric constant range. On the other hand, modified lead titanates such as samarium doped materials have high piezoelectric anisotropy: the planar coupling factor k_p is much less than the thickness coupling factor k_t. This absence of lateral coupling leads to reduced interference from spurious lateral resonances in longitudinal oscillators. This is very useful in high-frequency array transducer applications. One disadvantage to PZT and other lead based ceramics is their large acoustic impedance (approximately 30-$kgm^{-2}s^{-1}$ (Mrayls) compared to body tissue (1.5 Mrayls). Single or multiple matching layers with intermediate impedances needed to be used in the case of PZT to improve acoustic matching.

On the other hand, piezoelectric polymers, such as polyvinyliden-difluoride-trifluoroethylene, have much lower acoustic impedance (4 - 5 Mrayls) than the ceramics and thus provide better matching with soft tissues. However, piezopolymers are less sensitive than the ceramics and they have relatively low dielectric constants, requiring

large drive voltage and giving poor noise performance due to electrical impedance mismatching.

An alternative to ceramics and polymers is piezoelectric ceramic/polymer composites. Piezocomposites having 2-2 or 1-3 connectivity are commonly used in ultrasonic medical applications. These combine the low acoustic impedance advantage of polymers with the high sensitivity and low electrical impedance advantages of ceramics.

The design frequency of a transducer depends on the penetration depth imposed upon by the application. Resolution is improved with increasing frequency. Although a high frequency transducer is capable of producing a high resolution image, higher frequency acoustic energy is more readily attenuated by the body. A lower frequency transducer is used as a compromise when imaging deeper structures. Most medical ultrasound imaging systems operate in the frequency range from 2 to 10 MHz and can resolve objects approximately 0.2 to 1 mm in size. At 3.5 MHz, imaging to a depth of 10 -20 cm is possible, while at 50 MHz, increased losses limit the depth to less than 1 cm. Higher-frequency transducers (10 - 50 MHz) are used for endoscope-based imaging and for catheter-based intravascular imaging. At a higher frequency over 100 MHz applications are being done in the field of ultrasound microscopy. The operating frequency of the transducer is directly related to the thickness and velocity of sound in piezoelectric materials employed. As frequency increases resonator thickness decreases. For a 3.5 MHz transducer, PZT ceramic thickness needs to be roughly 0.4 mm. Most conventional

ceramic transducers, such as PZT are limited to frequencies below nearly 80 MHz because of the difficulty of fabricating thinner devices. (20) For microscopic applications at a frequency over 100 MHz, corresponding to the thickness of less than 20 μm piezoelectric thin-film transducers such as ZnO have to be used. (21)

Actuators and motors

Actuators

Currently the other important applications of piezoelectric materials exist in actuator fields. (22) Actuators are defined as the transducers capable of transferring input energy into a mechanical output energy. Using the converse piezoelectric effect, small displacement can be produced by applying a field to a piezoelectric materials. Vibrations can be generated by applying an alternating field. In advanced precision engineering, the demand for a variety of types of actuators which can adjust positions precisely (micropositioning devices), suppress noise vibrations (dampers), or drive objects dynamically (ultrasonic motors) exist. These devices are used in broad areas including optics, astronomy, fluid control and precision machinery. For actuator applications, piezoelectric strain and electrostriction induced by an electric field are used. Especially, electrostrictive materials such as lead magnesium niobate [PMN] ceramics are preferred because of their little degradation under severe operating conditions. The PMN is easily

electrically poled when an electric field is applied around the transition temperature and depoled completely without any remanent polarization. This provides extraordinary large apparent electrostriction though it is a secondary phenomenon of the electromechanical coupling. Figure 6 shows the longitudinal induced strain curve at room temperature in 0.9PMN- 0.1PT. The magnitude of the electrostriction is 10^{-3} and this material has almost no hysteresis.

Figure 7 shows the design classification of ceramic actuators. Simple devices composed of a disk and multilayer type directly use the strain induced in a ceramic by the applied electric field. Complex devices do not use the induced strain directly but use the magnified displacement through a special magnification mechanism such as unimorph, bimorph and moonie. The most popularly used multilayer and bimorph types have the following characteristics: The multilayer type does not show a large displacement (10 μm), but has advantages in generation force (100 kgf), response speed (10 μsec), life time (10^{11} cycles) and the electromechanical coupling factor k_{33} (0.70). The bimorph type exhibits a large displacement (300 μm), but shows disadvantages in generation force (100 gf), response speed (1 msec), life time (10^{8} cycles) and the electromechanical coupling factor k_{eff} (0.10). For instance, in a 0.65 PMN- 0.35 PT multilayer actuator with 99 layers of 100-μm thick sheets ($2\times3\times10$ mm^3), a 8.7 μm displacement is generated by a 100 V voltage, accompanied by a slight hysteresis. The transmit response of the induced

displacement after the application of a rectangular voltage is as quick as 10 μsec. In conclusion, the multilayer exhibits the field induced strain of 0.1% along the length.

Unimorph and bimorph devices are defined by the number of piezoelectric ceramic plates: only one ceramic plate is bonded onto an elastic shim., or two ceramic plates are bonded together simultaneously. The bimorph causes bending deformation because each piezoelectric plate bonded together produces extension or contraction under an electric field. In general, there are two types of piezoelectric bimorph: antiparallel polarization type and parallel polarization type, as shown in Fig. 8. Two poled piezoelectric plates with $t/2$ in thickness and L in length are bonded with their polarization directions opposite or parallel to each other. In cantilever bimorph configuration whose one end is clamped, the tip displacement δ_z under an applied voltage V is provided as follows;

$$\delta_z = 3/2 \cdot d_{31} (L^2/t^2) V \quad \text{(antiparallel type)} \tag{9}$$

$$\delta_z = 3 d_{31} (L^2/t^2) V \quad \text{(parallel type)} \tag{10}$$

The resonance frequency f_r for both types is given by

$$f_r = 0.16\, t / L^2 (\rho S_{11}^{E})^{-1/2} \tag{11}$$

where ρ is density and S_{11}^{E} is elastic compliance. A metallic sheet (called shim) is occasionally sandwiched between the two piezoelectric plates to increase the reliability, that is, the structure can be maintained even if the ceramics fracture. Using the bimorph structure, a large magnification of the displacement is easily obtainable. However, the disadvantages include a low response speed (1 kHz) and low generative force.

A composite actuator structure called "moonie" has been developed to amplify the small displacements induced in a piezoelectric ceramic. The moonie consists of a thin multilayer element and two metal plates with a narrow moon-shaped cavity bonded together. This device has intermediate characteristics between the conventional multilayer and bimorph actuators; this shows an order of magnitude larger displacement (100 μm) than the multilayer, and much larger generative force (10 kgf) with quicker response (100 μsec) than the bimorph.

Some examples of applications of piezoelectric and electrostrictive actuators mentioned above are described below. The piezoelectric impact dot-matrix printer is the first mass-produced device using multilayer ceramic actuators. The advantage of the piezoelectric printer head compared to the conventional magnetic types are: low energy consumption, low heat generation and fast printing speed. The longitudinal multilayer actuators do not exhibit a large displacement and thus a suitable displacement magnification mechanism is necessary. The displacement induced in a multilayer actuator pushes up the force point, and its displacement magnification is carried out through hinge levers so as to generate a large wire stroke. When the displacement in the piezoactuator is 8 μm, the wire stroke of 240 μm can be obtained, that is the magnification rate is 30 times.

Bimorph structures are commonly used for VCR head tracking actuators, because of their large displacements. An auto tracking scan system uses the piezoelectric actuators so that the head follows the recording track even driven at both still and quick modes. As can be anticipated, the bimorph drive is inevitably accompanied by a torsional motion. To obtain a perfect parallel motion a special mechanism has to be employed. Piezoelectric bimorphs have also been used in gramophone pick-up cartridges and cantilever bimorphs with small masses attached to their free end can be used as accelerometers. Piezoelectric pumps for gas or liquid utilizing an alternating bending motion of bimorph have been developed for intravenous drip injection in hospitals and for medication dispensers in chemotherapy, chronic pain and diabetes. Piezoelectric fans for cooling electronic circuits are made from a pair of bimorphs which are driven out of phase so as to blow effectively. Furthermore, piezo-bimorph type camera shutters have been widely commercialized.

In optical control systems, lenses and mirrors require micropositioning and even the shapes of mirrors are adjusted to correct image distortions. For instance, a space qualified active mirror called articulating fold mirror utilizes six PMN electrostrictive multilayer actuators to precisely position a mirror tip and tilt in order to correct the focusing aberration of the Hubble Space Telescope.

Piezoelectric actuators are also useful for vibration suppression systems of an automobile. An electronic controlled shock absorber was developed by Toyota. The

piezoelectric sensors detecting a road roughness is composed of 5 layers of 0.5 mm thick PZT discs. The actuator is made of 88 layers of 0.5 mm thick discs. Applying 500 V generates about 50 μm displacement, which is magnified by 40 times through a piston and plunger pin combination. This stroke pushes the change valve of the damping force down, then opens the bypass oil route, leading to decrease in the flow resistance. This electronically controlled shock absorber has both controllability and comfortablility simultaneously.

Ultrasonic motors

An ultrasonic motor is an example of piezoelectric actuators using a resonant vibration. In ultrasonic motors linear motion is obtained from the elliptical vibration through frictional force. The motor basically consists of a high-frequency power supply, a vibrator and a slider. The vibrator is composed of a piezoelectric driving component and an elastic vibrator part, and the slider is composed of an elastic moving part and a friction coat. The characteristics of the ultrasonic motors are low speed and high torque compared to the conventional electromagnetic motors with high speed and low torque. (22)(24)

The ultrasonic motors are classified into two types: a standing-wave type and a propagating-wave type. The standing wave is expressed by

$$Vs\,(x, t) = A\cos(kx)\cdot\cos(\omega t), \tag{12}$$

while the propagation wave is given by

$$Vp\,(x, t) = A\cos(kx - \omega t)$$

$$= A\cos(kx)\cdot\cos(\omega t) + A\cos(kx - \pi/2)\cdot\cos(\omega t - \pi/2) \tag{13}$$

A propagating wave can be generated by superimposing two standing waves whose phases differ by 90 degree to each other both in time and in space. The standing-wave type is sometimes called as a vibratory-coupler or a "woodpecker" type, where a vibratory piece is connected to a piezoelectric driver and the tip portion generates flat-elliptic movement. Figure 9 shows a vibratory coupler type motor. A vibratory piece is attached to a rotor or a slider with a slight cant angle. The standing-wave type has high efficiency up to 98% theoretical. However, a problem of this type is lack of control in both clockwise and counter-clockwise directions. The principle of the propagation type is shown in Fig. 10. In the propagating-wave type, also called "surfing-type", in which a surface particle of the elastic body draws an elliptic locus due to the coupling of longitudinal and transverse waves. This type generally requires two vibration sources to generate one propagating wave, leading to low efficiency (not more than 50%), but is controllable in both the rotational directions. An ultrasonic rotatory motor is successfully used in autofocusing camera to produce precise rotational displacements. The advantages of this motor over the conventional electromagnetic motor are: silent drive (inaudible), thin motor design and energy saving.

Resonators and filters

When a piezoelectric body vibrates at its resonant frequency it absorbs considerably more energy than at other frequencies resulting in the fall of impedance. This phenomenon enables piezoelectric materials to be used as a wave filter. A filter is required to pass a certain selected frequency band or to stop a given band. The band width of a filter fabricated from a piezoelectric material is determined by the square of the coupling coefficient k, that is, nearly proportional to k^2. Quartz crystals with very low k value of about 0.1 can pass very narrow frequency bands of approximate 1% of the center resonance frequency. On the other hand, PZT ceramics with a planar coupling coefficient of about 0.5 can easily pass a band of 10% of the center resonance frequency. The sharpness of the passband is dependent on the mechanical quality factor Q_m of the materials. Quartz has also a very high Q_m of about 10^6 which results in a sharp cut-off to the passband and well-defined frequency of the oscillator.

A simple resonator is a thin disc type, electroded on its plane faces and vibrating radially for applications in filters with a center frequency ranging from 200 kHz to 1 MHz and with a bandwidth of several percent of the center frequency. For a frequency of 455 kHz the disc diameter needs to be about 5.6 mm. However, if the required frequency is higher than 10 MHz, other modes of vibration such as the thickness extensional mode are exploited, because of its smaller size disc. The trapped-energy type filters made from PZT ceramics have been widely used in the intermediate frequency range for such as 10.7

MHz for FM radio receiver and transmitter. By employing the trapped-energy phenomena, the overtone frequencies are suppressed. The plate is partly covered with electrodes of a specific area and thickness. The fundamental frequency of the thickness mode beneath the electrode is less than that of the unelectroded portion, because of the extra inertia of the electrode mass. The longer wave characteristic of the electrode region cannot propagate in the unelectroded region. The higher-frequency overtones can propagate away into the unelectroded region. This is called as trapped-energy principle. Figure 11 shows a schematic drawing of trapped-energy filter. In this structure the top electrode is split so that coupling between the two parts will only be efficient at resonance. More stable filters suitable for telecommunication systems have been made from single crystals such as quartz or $LiTaO_3$.

SAW devices

A surface acoustic wave (SAW) also called a Rayleigh wave is composed of a coupling between longitudinal and shear waves in which the SAW energy is confined near the surface. An associated electrostatic wave exists for a SAW on a piezoelectric substrate, which allows electroacoustic coupling via a transducer. The advantages of SAW technology are: the wave can be electroacoustically accessed and tapped at the substrate surface and its velocity is approximately 10^4 times slower than an electromagnetic wave. The SAW wavelength is on the same order of magnitude as line dimensions which can be

photolithographically produced and the lengths for both short and long delays are achievable on reasonable size substrates. (25)(26)

There are a very broad range of commercial system applications which include front-end and IF (Intermediate Frequency) filters, CATV (Community Antenna Television) and VCR (Video Cassette Recorder) components, synthesizers, analyzers and navigators etc. In SAW transducers, finger electrodes provide the ability to sample or tap the wave and the electrode gap gives the relative delay. A SAW filter is composed of a minimum of two transducers. A schematic of a simple SAW bi-directional filter is shown in Fig. 12. A bi-directional transducer radiates energy equally from each side of the transducer. Energy not being received is to be absorbed to eliminate spurious reflection.

Various materials are currently being used for SAW devices. The most popular single-crystal SAW materials are lithium niobate and lithium tantalate. The materials have different properties depending on the cut of the material and the direction of propagation. The fundamental parameters considered when choosing a material for a given device applications are SAW velocity, temperature coefficients of delay (TCD), electromechanical coupling factor and propagation loss. Surface acoustic waves can be generated and detected by a spatially periodic, interdigital electrodes on the plane surface of a piezoelectric plate. A periodic electric field is produced when an RF source is connected to the electrode, thus permitting piezoelectric coupling to a traveling surface

wave. If an RF source with a frequency, f, is applied to the electrode having periodicity, d, energy conversion from an electrical to mechanical form will be maximum when

$$f = f_0 = V_s / d \tag{14}$$

V_s is the SAW velocity and f_0 is the center frequency of the device. SAW velocity is an important parameter determining the center frequency. Another important parameter for many applications is temperature sensitivity. For example, the temperature stability of the center frequency of SAW bandpass filters is a direct function of temperature coefficient for the velocity and delay for the material used. The first-order temperature coefficient of delay is given by

$$(1/\tau)\cdot(d\tau / dT) = (1/L)\cdot(dL / dT) - (1/V_s)\cdot(dV_s / dT) \tag{15}$$

where $\tau = L / V_s$ is the delay time and L is the SAW propagation length. The surface wave coupling factor, k_s^2, is defined in terms of the change in SAW velocity which occurs when the wave passes across a surface coated with a thin massless conductor, so that the piezoelectric field associated with the wave is effectively shorted-circuited. The coupling factor, k_s^2, is expressed by

$$k_s^2 = 2\,(V_f - V_m) / V_f \tag{16}$$

where V_f is the free surface wave velocity, V_m the velocity on the metallized surface. In actual SAW applications, the value of k_s^2 relates to the maximum bandwidth obtainable and the amount of signal loss between input and output, determining the fractional bandwidth versus minimum insertion loss for a given material and filter. Propagation loss is one of the major factors that determine the insertion loss of a device and is caused by

wave scattering at crystalline defects and surface irregularities. Materials which show high electromechanical coupling factors combined with small temperature coefficients of delay are likely to be required. The free surface velocity, V_0, of the material is a function of cut angle and propagation direction. The TCD is an indication of the frequency shift expected for a transducer due to a temperature change and is also a function of cut angle and propagation direction. The substrate is chosen based on the device design specifications and includes consideration of operating temperature, fractional bandwidth, and insertion loss.

Piezoelectric single crystals such as 128°Y-X (128°-rotated-Y-cut and X-propagation) - $LiNbO_3$ and X-112°Y (X-cut and 112°-rotated-Y-propagation) - $LiTaO_3$ have been extensively employed as SAW substrates for applications in VIF filters. A c-axis oriented ZnO thin films deposited on a fused quartz, glass or sapphire substrate are also commercialized for SAW devices. Table 4 shows some important material parameters for some SAW materials.

Delay lines

A delay line can be formed from a slice of glass such as PbO or K_2O doped SiO_2 glass in which the velocity of sound is nearly independent of temperature. PZT ceramic transducers are soldered on two metallized edges of the slice of glass. The input

transducer converts the electrical signal to a shear acoustic wave which travels through the slice. At the output transducer the wave is reconverted into an electrical signal delayed by the length of time taken to travel around the slice. Such delay lines are used in color TV sets to introduce a delay of approximately 64 μsec and are also employed in videotape recorder.

Piezoelectric transformer

The transfer of vibration energy from one set of electrodes to another on a piezoelectric ceramic body can be used for voltage transformation. This device is called a piezoelectric transformer. Recently, the office automation equipments with liquid crystal displays are successively commercialized such as notebook type personal computers and car navigation systems. These equipments with a liquid crystal display require a very thin, no electromagnetic-noise transformer to start the glow of a fluorescent back-lamp. This application has recently accelerated the development of the piezoelectric transformers. Figure 13 shows a fundamental structure where two differently-poled parts coexist in one piezoelectric plate. The plate has electrodes on half its major faces and on an edge, which is then poled in its thickness direction at one end and parallel to the long axis over most of its length. A low-voltage AC supply is applied to the large-area electrodes at a frequency that excites a length extensional mode resonance. A high-voltage output can then be taken from the small electrode and one of the larger electrodes. After the proposal by C.A.

Rosen such as mentioned above, piezoelectric transformers with several different structures have been reported. A multilayer type transformers are proposed in order to increase the voltage rise ratio. The input part is of the multilayer structure with internal electrodes and the output electrodes are formed at the side surface of the half part of rectangular plate. This transformer uses piezoelectric transverse mode for the input and output part.

3220BI00.MWM

Bibliography

1. B. Jaffe, W. Cook and H. Jaffe, *Piezoelectric Ceramics*, London: Academic Press, 1971.
2. W. G. Cady, *Piezoelectricity*, New York: McGraw-Hill, Revised Edition by Dover Publications, 1964.
3. F. Jona and G. Shirane, *Ferroelectric Crystals*, London: Pergamon Press, 1962.
4. M. E. Lines and A. M. Glass, *Principles and Applications of Ferroelectric Materials*, Oxford: Clarendon Press, 1977.
5. IEEE Standard on Piezoelectricity, New York, IEEE, Inc., 1978.
6. Landold and Boernstein, *Numerical Data and Functional Relationships in Science and Technology: Crystal and Solid State Physics, vol.11,* Berlin: Springer-Verlag, 1979.
7. W. A. Smith, *Proc. SPIE - The International Society for Optical Engineering* 1733, 1992.
8. H. Takeuchi, S. Jyomura, E. Yamamoto and Y. Ito, *J. Acoust. Soc. Am.*, 74, 1114, 1982.
9. Y. Yamashita, K. Yokoyama, H. Honda and T. Takahashi, *Jpn. J. Appl. Phys.*, 20, Suppl. 20-4, 183, 1981.
10. Y. Ito, H. Takeuchi, S. Jyomura, K. Nagatsuma and S. Ashida, *Appl. Phys. Lett.*,

35, 595, 1979

11. R. E. Newnham, D. P. Skinner and L. E. Cross, *Materials Research Bulletin*, 13, 525, 1978.

12. W. A. Smith, *Proc. 1989 IEEE Ultrasonic Symposium*, 755, 1989

13. H. Takeuchi, H. Masuzawa, C. Nakaya and Y. Ito, *Proc. IEEE 1990 Ultrasonics Symposium*, 697, 1990.

14. T. R. Shrout, Z. P. Chang, N. Kim and S. Markgraf, *Ferroelectric Letters*, 12, 63, 1990.

15. J. Kuwata, K. Uchino and S. Nomura, *Jpn. J. Appl. Phys.*, 21, 1298, 1982.

16. B. A. Auld, *Acoustic Fields and Waves in Solids*, 2nd ed., Melbourne: Robert E. Krieger, 1990.

17. G. S. Kino, *Acoustic Waves: Device Imaging and Analog Signal Processing*, Englewood Cliffs, N. J.: Prentice-Hall, 1987.

18. C. S. Desilets, J. D. Fraser and G. S. Kino, *IEEE Trans. Sonics Ultrason.*, SU-25, 115, 1978.

19. T. R. Gururaja, *Am. Ceram. Soc. Bull.*, 73, 50, 1994.

20. F. S. Foster, L. K. Ryan and D. H. Turnbull, *IEEE Trans. Ultrason. Ferroelec. Freq. Cont.*, 38, 446, 1991.

21. Y. Ito, K. Kushida, K. Sugawara and H. Takeuchi, *IEEE Trans. Ultrason. Ferroelec. Freq. Cont.*, 42, 316, 1995.

22. K. Uchino, *Piezoelectric Actuators and Ultrasonic Motors*, Boston: Kluwer

Academic Publishers, 1997.

23. L. E. Cross, S. J. Jang, R. E. Newnham, S. Nomura and K. Uchino, *Ferroelectrics*, 23, 187, 1980.

24. S. Ueha and Y. Tomikawa, *Ultrasonic Motors*, Oxford, Clarendon Press, 1993.

25. C. Campbell, *Surface Acoustic Wave Devices and Their Signal Processing Applications*, San Diego, Calif. Avcademic Press, 1989.

26. H. Matthews, *Surface Wave Filters*, New York: Wiley Interscience, 1977.

3220FL00.MWM

Figure 1. Perovskite structure ABO_3.

Figure 2. Dielectric constants of $BaTiO_3$ as a function of temperature.

Figure 3. Phase diagram of the PZT system.

Figure 4. Piezoelectric d strain coefficients versus composition for the PZT system.

Figure 5. Prototype transducer geometry.

Figure 6. Strain of PMN as a function of electric field.

Figure 7. Structures of ceramic actuators.

Figure 8. Two types of piezoelectric bimorphs: (a) antiparallel polarization type and (b) parallel polarization type.

Figure 9. Vibratory coupler type ultrasonic motor.

Figure 10. Principle of the propagating wave type ultrasonic motor.

Figure 11. Trapped-energy type filter.

Figure 12. Typical SAW bi-directional filter consisting of two interdigital transducers.

Figure 13. Piezoelectric transformer

3220FG01MWM

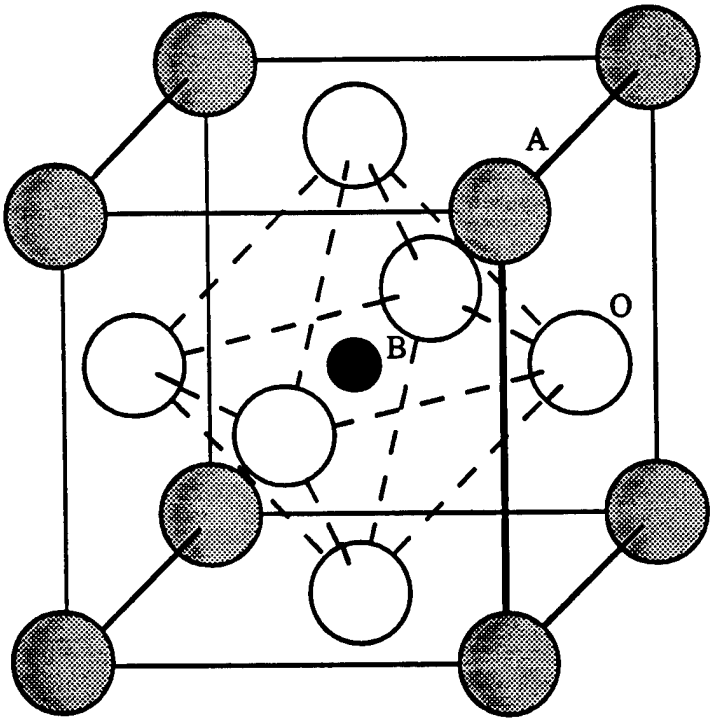

3220FG02MWM

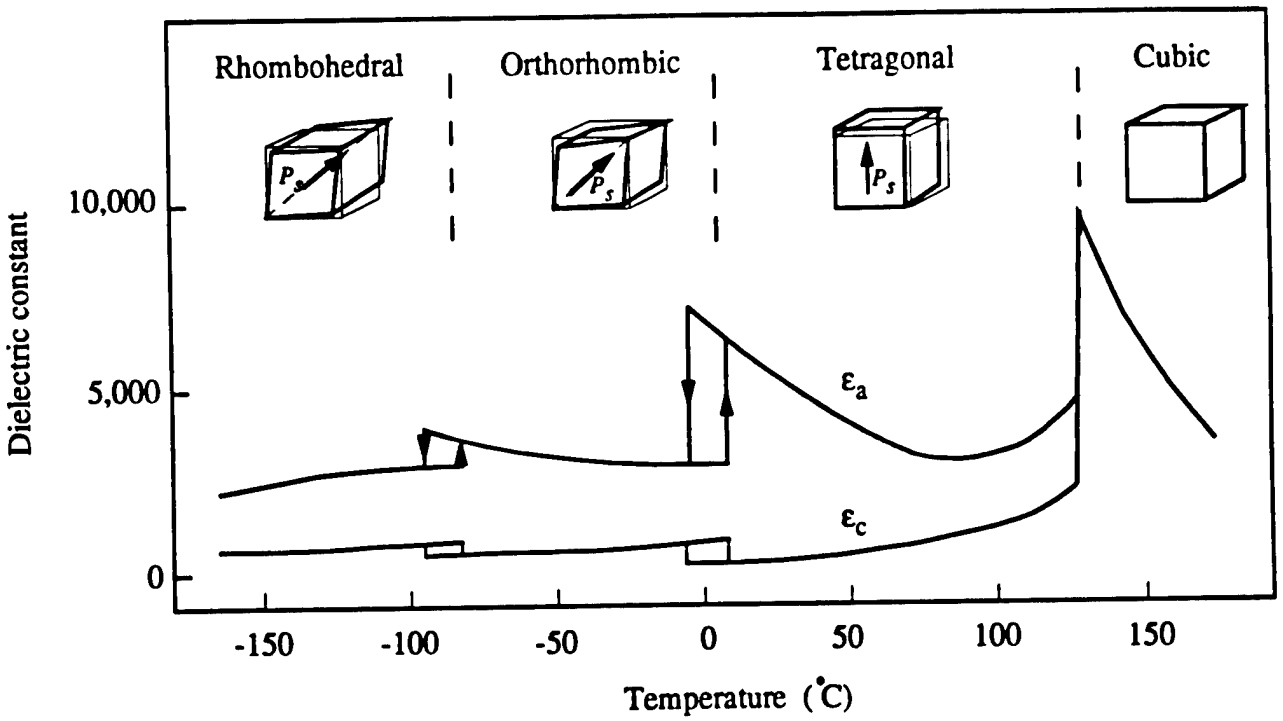

3220FG03MWM

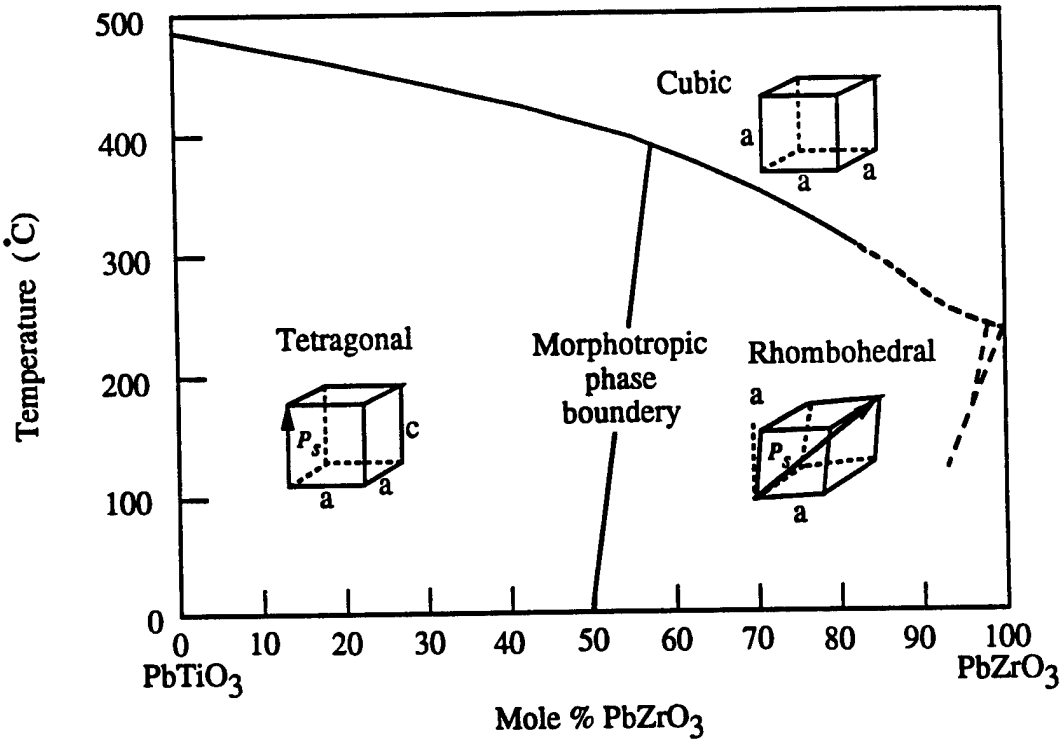

3220FG04MWM

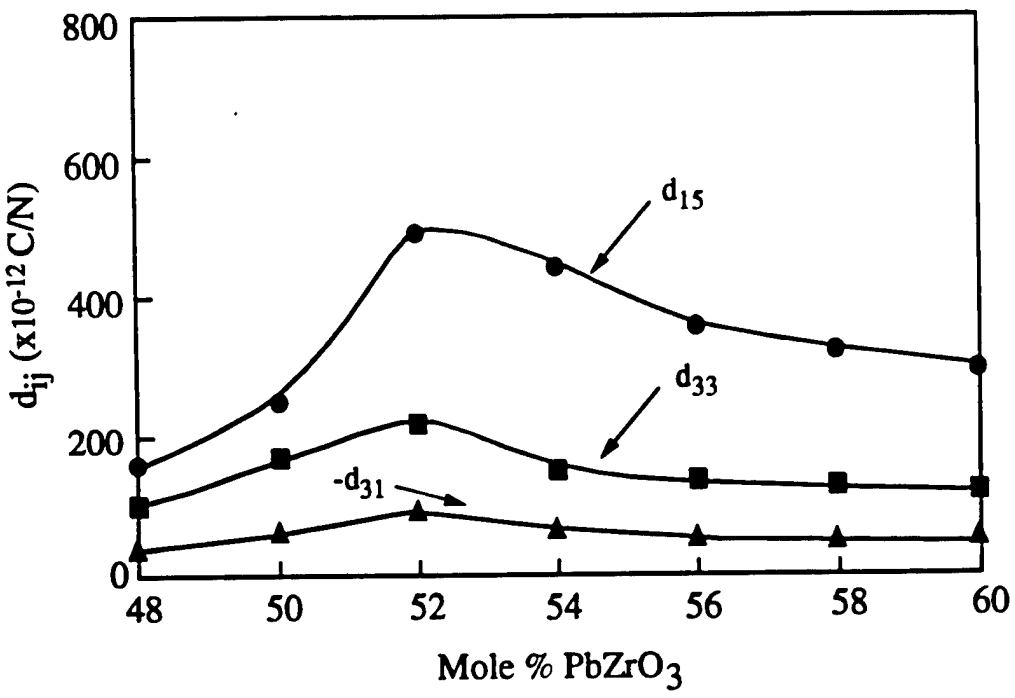

3220FG05.MWM

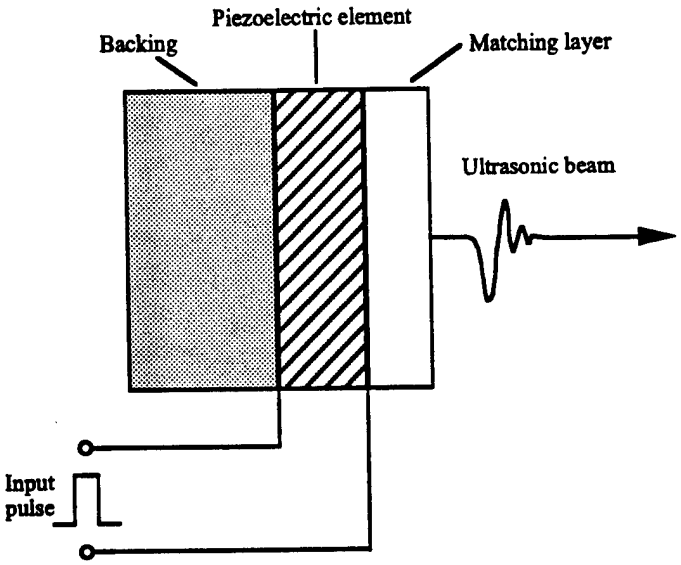

3220FG06MWM

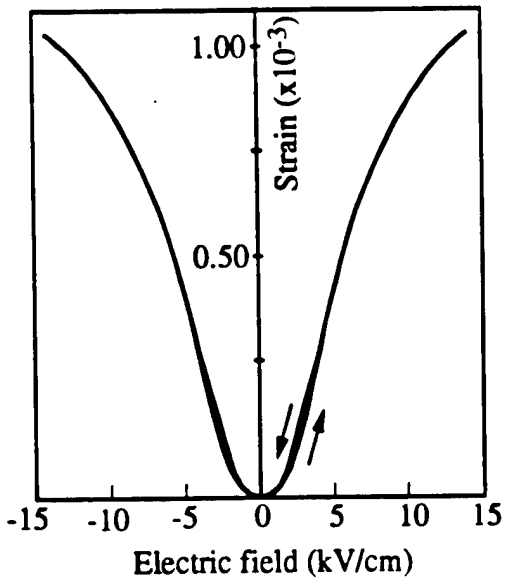

3220FG07.MWM

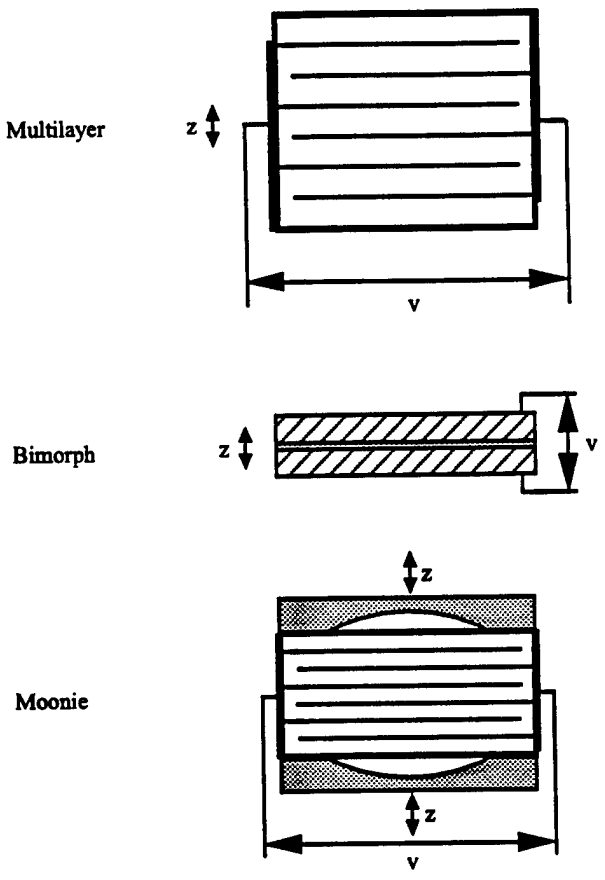

3220FG08.MWM

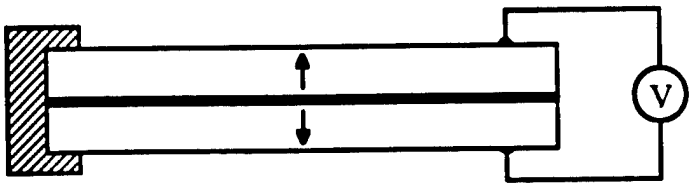

(a)

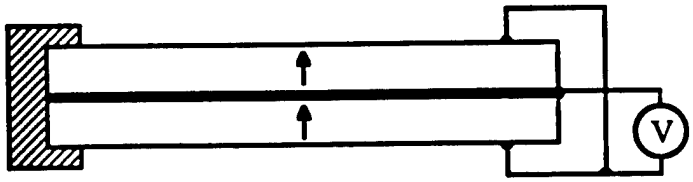

(b)

3220FG09.MWM

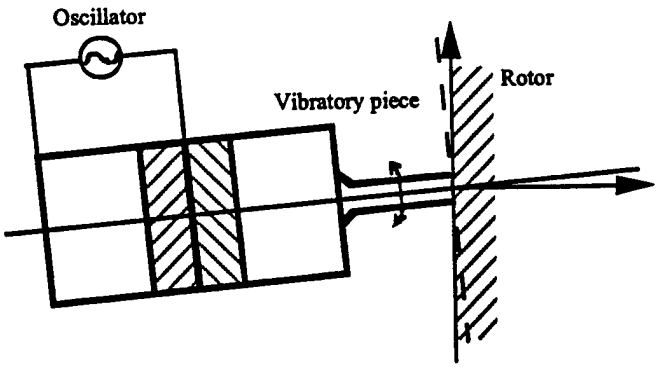

3220FG10MWM

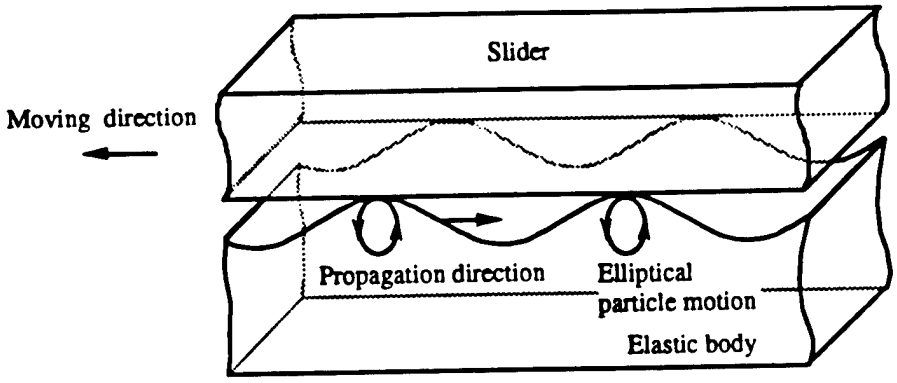

3220FG11.MWM

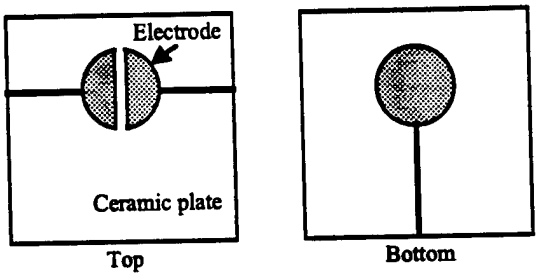

3220FG12.MWM

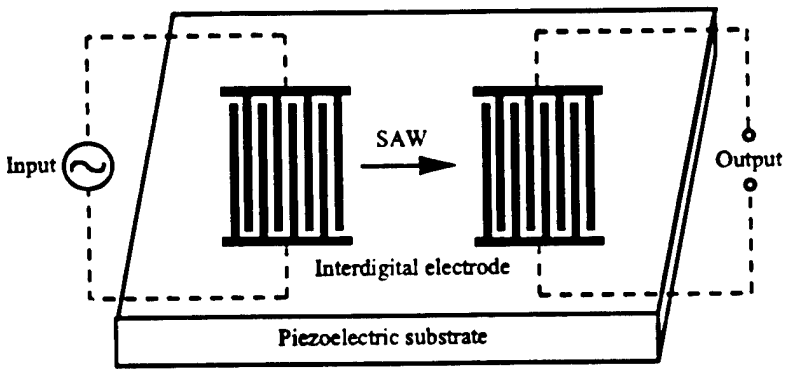

3220FG13.MWM

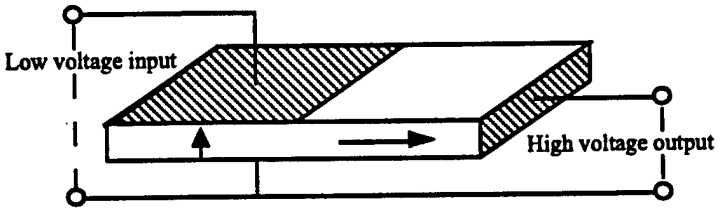

3220TB01.MWM

Table 1 Crystallographic classification in terms of polarity and centro-symmetry

Polarity	Symmetry	Crystal system										
		Cubic		Hexagonal		Tetragonal		Rhombo-hedral		Ortho-rhombic	Mono-clinic	Triclinic
Non-polar (22)	Centro (11)	m3m	m3	6/mmm	6/m	4/mmm	4/m	$\bar{3}$m	$\bar{3}$	mmm	2/m	
	Non-centro (21)	432	23	622	$\bar{6}$	422	$\bar{4}$	32		222		
		$\bar{4}$3m		$\bar{6}$m2		$\bar{4}$2m						
Polar (Pyroelectric) (10)				6mm	6	4mm	4	3m	3	mm2	2 m	1

Inside the bold line are piezoelectrics.

Table 2 Properties of piezoelectric materials

Parameter	Quartz	$BaTiO_3$	PZT 4	PZT 5H	$(Pb,Sm)TiO_3$	PVDF-TrFE
d_{33} (pC/N)	2.3	190	289	593	65	33
g_{33} (10^{-3}Vm/N)	57.8	12.6	26.1	19.7	42	380
k_t	0.09	0.38	0.51	0.50	0.50	0.30
k_p		0.33	0.58	0.65	0.03	
$\varepsilon_{33}{}^T/\varepsilon_0$	5	1700	1300	3400	175	6
Q_m	$> 10^5$		500	65	900	3 - 10
T_c(°C)		120	328	193	355	

Table 3 Comparison of ultrasonic transducer materials

	PZT ceramic	PVDF polymer	PZT-polymer composite	ZnO film
k_t	0.45 - 0.55	0.20 - 0.30	0.60 - 0.75	0.20 - 0.30
Z (Mrayls)	20 - 30	1.5 - 4	4 - 20	35
$\varepsilon_{33}^T/\varepsilon_0$	200 - 5000	10	50 - 2500	10
tanδ (%)	< 1	1.5 - 5	< 1	< 1
Q_m	10 - 1000	5 - 10	2 - 50	10
ρ (g/cm^3)	5.5 - 8	1 - 2	2 - 5	3 - 6

Table 4 SAW material properties

	Material	Cut - Propagation direction	k^2 (%)	TCD (ppm/ C)	V_0 (m/s)	ε_T
Single crystal	Quartz	ST - X	0.16	0	3158	4.5
	$LiNbO_3$	128°Y - X	5.5.	-74	3960	35
	$LiTaO_3$	X112°- Y	0.75	-18	3290	42
	$Li_2B_4O_7$	(110)-<001>	0.8	0	3467	9.5
Ceramic	PZT-$In(Li_{3/5}W_{2/5})O_3$		1.0	10	2270	690
	$(Pb,Nd)(Ti,Mn,In)O_3$		2.6	< 1	2554	225
Thin film	ZnO / glass		0.64	-15	3150	8.5
	ZnO / Sapphire		1.0	-30	5000	8.5

APPENDIX 2

Molecular Mechanisms in Smart Materials

Robert E. Newnham

The following is an edited version of the David Turnbull Lectureship address, given by recipient Robert E. Newnham at the 1996 MRS Fall Meeting. Newnham received the lectureship for "pioneering the field of ceramic composites for electronic and optical applications, and in recognition of a distinguished career of guiding students, lecturing, and writing." Newnham is the Alcoa Professor of Solid State Science at The Pennsylvania State University.

Introduction

It is a great honor to be named the Turnbull Lecturer of the Materials Research Society. Thirty years ago, David Turnbull was a professor at Harvard University, and I was a young professor at Massachusetts Institute of Technology. He and I share a common interest in phase transformations, an underlying theme of this lecture. Professor Turnbull's papers and the Solid State Physics Series he edited with Frederick Seitz are classics in the field. I refer you to his review entitled "Phase Changes [1] for a deeper understanding of today's subject.

The outline of my talk is as follows: I will begin with a brief introduction of what is meant by smart, very smart, and intelligent materials, differentiating the role of sensing, actuating, and signal processing. I will then cover a few of the applications, followed by a discussion of the atomic mechanisms important in piezoelectrics, electrostrictors, magnetostrictors, and shape-memory alloys. I then summarize the common themes for these mechanisms, and end with a few thoughts about biomimetic design and functional composites, as well as a glimpse of the future as typified by thin-film sensors and actuators. .

The concept of a smart material is exemplified by a videotape-head positioner (Figure 1). Bimorph piezoelectric ceramics are usually made from lead zirconate titanate (PZT). The positioner has large actuator electrodes that move the material, as well as smaller electrodes to sense the position and orientation of the tape head. This combination of sensing and actuating mimics two of the functions of a living system—namely being aware of the surroundings and being able to respond to that signal with a useful response, usually in the form of a motion. A smart material is not simply a sensor. A sensor receives a stimulus and responds with a signal. A smart material is not simply an actuator either. An actuator produces a useful motion or action. **Smart materials function as both sensors and actuators.** Smart materials sometime have a control system and sometimes not. Some function like our spinal cord in that they are **passively smart** and respond without thought- or signal-processing. They are analogous to the reflex responses of the human body.

In other cases, smart materials analyze the sensed signal, perhaps for its frequency components, and then make a choice as to what type of response to make. We call that an **actively smart system.** We have also been developing a family of **very smart materials**—I am not willing to call them intelligent—which have a learning or tuning function, making it possible for them to get slightly smarter with age.[2] Nonlinear properties like electrostriction or higher order elastic constants are used in these materials.

Looking ahead to the use of thin-film microelectromechanical systems (MEMS), more intelligent materials are coming on the scene that integrate the control system with the sensors and actuators, all in one common piece of material. At this stage, I think the system deserves the name **intelligent.** Perhaps someday we will manufacture **wise** materials that make correct moral decisions. Perhaps they will evolve in some way like living systems. A few forecasts for smart systems appear in Table I.

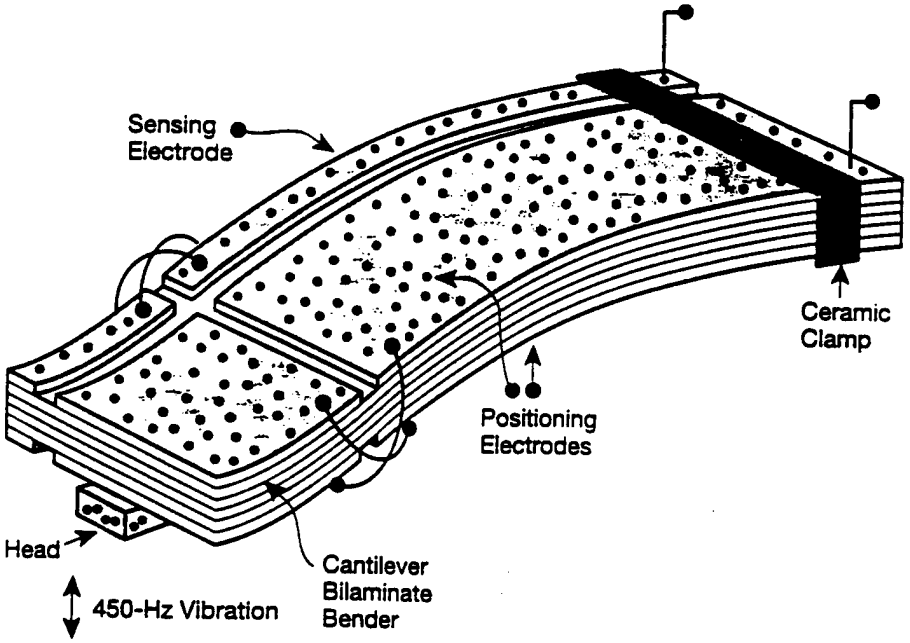

Figure 1. A videotape-head positioner senses and follows the tape track path. Using the direct and converse piezoelectric effects, the lead zirconate titanate bender acts as a smart material with separate electrodes for sensing and actuating. Articulation keeps the head perpendicular. Automatic scan tracking used.

Recent work on smart ceramics[3] and on various types of actuator materials[4] appears in the literature. Vibration suppression as in the smart shock absorber is the chief focus. Inside the smart absorber developed by Toyota,[5] a multilayer piezoelectric ceramic exists that has about five layers for sensing road vibrations. The multilayer stacks positioned near each wheel of the auto also have about 100 layers that act as the actuator, all part of the same PZT ceramic. After analyzing the vibration signals, a voltage is fed back to the actuator stack, and a response occurs by pushing on the hydraulic system of the auto to enlarge the motion. In this way, the auto is able to analyze acceleration signals from road bumps and respond with a motion that cancels the vibration. This is the Toyota Electronic Modulated System that produces force in the kilonewton range and displacements in the micron range.

Molecular Mechanisms

Rather than continuing with applications, I will now shift to the underlying structure-property relationships in smart materials. First I will provide a summary, giving you the main idea of my presentation.

All of these materials have at least two phase transitions. When described in terms of a thermodynamic function, two ordering parameters exist. The situation is similar to the feldspar crystals I studied as a student at Cambridge University many years ago. There are two transformations in this family of minerals: one due to an ordering of the aluminum and silicon atoms, and another arising from a ferroelastic transition caused by a distortion of the silicate network. A strong interaction between the two ordering parameters takes place in calcium and sodium feldspar.[7]

Similar phenomena are found in all four major families of smart materials. Nitinol and other shape-memory alloys have a broad phase transition with partially ordered cesium chloride-like structures transforming to a martensitic-like phase of lower symmetry. Like the feldspars, both atomic ordering and atomic displacements are involved. In lead magnesium niobate (PMN), an outstanding electrostrictive material, a similar diffuse phase transition from a partially ordered high-temperature state to a ferroelectric low-temperature state exists. Lead magnesium niobate is a ferroelectric analogue to ferroelastic Nitinol.

Terfenol is a typical magnetostrictive actuator with strong coupling between magnetic field and mechanical motion. It is an iron-rare-earth alloy with a paramagnetic to ferrimagnetic phase change at high temperature. Magnetostrictive actuators operate near a second phase transformation where the magnetic spins undergo reorientation to different crystallographic directions. In piezoelectric PZT, the best known of the actuator materials, there are similar changes in symmetry. Lead zirconate titanate is cubic at high temperatures and then is operated near a boundary between rhombohedral and tetragonal states. Terfenol is a magnetic analogue to ferroelectric PZT.

Table I: Top 10 Forecasts by the World Future Society for the Coming Decade.*

- Cash will disappear (smart cards)
- Electronic immigration (lone eagles).
- Robots smarter than humans (inorganic evolution).
- Prisons outmoded by implants (automated parole).
- Voice-driven furniture (smart chairs).
- Population shifts north (smart houses).
- Defective gene replacement (nanosensors and nanoactuators).
- Collision avoidance systems (smart automobiles).
- Older generation families (smart medical-delivery system).
- Automatic gardens (just-in-time farming)

*Several involve the use of smart materials with sensing and actuating capabilities

Ferroelectrics

To illustrate the behavior of piezoelectric and electrostrictive actuators, we have chosen $Pb(Zr,Ti)O_3$ and $Pb(Mg,Nb)O_3$, usually referred to as PZT and PMN, respectively. Lead zirconate titanate is a well-behaved normal ferroelectric with a large spontaneous polarization appearing at the Curie temperature. Lead mag-

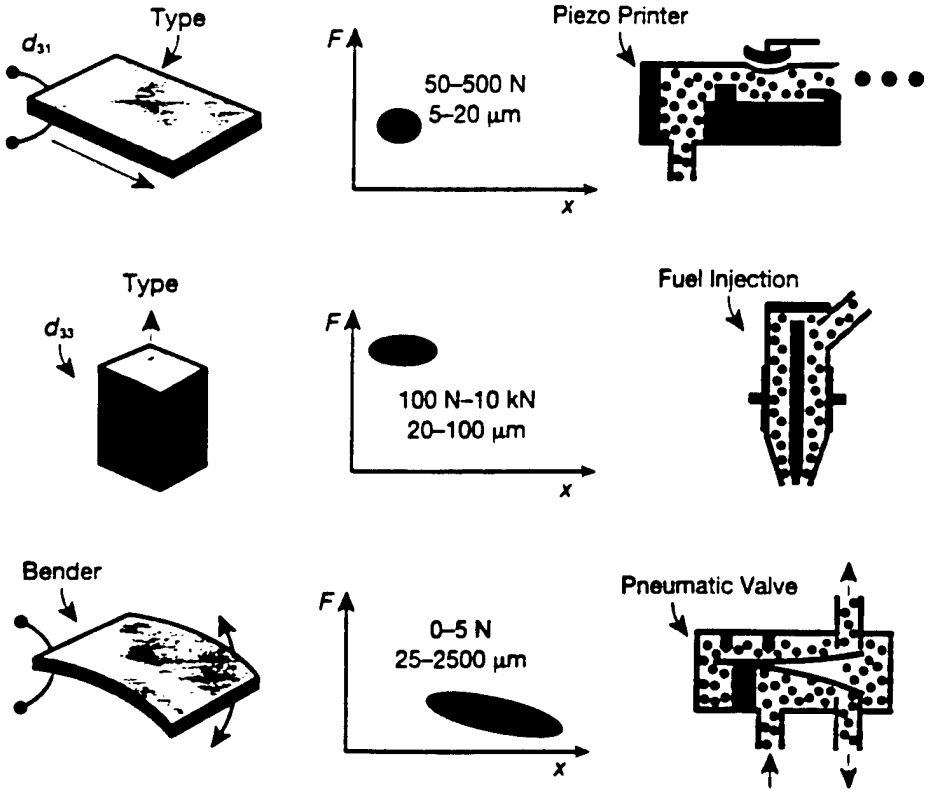

Figure 2. Ceramic multilayer actuators consist of thin layers of piezoelectric ceramic and metal electrodes. In contrast to traditional piezoceramics, even low voltages produce large forces and substantial displacements. A tradeoff exists between force and displacement. The multilayer stack utilizing the d_{33} coefficient gives kilonewton forces capable of pushing heavy weights through small distances. Bimorph benders make use of the smaller transverse d_{31} coefficient to give larger displacements in the millimeter range. (Figure courtesy of Philips Components, Roermond, Netherlands.)

nesium niobate is a relaxor ferroelectric with a partially ordered perovskite structure and a broad, diffuse phase transition. Very large dielectric constants and electrostriction coefficients are observed in this temperature range.

The multimillion-dollar market for PZT multilayer actuators includes d_{33} thickness mode transducers, d_{31} transverse mode transducers, and bender types. Typical applications, forces, and displacements for these three families of multilayer actuators appear in Figure 2. Each actuator has about a hundred layers and overall dimensions in the millimeter to centimeter range. Piezoelectric printers, fuel injectors, and pneumatic valves are well-developed markets for these multilayer actuators.

Multilayer actuators make use of ferroelectric oxides such as PZT and PMN with the perovskite structure. Ferroelectric oxides with the perovskite, tungsten bronze, pyrochlore, and bismuth titanate layer structures all have high dielectric constants, high refractive indices, and large electromechanical coupling coefficients, and all contain corner-linked octahedral networks of Ti^{4+}, Nb^{5+}, or other d^0 ions. These transition-metal elements are the highly polarizable "active" ions promoting ferroelectricity, and the high permittivities and piezoelectric constants required for transducers and capacitors.[7] With reference to the periodic system, there are two major groups of active ions, and both are near electronic "crossover" points where different types of atomic orbitals are comparable in energy and where hybrid bond formation is prevalent. The first group, typified by Ti^{4+}, Nb^{5+}, and W^{6+}, consists of d^0 ions octahedrally coordinated to oxygen. For Ti^{4+} the electronic crossover involves the $3d$, $4s$, and $4p$ orbitals, which combine with the σ and π orbitals of its six O^{2-} neighbors to form a number of molecular orbitals for the $(TiO_6)^{8-}$ complex. The bond energy of the complex can be lowered by distorting the octahedron to a lower symmetry. This leads to molecular dipole moments, ferroelectricity, large dielectric constants, piezoelectricity, and electrostriction. A second group of active elements contributing to polar distortions in ceramic dielectrics are the lone-pair ions having two electrons outside a closed shell in an asymmetric hybrid orbital. Among oxides the most important of these lone-pair ions are Pb^{2+} and Bi^{3+}, which are involved in a number of ferroelectrics ($PbTiO_3$, $Bi_4Ti_3O_{12}$, $PbNb_2O_6$) with high Curie temperatures. In many of these compounds, Pb^{2+} and Bi^{3+} are in pyramidal coordination with oxygen and therefore contribute to the spontaneous polarization.

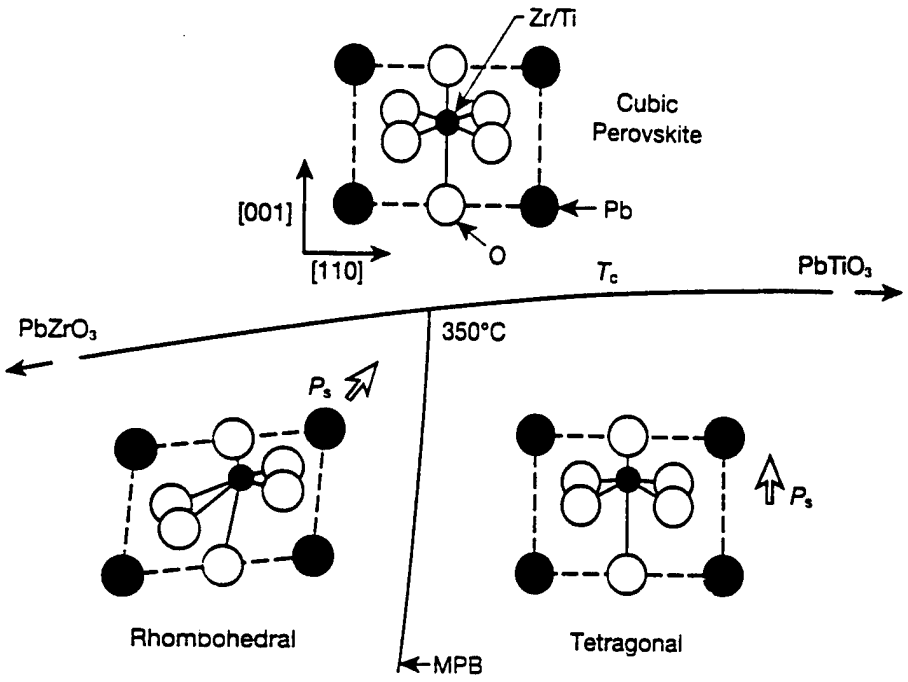

Figure 3. A portion of the $PbZrO_3$-$PbTiO_3$ phase diagram showing the structure changes at the Curie temperature (T_c) and the morphotropic phase boundary. Compositions near morphotropic phase boundary have 14 possible poling directions.

Piezoelectric PZT

Most piezoelectric-transducer formulations are based on $Pb(Zr,Ti)O_3$, one of a number of ferroelectric substances crystallizing with the perovskite structure.[7] Lead atoms appear at the corners of the unit cell and oxygens at the face centers. Both lead and oxygen ions have radii of about 1.4 Å. Together they make up a face-centered-cubic array, having a lattice parameter near 4 Å. Octahedrally coordinated titanium or zirconium ions are located at the center of the unit cell.

On cooling from high temperature, the crystal structure of PZT undergoes a displacive phase transformation with atomic displacements of about 0.1 Å. For titanium-rich compositions, the point symmetry changes from cubic m3m to tetragonal 4mm at the Curie temperature. The tetragonal state with its spontaneous polarization along [001] persists to 0 K. The structural changes appear in Figure 3.

To make use of these piezoelectric ceramics with their large polarizations, compositions near a second phase transition are chosen. At the Curie point, PZT converts from a paraelectric state with the ideal cubic perovskite structure to a ferroelectric phase located near a morphotropic phase boundary between the tetragonal and rhombohedral states. Very large piezoelectric coupling between electric and mechanical variables is obtained near this phase boundary. Much of the current research in this field involves looking for other morphotropic phase boundaries to further enhance the electromechanical-coupling factors.

The two effects utilized in PZT transducers are the direct and the converse piezoelectric effect. The direct effect relates polarization to stress and is used in sensors. The converse effect relates strain to electric field and is used in actuators.

For a poled ceramic having symmetry ∞m, d_{31}, d_{33}, and d_{15} are the appropriate tensor coefficients. Both intrinsic and extrinsic contributions to these piezoelectric coefficients exist. The intrinsic effects coming from the distortions of the crystal structure under mechanical stress appear in Figure 4. Under mechanical stress parallel to the dipole moment, there is an enhancement of the spontaneous polarization P_s along x_3. When stress is applied perpendicular to that dipole moment, electric charges develop transversely. These are the d_{33} and d_{31} effects, respectively. When the dipole is tilted by shear stress, charges appear on the side faces, the d_{15} coefficient. There are ex-

trinsic contributions to the piezoelectric coefficient as well. These can be extremely large, often involving the domain-wall motions.

Ferroelectric ceramics such as PZT do not become piezoelectric until electrically poled. Poling occurs under intense electric fields at elevated temperatures below the ferroelectric Curie point where the domains are easily aligned.

Titanium-rich compositions in the PZT system favor a tetragonal modification with sizable elongation along [001] and a large spontaneous polarization in the same direction. There are six equivalent polar axes in the tetragonaphase corresponding to [100], [$\bar{1}$00], [010], [0$\bar{1}$0], [001], and [00$\bar{1}$] directions of the cubic paraelectric state. A rhombohedral ferroelectric state is favored for zirconium-rich compositions. Here the distortion and polarization are along [111] directions, giving rise to eight possible domain states: [111], [$\bar{1}$11], [1$\bar{1}$1], [11$\bar{1}$], [1$\bar{1}\bar{1}$], [$\bar{1}\bar{1}$1], [$\bar{1}$1$\bar{1}$], and [$\bar{1}\bar{1}\bar{1}$].

The compositions that pole best lie near the morphotropic boundary between the rhombohedral and tetragonal ferroelectric phases. For these compositions, there are 14 possible poling directions over a very wide temperature range. This explains in part why the ceramic piezoelectric coefficients are largest near the morphotropic boundary. Phase changes between the rhombohedral and tetragonal phases also occur during the poling process.

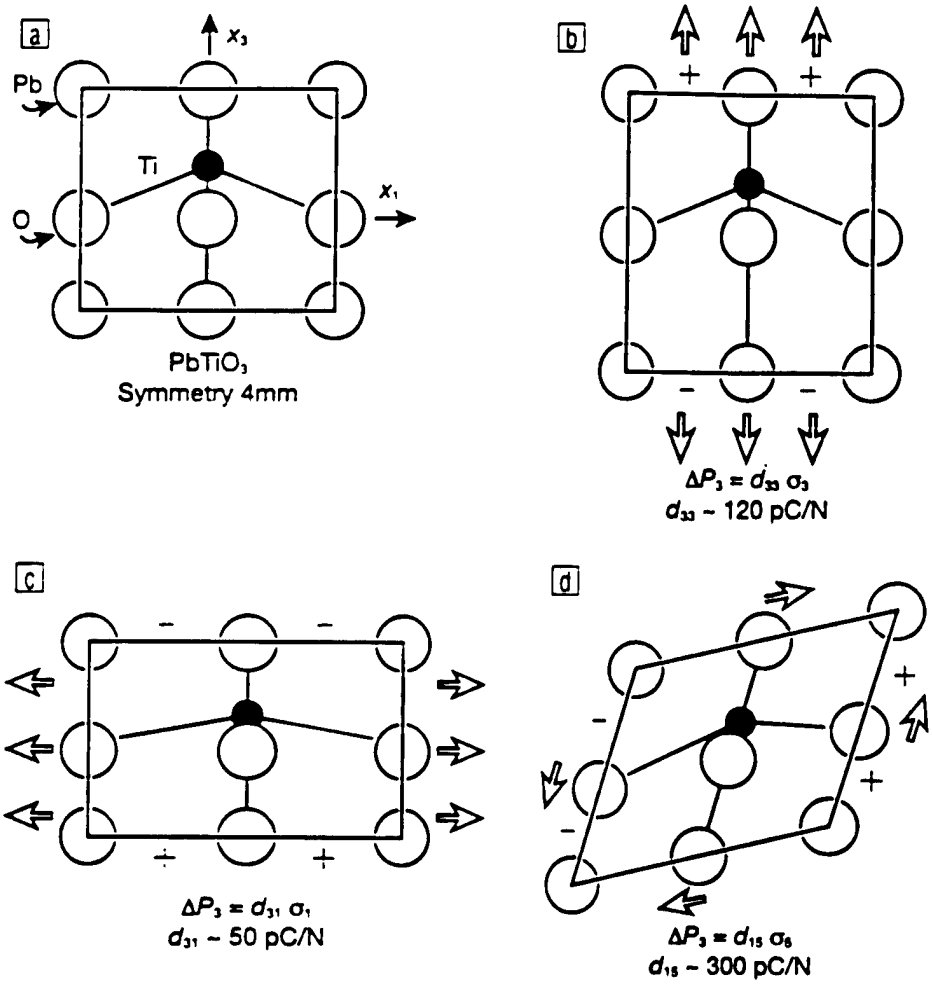

Figure 4. Intrinsic piezoelectric effect in polar lead titanate.

Electrostrictors

Piezoelectricity is a third-rank tensor relating strain and electric field. Electrostriction is a fourth-rank tensor relating strain to the square of the electric field.

Above the Curie temperature, the perovskite structure is cubic, and the electrostriction effect is more important than the piezoelectric effect because third-rank tensors disappear in centrosymmetric media. This leads to what we call very smart ceramics. In a smart ceramic, the direct piezoelectric effect is used for sensing, followed by feedback through the converse piezoelectric effect. In a very smart material, we monitor the change in capacitance of the material. We then monitor feedback with both direct-current (dc) and alternating-current (ac) fields to tune the magnitude of the electromechanical-coupling coefficient and then to drive it. For higher order coupling coefficients like electrostriction, there are three rather than two coupled effects: the change in the dielectric constant with stress, the field dependence of the piezoelectric voltage coefficient, and the electrically driven mechanical strain. The electrostrictive ceramic becomes a tunable transducer.[2]

We began work on a number of these electrostrictive materials nearly 20 years ago[9] for active optic systems. Much of this work took place with the ITEK Corporation in Lexington, MA. During the Cold War, there were many satellites flying over what was then the Soviet Union, utilizing active optic systems to eliminate atmospheric turbulence. In adjusting the position of optical components, electrostrictive materials have an advantage over piezoelectrics because there is much less hysteresis associated with the motions.

Work on active optic systems has continued over the years, and similar multilayer actuators were used to correct the positioning of the optical elements in the Hubble telescope. Supermarket scanners use actuators and flexible mirrors to optically interrogate bar codes.[10]

Relaxor Ferroelectrics

Ordered perovskites generally have low dielectric constants because the linkage between "active" ions is severed. In partially disordered structures such as the relaxor ferroelectrics, the dielectric constant can be extremely large, making them useful as capacitor dielectrics and as electrostrictive actuators. The most widely used compositions are modifications of lead magnesium niobate, $Pb_3MgNb_2O_9$.

Relaxor ferroelectrics consist of temperature-sensitive microdomains resulting from the many different "active" ion linkages in the disordered octahedral framework. Each NbO_6 octahedron may bond to anywhere from 0 to 6 other NbO_6 octahedra. Connections between these octahedra are essential to ferroelectricity and high dielectric-constant K values. As temperature decreases from the high-temperature paraelectric state, ferroelectric microdomains gradually co-

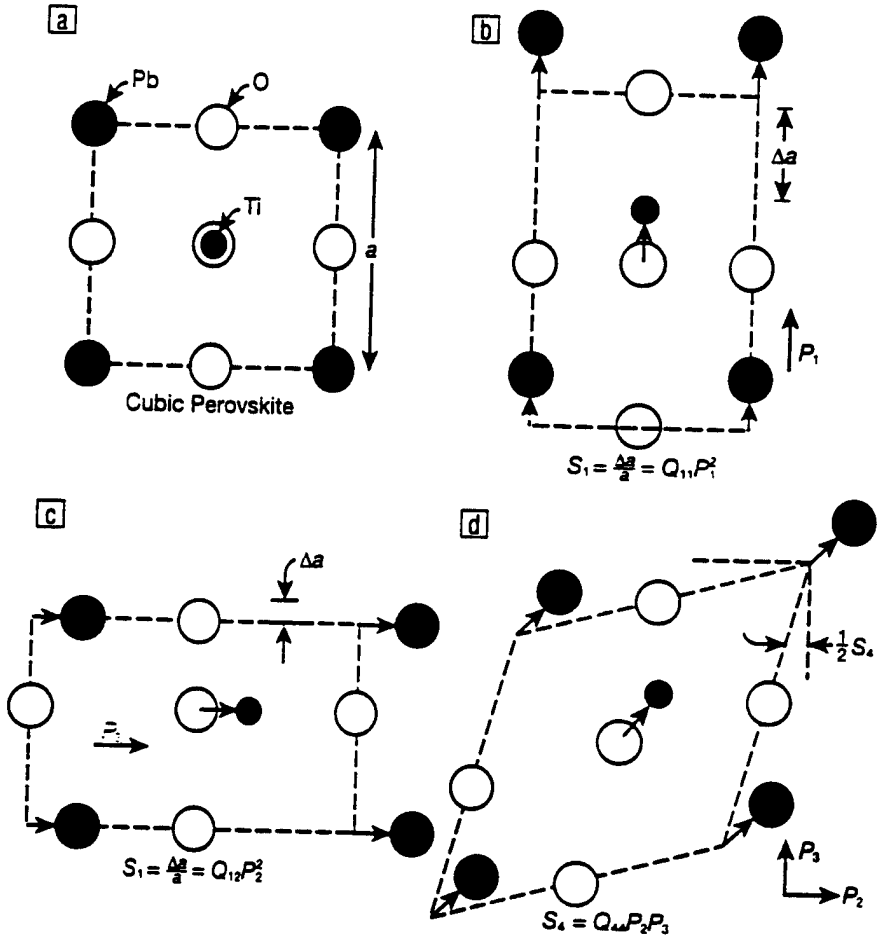

Figure 5. Electrostriction in cubic perovskite, showing the physical origin of electrostrictive coefficients Q_{11}, Q_{12}, and Q_{44}.

alesce to macrodomains, giving rise to a diffuse phase transformation. These polarization fluctuations are also dependent on bias field and measurement frequency. The dielectric constant drops off rapidly with frequency (hence the name "relaxor") because it takes time for the polarization fluctuations to respond. Direct-current bias fields favor coalescence, giving the same effect as results from lowering the temperature.

Relaxor behavior is very common among Pb-based perovskites, suggesting that Pb^{2+} and its "lone-pair" electrons play a role in the microdomain process, possibly by adjusting the orientation of the lone pair.

Electrostriction is a 6 × 6 matrix, relating strain to the square of the electric polarization. This type of matrix is familiar to most materials scientists because electrostriction is a fourth-rank tensor almost identical in form to elasticity. For a cubic crystal, we deal with the same coefficients—11, 12, and 44—that would normally be used to describe the elastic properties of a cubic crystal. In this case, strain is induced electrically rather than mechanically.

Compared to piezoelectricity, which utilizes a polar material, electrostrictive transducers use a cubic material, a material poised on an instability with microregions fluctuating in polarization. On the average, the atoms reside in the ideal cubic sites but are continually shifting off these positions. An atomic view of the Q_{11}, Q_{12}, and Q_{44} motions[2] in an electrostrictive material appears in Figure 5. The underlying origin of these effects is a partial ordering of the PMN perovskite structure, in which the niobium and the magnesium atoms of PMN alternate in position but only over short ranges, typically 30–50-Å units—just a few unit cells. Within these ordered islands, fluctuating dipoles exist that are acted upon by an external field to make large electrostrictive motion.

Magnetostrictive Actuators

Lead zirconate titanate and PMN ceramics are outstanding ferroelectric actuators, but equally interesting developments are taking place in ferroelastic and ferromagnetic materials. All these ferroic materials have a domain structure in which the walls can be moved with electric fields, magnetic fields, or mechanical stresses.

Magnetostrictive alloys like Terfenol-D ($Tb_{1-x}Dy_xFe_2$) function well as both sensors and actuators.[11] High-power actuators can deliver forces greater than 50 MPa with strains up to 0.6% while magnetostrictive sensor materials can provide hundreds of times the sensitivity of semiconductor strain gauges. Magnetoelastic materials also have tunable elastic moduli that can be controlled by external magnetic fields.

A large number of magnetomechanical transducers and actuators utilizing Terfenol-D have been designed and manufactured. The high-energy density of these actuators, plus their ruggedness and reliability, make them attractive for vibration suppression and high-power sonar. Thin films of magnetostrictive iron-rare-earth alloys can be sputtered on silicon and patterned by etching or sputtering through masks. Micropump and microvalve membranes and cantilevers appear to be promising MEMS components.[12]

The rare-earth atoms in Terfenol have large orbital moments that interact with fields to give large magnetostrictive strains. Rotation of the magnetization is largely responsible for the shape change. The symbol λ denotes the saturation strain. The field-induced strain in Terfenol D is about a hundred times larger than those in iron and nickel.

The iron in Terfenol produces the high Curie temperature. The rare-earth terbium and dysprosium atoms produce the large magnetostriction. In combination these three elements produce the useful alloys. What I wish to point out here is the analogy to PZT. Plotted in Figure 6 is a portion of the magnetic phase diagram of the material. It is cubic and paramagnetic at high temperature, and then undergoes a magnetic phase transformation to a rhombohedral structure with magnetic spin parallel to ⟨111⟩ directions. Near room temperature, it is poised on an instability with the spins ready to reorient into the tetragonal directions, the former ⟨100⟩ directions of the cube. There is a complex domain structure both above and below the transition. Like PZT it is poised on a rhombohedral-tetragonal phase boundary. The phase diagram of Terfenol has the magnetic equivalent to the morphotropic boundary of PZT.

The figure of merit for magnetostrictive actuators is proportional to the saturation strain coefficient. In addition to a large shape change, the strain must be easy to move. Therefore the anisotropy coefficient κ, which controls the rotation of the magnetization, also comes into the figure of merit λ/k. $TbFe_2$ has a very large λ coefficient but also has a large anisotropy constant k, which reduces the figure of merit. $DyFe_2$ has an anisotropy coefficient of opposite sign. By tuning the composition to be near the point where the anisotropy coefficient goes to zero, one can make an easily movable strain in this magnetostrictive alloy. This maximizes the figure of merit.

Figure 7 shows the two magnetic phase changes for Terfenol-D. At high temperature, it is paramagnetic. Below T_c near 700 K, the spins are aligned along a [111] direction, giving a rhombohedral distortion of the unit cell. The strong antiferromagnetic interactions between the iron and rare-earth spins make the alloy ferrimagnetic rather than ferromagnetic. Near room temperature, there is a spin reorientation to the tetragonal ⟨100⟩ directions of the cube. The magnetic point group changes from 3 m′ (the prime indicating a time reversal operator) to 4/mm′m′.

An explanation of the large magnetostrictive effect in $TbFe_2$ and iron-rare-earth intermetallic compounds has been put forward by Clark and co-workers.[13] Pure rare-earth metals possess large magnetostrictive strains but are not used as actuators because of their low Curie temperatures. When alloyed with iron however, the RFe_2 compounds are magnetic at room temperature with T_c values near 700 K.

The large magnetostriction coefficients are caused by the orbital motion of the rare-earth 4*f* electrons, which impart a shape anisotropy to the atoms. Trivalent terbium and dysprosium ions resemble flattened oblate ellipsoids while erbium, samarium, and thulium have elongated prolate shapes. Under strong magnetic fields, the magnetization rotates to a new orientation and is accompanied by a shape change.

The resulting magnetostrictive strain is especially large for RFe_2 compounds with the cubic Laves C15 structure. The structure distorts to a pseudocubic ferrimagnetic phase below the Curie temperature with the iron sublattice magnetization opposed to that of the rare earths. At room temperature, the preferred directions for magnetization are the six ⟨100⟩ cube axes for domains in $DyFe_2$. For $TbFe_2$ the eight ⟨111⟩ body diagonals are the easy axes of magnetization.

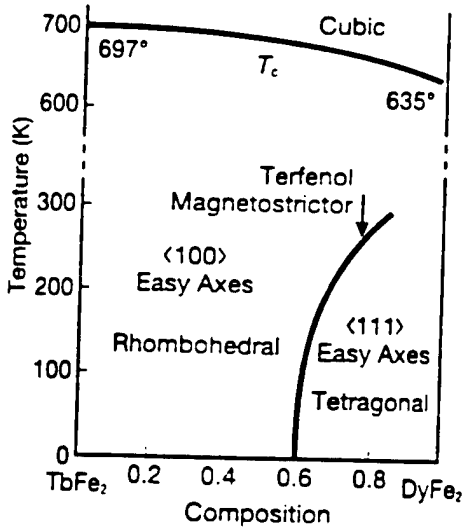

Figure 6. Binary phase diagram for the $Tb_{1-x}Dy_xFe_2$ system. Compositions near the magnetic spin boundary at $x = 0.7$ are used in magnetostrictive applications.[14] Courtesy of A.E. Clark.

The magnetostriction coefficients are largest for the rhombohedrally distorted alloys with ⟨111⟩ easy axes. This can be understood by examining the crystal structure. In the C15 structure, the rare-earth ions form a diamondlike lattice in which each rare-earth atom is bonded along ⟨111⟩ directions to four other rare earths. When a magnetic field is applied along [111] and the RFe_2 compound magnetizes in this direction, there is a redistribution of electron density, and a change in the R–R bonding. For oblate atoms like terbium, the bonds along $[1\bar{1}\,\bar{1}]$, $[\bar{1}1\bar{1}]$, and $[\bar{1}\,\bar{1}1]$ are enhanced when the 4*f* electron contribution to the Tb–Tb bond along [111] is decreased. This causes expansion along [111] and contraction in the perpendicular directions. For $ErFe_2$ the prolate erbiums also align along ⟨111⟩ directions, but a field along [111] causes a contraction along [111] rather than an expansion. In this case, the Er–Er bond along [111] grows stronger and shorter as magnetization develops along [111]. Thus $TbFe_2$ has a large **positive** magnetostriction coefficient, and $ErFe_2$ has a large **negative** coefficient.

Other RFe_2 compounds magnetize along ⟨100⟩ directions and have rather modest magnetostrictive coefficients. The enhancement in electron density is the same for all four R–R bonds pointing along different ⟨111⟩ directions. This applies to both oblate and prolate rare-earth atoms. As a result, the magnetostriction coefficient of $DyFe_2$ is an order of magnitude smaller than that of $TbFe_2$.

Nevertheless it is important to alloy $TbFe_2$ with $DyFe_2$. In actuators and transducers, it is very useful to have a large shape change, but it is also important to be able to control the shape change with small applied fields. A large shape change frozen in position is of no practical value. To lower the driving field, a second phase change is positioned near room temperature. This can be done by lowering the Curie temperature, but this has the effect of demagnetizing the actuator and greatly reducing the magnetostriction coefficient. It is preferable to choose a composition near the rhombohedral-tetragonal phase boundary where

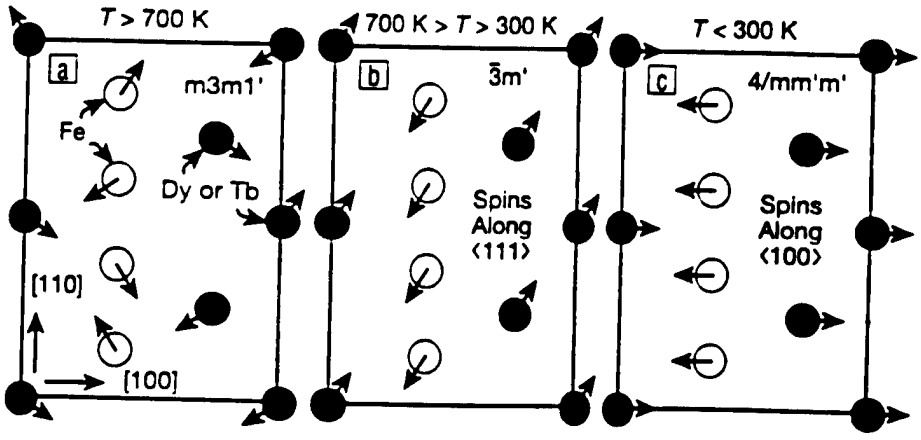

Figure 7. Magnetic phase transformation in Terfenol-D $Tb_{0.3}Dy_{0.7}Fe_2$ magnetostrictive actuator. At the Curie temperature, the paramagnetic phase converts to a rhombohedral ferrimagnetic phase (b) with spins parallel to ⟨111⟩ directions. Under operating conditions near room temperature, Terfenol is poised on a second transition to a tetragonal ferrimagnetic state (c) with spins parallel to ⟨100⟩ axes.

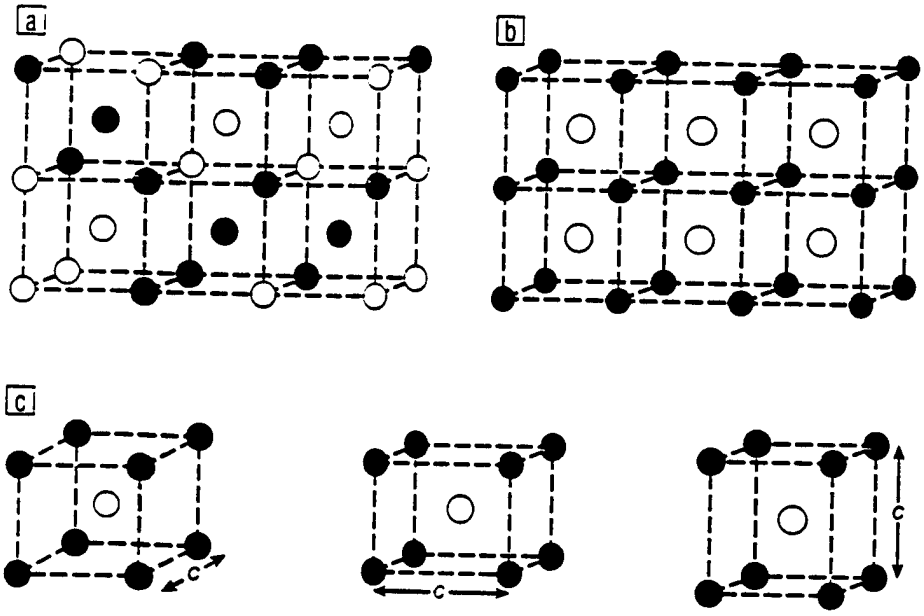

Figure 8. Body-centered intermetallics often show a structural transformation from a high-temperature disordered body-centered-cubic phase (space group Im3m) (a) to an annealed ordered austenite phase with the CsCl structure (space group Pm3m). (b) At lower temperatures, there is a second phase transition from austenite to a twinned martensite phase, pictured here as three variants of a body-centered tetragonal phase (space group P4/mmm) (c) with ferroelastic and antiphase domain walls.

the easy axis switches from ⟨111⟩ to ⟨100⟩. Compositions near $Dy_{0.7}Tb_{0.3}Fe_2$ have large magnetostrictive coefficients with easily controlled shape changes. Below room temperature, the magnetic symmetry changes from rhombohedral to tetragonal with a large decrease in the magnetostrictive shape change.

Shape-Memory Metals

My last example of an actuator material involves the shape-memory alloys, which are thermally driven rather than the magnetic drive of magnetostrictors or the electrical drive of piezoelectric and electrostrictive materials. This material too has phase transitions associated with the large thermomechanical-coupling coefficients. A commonly used material is Nitinol, nickel titanium alloys investigated initially at the Navy laboratories.[14] Working near 1:1 compositions, the nickel titanium intermetallic compound melts congruently at about 1300°C and has a martensitic phase transformation near room temperature.

The shape-memory alloys undergo martensitic transformations similar to those observed in the processing of steel. Two characteristics of martensitic phase changes are the absence of long-range diffusion and the appearance of a shape change.[15] Ferroelastic phase transformations are also distortive and diffusionless, and have much in common with the martensites. Ferroelastic crystals exhibit mechanical hysteresis between stress and strain caused by the stress-induced movement of domain walls. Martensites are also internally twinned, but mechanical stress causes phase changes as well as domain-wall movements.

Typically these materials are partially ordered as they undergo a transition from body-centered-cubic structure to a partially ordered CsCl structure (Figure 8). The shape-memory effect takes place at a martensitic transformation from the cesium chloride-like structure into a distorted multidomain martensite phase. Under stress the martensite easily deforms, and when reheated, goes back to the original morphology of the high-temperature structure. This is the shape-memory effect.

Some of the martensitic structures are very complex (Figure 9). The monoclinic structure of nickel titanium belongs to point group 2/m and has a β angle about 8° different from 90°. This generates a large spontaneous strain accompanying the martensitic phase change and is the shape change upon which external mechanical stresses and thermally induced stresses act. In the case of ferroelectrics, external fields act upon electric dipoles. For magnetic actuators, there are magnetic dipoles. With ferroelastics there is a shape change.

In the diffuse martensitic phase change, the partially ordered high-temperature austenite phase partially transforms into the martensite phase (Figure 10). Then under mechanical stress, two things happen. Domain reorientation takes place as indicated by the little bars in Figure 10, and phase changes occur as well. This behavior is very similar to the electrical behavior of the PMN relaxor ferroelectrics.

To summarize, most of the best actuators are primary ferroics. These ferroelastic, ferromagnetic, or ferroelectric solids are poised on an instability, often with two or more phase changes involved. Lead zirconate titanate is cubic at high temperature and is poised on a tetragonal-rhombohedral phase boundary. Partially ordered PMN is poised on a cubic-rhombohedral transition. The shape-memory alloys are also partially ordered and are poised on a martensitic phase transformation. Magnetostrictive terbium dysprosium iron alloys are cubic at high temperatures and are operated at a rhombohedral-tetragonal spin reorientation.

In addition to the four materials just discussed, other types of actuators are under development. Field-induced phase transitions in modified lead zirconate ceramics involve transitions between paraelectric, antiferroelectric, and ferroelectric phases.[18] Two phase transitions are involved in photostrictive materials in which the material changes its electri-

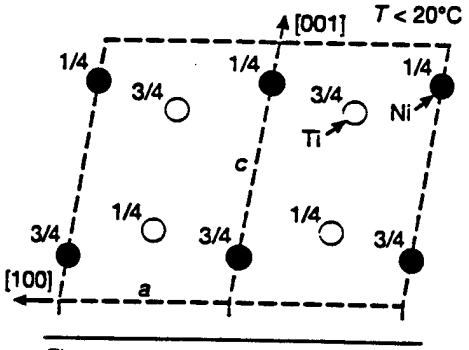

Figure 9. Crystal structure of the martensitic phase of Nitinol, NiTi. The space group is $P2_1/m$ with lattice parameters a = 2.884, b = 4.110, c = 4.665 Å, β = 98.10°. Sometimes referred to as the low AuCd structure, there are 12 orientation states of this monoclinic phase with respect to the cubic austenite phase.[16]

cal and mechanical characteristics under illumination.[14] The same number of phase transitions is also involved in chemostrictive materials with partially hydrated polymeric systems in which there are phase transitions both in the polymer and in the surrounding sheath of water molecules during the actuation process.

Biomolecular Actuators

Phase transformations also take place in protein-water systems during muscle action.[15] Protein molecules consist of polypeptide chains with amino-acid residues as side groups. The dielectric relaxation spectrum of protein molecules in aqueous solution provides evidence of the dynamic interaction between proteins and the surrounding sheath of water molecules. Based on dielectric loss measurements, there are five relaxation processes between 10^{-2} Hz and 10^{11} Hz. Conductive space-charge effects occur at frequencies below 1 kHz, followed by orientational fluctuations of the entire protein molecule near 1 MHz. Dipolar relaxation for bound water molecules lie near 10^8 Hz and for free water are at 10^{10} Hz. At high frequencies, picosecond (10^{12} Hz) fluctuations arise from the structural substates of the hydrogen bonds within the polypeptide chain. Changes in the dielectric spectrum with temperature and pH help decipher the protein-water interactions.

At low temperatures, the water surrounding the protein molecule forms clathrate-like cages consisting of hydrogen-bonded pentagonal and hexagonal rings. This ordered configuration of the water molecules keeps the polymerlike protein in a disordered extended form with its side groups trapped in the cages of water molecules.

On heating, the water molecules begin to move, breaking the hydrogen bonds and the clathrate cages. The side groups of the protein molecule are thereby released, allowing the protein to collapse into its folded form. It is held in this spiral-like collapsed configuration by internal hydrogen bonds between neighboring turns in the spiral.

Thus *two* transformations occur simultaneously. When heated the water molecules become more disordered while the protein molecules become more ordered. For the system as a whole, entropy must increase with temperature as required by the second law of thermodynamics. Therefore the entropy increase of the water molecules must exceed the decrease in entropy of the protein molecules. This coupled phase change leads to a sizable *decrease* in volume caused by the coiling motion of the protein polymer. As demonstrated by Urry,[20] this abrupt change in volume can be driven by temperature, pressure, light, electric field, or chemical change. Molecules like glutamic acid are especially good *chemostrictors*. The key side groups are COOH under acidic conditions and COO^- at neutral pH. The COOH group is more hydrophobic than the charged COO^- complex, causing the glutamic molecule to expand with increasing pH. Small changes in acidity can produce large mechanical movements.

Some inorganic substances behave in a similar way. The surface of a dry silicate tends to adsorb water, causing the material to swell. Although many minerals exhibit this phenomenon, layer silicates like Na-saturated montmorillonite ($Na_xSi_{2-x}Al_{1-x}O_5(OH) \cdot nH_2O$) show the greatest swelling potential.[21] When Na-montmorillonite is mixed with water, it dissociates into platelets only a few unit cells thick. The resulting sol has a gellike

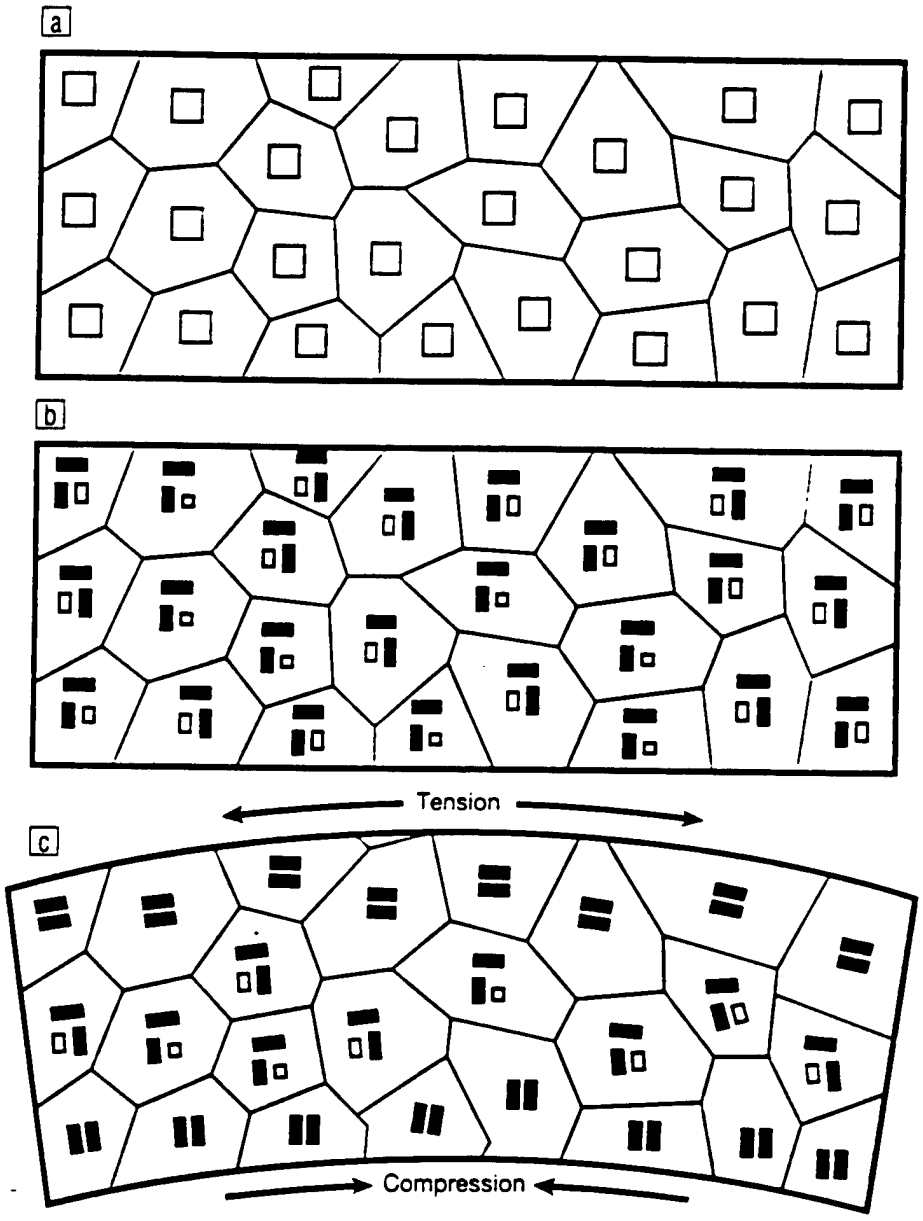

Figure 10. Shape-memory alloys transform from a partially ordered high-temperature cubic austenitic phase (a) to a mixed austenite-martensitic partially transformed low-temperature state (b) at the operating temperature. When deformed under mechanical stress (tension and compression) (c) phase changes and domain-wall movements take place. The metal returns to its original shape when the austenite phase reappears under heating.[13] Both twin orientation and phase changes occur.

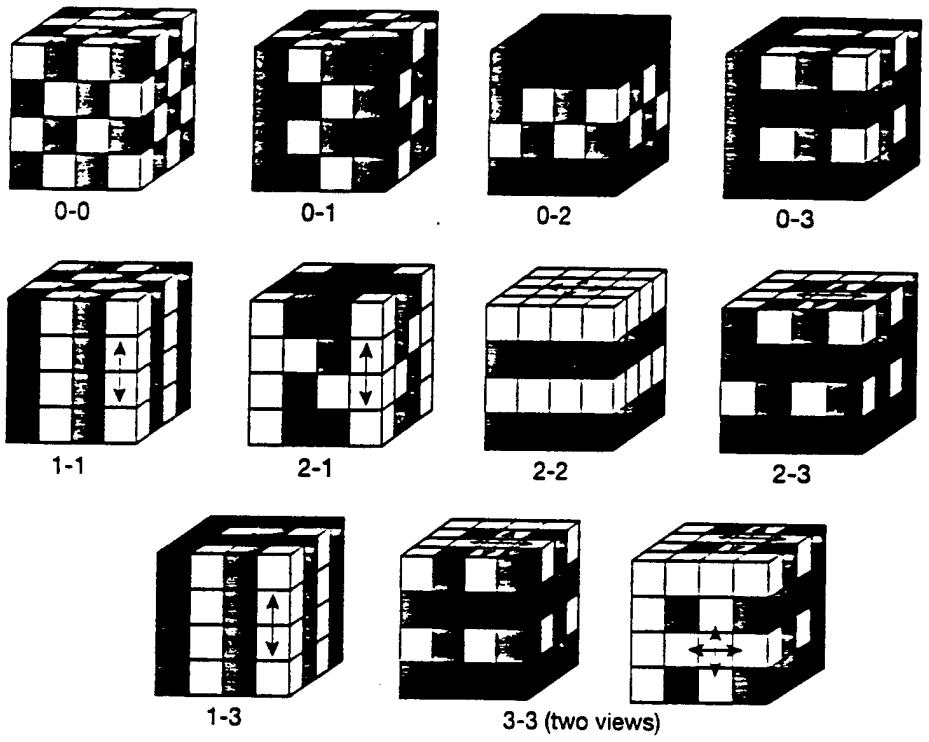

Figure 11. Ten connectivity patterns used in composite smart materials. By arranging two materials in series and parallel patterns, internal stress and field distributions can be optimized to improve device performance.[22]

character that tends to be thixotropic. Water adsorption is very rapid in the first few minutes with slower expansion over the long term. The chemostrictive effects resulting from the hydrophilic nature of silicate surfaces are capable of generating strains of 50% or more with large forces.

Functional Composites

My last few comments have to do with another approach to actuation and sensing, and are closer to my own interests: composite materials. What we have described so far are materials that, at least at high temperature, are single-phased. Another approach to making smart materials is to bring together two or more different materials, each of which has a phase transition associated with it. In our transducer program, we combine polymeric materials having phase transitions in which the elastic properties undergo large changes and ferroelectric materials in which the dielectric properties have an associated instability. The two materials have different types of instability, enabling us to build up structures especially good for sensing and actuating.

What we have tried to do in this family of functional composites is to take advantage of the fact that when optimizing a material, generally one is not trying to optimize all of the tensor coefficients but only those appearing in the figure of merit. Therefore we have built into these materials different connectivity patterns with an electrically soft material (a ferroelectric) and an electrically hard material (a polymer) having a very low dielectric constant. On the other hand, the polymer is mechanically soft with compliance coefficients several orders of magnitude larger than those of the ceramic. Using the connectivity patterns in Figure 11, we build up parallel and series connections that optimize particular combinations of tensor coefficients.[22]

Reductions in acoustic impedance are obtained by partially replacing ceramic with a soft polymer that couples the transducer vibrations better to water and to human tissue. Inserting electrodes inside the transducers lowers the drive voltage, and improved sensitivity to hydrostatic waves and enlarged displacements are among the other advantages listed in Table II. The composite transducers illustrate a very general approach that applies not only to piezoelectric materials but to many other functional composites.

Table II: Composite Electromechanical Tranducers Offer a Number of Advantages Over Single-Phase Transducers.

- Reduced acoustic impedance—better coupling to water and human tissue.
- Lower drive voltage with internal electrodes.
- Improved sensitivity to hydrostatic waves.
- Enlarged displacements.
- Acoustic isolation of adjacent sound sources.
- Passive and active vibration absorption.
- Improved high-frequency performance with smaller active regions.
- Mechanical strength and flexibility.
- Backing layers to absorb unwanted vibrations.
- Reduced hysteresis.
- Internal stress and field rearrangement.
- Improved breakdown strength.
- Tuned coupling coefficients, permittivity, and elasticity.
- Beam-forming capability.
- Rapid ringdown.

Composite Sensors and Actuators

Composite materials have found a number of structural applications, but their use in the electronics industry has been relatively limited. As the advantages and disadvantages of composites, sensors, and actuators become more clear, we expect this picture to change.

We have manufactured and tested composite piezoelectric transducers in our laboratory for the past two decades. These functional composites make use of a number of underlying ideas, including the following: connectivity patterns (Figure 11) leading to field and force concentration; the use of periodicity and scale in resonant structures; the symmetry of a composite structure and its influence on physical properties; polychromatic percolation and coupled conduction paths; varistor action and other interfacial effects; sum, combination, and product properties; coupled phase-transformation phenomena; and the important role that porosity and inner surface play in many functional-composite materials. These ideas[23] provide a basic understanding of functional-composite sensors and actuators. A few examples of composite piezoelectrics and their applications appear here. As I will point out later, some of these transducers mimic the geometries of the sound-sensing organs of fish:

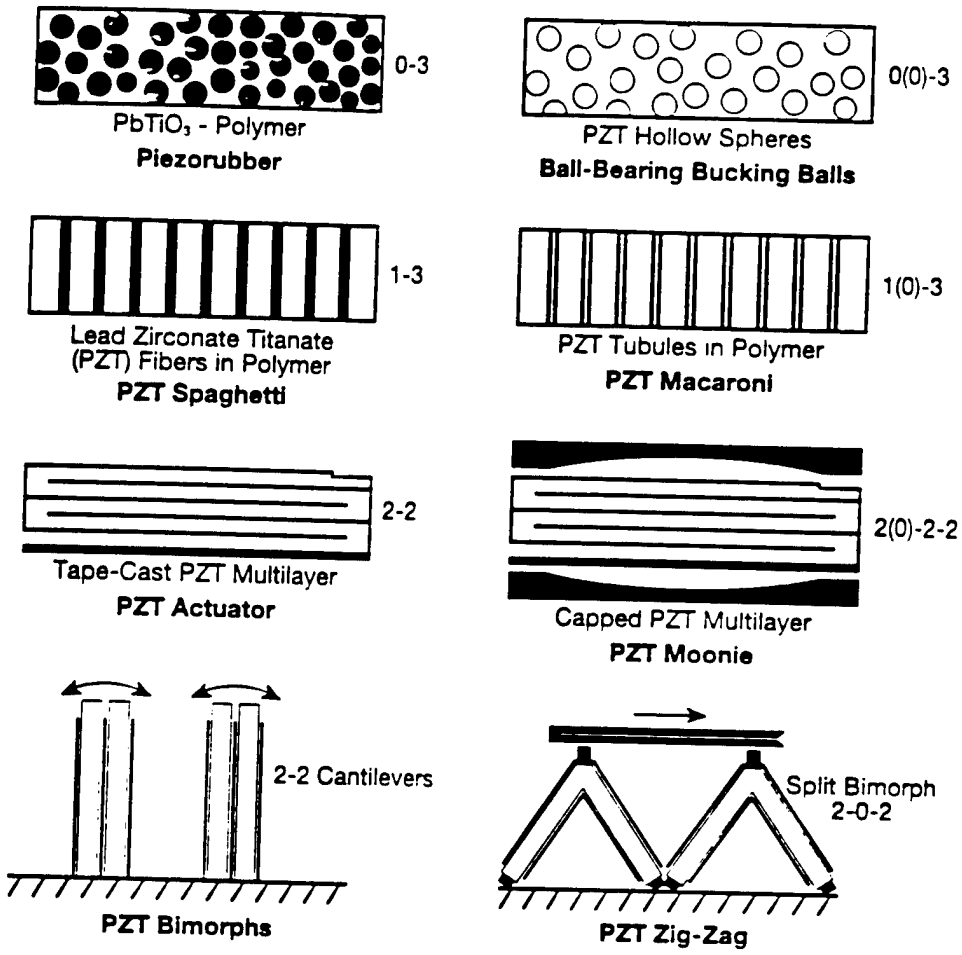

Figure 12. Piezoelectric composites for use as sensors, actuators, and transducers. The numbers describe the connectivity patterns utilized in the transducers.

elongated feelers, vibrating air bladders, and spherical inner ears. As illustrated in Figure 12, composite transducers come in a variety of different geometries.

Initially these studies concentrated on polymer-ceramic composites for use as hydrophones. Several interesting connectivity patterns[22] were developed including 3-3 structures made by the replamine process[24] and by fugitive phase technique.[25] Then came the more useful 1-3 composites, consisting of parallel PZT fibers embedded in a polymer matrix. These structures were made by extrusion,[26] by dicing,[27] and more recently by injection molding[28] and lithographic lost-wax techniques.[29] The coupling between the ceramic fibers and the polymer matrix is important.[30] In optimizing hydrophone performance, the $d_h g_h$ product was chosen as a figure of merit (Figure 13), where d_h is the hydrostatic-piezoelecric charge coefficient and g_h is the hydrostatic-piezoelectric voltage coefficient. The 1-3 composite increases d_h and g_h by reducing the d_{31} piezoelectric coefficient and the dielectric constant while maintaining a large d_{33} coefficient.

The usefulness of the 1-3 composite in high-frequency applications for nondestructive testing and medical diagnostics surfaced later.[31,32] Biomedical transducers require resonant frequencies in the 1–10-MHz range, as well as requiring high electromechanical-coupling coefficients, low acoustic impedance, and broad bandwidth. The 1-3 transducers manufactured by Siemens[29] have thickness resonances of 5–10 MHz, an electromechanical-coupling coefficient $k_t = 0.67$, a dielectric constant $K = 600$, a dielectric loss factor $\tan \delta < 0.025$, and an inverse mechanical loss Q of about 10.

Poling is sometimes difficult for the long, slender PZT fibers used in 1-3 composites. Electric breakdown often occurs before poling is complete, and the transducer is ruined. Lower poling and driving fields are obtained when the spaghettilike PZT fibers are replaced with macaronilike PZT tubules. When electroded inside and out, the thin-walled tubes are poled and driven radially at relatively modest voltages. Radial motions are coupled to length-wise displacements through the d_{31} coefficient. Effective piezoelectric constants of about 8,000 pC/N and large $d_h g_h$ products are achieved with these composites.[33] Other variants on the basic 1-3 structure include the 1-2-3 composite with transverse load-bearing fibers,[30] the 1-3-0 composite with a foamed polymer matrix,[34] and the interesting woven-fiber composites devised by Safari and coworkers.[35]

Perhaps the simplest piezoelectric composite is the 0-3 transducer made by dispersing ceramic particles in a polymer matrix. The NTK PiezoRubber films and cables are used as flexible hydrophones, keyboards, blood-pressure cuffs, and musical instruments. They are manufactured by hot-rolling $PbTiO_3$ particles into a chloroprene rubber matrix.[36]

Composites with 3-1 and 3-2 connectivity were prepared by drilling either circular or square holes in prepoled PZT blocks. Drilling was carried out in a direction perpendicular to the poled axis and by filling the drilled holes with epoxy.[37] On samples optimized for hydrophone performance, the g_h and $d_h g_h$ coefficients were about 4 and 40 times greater, respectively—for the 3-1 composites—and 25 and 150 times greater for the 3-2 composites compared to those of solid PZT.

Ball-bearing (bb) transducers are made from hollow spheres of PZT and are a few millimeters in diameter, about the same size as the metallic pellets used in air rifles (bb guns). PZT bbs are mass-produced by a patented forming process[38] in which air is blown through a PZT slurry of carefully controlled viscosity. The hollow spheres are 1–6 mm in diameter with wall thicknesses of 0.1 mm. Densities are about 1.3 g/cm^3, giving the bb a low acoustic impedance close to that of water and human tissue. When embedded in a polymer matrix to form a 0-3 composite, the bb spheres are surprisingly strong, and are able to withstand large hydrostatic pressure without collapse. Close-packed transducer arrays are easily assembled.

When electroded inside and out, and poled radially, the bb becomes an omnidirectional transducer suitable for underwater or biomedical applications. For spheres, 2.6 mm is the diameter with 90-μm-thick walls. The resonant frequencies are 700 kHz for the breathing mode (d_{31}) and 10 MHz for the wall-thickness mode (d_{33}). The bbs are small enough for use in catheters for noninva-

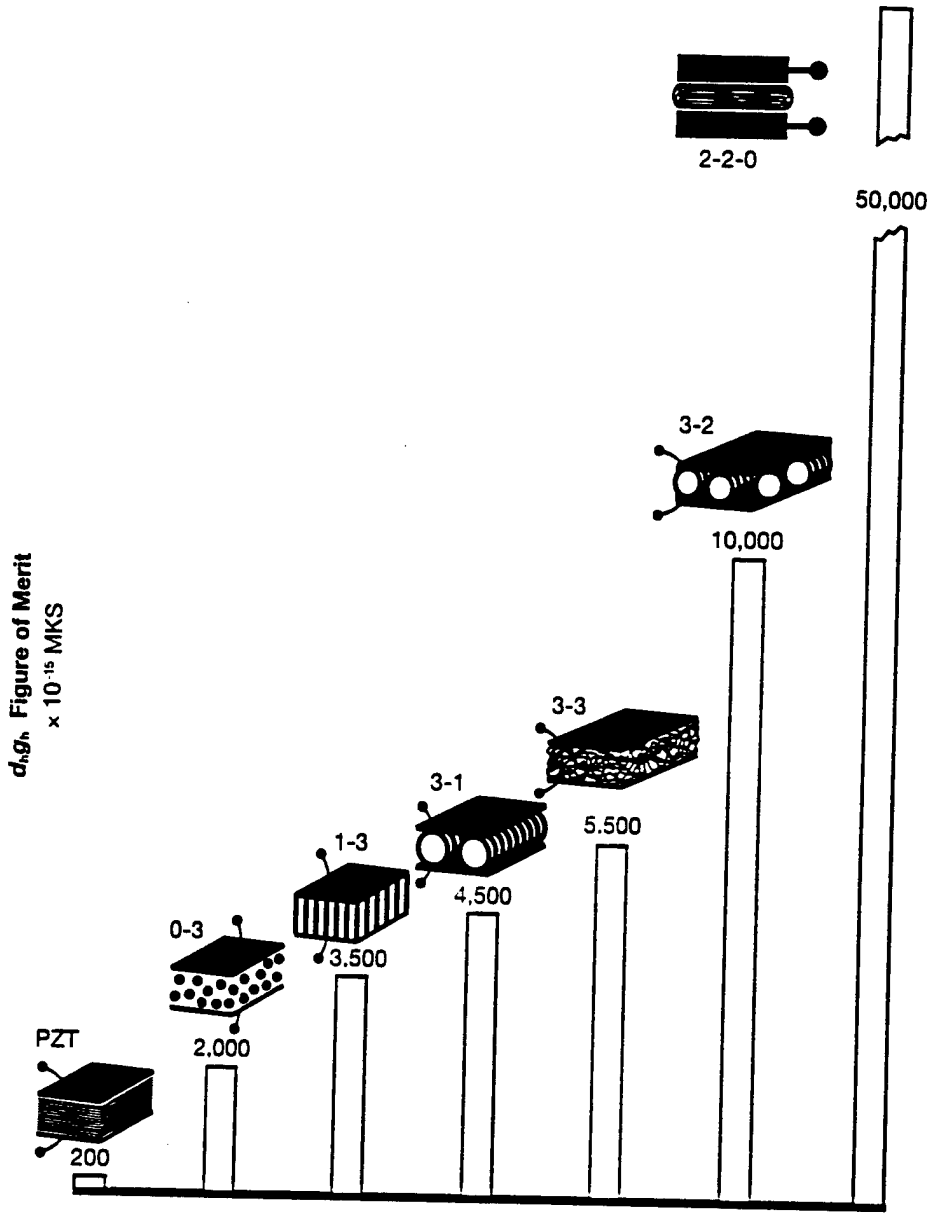

Figure 13. Hydrophone figure of merit for composite transducers and various piezoelectric materials. Values reported are for transducers approximately 1 cm in diameter when possible.[42]

sive surgery to act as beacons, sensors, and actuators.

In recent years, piezoelectric and electrostrictive ceramics have been used in many actuator applications.[39] To meet these needs, a new type of composite actuator based on a flextensional transducer has been developed.[40] This ceramic-metal composite actuator, or "moonie" consists of either a piezoelectric ceramic disk or a multilayer stack, sandwiched between two specially designed metal end caps. This design provides a sizable displacement, as well as a large generative force. In other words, it bridges the gap between the most common types of actuators, the multilayer and the bimorph. The shallow spaces under the end caps produce a substantial increase in strain by combining the d_{33} and d_{31} contributions to the ceramic. The design is attractive for hydrophone, transceiver,and actuator applications, and is especially advantageous for use as a nonresonant, low-frequency projector in deep water.[41] Patents describing the manufacture and testing of many of these composite transducers appear in Table III.

In this way, we have optimized a number of the properties of these materials. Figure 13 illustrates the hydrophone capabilities of these composites.[42] Hydrophones or underwater listening devices are normally made from pure PZT. However by developing the right combination of metals, ceramics, and polymers in the systems, the hydrostatic piezoelectric coefficients can be made far more sensitive for fish finding, biomedical applications, and geophysical exploration.

Biomimetic Transducers

The word "biomimetic" comes from the Greek words "bios" meaning "life" and "mimetikos" meaning "to imitate." Biomimetic means to imitate life or to use the biological world as a source of ideas for device concepts. For the past 20 years, we have been making biomimetic transducers from polymers, metals, and piezoelectric ceramics, arranged in various connectivity patterns. Some of the biomimetic ideas we have pursued appear in Figure 14 in cartoon form.

Our very first biomimetic transducer was copied from coral using a lost-wax method. The resulting PZT skeleton was back-filled with a flexible polymer to form a transducer with 3-3 connectivity and excellent piezoelectric properties.[24]

Fish and the other inhabitants of the underwater world have some interesting ways of talking and listening that we have copied using piezoelectric ceramics. For most fish, the principal sensors are the lateral line and the inner ear coupled to the swim bladder. The pulsating swim bladder also acts as a voice, as do chattering teeth in certain fish species. The lateral line runs from the head to the tail of the fish and resembles a towed array with sensing organs (stitches) spaced at intervals along the nerve fiber. Each stitch contains several neuromasts made up of gelatinous cupulae resembling pimples in shape. Within each cupulae are a number of fibers that vibrate as the fish swims through the water and that act as sensors for flow noise. The hairlike fibers are extremely thin in diameter, ranging from 0.5 to 10 μm. When stimulated by turbulence, the motion of the hairs produces changes in the synapses that are in turn connected to the nerve fiber. The electric signal originates from impedance changes in cell walls that modulate the flow of K^+ ions. The lateral line is especially sensi-

Table III: Patents on Composite Transducers.

	Patent No.	Issue Date
Flexible Piezoelectric Composite Transducers	4227111	10/07/80
Perforated PZT Polymer Composites	4422003	10/20/83
PZT Composite and a Fabrication Method Thereof	4412148	10/25/83
Broad-Bandwidth Composite Transducers	4485321	11/27/84
Piezoelectric Filler and Flexible Piezoelectric Composites	4624796	11/25/86
Transversely Reinforced Piezoelectric Composites	4613784	12/21/86
1-3-0 Connectivity Piezoelectric Composite with Void	4728845	03/01/88
Easily Poled 0-3 Piezoelectric Composite for Transducer Applications	4944891	07/31/90
Method of Detecting Sound in Water Using Piezoelectric-Polymer Composites with 0-3 Connectivity	4977547	12/11/90
Transformed-Stress-Direction Acoustic Transducer	4999819	03/12/91
Frequency Agile Sonic Transducer	5166907	11/24/92
Metal-Electroactive Ceramic Composite Actuators	5276657	01/04/94

tive to low-frequency fluid motion parallel to the length of the fish. In the 50-Hz range, threshold signals appear for displacements as small as 30 nm.[43]

The 1-3 composite hydrophones we patented 15 years ago mimic the hair-filled cupulae of the lateral line. Thin PZT fibers embedded in polymer provide excellent electromechanical coupling to a liquid medium and have potential uses as both sensors and actuators. Transducers (1-3) function well in both the low- and high-frequency ranges.[44] The Materials Systems Corporation now manufactures these transducers using injection molding. Other manufacturers continue to use the dice-and-fill method developed in our laboratory 20 years ago.

Another of our piezoelectric hydrophone composites maximizes the figure of merit or sensitivity by simply redirecting the applied stresses using specially shaped electrodes.[45] These are the flextensional moonie and cymbal transducers that mimic the motions of the swim bladder. Shallow air spaces reside under the metal electrodes while the PZT ceramic plays the role of the muscle lining of the swim bladder. When subjected to a hydrostatic stress, the thick metallic electrodes convert a portion of the z-direction stress into large radial and tangential stresses of opposite signs. The result is an inexpensive compact transducer with superb piezoelectric properties. Benthos and Input/Output-manufactured moonie tranducers for towed arrays and undersea oil exploration.

The hollow-sphere PZT transducers mimic the inner ear of a fish. The inner ear consists of inertia-sensing chambers resembling accelerometers. Within each chamber is a dense ear stone (otolith) that vibrates in a near-field sound wave. The inertia of the ear stone causes it to lag behind the motion of the fish, and to push against hair cells which line the chamber (sacculus). On bending, the hair cellular membranes deform, stimulating neural transmissions to the brain. Connections to the air bladder improve the sensitivity to far-field sound.[46]

As an example of a bio-inspired transducer, consider the doubly-resonant cymbal transmitter.[47] Male coqui frogs in the Caribbean National Forest of Puerto Rico communicate with nearby frogs by emitting a two-tone "co-qui" call. The low-frequency "co" note at 1160 Hz is a warning to other male frogs marking territorial boundaries. The "qui" note at 2090 Hz is a "come hither" mating call to females.[48]

A doubly resonant transducer mimicking the frog call in the low-kHz range has been constructed from an asymmetrically-capped PZT disk. The two resonances can be tuned individually by selecting cap metals of different stiffness or different geometry (Figure 15). Effi-

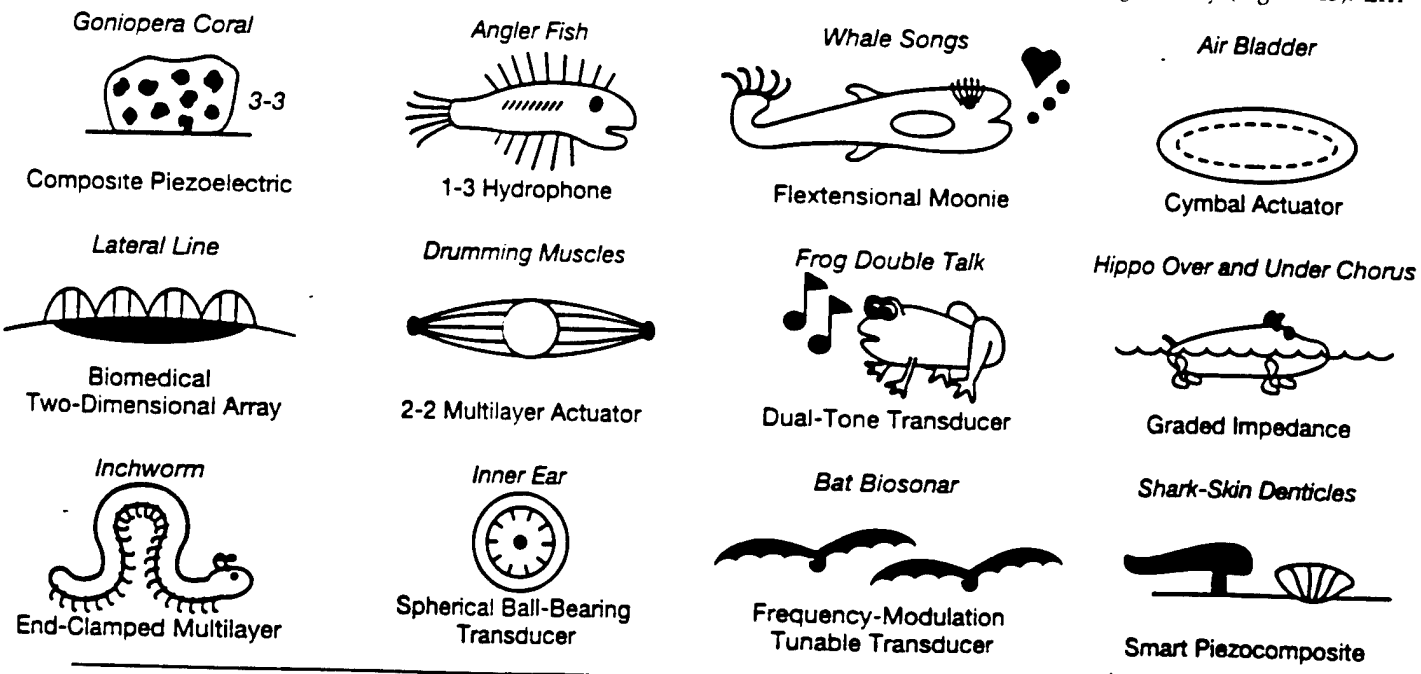

Figure 14. Some of the biomimetic structures and transduction mechanisms we have copied in past studies of piezoelectric composites.

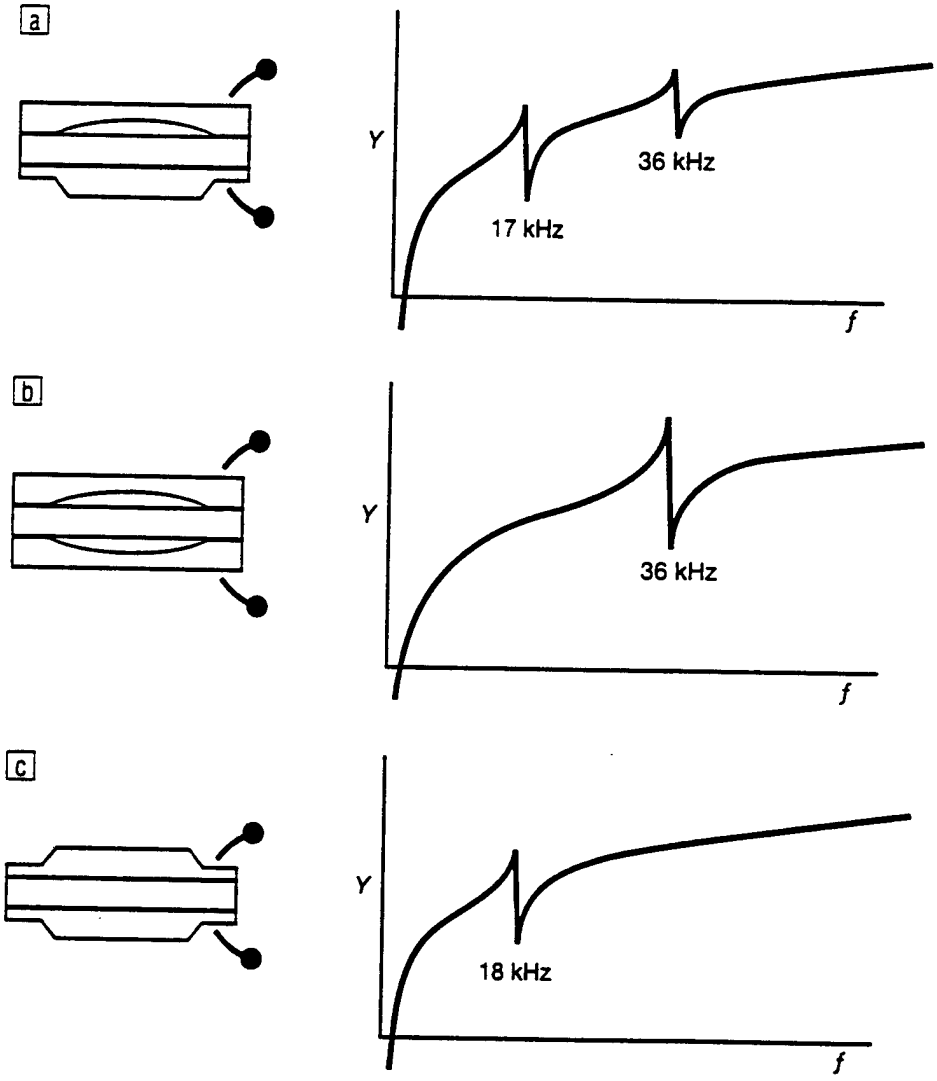

Figure 15. An asymmetric flextensional two-tone transducer (a) combining the end-cap geometries of the standard moonie (b) and cymbal (c) designs. The asymmetric transducer gives an admittance spectrum with two resonances. This mimics the dual-note call of the coqui frog.[48]

cient underwater transmitters with broad bandwidth can be obtained by coupling the two frequencies together.[49] Dual-tone transducers are under development for imaging breast cancer tumors.[5]

Summary

Several common themes appear in this talk. Two transformations are involved in most of these smart materials, often a primary ferroic (ferroelastic, ferroelectric, or ferromagnetic) with domain-wall motions that assist in the sensing and actuating processes. The ferroics are operated near an instability to make these domain walls with their associated dipoles and strains movable. We have identified several types among the commonly used actuator materials, and others appear to be possible too. In one type, a high Curie temperature exists as in PZT or Terfenol, and the actuator is operated near an orientational change of the electric or the magnetic dipole moment. The second type involves a partially ordered phase, as in electrostrictive PMN or the shape-memory alloys. These materials are operated near a diffuse phase transition with two coexisting phases, the high-temperature or austenitelike phase and the low-temperature or martensitic-type phase. A third type involves composite materials with coupled phase transformations.

The underlying strategies to optimize smart materials are fairly obvious. Why primary ferroic? These materials provide a handle for external fields or forces, whether it be a strain or an electric dipole or magnetic dipole. Why a cubic prototype phase? The answer is that it gives many equivalent orientation states and makes it possible then to use polycrystalline materials without the necessity of growing single crystals. Why partial ordering? This structure provides many nucleation sites for generating a diffuse phase transformation. Why a morphotropic transition? This instability ensures persistent disequilibrium over quite a wide range. In his recent book, *Out of Control*,[51] author Kevin Kelly describes how biological systems evolve into more complex life forms: Neither constancy nor relentless change will support a complex dynamic system. Equilibrium is death, and complete chaos leads to explosive behavior, also followed by death. On the other hand, persistent disequilibrium optimizes dynamic behavior by staying on the hairy edge of rapid response. The behavior of the sensor and actuator materials used in smart systems appears to be consistent with this idea.

As we look to the future, many new types of smart systems will be developed. Aerospace engineers are interested in smart air foils to control drag and turbulence. Diabetics need medical systems to sense sugar level and deliver insulin. Architects are designing smart buildings that incorporate self-adjusting windows to control the flow of energy into houses. Tennis players will want smart racquets to make overhead smashes and delicate drop shots. Smart systems will identify burglars and other dishonest people, and control their movements. Smart toilets are capable of analyzing urine to identify health problems. Smart irrigation systems are needed to optimize the world's food supply. Fish are the leading source of protein in many parts of the world. We can farm the oceans using smart transducers to talk to the fish and herd them like cattle. The word "smart" is being used everywhere, including the comic strips. Dagwood and Blondie recently visited a used-car dealer who told them about a smart car, and they asked what was meant by a "smart car"? The dealer replied that the car is so smart, if the payments are not made, it will drive itself back to the dealership!

Acknowledgments

It is a pleasure for me to acknowledge Eric Cross and my other colleagues in the ferroelectrics group at Penn State. We have worked together in great harmony for many years. The financial sup-

port of the Office of Naval Research, the National Science Foundation, the Advanced Research Projects Agency, and the Alcoa Corporation are also acknowledged with gratitude. Debra Shav and Laura Gallagher were very helpful in preparing the manuscript.

References

1. D. Turnbull. *Solid State Phys.* 3 (1956) p. 225.
2. R.E. Newnham. *NIST Spec. Pub.* 804 (1991) p. 39.
3. R.E. Newnham and G.R. Ruschau, *J. Am. Ceram. Soc.* 74 (1991) p. 463.
4. R.E. Newnham. *MRS Bulletin* XVIII (4) (1993).
5. K. Uchino. *Piezoelectric Actuators and Ultrasonic Motors* (Kluwer Academic Publishers, Boston, 1997).
6. E.K.H. Salje. *Phase Transitions in Ferroelastic and Co-Elastic Crystals* (Cambridge University Press, Cambridge, UK, 1990).
7. H.D. Megaw. *Ferroelectricity in Crystals* (Methuen & Company, Limited, London, 1957).
8. B. Jaffe, W.R. Cook, and H. Jaffe. *Piezoelectric Ceramics* (Academic Press, New York, 1971).
9. K. Uchino, S. Nomura, L.E. Cross, and R.E. Newnham. *J. Phys. Soc. Jpn.* 49B (1980) p. 45.
10. K. Uchino. *MRS Bulletin* XVIII (4) (1993) p. 42.
11. K.B. Hathaway and A.E. Clark, *ibid.* p. 34.
12. M. Wun-Fogle, H.T. Savage, and A.E. Clark, *Sensors and Actuators* 12 (1987) p. 323.
13. A.E. Clark, in *Ferromagnetic Materials 1*, edited by E.P. Wohlfarth (North Holland Publishing Company, Amsterdam, 1980).
14. G.R. Purdy and J.G. Parr, *Trans. Am. Inst Min. Eng.* 221 (1961) p. 631.
15. C.M. Wayman, *MRS Bulletin* XVIII (4) (1993) p. 49.
16. Y. Kudoh, M. Tokonami, S. Miyazaki, and K. Otsuka, *Acta. Metall.* 33 (1985) p. 2049.
17. R.G. deLange and J. Zijderveld, *J. Appl. Phys.* 39 (1968) p. 2195.
18. K. Uchino and S. Nomura, *Ferroelectrics* 50 (1983) p. 191.
19. M. Tanimura and K. Uchino, *Sensors and Mater.* 1 (1988) p. 47.
20. D.W. Urry, *Sci. Am.* (1995) p. 64.
21. R.E. Grim, *Clay Mineralogy* (McGraw-Hill Book Company, New York, 1953).
22. R.E. Newnham, D.P. Skinner, and L.E. Cross, *Mater. Res. Bull.* 13 (1978) p. 525.
23. R.E. Newnham, *Annu. Rev. Mater. Sci.* 16 (1986) p. 47.
24. D.P. Skinner, R.E. Newnham, and L.E. Cross, *Mater. Res. Bull.* 13 (1978) p. 599.
25. T.R. Shrout, W.A. Schulze, and J.V. Biggers, *Mater. Res. Bull.* 14 (1979) p. 1553.

Terminology for "Smart" Materials

Piezoelectricity: A linear relationship between electric and mechanical variables. Electric polarization is proportional to mechanical stress in the direct piezoelectric effect. The thermodynamically related converse piezoelectric effect relates mechanical strain to the applied electric field. Only solids lacking a center of symmetry show piezoelectricity, a third-rank tensor property.

Electrostriction: A quadratic relationship between mechanical strain and the square of the electric polarization. Electrostriction is normally a small effect, but electrostrictive strains can be surprisingly large near the Curie temperature of a ferroelectric substance. Electrostriction is a fourth-rank tensor property observed in both centric and acentric insulators.

Magnetostriction: Mechanical deformation induced by a magnetic field. The shape change is largest in ferromagnetic or ferrimagnetic solids in which mechanical strains accompany the motion of domain walls and the rotation of the magnetization vector.

Shape Memory: A thermomechanical phenomenon in which a solid returns to its undeformed shape after being heated to an elevated temperature. Large shape-memory effects occur in certain intermetallic compounds with martensitic phase transformations. Such metals are easily deformed in the low-temperature martensitic phase but return to their original shape when transformed to the high-temperature austenitic state.

Ferroic Solids are characterized by the presence of domain walls, which can be moved by external fields or forces. Ferroelectrics, ferromagnetics, and ferroelastics are the three primary types of ferroics. There are also six kinds of secondary ferroics of less practical importance.

Ferroelectrics are ferroic solids in which domain walls can be repositioned with applied electric fields. This leads to hysteresis between electric polarization and the applied field. Most ferroelectrics undergo a displacive phase transformation at the Curie temperature (T_c) where the spontaneous polarization and the domain structure disappear. Above T_c a normal ferroelectric is in its *paraelectric* state, in which dielectric permittivity follows a Curie-Weiss law. This is not true for *relaxor ferroelectrics*, which are characterized by a broad, diffuse phase transition and large permittivity values that are strongly dependent on frequency and do not obey a Curie-Weiss law.

Ferromagnetic materials are the magnetic analogue to ferroelectrics. Hysteresis between magnetization and an applied magnetic field arises from the movement of magnetic domain walls. The spontaneous magnetization, hysteresis, and domain walls disappear when a ferromagnetic is heated above T_c into its *paramagnetic* state. *Ferrimagnetic* materials show macroscopic properties similar to ferromagnets but differ on the atomic scale. Within a given domain, the magnetic dipoles of a ferromagnetic solid are parallel to one another. In a ferrimagnetic, some of the dipoles are aligned in other directions. Nevertheless there is a net magnetization within each domain, as in a ferromagnet.

Ferroelasticity is the mechanical analogue to ferroelectricity and ferromagnetism. These materials exhibit hysteresis between strain and stress caused by the motion of ferroelastic domain walls. The effect is more complicated near a *martensitic phase transformation* where mechanical stress induces changes in crystal structure as well as domain-wall motion. Martensitic shape-memory alloys have broad, diffuse phase transformations with coexisting high- and low-temperature phases. Domains disappear when fully transformed to the high-temperature austenitic (paraelastic) state.

Photostrictive and *Chemostrictive* materials show sizable changes in shape due to light or chemical environment. These effects are caused by changes in electronic structure or in chemical bonding and are usually not connected with domain-wall motion.

26. K.A. Klicker, J.V. Biggers, and R.E. Newnham, *J. Am. Ceram. Soc.* **64** (1981) p. 5.
27. H.P. Savakus, K.A. Klicker, and R.E. Newnham, *Mater. Res. Bull.* **15** (1981) p. 677.
28. C.P. Bowen, T.R. Shrout, R.E. Newnham, and C.A. Randall, *J. Intell. Mater. Syst. Struct.* **6** (1995) p. 159.
29. G. Preu, A. Wolff, and D. Crames, *U. Bast Euro-Ceramics II* **3** (1991) p. 2005.
30. M.J. Haun, R.E. Newnham, and W.A. Schulze, *Adv. Ceram. Mater.* **1** (1986) p. 361.
31. T.R. Gururaja, W.A. Schulze, L.E. Cross, R.E. Newnham, B.A. Auld, and Y.J. Wang, *IEEE Trans. Ultrason. Ferroelec., Freq. Cont.* **32** (1985) pp. 481, 499.
32. W.A. Smith and B.A. Auld, *ibid.* **38** (1991) p. 40.
33. W. Pan, Q.M. Zhang, A. Bhalla, and L.E. Cross, *J. Am. Ceram. Soc.* **72** (1989) p. 571.
34. M.J. Haun and R.E. Newnham, *Ferroelectrics* **68** (1986) p. 123.
35. V.F. Janas and A. Safari, *J. Am. Ceram. Soc.* **78** (1995) p. 2945.
36. H. Banno, *Ferroelectrics* **50** (1983) p. 329.
37. A. Safari, S. DaVanzo, and R.E. Newnham, *ibid.* **50** (1983) p. 257.
38. R. Meyer, H. Weitzing, Q.C. Xu, Q.M. Zhang, R.E. Newnham, and J.K. Cochran, *J. Am. Ceram. Soc.* **77** (1994) p. 1669.
39. D. Damjanovic and R.E. Newnham, *J. Intell. Mat. Syst. Struct.* **3** (1992) p. 190.
40. Y. Sugawara, K. Onitsuka, S. Yoshikawa, Q. Xu, R.E. Newnham, and K. Uchino, *J. Am. Ceram. Soc.* **75** (1992) p. 996.
41. Q.C. Xu, S. Yoshikawa, J. Belsick, and R.E. Newnham, *IEEE Trans. Ultrason. Ferroelec., Freq. Cont.* **38** (1991) p. 634.
42. J. Tressler, private communication.
43. D.B. Webster, R.R. Fay, A.N. Popper, eds. *The Evolutionary Biology of Hearing* (Springer-Verlag, New York, 1992).
44. T.R. Gururaja, A. Safari, R.E. Newnham, and L.E. Cross in *Electronic Ceramics 92*, edited by L. Levinson (Marcel Dekker, New York, 1988).
45. A. Dogan, Q.C. Xu, K. Onitsuka, S. Yoshikawa, K. Uchino, and R.E. Newnham, *Ferroelectrics* **156** (1994) p. 1.
46. W. Tavolga, A. Popper, and R. Fay, eds., *Hearing and Sound Communication in Fishes* (Springer-Verlag, New York, 1981).
47. J.F. Tressler and R.E. Newnham, *IEEE Trans. Ultrason., Ferroelec., Freq. Cont.* (in press).
48. P.M. Narins, *Sci. Am.* (August 1995) p. 78.
49. McLaughlin and J.F. Lindberg, *Proc. 3rd Int. Workshop on Transducers for Sonics and Ultrasonics*, edited by M. McCollum, B. Hamonic, and O. Wilson (Technomic Press, 1993) p. 239.
50. J. Ophir, *Ultrasonic Imaging* **13** (1991) p. 111.
51. K. Kelly, *Out of Control* (Addison-Wesley Press, 1994).

Robert E. Newnham received a BS degree in mathematics from Hartwick College in 1950; an MS degree in physics from Colorado State University in 1952; and two PhD degrees, one in physics from The Pennsylvania State University (1956), and a second in crystallography from Cambridge University (1960). He was a research fellow at Cavendish Laboratory, Cambridge, from 1956 to 1958, when he joined the Massachusetts Institute of Technology (MIT). After eight years at MIT, he then joined the faculty at Penn State, where he is now Associate Director and Alcoa Professor of Solid State Science, Intercollege Materials Research Laboratory and Department of Materials Science and Engineering. Newnham has published more than 400 research papers, written four books and 14 book chapters or review articles, served in an editorial capacity on eight journals, guest edited the April 1993 issue of MRS Bulletin, *and received more than 30 honors. He is a fellow of the Mineralogical Society of America and the American Ceramic Society, and a member of the National Academy of Engineering. Newnham can be reached at The Pennsylvania State University, 251-A Materials Research Laboratory, University Park, PA 16802-4801, USA; fax 814-865-7593; e-mail bobnewnham@psu.edu.*

APPENDIX 3

Electronic Ceramics R&D in the U.S., Japan

Part I: Patent History

U.S. and Japanese patent history for dielectric ceramics, piezoelectric ceramics and ferroelectric thin films is reviewed to help predict future R&D trends.

Scott L. Swartz
NexTech Materials Ltd., Worthington, Ohio

Thomas R. Shrout
Materials Research Laboratory, The Pennsylvania State University, University Park, Pa.

Tadashi Takenaka
Science University of Tokyo, Noda, Japan

A survey of ongoing R&D in the United States and Japan was conducted to identify and characterize future development of electronic ceramics. The types of electronic ceramics included in this study were:

- Dielectric ceramics for capacitors and microwave filters;
- Piezoelectric ceramics for transducers and actuators;
- Ferroelectric thin films for semiconductor memories and microactuators.

Information for this survey was obtained by an analysis of U.S. patent literature from January 1990 through August 1996 and through responses to questionnaires sent to Japanese technologists. This was supplemented by recent review articles[1-5] and by information presented at workshops and symposia[17-20] dedicated to electronic ceramics. This assessment confirmed that the field of electronic ceramics will remain a fertile area for R&D. The biomedical and telecommunication industries were identified as potential growth areas.

For dielectric ceramics, development of multilayer ceramic capacitors (MLCs) will continue, and miniaturization—e.g., thinner dielectric layers—and cost reduction—e.g., nickel electrodes—will be primary drivers. However, the need for discrete components may decrease as technology evolves toward increasing integration, with capacitors, resistors and inductors incorporated into multifunctional ceramic packages and/or semiconductors.

New applications for piezoelectric ceramic transducers and sensors continue to emerge. However, difficulties in reducing manufacturing costs have limited several high-volume applications of piezoelectric actuators. Increased applications of piezoelectric ceramics are expected for the biomedical and aerospace industries, which can tolerate the relatively high cost of piezoelectric ceramic components.

Successful development of high-capacity semiconductor memories, incorporating ferroelectric thin-film materials, is expected within several years. Many of the technical issues related to thin-film deposition and integration with semiconductors have been solved. Additional near-term applications of ferroelectric thin-film technology include microactuators and microelectromechanical systems (MEMS).

Development times for electronic ceramic products are expected to be reduced, with fewer resources available for R&D. This will result in an increased emphasis on matching R&D resources to identified market needs.

Finally, there is a growing awareness of environmental issues in Japan, which may result in a shift in priorities for future R&D of electronic ceramic products. Of particular concern is the use of lead in electronic ceramic products—e.g., lead-based solders, lead-based relaxors and lead zirconate titanate-based piezoelectric ceramics. Future research may be directed toward identifying alternatives to these materials.

Electronic ceramics encompasses a broad range of existing device markets and future applications currently under development. Several technical reviews providing specific details of electronic ceramics materials and associated device manufacturing technologies are available[1-5] as evidence of the breadth and scope of this field. Electronic ceramics markets are dominated mostly by U.S. and Japanese companies, with a small but significant European market presence and a growing presence by companies in Korea, Singapore and China.

Dielectric Ceramics

Besides ceramic substrates and packages—which were not directly addressed by this study—MLCs and microwave filters provide the largest markets for electronic ceramics materials. The ceramic capacitor market in the United States is >$900 million/year, and this market is growing at 10%/year.[6] The Japanese ceramic capacitor market is usually estimated at 3–4 times that of the U.S. market. The U.S. microwave dielectric filter market is conservatively estimated at $300–$400 million, which is similar to that of the Japanese market.

The dielectric ceramics materials used in these passive devices represent intense past and future development activity. The dielectric materials used in MLCs have continually evolved to meet ever-increasing demands for miniaturization, higher-frequency operation, stable response over a wide temperature range, improved reliability and reduced manufacturing costs. Meeting these market demands requires the development of new dielectric materials and improved manufacturing methods for reducing dielectric layer thicknesses in MLCs. An example is the current activity in Japan toward using nickel electrodes in MLCs as a replacement for more-expensive silver and silver–palladium electrodes.

Mobile telephones, pagers and microwave communications have created a large market for dielectric ceramic filters during the past 10 years. The stringent requirements for this application include high dielectric permittivity, negligible temperature dependence and extremely low microwave dielectric loss.

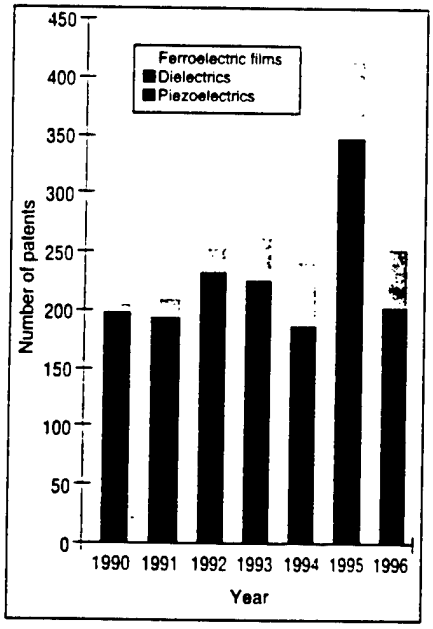

Total number of U.S. electronic ceramics patents for piezoelectric ceramics, dielectric ceramics and ferroelectric thin films for January 1990 through August 1996. Steady increase in the total number of patents each year is caused by expanded patent activity for piezoelectric ceramics and ferroelectric thin films.

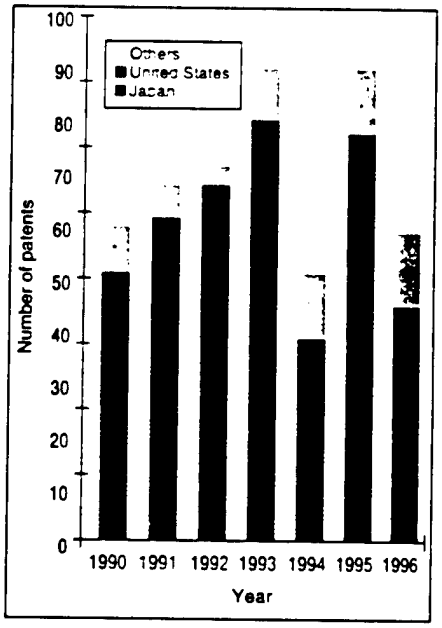

Total number of U.S. dielectric ceramics patents, assigned to organizations in the United States, Japan and other countries for January 1990 through August 1996. Japanese and U.S. organizations received 50% and 37%, respectively, of the total number of patents.

Piezoelectric Ceramics

Piezoelectric and electrostrictive ceramics are used in the consumer, automotive, medical and aerospace industries. These applications range from low-cost buzzers and filters through high-performance transducers for ultrasonic imaging systems[7,8] and towed array sonars.[9,10] Relatively new uses of piezoelectric ceramics include actuators in cameras and ink-jet printers.

This diversity makes accurate assessments difficult, but the U.S. market for piezoelectric ceramic components has been estimated at $128 million in 1994, with a 10%/year growth rate.[6] The Japanese market for piezoelectric ceramic components is estimated at >>$500 million. The markets for the systems that rely on piezoelectric ceramics are much larger, hence, the importance of these materials.

There has been an ever-increasing trend toward improving the performance and reliability of piezoelectric ceramics. Therefore, new applications of ultrasonic motors, actuators and transformers have been proposed.

The promise of developing "smart" materials,[11,12] providing both sensing and actuating functions, has increased the focus on development of piezoelectric, electrostrictive and other active materials. A current smart application of piezoelectric ceramics is the suspension systems in high-end luxury cars.[13] Other smart applications involving piezoelectric ceramics in combination with other materials are under development to meet U.S. military needs.

Ferroelectric Thin Films

Ferroelectric thin films are defined here as inorganic ferroelectric films with thicknesses <10 mm. Liquid-crystalline and other polymeric thin-film ferroelectric materials for displays and other applications are subjects of intense R&D activity, but these materials have not been included in this assessment.

The development of inorganic ferroelectric thin films is in its infancy, when compared to dielectric and piezoelectric ceramics. Although research on ferroelectric films was initiated in the 1960s,[14,15] large-scale development efforts did not begin in earnest until the late 1980s.

Two reasons for the rapid expansion of R&D activity directed at ferroelectric films are the availability of improved thin-film deposition techniques and the identification of ferroelectric films as an enabling technology development of high-capacity nonvolatile memories (NVMs) and high-capacity dynamic random-access memories (DRAMs). Although most of the current development of ferroelectric films focuses on semiconductor memories, other applications have been identified,[16] including microactuators, pyroelectric detectors and optical waveguide devices.

Information Gathering

A keyword search of U.S. and Japanese patent literature was performed for dielectric ceramics, piezoelectric ceramics and ferroelectric thin films, covering January 1990 through August 1996. Abstracts of identified patents were obtained and reviewed. Patents were classified by the type of research conducted—e.g., materials or devices—the specific application—e.g., MLC or microwave filter, sensor or actuator, NVM or DRAM—and the nature of the assignee organization—industrial, government, university, individual. Trends in patent activities were identified based on these classifications.

Questionnaires were distributed to >400 Japanese technologists active in electronic ceramics research, development and manufacturing. Analysis of the questionnaire responses provided an important perspective on how Japanese technologists view the past and look toward the future. The content and results of this questionnaire will be reported in the August 1997 issue of ***Ceramic Bulletin***.

Patent Literature Review

Dielectric ceramics and piezoelectric ceramics have relatively long technical histories and represent areas where electronic ceramics technology is being applied to the improvement of existing products and to the development of new applications. Searches of the U.S. and Japanese patent literature for these two types of ceramics provided comparable results. Therefore, the discussions that follow are based on statistics compiled for U.S. patents—because many more U.S. patents were identified in our searches.

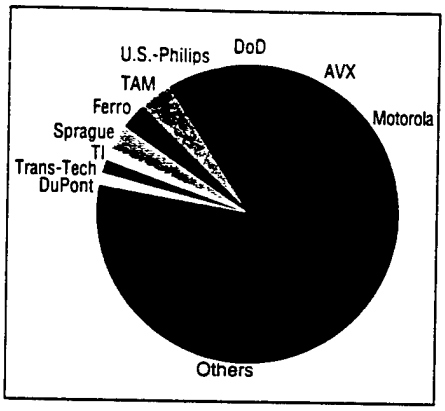

Distribution of U.S. patents assigned to U.S. organizations for dielectric ceramics January 1990 through August of 1996. Two companies with the largest number of patents were Motorola and AVX, the largest U.S. producers of microwave filters and capacitors, respectively. However, most of the dielectric patents were assigned to research organizations—individuals, small companies, DoD laboratories and universities—not currently involved in the manufacture of dielectric ceramics or related devices.

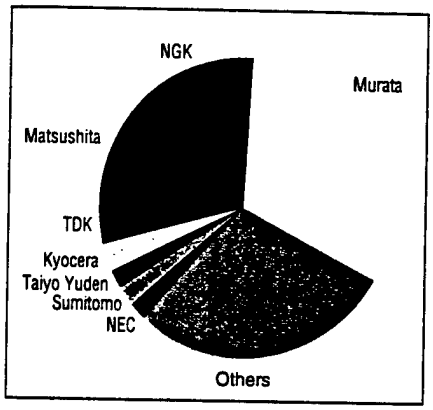

Distribution of U.S. patents assigned to Japanese organizations for dielectric ceramics for January 1990 through August 1996. More than 95% of these patents were received by large Japanese companies, and 70% were received by only 15 companies. Murata was the leading patenter of dielectric ceramics, with 62 patents, or about one in every six of all U.S. patents.

In comparison, ferroelectric thin films have a short technical history based on the limited number of patents published prior to 1990. Only eight U.S. patents on ferroelectric thin films were found for 1976–1989. Thus, for the most part, our searches of the U.S. and Japanese patent literature covered the entire patent history of ferroelectric films. Furthermore, these searches provided complementary information. Therefore, the following discussion on ferroelectric thin films is based on both U.S. and Japanese patents.

During the period covered, 1834 U.S. patents were found for dielectric ceramics (21%), piezoelectric ceramics (65%) and ferroelectric films (14%). U.S. and Japanese organizations were assigned a similar number

U.S. Patents on Piezoelectric Ceramics Assigned to U.S. Organizations

Organization	Primary patent subtopic	Number of patents		
		1990–1993	1994–1996	Total
U.S. DoD*	Micropositioners, hydrophones, sonars, composites, SAW devices	43	35	78
Individuals	Sensors, optics, rainbow actuators	34	20	54
Hewlett–Packard	Ultrasonic transducers (biomedical)	8	20	28
General Electric	Ultrasonic transducers (biomedical)	14	11	25
Motorola	SAW filters, buzzers	5	15	20
Caterpillar	Actuators (fuel injection systems)	11	1	12
Rockwell	Motors, gyroscopes, MEMS	10	1	11
IBM	Actuators for ink-jet printers, MEMS, positioning heads for magnetic recording, toner-level sensors	5	6	11
Compaq	Ink-jet printers	0	11	11
All others	Composite processing, bar-code readers, actuators, motors, nondestructive testing, ultrasonic bone healing	105	150	265
Total		235	270	505

*Includes DoD laboratories and DoD-funded universities.

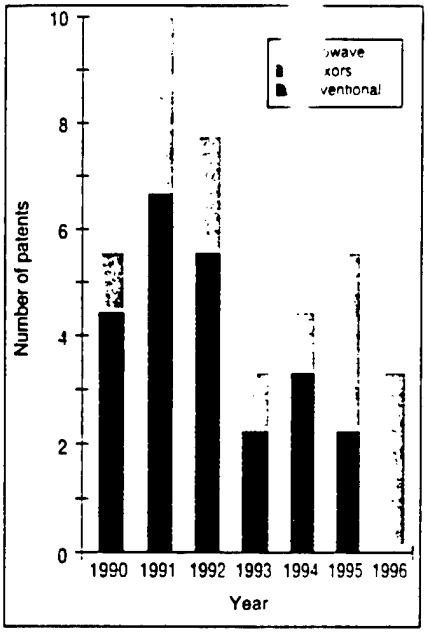

Types of dielectric compositions covered by U.S. compositional patents received by U.S. organizations for January 1990 through August 1996. These patents covered primarily conventional $BaTiO_3$-based dielectric compositions in the early 1990s, with emphasis shifting to microwave compositions by the mid-1990s.

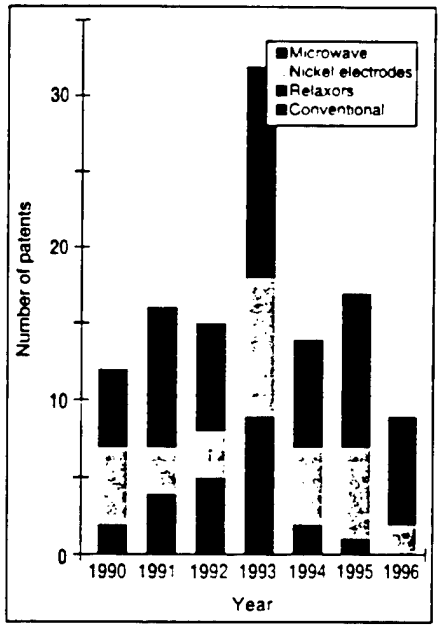

Types of dielectric compositions covered by U.S. compositional patents received by Japanese organizations for January 1990 through August 1996. Slightly less than half of these patents covered microwave dielectric compositions, and a significant proportion covered dielectric compositions compatible with manufacture of MLCs with internal nickel electrodes.

U.S. Patents on Piezoelectric Ceramics Assigned to Japanese Companies

Organization	Primary patent subtopic	Number of patents		
		1990–1993	1994–1996	Total
Murata	SAW filters, gyroscopes, buzzers, accelerometers, bimorph actuators	15	39	54
NEC	Actuators, ultrasonic motors, transformers	24	12	36
Matsushita	SAW filters, ultrasonic motors, ultrasonic probes	16	18	34
Brother	Ink-jet and dot-matrix printers	18	12	30
Seiko–Epson	Ultrasonic motors, ink-jet printers	9	15	24
NGK	SAW filters, composites, actuators, sensors	10	12	22
Mitsubishi	Actuators, knock sensors, gyroscopes	16	5	21
Hitachi	SAW filters, ultrasonic probes, ultrasonic motors	16	2	18
Fujitsu	Ink-jet printers, ultrasonic probes, transformers, bimorph actuators	10	8	18
Toshiba	Ultrasonic probes, transformers, bimorph actuators	10	8	18
Toyota	Fuel injection systems	10	5	15
Canon	Micromotors, ultrasonic motors, cantilever actuators	5	10	15
Nikon	Ultrasonic motors	8	6	14
Sumitomo	SAW devices	3	7	10
Olympus	Ultrasonic motors, cantilever actuators, atomic-force microscope	4	6	10
All others	Motors, micropositioners, sensors, automotive suspension systems	83	64	147
Total		257	229	486

*No differentiation was made between like-named companies within the same kyoritsu, e.g., Matsushita, NGK, Mitsubishi and Sumitomo.

of patents, 783 and 787, respectively, accounting for 86% of the total. Most of the remaining 264 patents were assigned to European and Korean organizations. A gradual increase in the number of patents each year was noted, except for a reduction in the total number of patents in 1994, primarily caused by a significantly reduced patent activity in dielectric ceramics.

Dielectric Ceramics Patents

A total of 391 U.S. patents were found for dielectric ceramics, with Japanese and U.S. organizations receiving ~50% and ~37%, respectively.

More than 95% of the Japanese organizations that received U.S. patents on dielectric ceramics were large companies, with Murata leading with 62 patents, 32% of the Japanese-assigned patents. Other large Japanese companies with a significant number of U.S. patents include NGK Insulators, Matsushita Electric Industrial, TDK, Kyocera, Taiyo Yuden and NEC. The large number of patents assigned to Murata is consistent with its dominance of the worldwide ceramic capacitor and microwave filter markets.

A diverse range of U.S. organizations received patents on dielectric ceramics, with Motorola—the world market leader in the cellular telephone market—leading the way with 17 patents, 12% of the U.S.-assigned patents. U.S. capacitor and dielectric materials suppliers—AVX, U.S. Philips, TAM, Ferro and Sprague—also received significant numbers of patents. However, >60% of the U.S.-assigned patents were received by organizations not currently involved in the manufacture of ceramic capacitors or microwave filters. This list includes U.S. Army and U.S. Navy laboratories, defense contractors, universities and small businesses.

The patent review indicated differing dielectric composition development strategies between U.S. and Japanese companies. U.S. companies were more aggressive than Japanese companies in developing new dielectric compositions for conventional $BaTiO_3$-based (X7R/Z5U) MLCs (19 vs 8 patents).

Japanese companies were more aggressive in developing microwave

compositions (59 vs 6 patents) and PbO-based relaxor dielectrics (14 vs 2 patents). It is significant that the Japanese have developed rare-earth-modified $BaTiO_3$ (X7R) dielectric compositions that can be sintered with nickel internal electrodes under reducing atmospheres. Japanese companies received 33 U.S. patents on these compositions, while U.S. companies received none. Korean companies had seven compositional patents, most for microwave compositions.

Several patents were obtained by the U.S. Department of Defense (DoD) and its contractors, primarily on dielectric materials used in microwave phase shifters. These dielectric materials essentially were ignored by Japanese developers. This is indicative of an overall trend in the U.S. electronic ceramics field, where the U.S. government funds a substantial amount of R&D toward developing materials that meet military needs.

Several U.S. companies and fewer Japanese companies received patents for their development of dielectrics used in low-temperature cofired ceramic (LTCC) packages. These patents were obtained mostly by large materials suppliers and electronic system manufacturers, including TRW, Hughes, Westinghouse, Ferro and DuPont in the United States and Fujitsu, NEC and Kyocera in Japan.

Piezoelectric Patents

A total of 1187 U.S. patents were found for piezoelectric ceramics, with U.S. and Japanese organizations receiving 41% and 42%, respectively. From 1990 through 1994, 140–175 patents/year were issued on piezoelectric ceramics. However, a substantial increase in patent activity was observed for 1995 and 1996, 275 and 231, respectively—a prorated total was used for 1996. The wide range of applications that involves piezoelectric ceramics led to extreme diversity in the nature of the inventions and the types of organizations receiving patents, thus making it difficult to provide concise classifications. However, the results of the patent search can be summarized by identified trends.

From 1990 through 1993, Japanese companies received 273 U.S. patents on piezoelectric ceramics, compared to 219 patents received by U.S. organizations. This trend was reversed during 1994 through 1996, with U.S. organizations receiving 270 patents and Japanese companies 229 patents. This shift appears to be more related to an expansion of development activity in the United States, rather than a reduction of Japanese activity.

Only seven U.S. companies received 10 or more patents on piezoelectric ceramics. They accounted for 118 patents, only 23% of the total number of patents assigned to U.S. organizations. On the other hand, there were 15 Japanese companies with 10 or more patents, accounting for 339 patents (70%).

Research at DoD laboratories and funded universities resulted in 70 patents on piezoelectric ceramic materials and devices. Another 54 patents were assigned to individuals affiliated with universities or their own small businesses. The four companies receiving the most U.S. patents were Japanese, with Murata clearly dominant with 54.

The two U.S. companies receiving the most U.S. patents were Hewlett–Packard and General Electric. They

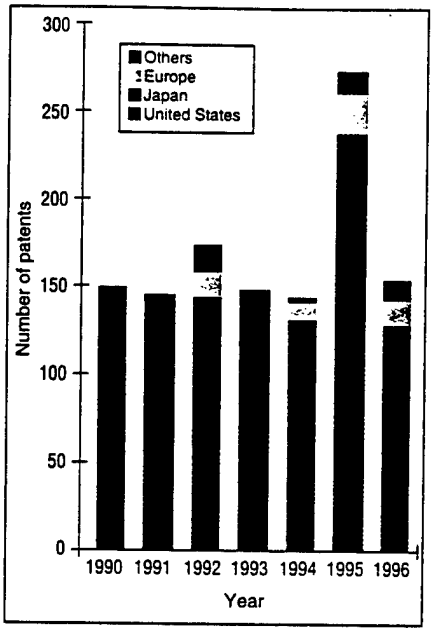

Total number of U.S. patents for piezoelectric ceramics assigned to organizations in the United States, Japan and other countries for January 1990 through August 1996. Japanese and U.S. organizations received 41% and 42%, respectively, of the total number of patents.

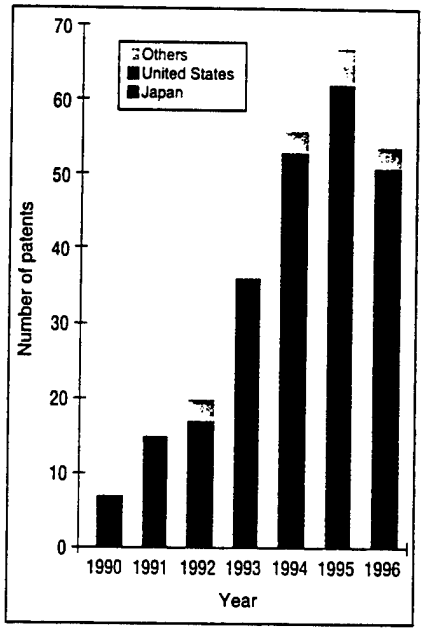

Total number of U.S. patents for ferroelectric thin films assigned to organizations in the United States, Japan and other countries for January 1990 through August 1996. U.S. and Japanese organizations received 54% and 40%, respectively of the total number of patents.

Patents on Ferroelectric Thin Films by Technical Subtopic

Technical subtopic	Number of U.S. patents		Number of Japanese patents
	United States	Japan	Japan
Integration with semiconductors	46	18	65
NVMs	50	61	55
DRAMs	4	4	32
Other applications	13	12	5
Sputtering deposition processes	2	5	14
MOCVD processes	8	1	3
Sol–gel deposition processes	11	1	8
Laser-deposition processes	4	1	1
Total	138	103	183

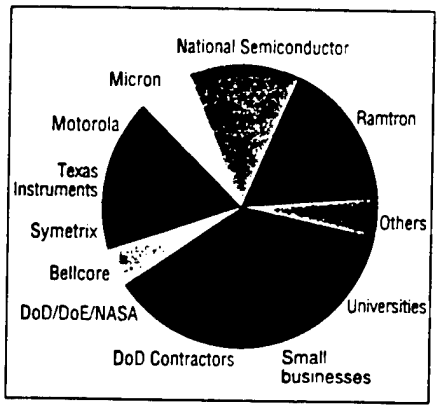

Distribution of U.S. patents assigned to U.S. organizations for ferroelectric thin films for January 1990 through August 1996. Semiconductor manufacturers accounted for ~50% of these patents, with the remainder being distributed among a variety of research organizations including universities, small businesses, U.S. government laboratories and DoD contractors.

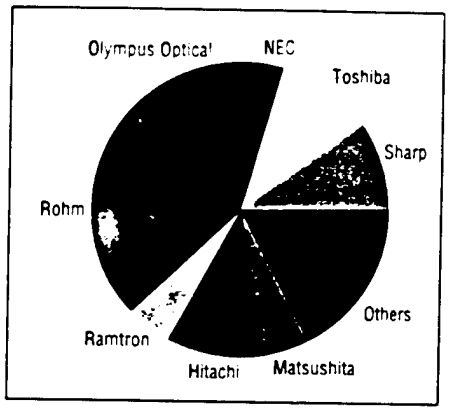

Distribution of U.S. patents assigned to Japanese organizations for ferroelectric thin films, January 1990 through August 1996. Rohm, a Japanese semiconductor manufacturer, received more than 26% of these patents, and large Japanese companies, such as Olympus, Toshiba, Sharp and Hitachi accounted for an additional 44%.

were active in the development of ultrasonic transducers for biomedical applications. The United States is dominant in the biomedical field, with numerous other patents related to ultrasonic transducers, medical imaging systems, drug delivery devices and surgical tools. Japanese companies received few, if any, biomedical-related patents involving piezoelectric ceramics.

Use of piezoelectric actuators in ink-jet printing heads was the subject of considerable patent activity and recent commercial successes. Companies, similar to IBM and Compaq in the United States, and Brother and Seiko–Epson in Japan, were active developers of these devices. Successful development and commercialization also was achieved for ultrasonic motors used in cameras and other specialized optical systems. Japanese companies with U.S. patents on ultrasonic motors included NEC, Matsushita, Seiko–Epson, Canon, Nikon and Olympus.

Several recent patents were received by Japanese companies—NEC, Fujitsu and Toshiba—on piezoelectric transformers. This application has considerable commercial potential, because successful development of piezoelectric transformers will allow miniaturization of flat-panel displays.

Many patents were awarded to U.S. and Japanese companies active in the automotive industry. Piezoelectric ceramics continue to find new automotive applications as sensors, e.g., for antilock braking systems. Japanese companies, especially Murata, have been active in the development of piezoelectric gyroscopes, which may find applications in automotive guidance (global positioning) systems.

Several automotive companies were active in the development of multilayer piezoelectric actuators for fuel-injection systems. Companies receiving patents on these systems included General Motors, Ford and Caterpillar in the United States, and Toyota, Nissan and Honda in Japan. Most of these patents were issued in the early 1990s, but the technology has not been commercialized because of the difficulty in reducing manufacturing cost for the multilayer actuators, even at the high production volumes that this application would provide.

Japan appears to be dominating the development of surface acoustic wave (SAW) devices, which may become competitive with dielectric filters for telecommunications if their operation can be pushed to higher frequencies. Japanese developers of SAW devices include Murata, Matsushita, NGK, Hitachi and Sumitomo, whereas Motorola is one of few U.S. companies with patents in this area. In general, SAW device patents covered electroding patterns and methods, with a few patents on new materials, e.g., $La_2B_4O_7$ and ZnO–diamond composites.

A relatively new development in the United States is microelectromechanical systems (MEMS), with patents received by IBM, Rockwell and Massachusetts Institute of Technology. Anticipated MEMS applications include biomedical devices, semiconductor manufacturing and robotics.

Few patents were found on "smart" systems, i.e., where piezoelectric sensors and actuators are integrated within a composite material or structure. These smart systems are being heavily funded by the U.S. government, with several anticipated military aerospace applications—e.g., vibration damping, signature reduction and structural health monitoring.

Patents on Ferroelectric Thin Films Assigned to Japanese Companies

Company	Number of patents Primary patent subtopic	U.S.	Japan	Total
Rohm	NVMs	27	8	35
Sharp	NVMs	10	22	32
Hitachi	Integration with semiconductors	11	19	30
Toshiba	Integration with semiconductors	11	15	26
Matsushita Electric Industrial	Sputtering deposition processes	5	14	19
NEC	Integration with semiconductors	3	15	18
Olympus Optical	NVMs	13	5	18
Seiko–Epson	Integration with semiconductors	2	16	18
TDK	NVMs	2	7	9
Fujitsu	Integration with semiconductors	0	9	9
Total		84	139	223

Ferroelectric Patents

A total of 255 U.S. patents were found for ferroelectric thin films, with U.S.

and Japanese organizations receiving ~54% and 40%, respectively. Our search of the Japanese patent literature identified 183 patents, all assigned to Japanese organizations. The patents issued for ferroelectric thin films increased steadily from 1992 through 1996. This trend is consistent with the rapid expansion of research activity in ferroelectric thin films that began in the late 1980s and continued through the 1990s.

Of 286 U.S. and Japanese patents assigned to Japanese organizations, 282 patents (98%) were assigned to large Japanese manufacturing companies. Of 138 U.S. patents assigned to U.S. organizations, only 61 patents (44%) were assigned to large U.S. manufacturing firms, and 46 patents (33%) were assigned to small businesses. The remaining 31 patents were distributed among universities, the U.S. government and contract research organizations.

In contrast to dielectric and piezoelectric ceramics, the precompetitive nature of ferroelectric thin-film technology has fostered several alliances between U.S. and Japanese organizations. Virginia Tech, a U.S. university, has assigned many of its patents to Sharp. Symetrix, a U.S. small business, and Olympus Optical are jointly developing and patenting ferroelectric thin-film technology. Other examples of active U.S.–Japanese alliances include Ramtron International, Fuji–Xerox and Texas Instruments–Japan.

The semiconductor industry is the market-driving force behind development of ferroelectric thin-film technology. Of 424 patents assigned to U.S. and Japanese organizations, 335 patents (79%) were directly related to semiconductor memories (NVMs and DRAMs) or to semiconductor fabrication processes for integrating ferroelectric films on silicon. Most of the remaining 89 patents were specific to thin-film deposition processes for semiconductor substrates or to applications involving ferroelectric films deposited onto semiconductors. The 10 most prolific Japanese developers of ferroelectric thin-film technology, accounting for 223 of 284 patents, are manufacturers of semiconductor components and/or electronic systems.

Of the 216 U.S. and Japanese patents related to semiconductor memories, 176 patents were specific to NVMs and 40 to DRAMs. The disparity between NVM and DRAM patents may have been skewed by the large number of patents assigned to semiconductor integration. Another explanation may be related to the relatively recent entry of U.S. semiconductor manufacturers into focused DRAM development programs.

However, 32 of 40 DRAM-specific patents (80%) were Japanese. This suggests that Japanese companies decided not to pursue U.S. patents for their DRAM-specific inventions or that corresponding U.S. patents were disallowed. Furthermore, two Japanese companies—Rohm and Olympus Optical—received significantly more U.S. than Japanese patents, which is consistent with their alliances with U.S. research organizations. However, the opposite trend was observed for other Japanese companies with patents on ferroelectric films.

It is difficult to make precise conclusions on deposition methods, because most of the identified patents were nonspecific with respect to the thin-film deposition processes. However, of the 25 process-specific patents assigned to U.S. organizations, nine thin-film deposition processes were developed by universities, eight by small businesses, three by contract research organizations and five by large U.S. manufacturing firms. Japanese companies were assigned only eight process-specific U.S. patents, but were assigned 26 such patents in Japan. Relatively new thin-film deposition processes—sol–gel, MOCVD and laser-deposition—were patented first by U.S. organizations, before any patents on these processes were received by Japanese companies.

Several patents assigned to U.S. and Japanese organizations addressed issues related to integrating ferroelectric thin films on semiconductor substrates. Many of these patents described interlayers of various materials to prevent diffusion of film constituents into the semiconductor. In some patents, interlayer films were described that served as templates for improving crystallinity and performance and/or promoting epitaxial growth of subsequently deposited ferroelectric films. Several other patents described novel electrode materials that resulted in reduced fatigue or lower leakage currents in semiconductor memories.

A significant patent assigned to Symetrix was based on the development of $SrBi_2Ta_2O_9$—the so-called Y-1 material—as a ferroelectric thin-film material providing fatigue-free polarization reversal. This patent alone led to subsequent development and several additional patents on deposition methods and semiconductor integration methods for the Y-1 material. ■

Acknowledgments

The authors are grateful to the Air Force Office of Scientific Research (AFOSR/AORD) for providing funding for this work and to Dr. Shiro Fujishiro (AFOSR) for his encouragement throughout the project. The authors also wish to acknowledge the following people for their input to the assessment: T. R. Gururaja (Hewlett–Packard), Angus Kingon (North Carolina State University), Harlan Anderson (University of Missouri-Rolla) and Clive Randall (The Pennsylvania State University).

The second part of this two-part article on the future trends of R&D of electronic ceramics in the United States and Japan will present details of a questionnaire sent to Japanese technologists. The results of the questionnaire and general conclusions derived from it and the patent review described here will be presented in the August 1997 issue of ***Ceramic Bulletin***.

For the complete set of references to parts I and II of this article, please FAX or mail your request with your name and address to Editorial Assistant at 614-794-5822 or headquarters, respectively. Request ACerS Data Depository File No. 273

Electronic Ceramics R&D in the U.S., Japan

Part II: Japanese View

The results of a questionnaire completed by Japanese technologists were used to help predict future R&D trends for dielectric ceramics, piezoelectric ceramics and ferroelectric thin films.

Scott L. Swartz
NexTech Materials Ltd., Worthington, Ohio

Thomas R. Shrout
Materials Research Laboratory, The Pennsylvania State University, University Park, Pa.

Tadashi Takenaka
Science University of Tokyo, Noda, Japan

R&D of electronic ceramics in the United States and Japan was studied to identify and characterize its future development. Dielectric ceramics, piezoelectric ceramics and ferroelectric thin films were included in the study.

Information for this survey was obtained by an analysis of U.S. patent literature from January 1990 through August 1996 and through responses to questionnaires sent to Japanese technologists. The results of the patent survey were reported in the July 1997 issue of ***Ceramic Bulletin.***

Questionnaires were distributed to >400 Japanese technologists active in electronic ceramics research, development and manufacturing, and 61 responses were obtained. The questionnaires addressed:

- Most significant developments during the previous five years;
- Important developments and applications anticipated to occur within the next five years;
- Development activities expected to have decreasing importance in the next five years;
- Economic and environmental factors that will impact future developments;
- Key requirements for commercializing new products.

This information was supplemented by review articles[1–5] and presentations at workshops and technical symposia[17–20] dedicated to electronic ceramics.

Japanese Technologists Surveyed

Questionnaires were sent to Japanese technologists active in the field of electronic ceramics. The questionnaire contained seven questions that were designed to obtain Japanese perspective on significant recent developments and expected future developments in electronic ceramics and to identify factors that will influence future R&D directions. The responses included 46 from Japanese industry and 15 from academia.

Information obtained during this assessment provided a definite contrast between development trends identified by the patent review and the survey of anticipated future R&D directions. There is significant lag time between the conception of an invention and publication of a patent, so that the patent review process, by its nature, tends to monitor development activities that are at least two years old. However, there usually is a significant amount of development time—typically three to five years—before a patented invention reaches commercial implementation. For this reason, one may have expected that the two assessment approaches would provide parallel results.

Dielectric Ceramics

During the past 15 years, much R&D has been devoted to PbO-based relaxor dielectric compositions, such as $Pb(Mg,Nb)O_3$ and related compounds.[21,22] The primary drivers

Survey Questions and General Responses

1. ***Background of Survey Participants*** Most of the respondents indicated experience in multiple electronic ceramics R&D fields. Dielectric ceramics were most often cited, followed by piezoelectric ceramics and ferroelectric thin films.

2. ***Most Significant Recent Developments*** Many responses addressed subtopics within the participant's area of expertise. Most of the developments cited contributed in reduction of manufacturing cost; component miniaturization; enabling new products or product improvements; saving energy; or fostering environmental consciousness. Many industrial respondents cited product-oriented developments rather than materials developments; i.e., miniaturized microwave filters were cited instead of low-loss microwave dielectric ceramics. In dielectric ceramics, thin-layer MLC fabrication methods were cited most often. In piezoelectric ceramics, several product-related developments—actuators, gyroscopes, ink-jet printing heads, etc.—were cited. The development of lead-free piezoelectrics also was mentioned, although this area of R&D is at its infancy. In ferroelectric films, semiconductor memories were cited most often, with memory-related thin-film materials and deposition processes. Four industrial participants stated that there were no major developments within the past five years.

3. ***Important New Electronic Ceramic Application(s)*** Responses ranged from generic to specific. In dielectric ceramics, new products based on multifunctional ceramic packages (with integrated capacitors, resistors and inductors) and microwave components for high-frequency telecommunications are expected. In piezoelectric ceramics, responses were distributed among several specific devices, all of which require the development of low-cost synthesis and fabrication processes for piezoelectric ceramics providing higher performance and better reliability than are available currently. Semiconductor-based devices incorporating ferroelectric thin films, such as memories and microactuators, are expected to be commercialized. Several responses indicated a growing awareness in Japan over environmental issues.

4. ***Anticipated Future Developments in Electronic Ceramics*** A wide range of generic and specific responses were received. In dielectrics and ceramic packaging, the responses are best summarized by "fusion of semiconductor and ceramic packaging industries." Thus, ceramic packaging and semiconductor processing are expected to provide increased multifunctionality, with passive components—capacitors, inductors and resistors—all incorporated into the same ceramic package or semiconductor substrate. Much future development is expected within ferroelectric thin films for semiconductor memories. Only a few future developments were cited under piezoelectric ceramics, and these primarily were related to specific actuator devices and low-cost fabrication methods for them. Several responses were related to advanced fabrication methods, such as artificial superlattices, nanoscale structural control and atomic-level control of thin-film deposition processes. Mostly, the future developments cited were consistent with that required to develop future products cited in response to the previous question.

5. ***Current Applications Expected to have Less Importance*** Nineteen of the respondents gave no answer to this question. There were only five citations in piezoelectric ceramics and ferroelectric thin films, consistent with the expectation of additional future R&D, as suggested by responses to earlier questions. Most of the responses were related to capacitors and packaging, based on the assumption that electronic functions will be integrated into a single package, within the ceramic substrate or the semiconductor itself. This integration is expected to lead to a decreased reliance on discrete components—capacitors, resistors and inductors—as well as the ceramic substrates upon which these components currently are attached. Several respondents suggested that ceramic packaging will continue to be replaced by polymer packaging.

6. ***Important Economic or Environmental Factors*** Responses to this question indicate an acute awareness of environmental issues by Japanese scientists. One-half of all respondents mentioned the need to reduce the use of toxic materials in electroceramics, including lead and lead oxide. Other potentially hazardous elements commonly used in electroceramics include bismuth, cadmium and nickel. The topics of energy conservation, clean energy sources and natural resource preservation also were cited. Of the economic factors, manufacturing cost was cited most often, with miniaturization, short development time and the need for development to keep pace with market demands.

7. ***Requirements for Commercialization of New Products*** This question received a wide range of responses, with manufacturing cost cited by ~50% of the respondents. Other responses with multiple citations included R&D, marketing, matching R&D with market needs, reliability, product performance, short development time and environmental consciousness.

for this development work were volumetric efficiency and low sintering temperature offered by high-permittivity relaxors. Successful development of these relaxor dielectrics has led to limited commercial use of these lead-based dielectrics, primarily in Japan.

However, the results of this assessment suggest that the development of lead-based dielectrics will be discontinued and their commercial use may even be phased out. This prediction is based on a growing concern in Japan over the use of toxic materials, e.g., lead compounds; recent development of green-sheet fabrication methods for producing MLC chip capacitors with ultra-thin dielectric layers; and increased use of temperature stable (X7R) capacitors needed by the automotive, appliance and consumer electronics industries.

Emphasis on MLCCs

With an increased emphasis on MLC capacitors with temperature-stable, dielectric response, the assessment indicates two different approaches are being pursued by Japanese and U.S. capacitor manufacturers. In the United States, development efforts have focused on existing $BaTiO_3$-based X7R compositions, with the goal of reducing capacitor size by increasing permittivity from ~3000 to ~5000.

Japanese capacitor manufacturers, especially Murata, TDK and Taiyo Yuden, have focused on reducing cost by developing $BaTiO_3$-based X7R compositions that can be sintered in reducing atmospheres, thus enabling the use of nickel electrodes.

Although the latter approach may limit maximum permittivity levels to ~3000, capacitor size reduction will be achieved by using ultrathin dielectric layers, i.e., ≤ 5 μm. With successful commercialization of the Japanese approach, continued domination of the capacitor market by Japanese manufacturers can be expected.

Dielectric Powders

Similar powder production methods are used in the United States and Japan, although the relative use a year of the various methods is different. In both countries, there is a widespread use of

chemically prepared dielectric powders. In the United States, development efforts have focused on oxalate precipitation[23] and other chemical synthesis methods[24,25] to prepare pure $BaTiO_3$ powders. Japanese efforts have focused on powders produced by hydrothermal synthesis.[26,27] This method[28] involves the synthesis of crystalline powders from aqueous solutions at temperatures <350°C.

The use of hydrothermal $BaTiO_3$ powder has enabled the Japanese development of X7R capacitors with nickel electrodes.[29] Sakai Chemical is the primary supplier of hydrothermal $BaTiO_3$ powder in Japan, and Cabot is supplying hydrothermal $BaTiO_3$ powder in the United States. Although their initial process patents[30,31] were issued during the late 1980s, Cabot remains at the pilot scale of production, whereas Sakai currently is producing ~50 tons/month of hydrothermal $BaTiO_3$.[32] It remains to be seen whether U.S. capacitor manufacturers embrace the hydrothermal $BaTiO_3$ technology or continue on their current development path.

Microwave Filters

The evolution of the telecommunications market has increased demand for microwave dielectric filters. Most current production is based on bulk dielectric filters comprised of temperature-stable and low-loss dielectrics, such as $BaTi_4O_9$-based compositions. As with capacitors, there is an ever-increasing demand for reducing the size of microwave filters, which can be achieved only by using higher-permittivity dielectrics or by adopting a multilayer device configuration.

Murata recently introduced smaller-sized filters based on high-permittivity microwave dielectrics. However, it is expected that the multilayer approach will be pursued for the next generation of dielectric filters. There is far greater potential for size reduction because a single multilayer device would replace several bulk filters. Commercialization of multilayer dielectric filters requires considerable additional development of dielectric and electrode materials, as well as multilayer fabrication methods.

The dielectric ceramic material also should have a low sintering temperature to allow cofiring with silver electrodes,[33–35] or be compatible with sintering under reducing atmospheres to allow use of copper electrodes.[36] Successful development of multilayer filters requires that the internal electrode must be fabricated with greater perfection than current multilayer fabrication methods allow:

- Precise internal electrode patterns are required to achieve the desired resonance frequency of the multilayer filter;
- Irregularity in dielectric thickness and/or roughness at the ceramic–electrode interface increase microwave losses;
- The electrode layers should be highly dense to assure maximum conductivity and minimize losses.

The patent review and questionnaire results also suggested that discrete dielectric filters, either in bulk or multilayer geometries, may find future competition from low-temperature cofired ceramic (LTCC) packages[37,38] and/or piezoelectric surface acoustic wave (SAW) devices.[39,40] LTCC packages may be developed with microwave filter components buried within the package itself, and SAW devices are being developed as a competing miniaturization technology for microwave filters.

Piezoelectric Ceramics

Current production of piezoelectric ceramics generally is based on lead zirconate titanate (PZT) ceramics, using conventional ball milling and calcination methods. PZT powders are acceptable for current piezoelectric ceramic applications, ranging from buzzers, filters, igniters and ultrasonic cleaners to towed array sonars, medical imaging systems, ink-jet printing heads, camera shutters, positioners for optical systems and sensors.

Multilayer piezoelectric actuator technology has been proved for several high-volume automotive applications—e.g., fuel-injection systems and suspension systems. Commercialization has been limited by difficulties in meeting performance and reliability requirements at acceptable manufacturing cost. For this reason, previous predictions[41] of enormous market growth for piezoelectric actuators have failed to materialize. Apparently, multilayer ceramic fabrication technology that allows capacitors to be manufactured at pennies per part, has not translated into the low-cost fabrication of multilayer actuators.

Despite the difficulties in achieving necessary cost reductions for high-volume production, piezoelectric ceramics continue to find new uses in low-volume, specialized applications where the relatively high costs can be tolerated. Examples include positioning heads for magnetic recording,[42] scanning tunneling microscopes,[43] bar-code readers,[44] sensors for antilock braking systems,[45] toner sensors for laser printers[46] and ultrasonic bone-healing devices.[47] There appear to be several specialized biomedical applications of piezoelectric ceramic materials, where high cost can be tolerated. For example, piezoelectric single crystals[48] can be used in future ultrasonic imaging systems.

New Fabrication Methods

Injection molding is being developed as a low-cost fabrication method for piezoelectric–polymer composites.[49] Targeted applications include ultrasonic transducer arrays for ultrasonic imaging systems and transducer–actuator arrays for vibration-damping systems. Higher-frequency operation and, thus, smaller feature sizes are required to increase the resolution of ultrasonic imaging systems. As feature sizes are reduced to the 50 μm size range and below, mechanical strength becomes an issue during fabrication.

The use of new synthesis and processing methods to allow preparation of fine-grained microstructures is a viable approach for improving mechanical properties, assuming that equivalent piezoelectric properties can be obtained.

Miniaturized piezoelectric ceramic transformers[50] are being developed for flat-panel displays and other computer-related applications. The need for a piezoelectric ceramic material with high mechanical Q and high driving voltages may require the use of new ceramic-processing methods.

Chemical synthesis methods have been applied successfully to capacitor dielectrics and provide significant advantages—e.g., thinner layers and nickel electrodes—despite higher powder costs. Hydrothermal synthesis[51,52]

and other advanced processing methods[9] also are being developed for piezoelectric ceramics.

However, despite the promise of improved performance and reliability, no method has been developed beyond the pilot-scale evaluation stage. It remains to be seen whether successful development and scale-up of these new PZT powder production methods can be achieved, and whether these powder-processing technologies can provide the impetus required for successful large-scale commercialization of ceramic actuators and other high-performance piezoelectric ceramic applications.

Japanese scientists identified the need for non-lead-containing piezoelectric ceramics. However, no such patents have appeared recently. It is doubtful that any "new" non-lead-containing piezoelectric ceramic systems will be identified. Therefore, research will focus on currently known materials.

Research on lead-free piezoelectrics is being conducted at U.S.[53] and Japanese universities,[54] and useful piezoelectric compositions in the $(Na_{1-x}Bi_x)TiO_3$ system[54] have been identified. Other candidate non-lead piezoelectric systems would include perovskites, such as $(Na,K)NbO_3$; bismuth-layer-structured compounds, such as $Bi_4Ti_3O_{12}$, $SrBi_2Nb_2O_9$; and tungsten–bronzes, such as $(Sr,Ba)Nb_2O_6$. However, it is doubtful that ceramics within these systems will exhibit piezoelectric responses even close to those of PZT ceramics.

If lead-free piezoelectric ceramics are mandated by future regulations, then considerable R&D will be required to identify suitable piezoelectric compositions and to develop ceramic-processing methods for these new materials. Also, system designers will be forced to compromise on the magnitude of piezoelectric strains and to focus on approaches to amplify the strains. Examples of recently commercialized strain-amplification technologies include rainbow actuators[55] and moonies.[56]

Ferroelectric Thin Films

Ferroelectric thin films have created excitement within the electronic ceramics community, with R&D beginning in earnest during the late 1980s and continuing throughout the 1990s. Although the promise of using ferroelectric films in semiconductor memories has been known for some time,[57, 58] the availability of suitable thin-film deposition techniques for multicomponent oxides is a relatively recent development. Many of these advanced deposition methods were developed for high-temperature superconductors and then applied to ferroelectric materials as government funding for thin-film superconductors diminished and increased funding for thin-film ferroelectrics became available.

In the United States, much of the government-funded initial ferroelectric thin-film R&D has been conducted at universities, small businesses and government laboratories. In the late 1980s, the U.S. government supported development of NVM, with programs led by Raytheon and McDonnell Douglas. However, these heavily funded development programs failed to produce a commercial memory product.

Current U.S. developers of NVM include two small companies, Ramtron and Symetrix, both of which are collaborating with several Japanese companies. Motorola and National Semiconductor appear to be funding their own development work, based on patent search and their contributions to recent technical symposia.

Beginning in 1992, the U.S. government shifted its priorities to the development of DRAMs, and work continues under a DoD-supported consortium[59] of U.S. DRAM manufacturers—Micron, IBM and Texas Instruments—with support provided by North Carolina State University, Advanced Technology Materials and Varian. Motorola is funding its own DRAM development work.

In recent years, the financial responsibility for much of the memory development work has been transferred from the U.S. government to semiconductor manufacturers, with a corresponding reduction in government support of R&D at universities and small businesses.

In Japan, industry has funded essentially all of the ferroelectric thin-film R&D to date, and this support has increased substantially in recent years. Japan's ferroelectric thin-film technology development work has received little direct support from the Japanese government, and there has been only limited Japanese university involvement in ferroelectric thin-film research, probably because of the high capital costs for semiconductor-processing equipment.

Similar to the United States, there is a strong interest in ferroelectric thin-film research by large industrial companies in Japan. Japanese companies involved with NVM development include Rohm, Toshiba, Hitachi, Fujitsu, Matushita Electronics and Olympus Optical. Japanese DRAM developers include Mitsubishi Electric, NEC, Toshiba and Hitachi.

With the considerable investment that will be required by both U.S. and Japanese industry to sustain the development of semiconductor memories and other ferroelectric thin-film devices, the future growth of this R&D will be contingent on steady technical progress toward commercial applications. Based on the rapidly increasing number of patents and the comments of Japanese questionnaire respondents, there appears to be considerable confidence that this progress will be achieved.

NVMs in Next Decade

The survey indicated Japanese confidence that semiconductor NVMs will be successfully developed within the next decade, and that development of other thin-film applications, such as microactuators, will follow thereafter. Many of the technical hurdles to commercialization of ferroelectric memories have been addressed, including deposition methods for high-quality thin films, interlayer and electrode materials, and integration onto semiconductors. However, a significant amount of development is required to assure success.

A current issue with PZT-based NVMs is fatigue after numerous polarization reversal cycles,[59] but recent reports indicate successful fabrication of PZT films that withstand up to 10^{13} cycles, which is sufficient for most memory applications.

An important development[60] is the identification of bismuth-layer-structured $SrBi_2Ta_2O_9$ (SBT) as a ferroelectric thin-film material with fatigueless polarization reversal properties.

However. SBT requires high deposition temperatures ($T > 750°C$), which are incompatible with successful integration into high-capacity memories. Development work to be conducted over the next few years will determine which ferroelectric material (PZT or SBT) will be successfully incorporated into commercial NVMs.

Although the development of SBT increases the chances for successful NVM development, the ultimate result may be to diminish the amount of R&D devoted to solving associated integration issues and optimizing performance of PZT films, the thin-film material of choice for microactuators. However. there remains an obvious synergy between the development of semiconductor memories and the subsequent development of other semiconductor-based ferroelectric thin-film applications.

The primary technical issue to be addressed is the fabrication of relatively thick PZT films, so that sufficiently large piezoelectric strains can be exploited. Currently, there are no inexpensive thick-film fabrication methods available that provide the required quality, although this is an area of considerable ongoing R&D.

Future Perspective

This survey was conducted to obtain a future perspective of electronic ceramics R&D in the United States and Japan. Patent literature was reviewed and a survey of Japanese technologists was conducted. The following conclusions are offered:

•Based on the patent review. there are substantial differences in the R&D structure of electronic ceramics between the United States and Japan. In the United States, much of the R&D is funded by the U.S. government and is focused on specific needs of the military. In Japan, electronic ceramics research is almost entirely supported by large industrial companies and targeted toward specific products. In the United States, universities, small businesses and government laboratories are active patenters of electronic ceramics materials technology. In Japan. patents are assigned almost exclusively to industrial companies.

•Enormous growth in applications of multilayer piezoelectric actuators and ultrasonic motors has not occurred because of difficulties in reducing manufacturing cost at high-volume production. Unless low-cost manufacturing methods for piezoelectric ceramic devices can be developed, this market will be restricted to low-volume, specialized applications.

•Continued miniaturization of electronic ceramic devices is expected as multilayer fabrication technologies continue to evolve. Ceramic packaging and semiconductor processing are expected to merge. with multifunctionality built into the ceramic package and into the semiconductor substrate.

•Successful development of high-capacity (>4 Mbyte) semiconductor memories is expected within several years. The key technical issue is integration of fabrication processes for the ferroelectric thin-film materials with semiconductor processing. because the relatively high processing temperatures (650°C) of ferroelectric films must not adversely affect underlying semiconductor circuitry. Current ferroelectric NVM materials include PZT and SBT, each having its own development hurdles. The primary ferroelectric thin-film material for DRAMs is $(Ba,Sr)TiO_3$. For this application, near-term success is critical, so that the technology can be implemented before competing high-capacity DRAM designs are selected.

•Successful commercialization of semiconductor memories is expected to be followed by the development and commercialization of ferroelectric films for microactuators and related microelectromechanical systems. The key development issue is the development of fabrication processes for relatively thick (>5 μm) ferroelectric films with high piezoelectric activity (e.g., PZT) and semiconductor integration processes for these thick films.

•Medicine and telecommunications are growth areas for electronic ceramics applications. especially in the United States. Piezoelectric ceramics will continue to be incorporated into diagnostic instruments and surgical tools, which can tolerate the relatively high costs associated with low-volume production of specialized piezoelectric ceramic components. Expansion of satellite broadcasting and personal communications will require new optoelectronic materials and devices, and new miniaturization/integration technologies for current microwave components.

•There is a growing awareness of environmental and energy-related issues pertaining to electronic ceramics in Japan, but not necessarily in the United States. This may result in a shift in priorities for future Japanese R&D of electronic ceramics products. New environmental regulations may result in the limited use of current materials—e.g., lead-based relaxor dielectrics—and development of alternative materials—e.g., lead-free piezoelectrics and lead-free solders. The development of environmentally friendly ceramic fabrication processes also is expected. An excellent review article[61] describing materials engineering concepts for a better global environment was recently published.

•The development time for electronic ceramics products is expected to become shorter, and the resources available for R&D are expected to be reduced. This will require substantial focusing of R&D resources toward specific product targets. An increased emphasis on marketing and market research will be required, so that limited R&D resources can be matched to market needs. ■

Acknowledgments

The authors are grateful to the Air Force Office of Scientific Research (AFOSR/AORD) for providing funding for this work and to Dr. Shiro Fujishiro (ASOFR) for his encouragement throughout the project. The authors also wish to acknowledg the following people for their input to the assessment: T. R. Gururaja, (Hewlett–Packard), Angus Kingon (North Carolina State University), Harlan Anderson (University of Missouri-Rolla) and Clive Randall (The Pennsylvania State University).

The first part of this two-part article on the future trends of R&D of electronic ceramics in the United States and Japan presented results of a patent review. The patent review was presented in the July 1997 issue of *Ceramic Bulletin*.

For the complete set of references to parts I and II of this article, please FAX or mail your request with your name and address to Editorial Assistant at 614-794-5822 or headquarters, respectively. Request ACerS Data Depository File No. 272.

For the list of Japanese organizations responding to the questionnaire or a more-detailed summary and analysis of the survey results (including unedited questions), please FAX or mail your request with your name and address to Editorial Assistant at 614-794-5822 or headquarters, respectively. Request ACerS Data Depository File No. 274.

MATERIALS STUDIES

Polycrystal Perovskite Ceramics

APPENDIX 4

Journal of the Korean Physical Society, Vol. 32, February 1998, pp. S1265~S1267

Piezoelectric Properties of $Pb(InNb)_{1/2}O_3$-$PbTiO_3$ Solid Solution Ceramics

Edward F. ALBERTA and Amar S. BHALLA
Materials Research Laboratory, The Pennsylvania State University, University Park, Pennsylvania 16802, USA

Piezoelectric and electrical properties of ceramics in the xPb(InNb)$_{1/2}$O$_3$-(1−x)PbTiO$_3$ [PIN:PT(x)] system are described. A high dielectric constant and remanent polarization were obtained for compositions near the morphotropic phase boundary. In this system, the morphotropic phase boundary is found to be located at the composition x = 62 mol% PIN. For this composition, the dielectric constant is 2100 at room temperature and increases to 23500 at it's transition temperature of 280 °C. The remanent polarization is approximately 35 μC/cm^2 and corresponds to a coercive field of 16 kV/cm. Finally, poled ceramics of the morphotropic phase boundary composition posses a d_{33} value of 395 pC/N, a d_{31} of -175 pC/N and a k_{31} of 30%.

I. INTRODUCTION

Lead indium niobate, $Pb(InNb)_{1/2}O_3$ (PIN) has been shown to be a relaxor ferroelectric in which the degree of B-site cation ordering can be thermally controlled. Disordered PIN has been found to have a pseudo-cubic perovskite structure. After thermal annealing, PIN orders into an antiferroelectric orthorhombic phase, isostructural with $PbZrO_3$. It has been reported that a morphotropic phase boundary exists in the solid solution system xPb(InNb)$_{1/2}$O$_3$-(1−x)PbTiO$_3$ [PIN:PT] near x = 0.62 separating the pseudo-cubic and tetragonal phases [1,2]. This paper reports the dielectric and piezoelectric properties for PIN:PT compositions in the vicinity of the morphotropic phase boundary.

II. EXPERIMENTAL PROCEDURES

Ceramic samples of various PIN:PT compositions near the morphotropic phase boundary were sintered in closed Al_2O_3 crucibles for 3 hours at 1250 °C. The atmosphere within the crucible was maintained using In_2O_3 and PbO source powders. Sintered samples were then polished and sputtered-platinum electrodes were applied.

The temperature dependence of the dielectric constant was measured using a computer controlled measurement system consisting of a multifrequency LCR meter (HP4274A. Hewlett Packard Co.), a desktop computer (HP9816) and a nitrogen-fed furnace (Delta Design Inc.).

Dielectric hysteresis measurements were made using a modified Sawyer-Tower circuit. Simultaneous strain measurements were made using an LVDT and lock-in amplifier (SR860, Stanford Research Inc.).

In preparation for the piezoelectric measurements, the samples were immersed in a silicone oil to prevent electrical breakdown and poled at 40 kV/cm for 10 min. The piezoelectric measurements were made with an HP 4194A impedance analyzer using the IEEE resonance method.

III. RESULTS

The temperature dependence of the dielectric constant was determined for several compositions across the PIN:PT solid solution. Figure 1 shows the frequency dependence of the dielectric constant for the composition x = 0.62. The room temperature dielectric constant, measured at 1 kHz, was found to be 2100. The transition temperature of 280 °C corresponds to a maximum dielectric constant of 23500. Figure 2 illustrates the presents of two maxima in the dielectric constant versus temperature measurements for poled samples. The lower temperature transition can be explained by the presence of a small curvature of the morphotropic phase boundary (Fig. 6). The morphotropic phase boundary composition (x = 62 mol% PIN) is also clearly shown.

The remanent polarization and coercive field for PIN:PT(62:38) was found to be 34.5 μC/cm^2 and

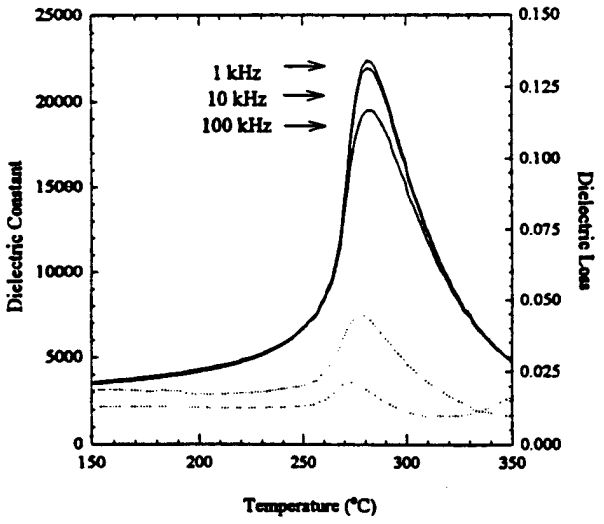

Fig. 1. Variation of the dielectric constant and loss for PIN:PT(62:38) ceramics.

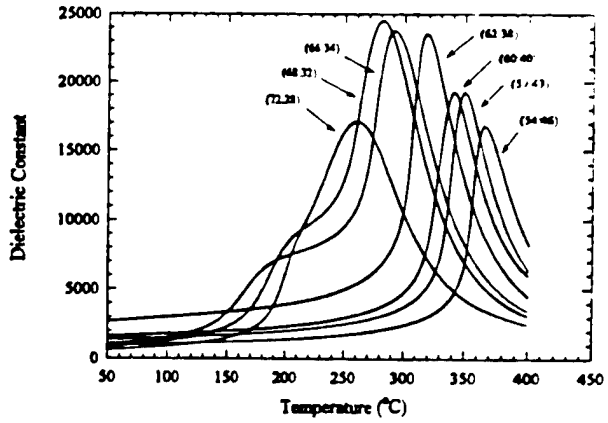

Fig. 2. Temperature dependence of the dielectric constant for various poled compositions in the PIN:PT (x:1$-x$) system measured while heating at 2 °C/min at 1 kHz.

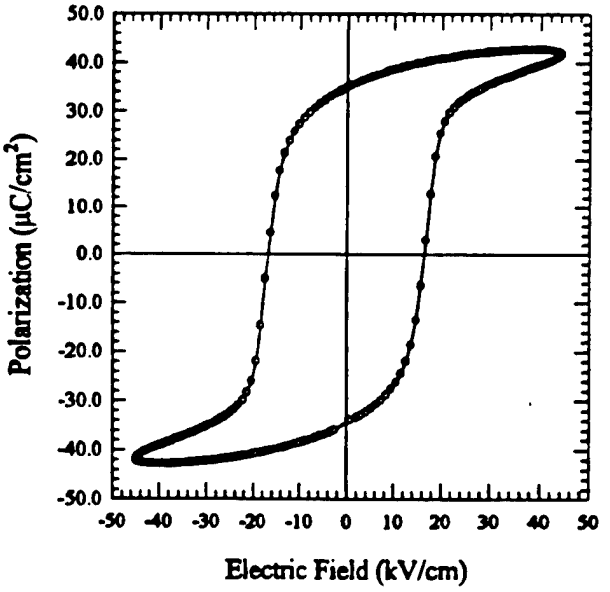

Fig. 3. Dielectric hysteresis loop for PIN:PT(62:38).

16 kV/cm, respectively. A summary of the hysteresis data for samples near the phase boundary is shown in Fig. 4. The addition of lead titanate increases the remanent polarization from nearly zero for pure PIN to a maximum value of 34.5 μC/cm^2 at the morphotropic phase boundary. In addition, the coercive field also increases with increasing lead titanate concentration.

Ceramics in the PIN:PT system were found to be easily poled with a field of 40 kV/cm applied at room temperature. After poling, the piezoelectric coefficient, d_{33}, was measured using a Berlincourt d_{33}-meter. The optimum poling time was determined to be approximately 10 minutes. The piezoelectric coefficient was found to reach a maximum value of 395 pC/N at the morphotropic phase boundary. The piezoelectric coupling coefficient, k_{33}, followed a similar trend, reaching a maximum of 30%.

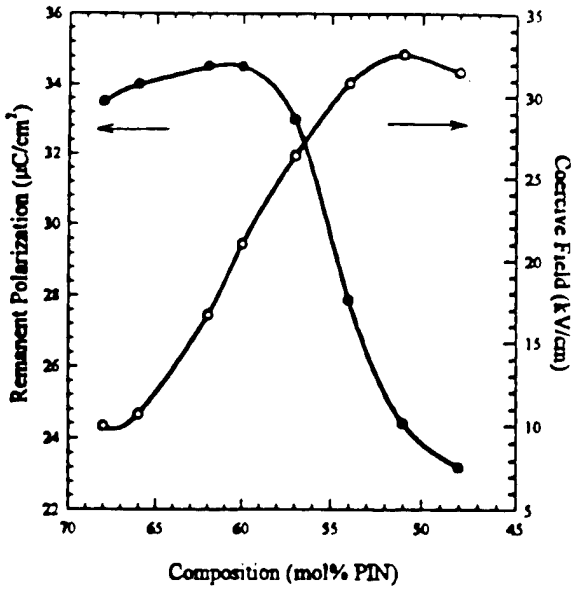

Fig. 4. Compositional dependence of the remanent polarization and coercive field for PIN:PT ceramics.

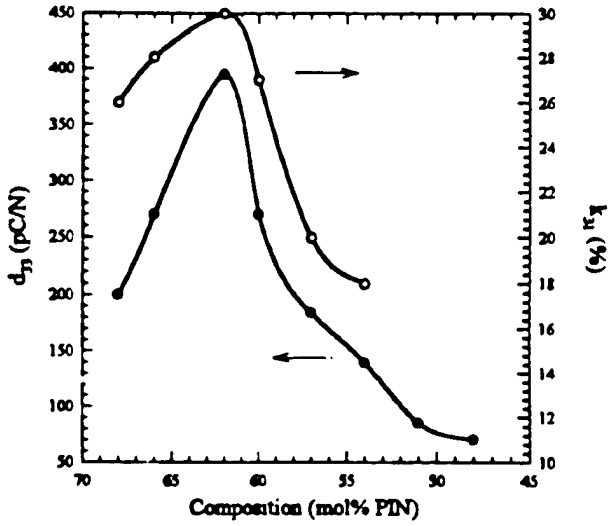

Fig. 5. Compositional dependence of the piezoelectric coefficient, d_{33}, and the piezoelectric coupling coefficient, k_{31}, for PIN:PT ceramics.

IV. SUMMARY

The PIN:PT solid solution has a morphotropic phase boundary at x = 0.62. The dielectric constant for this composition is 2100 at room temperature and increases to 23500 at it's transition temperature of 280 °C. The remanent polarization is approximately 35 μC/cm^2 and corresponds to a coercive field of 16 kV/cm. The poled ceramic was found to have a d_{33} value of 395 pC/N, a d_{31} of -175 pC/N and a k_{31} of 30%.

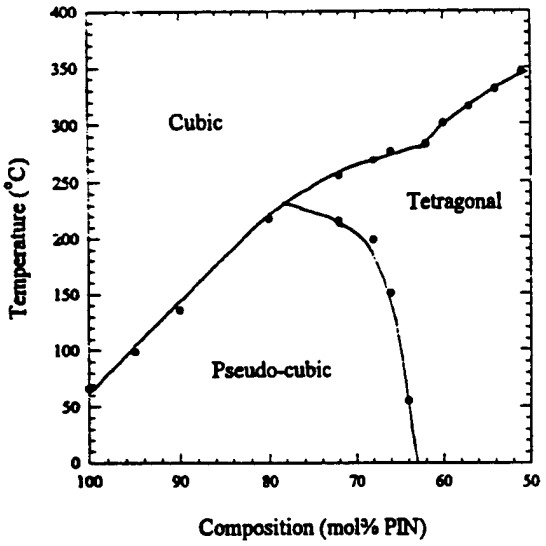

Fig. 6. PIN:PT phase diagram based on transition temperatures of poled ceramics.

REFERENCES

[1] U. Kodama, M. Osada, O. Kumon and T. Nishimoto, Ceram. Bull. **48**, 1123 (1969).

[2] E. F. Alberta and A. S. Bhalla, Mater. Lett. **29**, 127 (1996).

APPENDIX 5

High Strain and Low Mechanical Quality Factor Piezoelectric $Pb[(Sc_{½}Nb_{½})_{0.575}Ti_{0.425}]O_3$ Ceramics.

Edward F. Alberta and Amar S. Bhalla
Materials Research Laboratory, The Pennsylvania State University, University Park, PA.

Abstract

Piezoelectric properties of niobium doped $Pb(ScNb)_{½}O_3$: $PbTiO_3$ [PSN:PT] ceramics near the morphotropic phase boundary are investigated. The piezoelectric coupling factors $k_p \approx 82$ %, $k_{31} \approx 48$ % , $k_{33} \approx 77$ %, and $k_t \approx 57$ % are measured. In good samples, values of remanent polarization of 40.81 $\mu C/cm^2$ and the mechanical quality factor, Q_m, less than 10 show the potential of the material for designing high sensitivity and wide bandwidth sensors and transducers.

Introduction

Lead scandium tantalate - lead titanate [PST:PT] and isomorphous lead scandium niobate - lead titanate [PSN:PT] solid solutions possess morphotropic phase boundaries at compositions of $Pb[(Sc_{½}Ta_{½})_{0.60}Ti_{0.40}]O_3$ and $Pb[(Sc_{½}Nb_{½})_{0.575}Ti_{0.425}]O_3$, respectively.[1,2,3,4] Yamashita[5] and Adachi[6] have shown that niobium-doped PSN:PT has electromechanical coupling and piezoelectric constants that rival those of PZT and may prove to be of enormous technological interest. They report coupling factors of $k_p = 69\%$, $k_t = 52\%$ and $k_{33} = 76\%$ with a remanent polarization of 27 $\mu C/cm^2$ and room temperature dielectric constant of 2500. This paper reports the unusually low mechanical Q and high electrostrictive strain as well as further improvements in the electromechanical properties of PSN:PT ceramics. These improvements in the ceramic PSN:PT will have impact in

medical imaging devices and other applications requiring high coupling and wide bandwidth.

Experimental Procedures

Niobium doped PSN:PT samples were prepared by the Columbite precursor method[7]. The precursor material was synthesized using Sc_2O_3 and Nb_2O_5 to form stoichiometric $ScNbO_4$. PbO and Nb_2O_5 were then added to the $ScNbO_4$ and the mixture was vibratory milled for 24 hours. After drying, the powder was calcined for 2 hours at 850°C. The calcined powder was then pressed and sintered at 1275°C followed by hot isostatic pressing at 1000°C.

The electrical properties were measured on samples with sputtered platinum electrodes. P-E hysteresis loops were observed using a modified Sawyer-Tower circuit. The corresponding strain was measured using an LVDT and lock-in amplifier. Samples were then poled in a heated silicone oil bath. The optimum poling field of 30 kV/cm was used for 30 min at a temperature of 100°C. Samples were allowed to age for 24 hours before any piezoelectric or dielectric measurements were made. The IEEE resonance method[8] was followed for these measurements using an HP-4194A impedance analyzer.

Results and Discussion

Following the initial conventional sintering step, the ceramics were HIP'd to further enhance density. After the HIP'ing step the ceramics were almost translucent, having approximately 98% theoretical density and were single-phase perovskite. The room temperature dielectric constant of as-prepared samples was 2500 at 1 kHz and the dependence of the dielectric constant on temperature is shown in figure 1. The morphotropic phase boundary composition samples showed a transition temperature of 254°C at which the corresponding maximum permittivity value was 30500. A typical P-E hysteresis loop for the PSNT ceramics depicting the remanent polarization of

40.81 $\mu C/cm^2$, coercive field of 7.47 kV/cm, and maximum applied field of 88 kV/cm at room temperature is shown in figure 2. Electrostrictive strain measurements at room temperature showed the material's high tolerance for electric field. High electromechanical strain values of 0.6 % were measured at field levels of 90 kV/cm.

The samples were poled and aged for 1 day after which the dielectric constant and electromechanical properties were measured again. The dielectric constant increased to 3100 and the typical d_{33} was on the order of 595 - 600 pC/N (using a Berlincourt d_{33} meter.) The guidelines of the IEEE for determining the piezoelectric constants by the resonance method were followed for obtaining the various piezoelectric coefficients listed in table 1. The electromechanical coupling coefficients, k_p, k_{31}, k_{33} and k_t were on the order of 82 %, 48 %, 77 % and 57 %, respectively. In addition to these attractive properties, the mechanical quality factor, Q_m, values were rather low. For the radial mode $Q_m \approx 24$ and for the thickness mode $Q_m < 10$ were calculated from the experimental data. The low mechanical quality factor found in these materials provide an avenue to design large intrinsic-bandwidth transducers. Thus, PSN:PT is an attractive and technically important material for designing high sensitivity (high coupling) high bandwidth (low Q_m) transducers. The electrostrictive strain, on the order of 0.6 % is a significant value in ceramics and is one of the largest reported in electroceramics.

References

1. Giniewicz, J.R., "An Investigation of the Lead Scandium Tantalate-Lead Titanate Solid Solution System," *Ph.D. Thesis, The Pennsylvania State University,* University Park, PA (1991).

2. Giniewicz, J.R., A.S. Bhalla, and L.E. Cross, "Pyroelectric Response and Depolarization Behavior of (1-x)$Pb(Sc_{½}Ta_{½})O_3$ -(x)$PbTiO_3$ Materials," *Ferroelectrics,* **118**, 157 (1991).

3. Wang, J.F., J.R. Giniewicz, and A.S. Bhalla, "Soft Piezoelectric (1-x)$Pb(Sc_{½}Ta_{½})O_3$ - (x)$PbTiO_3$ Ceramics with High Coupling Factors and Low Q_m," *Ferroelectrics Letters,* **16**, 113 (1993).

4. Tennery, V.J., K.W. Hang, and R.E. Novak, "Ferroelectric and Structural Properties of the $Pb(Sc_{½}Nb_{½})_{1-x}Ti_xO_3$ System," *J. Am. Ceram. Soc.*, **51** 671 (1968).

5. Yamashita, Y., "Improved Ferroelectric Properties of Niobium-Doped $Pb[(Sc_{½}Nb_{½})Ti]O_3$ Ceramic Material," *Jpn. J. Appl. Phys.*, **32** 5036 (1993).

6. Adachi, M., T. Toshima, M. Takahahi, Y. Yamashita, and A. Kawabata, "Preparation and Properties of Niobium-Doped $Pb[(Sc_{½}Nb_{½})_{0.58}Ti_{0.42}]O_3$ Ceramics Using Hot Isostatic Pressing," Submitted for publication, (1995).

7. Swartz, S.L. and T.R. Shrout, "Fabrication of Perovskite Lead Magnesium Niobate," *Mat. Res. Bull.*, 17, 1245 (1982).

8. IEEE Standard on Piezoelectricity, ANSI/IEEE Std. 176-1978, The Institute of Electrical and Electronic Engineers, Inc., New York (1978).

Tables

1. Measured dielectric and electromechanical properties of $Pb[(Sc_{½}Nb_{½})_{0.575}Ti_{0.425}]O_3$ ceramics.

Figures

1. Variation of the dielectric constant and loss as a function of temperature for PSNT ceramics.

2. Hysteresis loop characteristics of PSN:PT ceramics.

3. Electrostrictive strain behavior of PSN:PT ceramics.

(Please adjust the size of the tables and figures as necessary.)

Table 1. Measured dielectric and electromechanical properties of $Pb[(Sc_{½}Nb_{½})_{0.575}Ti_{0.425}]O_3$ ceramics.

Property:	PSN:PT
Density (g/cm^3)	7.95
Dielectric constant:	
at 25°C (unpoled)	2500
at 25°C (poled)	3100
at T_c	30500
Dielectric Loss:	
at 25°C (unpoled)	0.020
at 25°C (poled)	0.017
at T_c	0.102
Transition temperature (°C)	254
Hysteresis:	
E_{max} (kV/cm)	88.00
E_c (kV/cm)	7.47
P_{max} ($\mu C/cm^2$)	50.10
P_r ($\mu C/cm^2$)	40.81
χ_{max} (%)	0.58
Resonance:	
N_r (Hz m)	2014
N_t (Hz m)	2114
σ	0.33
s_{11}^E ($x10^{-12}$ m^2/N)	14.97
d_{33} (pC/N)	595
d_{31} (pC/N)	-310
k_p (%)	82
k_{31} (%)	48
k_{33} (%)	77
k_t (%)	57
Q_m (radial mode)	24
Q_m (thickness mode)	< 10

Table 1. (Alberta and Bhalla, 1997)

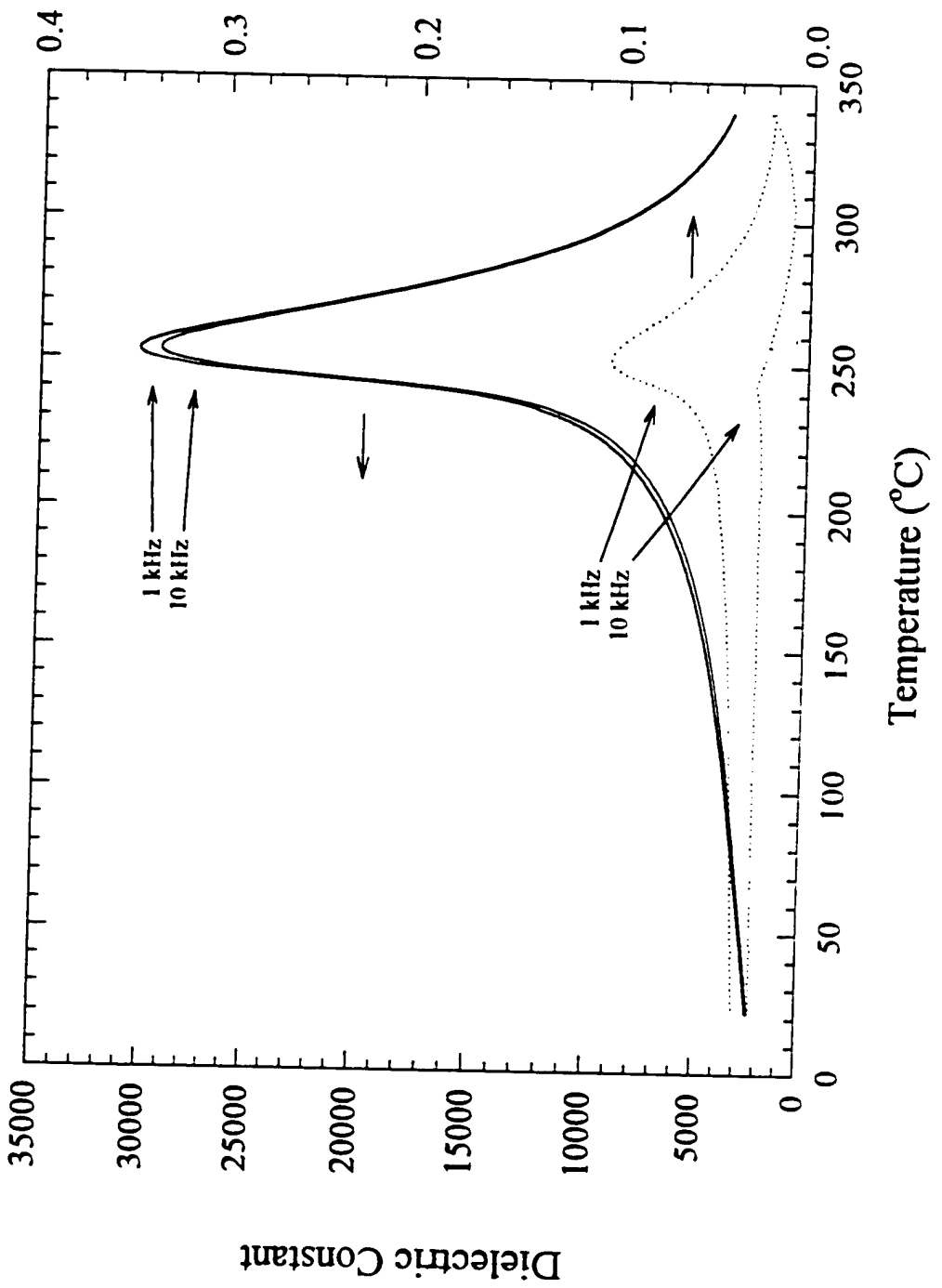

Figure 1. (Alberta and Bhalla, 1997)

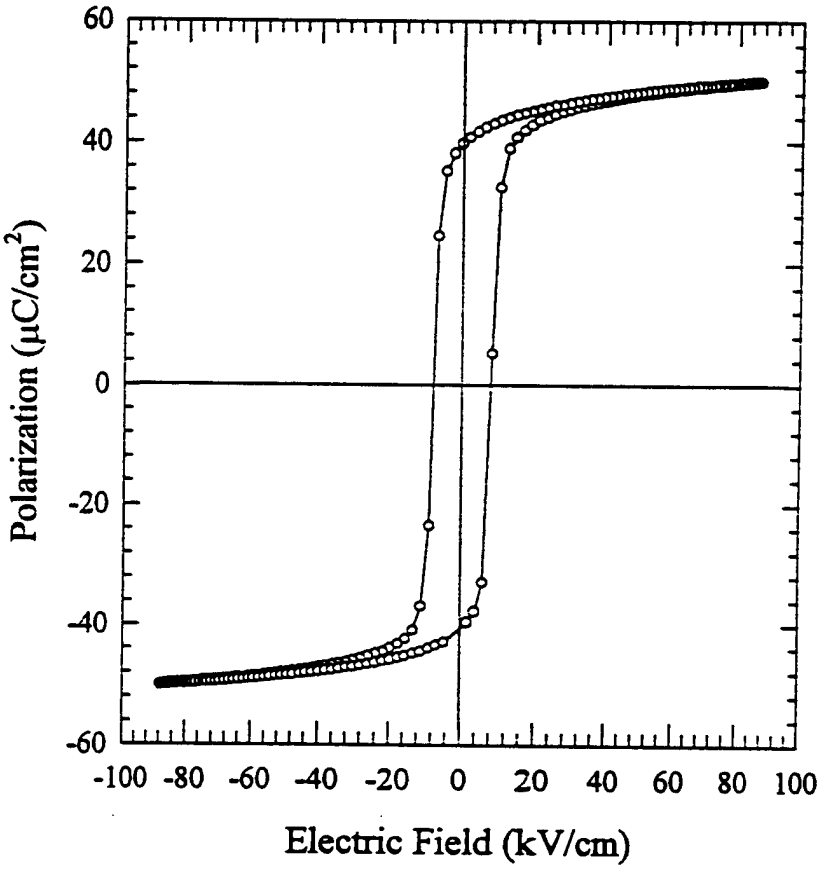

Figure 2. (Alberta and Bhalla, 1997)

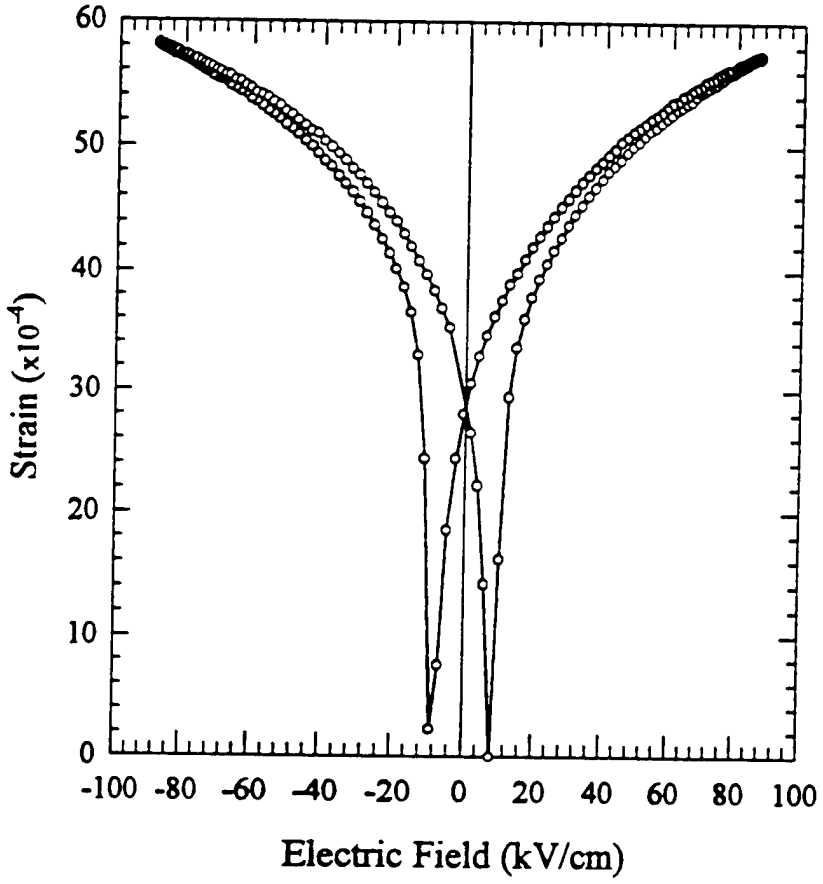

Figure 3. (Alberta and Bhalla, 1997)

APPENDIX 6

Polarization responses in lead magnesium niobate based relaxor ferroelectrics

Q. M. Zhang[a] and J. Zhao
Materials Research Laboratory and Department of Electrical Engineering, The Pennsylvania State University, University Park, Pennsylvania 16802

(Received 31 March 1997; accepted for publication 21 July 1997)

Changes in the electrostrictive coefficients Q_{ij}, especially the volumetric coefficient, with temperature and bias field provides important information regarding the nature of the polarization in lead magnesium niobate based relaxor ferroelectrics. We show that the polarization response at temperatures near the dielectric constant maximum is mainly through the polar-vector reorientation of the nanopolar regions, as suggested by the polar glass model. As the temperature is lowered through the freezing transition, the polarization response is governed by the phase switching and intrinsic contributions rather than by the domain wall motions found in normal ferroelectrics. © *1997 American Institute of Physics.* [S0003-6951(97)02638-7]

Relaxor ferroelectric materials have attracted a great deal of attention in the past several decades because of their technological importance and peculiar phase transition behavior.[1,2] One classical system is $Pb(Mg_{1/3}Nb_{2/3})O_3$ (PMN) and its solid solution with $PbTiO_3$ [$(1-x)$PMN–xPT, $x<0.3$]. The materials are characterized by a broad dielectric maximum with a strong frequency dispersion at temperatures just below the dielectric maximum T_m. Moreover, when cooled in zero field, the materials remain in the cubic phase macroscopically even at temperatures near zero Kelvin. Microscopically, the structure is divided into polar regions with a coherence length on the order of 10 nm. It has been observed that these nanopolar regions persist to temperatures far above T_m. Many models have been proposed for this class of material. Among them, the superparaelectric model, the polar glass model, and the random field model have received the most attention.[2–5] More recently, based on model calculation, it has been suggested that the dominant polarization mechanism at temperatures near T_m in PMN is through domain-wall-type motions rather than through polar region reorientation as suggested by the polar glass model.[6] Although each of these models has merit, there exists no direct experimental evidence related to the basic polarization mechanisms and on the nature of the nanopolar regions, which are crucial to the understanding of relaxor behavior and to attest different models.

In the absence of a poling field, the microstructure of PMN-based relaxors consists of nanopolar regions embedded in a nonpolar matrix.[2] The polarization response of the material can arise from several different mechanisms: the polar-vector reorientation of the polar regions, as suggested by the superparaelectric model and the dipole glass model, the expansion and shrinkage of these regions (breathing mode of the polar regions), and from an induced phase transformation between the cubic (paraelectric) and rhombohedral (ferroelectric) phases. In addition, there are induced changes in polarization from the cubic and rhombohedral phases which are known as intrinsic contributions to the polarization. One of the interesting features related to PMN-based relaxor materials is that these polarization mechanisms are also ferroelastic. Moreover, the polarization responses can be grouped into those generating a volume strain and those with zero volume strain. It is this difference in the volume change, that will be used to probe the nature of the polarization and its dynamics in PMN-based relaxors.[7]

Because of symmetry of the ceramic, the polar vectors of nanopolar regions are distributed randomly in all possible directions. Hence, the breathing mode motions of polar regions with opposite polar directions resemble the 180°-type-domain-wall motion in regular ferroelectric, while those with polar directions other than 180° resemble non-180°-type-wall motions. For the sake of simplicity, the polar region motions of these types are termed as quasidomain-wall motions. Regarding uncompensated breathing mode motions of polar regions, they involve phase transformation of the polar regions and are therefore included in the category of phase switching. Obviously, neither the polar vector reorientation nor the quasidomain-wall motion generates volume strain. On the other hand, the polarization changes arising from the phase switching and the intrinsic contributions are accompanied by a volume strain.

PMN and 0.9PMN–0.1PT were chosen for investigation. The dielectric maximum T_m is -10 °C for PMN and 38 °C for 0.9PMN–0.1PT (at 1 kHz). The use of two compositions instead of one ensures the reliability of the results. Ceramic samples were prepared following the procedures described in Ref. 8. Typical sample size is about $0.5\times0.5\times0.5$ cm^3. The strains S_1 and S_3, the transverse and longitudinal strains, respectively, were measured using both the strain gauge method and the laser dilatometer method. In the strain gauge method, S_1 and S_3 were measured simultaneously by attaching two strain gauges on faces parallel and perpendicular to the applied electric field direction. The signal output from the strain gauge amplifier was detected using both a lock-in amplifier and a digital oscilloscope. In the laser dilatometer method, S_1 and S_3 were acquired separately and the results are consistent with the strain gauge technique.[9] The polarization P_3 was obtained with a Sawyer–Tower circuit in which the output signal was monitored with a lock-in amplifier and a digital oscilloscope. Polarization measurements were car-

[a]Electronic mail: qxz1@psuvm.psu.edu

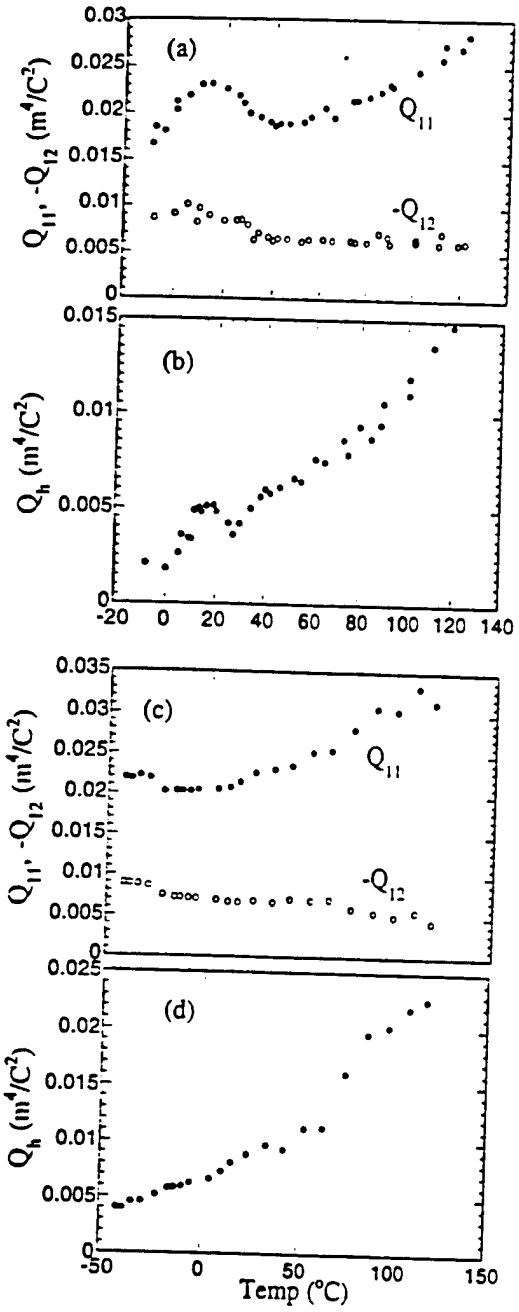

FIG. 1. The electrostrictive coefficients Q_{ij} as a function of temperature measured at 10 Hz. (a) Q_{11} and Q_{12} for 0.9PMN–0.1PT; (b) the volumetric electrostrictive coefficients $Q_h(=Q_{11}+2Q_{12})$ for 0.9PMN–0.1PT; (c) Q_{11} and Q_{12} for PMN; (d) Q_h for PMN.

ried out concurrently with the strain measurement. In the field range used, the difference between the data obtained from the lock-in amplifier and those from the digital oscilloscope is within the data scatter (about ±5%). The amplitude of applied AC voltage is about 200 V/cm with a frequency of 10 Hz. Experiments were carried out during both cooling and heating cycles, and except for 0.9PMN–0.1PT data below 15 °C, which is strongly affected by the freezing transition of the material, there are no significant differences between the data in the two temperature directions.

Presented in Fig. 1 are the electrostrictive coefficients Q_{11} and Q_{12} for PMN and 0.9PMN–0.1PT as functions of temperature, where Q_{11} and Q_{12} are defined as

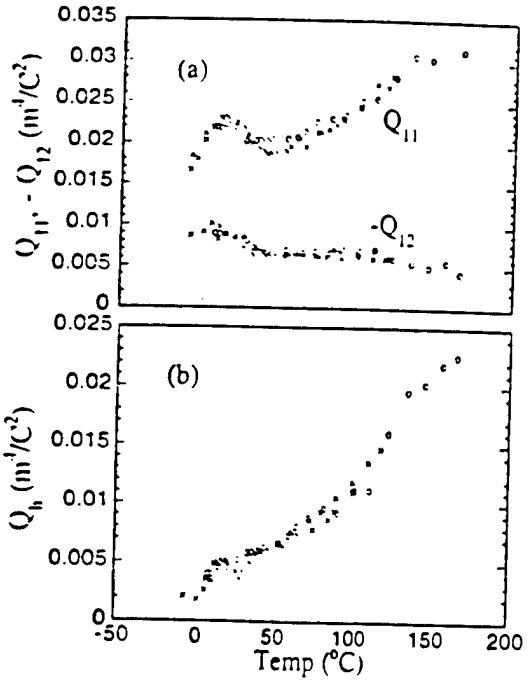

FIG. 2. By shifting the temperatures of PMN up 48 °C (to account for the difference in T_m between PMN and 0.9PMN–0.1PT), the data of PMN (open circles) overlap with those of 0.9PMN–0.1PT (crosses). Data show that as temperature increases, Q_{11} increases while Q_{12} decreases.

$$S_3 = Q_{11}P_3^2 \quad \text{and} \quad S_1 = Q_{12}P_3^2. \tag{1}$$

For PMN, between −45 °C and 125 °C, the measured Q_{ij} values do not change with the applied field amplitude. While for 0.9PMN–0.1PT, the data at temperatures above 10 °C depend only weakly on the field amplitude and below that temperature, the data exhibit a strong dependence on the field amplitude. The change in the field dependence in 0.9PMN–0.1PT is related to the freezing temperature T_f below which the polarization hysteresis loop exhibits substantial remnant polarization and the polarization-field relationship is strongly hysteretic. For 0.9PMN–0.1PT, T_f is about 10 °C while for PMN, it lies near −70 °C, well below the experimental temperature.[3,4,10] By combining Q_{11} and Q_{12}, the volumetric electrostrictive coefficient Q_h ($Q_h = Q_{11} + 2Q_{12}$) can be obtained as presented in Fig. 1.

One of the salient features of Fig. 1 is that the electrostrictive coefficients Q_{ij} change with temperature for both PMN and 0.9PMN–0.1PT. Moreover, compared with Q_{11} and Q_{12}, the relative change of Q_h with temperature is quite substantial. For 0.9PMN–0.1PT, it increases from 0.002 m^4/C^2 at −10 °C to about 0.013 m^4/C^2 at 120 °C. And for PMN, it increases from 0.004 m^4/C^2 at −45 °C to about 0.023 m^4/C^2 at 120 °C. If we shift the temperature scale for PMN upwards by 48 °C, it overlaps nicely with that of 0.9PMN–0.1PT. Hence, when adjusted for the difference in T_f, the results from the two systems are quite consistent with each other (Fig. 2). As pointed out earlier, Q_h measures the volume strain generated per unit polarization. The data presented in Fig. 2 reveal that compared with the polarization mechanisms at higher temperatures, the polarization response at low temperatures (near and below T_m) involves very little volumetric strain. In other words, the polarization

response is from either the quasidomain-wall-type motion or polar-vector reorientation or both.

Another interesting feature from Figs. 1 and 2 is that at high temperatures, the increase of Q_h is due to both the increase of Q_{11} and the decrease of $|Q_{12}|$ with temperature. From the available lattice constant data on the cubic and rhombohedral phases of PMN, it can be shown that for the phase transformation from the cubic to the rhombohedral,[10–12] both Q_{11} and Q_{12} in single crystals are positive where Q_{11} is measured along the [111] direction of the unit cell, which is the direction of the spontaneous polarization and Q_{12} is related to the strain in the plane perpendicular to the spontaneous polarization. Averaging over all the directions yields a near zero Q_{12} for a PMN ceramic sample,[13] which is consistent with the experimental data in which at 120 °C, $Q_{11}/|Q_{12}|$ of PMN is above 7. On the other hand, for the polar-vector reorientation or the quasi-non-180°-domain-wall-motion, Q_{12} should be equal to $-Q_{11}/2$, as observed at temperatures near T_m. The decrease of $|Q_{12}|$ with temperature in the ceramic samples and a large ratio of $Q_{11}/|Q_{12}|$ at high temperatures are clear indications that at high temperatures, the contribution to the polarization response from the phase switching becomes increasingly important. It should be pointed out that the experimental temperature here is still far below the temperature where the nanopolar regions disappear, which for PMN is above 300 °C, and at that temperature, the polarization response should be from the intrinsic.[2]

Hence, in PMN and 0.9PMN–0.1PT, the experimental results establish that in the experimental temperature range there exist at least two types of polarization processes: phase switching which involves volume strain P_v and quasidomain-type motion or polar-vector reorientation P_d which does not involve volume strain. It is apparent that the measured Q_h^m is related to Q_h^{Tr}, which is from P_v, through

$$Q_h^m = Q_h^{\mathrm{Tr}} \frac{P_v^2}{(P_v + P_d)^2}. \tag{2}$$

where we assume that the total polarization is $P_v + P_d$. Obviously, from the data in Fig. 2, $Q_h^{\mathrm{Tr}} > 0.023\ \mathrm{m}^4/\mathrm{C}^2$, which indicates that at near and below T_m, more than 90% of the polarization response is from either the quasidomain-wall-type or polarization reorientation which does not involve volume strain, while at higher temperatures, there is a substantial increase in P_v with respect to P_d.

In order to determine whether the quasidomain-wall-type motion or the polar-vector reorientation is responsible for the polarization response at temperatures near T_m, we note that there is a fundamental difference between the polarization due to the quasidomain-wall motions and the polarization due to the polar-vector reorientation. That is, for the quasidomain-wall-type motions of the nanopolar regions, under an external poling field, the system becomes no longer isotropic and part of the polar region motions will be converted from the qausidomain-wall-type to the phase switching which will produce volume change, while for polar-vector reorientation, there will still be no volume strain under external bias fields.

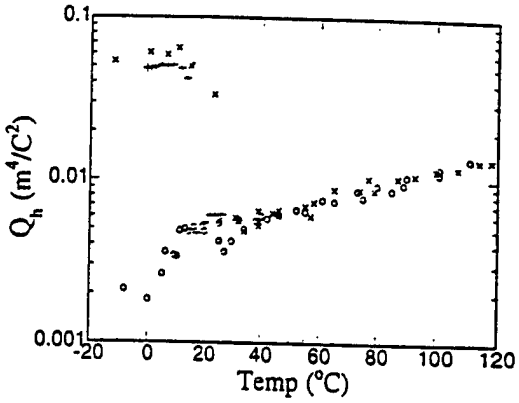

FIG. 3. The effect of DC bias field on the volumetric electrostrictive coefficient Q_h for 0.9PMN–0.1PT. Open circles are Q_h measured without bias field, pluses are under 800 V/cm, and crosses are under 3 kV/cm DC bias field. The large increase of Q_h with DC bias field at low temperatures indicates the polarization response is through the phase switching and intrinsic processes.

The influence of the DC electrical bias field on Q_h was investigated and the data presented in Fig. 3 show that for 0.9PMN–0.1PT at temperatures above 20 °C, Q_h does not exhibit significant changes with DC bias fields. The results presented here, hence, support the notion that at the temperatures near T_m the polarization response from the nanopolar region is through the polar-vector reorientation. On the other hand, at temperatures near and below T_f, a large increase of Q_h was observed for a bias field of higher than 800 V/cm, indicating that the major contribution to the polarization response is due to the phase switching and intrinsic contributions, rather than the domain wall motions or the polar vector reorientation. This is quite different from the behavior at temperatures near T_m. The experimental data, therefore, also establish a direct evidence of a polarization freezing process, i.e., as the system goes through the freezing transition, the polarization response of the nanopolar regions evolves from the polar-vector reorientation to the phase switching.

The authors wish to thank Professor L. E. Cross and Professor R. Newnham for stimulating discussions.

[1] G. A. Smolensky and A. I. Agranoskaya, Sov. Phys. Solid State **1**, 1429 (1959).
[2] L. Eric Cross, Ferroelectrics **76**, 241 (1987).
[3] V. Westphal, W. Kleeman, and M. D. Glinchuk, Phys. Rev. Lett. **68**, 847 (1992).
[4] D. Viehland, S. J. Jang, L. E. Cross, and M. Wuttig, J. Appl. Phys. **68**, 2916 (1990).
[5] E. V. Colla, E. Yu. Koroleva, N. M. Okuneva, and S. B. Vakhrushev, Phys. Rev. Lett. **74**, 1681 (1995).
[6] A. E. Glazounov, A. K. Tagantsev, and A. J. Bell, Phys. Rev. B **53**, 11 281 (1996).
[7] Q. M. Zhang, H. Wang, N. Kim, and L. E. Cross, J. Appl. Phys. **75**, 454 (1994).
[8] S. L. Swartz and T. R. Shrout, Mater. Res. Bull. **17**, 1245 (1982).
[9] Q. M. Zhang, S. J. Jang, and L. E. Cross, J. Appl. Phys. **65**, 2807 (1989).
[10] G. Calvarin, E. Husson, and Z. G. Ye, Ferroelectrics **165**, 349 (1995).
[11] P. Bonneau, P. Garnier, E. Husson, and A. Morell, Mater. Res. Bull. **24**, 201 (1989).
[12] N. de Mathan, E. Husson, G. Calvarin, and A. Morell, Mater. Res. Bull. **26**, 1167 (1991).
[13] A. F. Devonshire, Philos. Mag. **42**, 1065 (1951).

APPENDIX 7

Effect of nanopolar regions on electrostrictive coefficients of a relaxor ferroelectric

A. E. Glazounov, J. Zhao, and Q. M. Zhang

Materials Research Laboratory, The Pennsylvania State University[1], *University Park, PA 16802*

Abstract. Volumetric electrostrictive coefficient, Q_h, of $PbMg_{1/3}Nb_{2/3}O_3$ (PMN) relaxor ferroelectric is investigated using a high-resolution neutron powder diffraction and a conventional strain measurement. Using the results of these experiments we: (1) derive the value of Q_h of prototype cubic lattice of PMN, which is equal to $Q_h = (8.3 \pm 1.0) \times 10^{-2}$ (m^4/C^2); (2) find the temperature dependence of the volume fraction, δv, of the polar regions in the material, and estimate that at temperatures around the dielectric permittivity maximum, T_{max}, it is equal to $\delta v \approx 90\,\%$; (3) estimate the magnitude of the contribution of the crystal lattice to the polarization response of PMN at temperatures around and below T_{max}. These results are essential for the understanding of the nature of the polarization and strain response of relaxor ferroelectrics.

INTRODUCTION

In this paper, we investigate electrostrictive coefficients of a "classical" relaxor ferroelectric, complex perovskite $PbMg_{1/3}Nb_{2/3}O_3$ (PMN). The motivation is to understand the relationship between the microstructural feature of PMN, namely the partitioning of the structure into the small regions of local spontaneous polarization with a nanometer scale size, and the electrostrictive response of this material. The key results of this study are summarized in the abstract and provide a new insight into the physics of relaxor ferroelectrics. Particularly, the evidence derived from this study, such as the temperature variation of the volume fraction of the polar regions and the estimate for the relative contribution of the crystal lattice to the total polarization induced in the material, is very important for the understanding of the nature of the polarization response of relaxors. The latter still remains one of the open problems of the contemporary physics of ferroelectrics and challenges both experimentalists and theorists.

[1] This work was supported by the Office of Naval Research. The authors also wish to thank Dr.B.Toby and National Institute of Standards and Technology (NIST) for the help in experiment with neutron diffraction.

Proceedings Williamsburg Mtg., Williamsburg, VA (1998).

Electrostriction in a double-phase mixture

Contemporary models of relaxors consider them as structurally inhomogeneous materials consisting of small polar regions of nanometer scale size which are randomly distributed in a nonpolar matrix. In PMN, the polar regions appear at high temperatures, around T_d =600 K, far above the temperature of the dielectric permittivity maximum, T_{max}, which is located around 270 K, and persist down to 0 K [1–3]. They are elongated along the direction of the local spontaneous polarization, P_s, (the shape which minimizes the effect of the depolarizing field) which can be oriented in one of eight ⟨111⟩ pseudocubic directions allowed by the rhombohedral symmetry of the polar phase [3]. The presence of the polar regions results in that the material response (both electric and elastic) to the applied electric field can originate from different mechanisms: (a) thermally activated reorientation of vector $\vec{P}_s$ in the polar regions [2,4–7], (b) expansion and shrinkage of the regions (similar to the domain wall motion in ordinary ferroelectrics) [8–10], and (c) induced phase transformation between nonpolar and polar phases [11]. It is also possible that several mechanisms coexist, and that different mechanisms dominate in different temperature intervals [11]. In addition, one should also take into account a change in the polarization and strain due to the response of the (d) crystal lattice, both in polar and nonpolar phases, which is always present and is usually referred to as an intrinsic contribution. Taking into account the above picture of the response of the double-phase mixture "polar regions / nonpolar matrix", the experimentally measured components polarization and strain can be written as:

$$P_i = \sum_\alpha P_i^{(\alpha)} , \qquad S_{ij} = \sum_\alpha S_{ij}^{(\alpha)} , \tag{1}$$

where $P_i^{(\alpha)}$ and $S_{ij}^{(\alpha)}$ are the contributions to the polarization and strain from different mechanisms, (a)–(d), which are averaged over the crystal. Using Eq.(1) and the definition of the electrostriction, $S_{ij} = Q_{klij} P_k P_l$, the electrostrictive coefficients, Q_{klij}, of a relaxor can be written using the matrix notations as:

$$Q_{ij} = \frac{S_j}{P_i^2} = \frac{\sum_\alpha S_j^{(\alpha)}}{\left[\sum_\alpha P_i^{(\alpha)}\right]^2} . \tag{2}$$

This equation shows that coefficients Q_{ij} derived from strain measurements, which are performed with a reference to the structurally inhomogeneous state, are actually some "apparent" values, $Q_{ij} = Q_{ij}^{app}$, which must depend upon the properties of ensemble of the polar regions, such as their population in the crystal, average size, etc..

Is it possible to separate contributions to the electrostrictive strain of relaxor from different polarization mechanisms? One possible solution of this problem has been proposed by Cross [2]. He studied another relaxor, tungsten bronze $(Sr_{0.6}Ba_{0.4})Nb_2O_6$ (SBN), which has a tetragonal structure, and demonstrated that

a large qualitative difference observed in the behavior of electrostrictive coefficients Q_{33} (which was measured using electric field applied along the 4-fold axis in the crystal), and Q_{11} (for the field applied perpendicular to it), could be related to the presence of the polar regions, which local spontaneous polarization, $\bar{P}_s$, was along the 4-fold axis. In the present study, we will use another approach in order to separate the contributions to Q_{ij} from different mechanisms.

Approach of this study

The approach of the present study is to choose PMN as a model material and compare its electrostrictive coefficients derived from two experiments. The objective of one experiment is to determine the values Q_{ij} of prototype cubic lattice of PMN. In order to do that, one should eliminate from the material the inhomogeneity related to the presence of the double-phase mixture: "polar regions / nonpolar matrix" [12]. We will do that by measuring the change in the lattice constants related to the structural phase transition into the ferroelectric state induced in PMN during cooling under dc electric field (FC) at temperatures below T_f = 220 K, [13,14]. In this method, two measurements must be performed, where the lattice parameters of PMN are measured in the FC and zero-field cooling ZFC regimes. However, it should be stressed that because of the existence of the polar regions which introduce an additional strain in the cubic lattice of PMN [2,15] one cannot use as a reference the lattice parameters measured directly in the ZFC experiment at temperatures below T_d =600 K. Therefore, in order to determine the lattice parameters of the prototype cubic phase at temperatures below 600 K, one should adopt the approach employed in Refs. [1,2]. Namely, at T < 600 K the parameters of the prototype cubic phase can be found from the extrapolation of the experimentally measured lattice constants at temperatures above 600 K, which should change linearly according to the normal thermal expansion of the lattice. The comparison of the lattice parameters of rhombohedral ferroelectric state [14,16] with the extrapolated values of the cubic lattice thus will give us the electrostrictive strain related with the structural phase transition.

The second experiment will be a conventional measurement of the electrostrictive strain induced in PMN by small ac fields at temperatures below 600 K, in order to characterize the response of the double-phase mixture: "polar regions / nonpolar matrix".

In the present paper, we will focus on studying the volumetric electrostrictive coefficient, $Q_h = Q_{11} + 2Q_{12}$, of PMN ceramics. We choose Q_h because even though ceramics is the polycrystalline body, the volumetric electrostrictive coefficient remains the same as in the single crystals [17]. Therefore, even though in the experiments we are dealing with ceramics, by measuring Q_h we get the direct information about the properties of PMN single crystals.

EXPERIMENTAL AND RESULTS

Electrostrictive coefficient Q_h of prototype cubic phase of PMN

In this experiment, the lattice parameters of PMN were investigated over a wide temperature interval, from 100 K to 1050 K using a high-resolution neutron powder diffraction. The low temperatures were required to study the ferroelectric state induced in PMN during FC below $T_f = 220$ K [13,14], whereas the high temperature interval (600 K – 1050 K) was important to obtain reliable data on the prototype cubic phase to be extrapolated to low temperatures. The choice of neutron diffraction relied on the fact that neutrons have a larger penetration depth compared to conventional X-rays, thus allowing us to study the bulk properties of the material. High-resolution data were required in order to detect the phase transformation with a very small lattice distortion in the rhombohedral ferroelectric phase of PMN from the prototype cubic phase, $(90° - \alpha^{rh}) \leq 0.1°$, [19]. The neutron powder diffraction data were collected using the BT-1 high resolution diffractometer at the NIST Center for Neutron Research reactor, NBSR, and the details of the experiment are described in Ref. [12].

Experiment was first conducted in the ZFC regime where the diffraction patterns of PMN were recorded at several temperatures from 1050 K to 100 K. Afterwards, the dc field $E = 5$ kV/cm was applied to the same sample at 300 K, and the

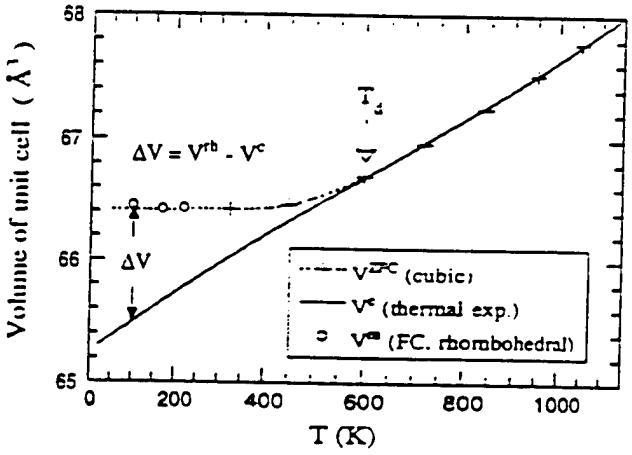

FIGURE 1. Temperature dependence of the volume of the unit cell of PMN measured in ZFC (plus signs, and the dotted line drawn through them in order to guide the eye) and FC (open circles) regimes. The linear dependence of the unit cell volume on temperature corresponds to the normal thermal expansion of prototype cubic lattice of PMN (solid line). During the FC regime, PMN is in the ferroelectric state with a rhombohedral structure at $T \leq 220$ K (open circles). ΔV denotes the volume change in the crystal lattice during the phase transition to the ferroelectric state. T_d is the temperature at which polar regions appear in PMN upon cooling.

sample was cooled down (FC regime). In this regime the diffraction patterns were recorded at several temperatures below $T_f = 220$ K, where the field induced phase transition was expected in PMN for the electric field larger than the threshold field, $E_{th} = 1.7$ kV/cm, [13].

The results of both ZFC and FC measurements were in a good agreement with similar experiments performed by other research groups. For ZFC, the crystal lattice of PMN is cubic in the whole studied temperature interval [3,15], whereas for FC using $E = 5$ kV/cm the crystal structure is rhombohedral at temperatures below 220 K [16,19]. In both cases, unit cell parameters, a^c (for cubic), and a^{rh} and α^{rh} (for rhombohedral), were determined using the structural refinement procedure [12].

Figure 1 presents the temperature dependence of the volume of the unit cell, V, of PMN for both ZFC and FC experiments, and also illustrates the approach which we used to calculate the volume strain of the crystal lattice related with the phase transition. In the plot, open circles show the volume V^{rh} of the unit cell of rhombohedral crystal lattice corresponding to the ferroelectric state induced in PMN at $T \leq 220$ K by the dc field $E = 5$ kV/cm. Pluses and dotted line connecting them correspond to the ZFC regime, $V^{ZFC}(T)$, with the cubic structure. Taking into account that no polar regions exist in the material above $T_d = 600$ K, the linear variation of V^{ZFC} in the high-temperature interval is the normal thermal expansion of the prototype cubic lattice of PMN, $[V^c(T) - V^c(T_d)] \propto \beta_V \cdot (T - T_d)$, where β_V is the volumetric thermal expansion coefficient and V^c is the volume of the unit cell of the prototype cubic lattice. Below 600 K, $V^{ZFC}(T)$ deviates from the linear dependence due to the appearance of polar regions in PMN, which introduce an additional strain in host cubic lattice equal to $Q_h\langle P_s^2\rangle$, where $\sqrt{\langle P_s^2\rangle}$ is the root mean squared local spontaneous polarization [1,2].

In order to find Q_h from the data in Fig. 1, the volumetric strain related to the structural phase transformation was calculated as $\Delta V/V^c$, where $\Delta V = V^{rh} - V^c$, Fig. 1. Below 220 K, the volume V^c of the prototype cubic lattice was found by the extrapolation of the high-temperature linear dependence down to low temperatures, as shown in Fig. 1 with the solid line. Afterwards, the volumetric electrostrictive coefficient was determined from the equation: $Q_h = 1/P_s^2 \cdot [V^{rh} - V^c]/V^c$, where P_s is the macroscopic spontaneous polarization, which was evaluated from saturated polarization hysteresis loops measured on PMN single crystal samples along $\langle 111\rangle$ direction using the ac field of 30 kV/cm amplitude [12].

TABLE 1. Volumetric electrostrictive coefficient Q_h of prototype cubic lattice of PMN relaxor calculated from the results of the structural study of PMN using high-resolution neutron powder diffraction.

T (K)	100	170	220
Q_h (10^{-2} m^4/C^2)	8.2 ± 1.0	8.1 ± 1.0	8.5 ± 1.0

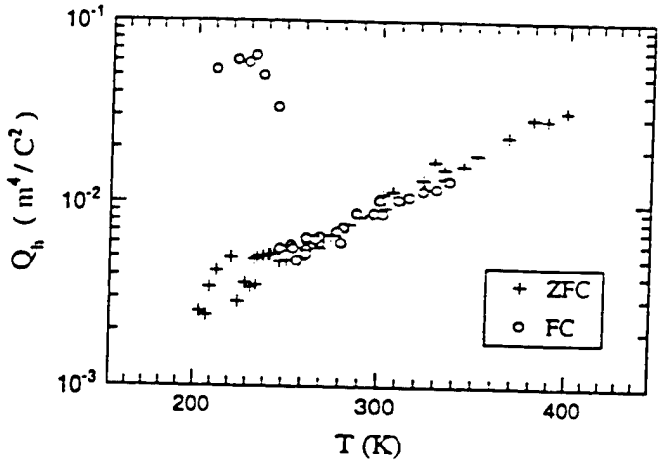

FIGURE 2. Temperature dependence of volumetric electrostrictive coefficient, Q_h, of PMN measured in ZFC (open circles) and FC under the dc bias $E_b = 3$ kV/cm (plus signs) regimes. The step-like change in Q_h at low temperatures coincides with the structural phase transition from mixed to normal ferroelectric state, which is induced in PMN by large dc bias. Therefore large values of Q_h below the step correspond to the electrostrictive strain of the crystal lattice only. The experimental uncertainty of the evaluation of Q_h is about 0.2×10^{-2} (m^4/C^2).

The Q_h data are summarized in Table 1. From that table, it can be seen that within the error of experiment, the electrostrictive coefficient remains temperature independent in the studied temperature interval of more than 100 K. This result is in agreement with the conventional wisdom that the electrostrictive coefficients coupling electric and elastic properties of the crystal lattice should be "proper" material constants, i.e., should be temperature independent [2].

Electrostrictive coefficient Q_h of mixed state of PMN

The electrostrictive coefficient, Q_h, of PMN in its mixed state, "polar regions / nonpolar matrix", was derived from the following experiment [11]. Small ac field of amplitude $E_m = 0.2$ kV/cm and frequency 10 Hz was applied to the sample, and the induced polarization, P_1, and longitudinal, S_1, and transverse, S_2, strains were measured simultaneously. The P_1 was measured using a Sawyer – Tower circuit, in which the output signal was detected with a SR 830 lock-in amplifier, and S_1 and S_2 were measured using the strain gauge technique, where the signal output from the strain gauge was measured with two other SR 830 lock-in amplifiers. Then, the volumetric electrostrictive coefficient was found from: $Q_h = \overline{Q}_{11} + 2\overline{Q}_{12}$, where $\overline{Q}_{11} = S_1/P_1^2$ and $\overline{Q}_{12} = S_2/P_1^2$ are the longitudinal and transverse electrostrictive coefficients of ceramics, respectively. These measurements were performed within the temperature interval from 200 K to 400 K, where the high temperature limit was caused by the increase in the electric conduction of the material at high tem-

peratures, which made the strain measurements very difficult. In addition, the same coefficient was measured in the FC regime, where the small ac probing field, $E_m = 0.2$ kV/cm, was superimposed on large dc bias, $E_b = 3$ kV/cm.

Figure 2 summarizes the results of these experiments by plotting Q_h as a function of temperature. Several features can be noticed in this plot. First, the electrostrictive coefficient of the mixed phase of PMN shows strong temperature dependence, it changes approximately by 10 times within the studied temperature interval. Second, at temperatures around $T_{max} \approx 270$ K, the value of Q_h corresponding to the mixed state is about 10 times smaller than the value derived from the neutron diffraction study, cf. Table 1. Third, when the large dc field is applied to the sample, Q_h undergoes the step-like change at temperatures around 230 K. The position of this step coincides with the temperature of structural phase transition from mixed to normal ferroelectric state, which is induced in PMN by the electric field larger than the threshold field, E_{th}, [13]. Thus, the dc bias "removes" the inhomogeneity related with "polar regions / nonpolar matrix", and Q_h measured at temperatures below the step corresponds to the electrostrictive strain of the crystal lattice only. This conclusion is supported by the fact that under the dc bias the electrostrictive coefficient is temperature-independent at low-temperatures, Fig.2, and has a value $Q_h = (6.0 \pm 0.2) \times 10^{-2}$ (m^4/C^2) which is very close to the average value $Q_h = (8.3 \pm 1.0) \times 10^{-2}$ (m^4/C^2) derived from the neutron diffraction study of PMN, Table 1.

DISCUSSION

The plot in Fig.3 combines all the data obtained in the present work. It clearly demonstrates that the temperature dependence of the electrostrictive coefficient Q_h, which was derived from strain measurements performed with a reference to the structurally inhomogeneous state (plus signs in Fig.3), most likely is related with the change in the properties of the ensemble of the polar regions in the temperature interval below 600 K. Above $T_d = 600$ K, no polar regions exist in the material, thus electrostrictive strain is only due to the distortion of the prototype cubic lattice of PMN, which is characterized by the electrostrictive coefficient Q_h^{lat}. The neutron diffraction data (closed circles in Fig.3) suggest that Q_h^{lat} is temperature independent and is equal to $Q_h^{lat} = (8.3 \pm 1.0) \times 10^{-2}$ (m^4/C^2), Table 1. When the polar regions appear in the material below 600 K, they, first, introduce an additional volumetric strain in the host cubic lattice, which is equal to $Q_h^{lat} \langle P_s^2 \rangle$ [2,15], and, second, bring "new" mechanisms of the polarization and strain response to the electric field, such as polar vector reorientation, (a), or expansion and shrinkage of the polar regions, (b). Therefore, the electrostrictive coefficient derived from the strain measurement will be now just an "apparent" parameter, Q_h^{app}, which must depend upon the properties of ensemble of the polar regions, such as their population in the crystal, average size, etc..

The relationship between the electrostrictive coefficients Q_h^{lat} and Q_h^{app} can be

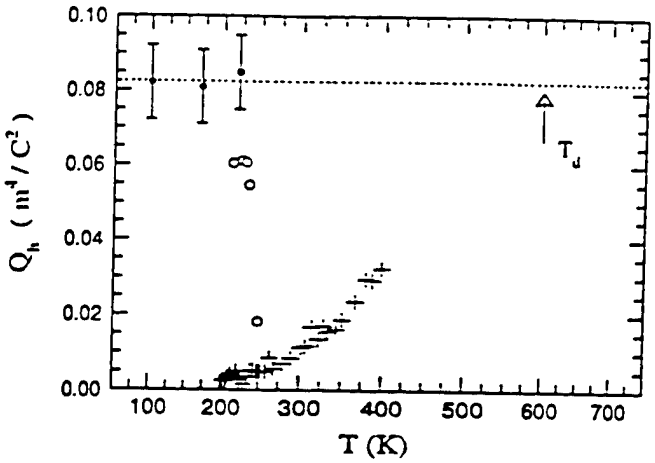

FIGURE 3. The plot combines all the data obtained in the present work, and shows the volumetric electrostrictive coefficient of prototype cubic lattice of PMN, Q_h^{lat}, (closed circles), and Q_h^{app} which describes the electrostrictive strain in the double-phase mixture, "polar regions / nonpolar matrix", (plus signs). When the structural inhomogeneity is removed by large dc bias field, which induces the normal ferroelectric state in PMN at low temperatures, the measured values of Q_h^{app} tend toward Q_h^{lat}, as shown with open circles in the plot. Therefore, the temperature dependence of the electrostrictive coefficient which is derived from strain measurements performed with a reference to the structurally inhomogeneous state is related with the change in the properties of ensemble of the polar regions, which appear in the material at temperatures below $T_d \approx 600$ K (shown with an arrow).

obtained from the comparison of the three states of PMN: *(i)* prototype cubic, *(ii)* mixed, consisting of "polar regions / nonpolar matrix", and *(iii)* completely polarized state. The latter can be obtained in the limit of very high electric field, E_m, applied to the sample, so that the whole volume of the crystal will have a homogeneous polarization, P_s, along [111] crystal axis (it is reasonable to expect that the symmetry of this state is the same as of the polar regions, i.e., rhombohedral), [20]. Therefore, one can write:

$$Q_h^{app} = \frac{S(E_m)}{P_s^2} = \frac{Q_h^{lat} P_s^2 - Q_h^{lat} \langle P_s^2 \rangle}{P_s^2} , \qquad (3)$$

where $Q_h^{lat}\langle P_s^2 \rangle$ is the strain introduced into the cubic lattice due to the appearance of the polar regions in the mixed state, $Q_h^{lat} P_s^2$ is the electrostrictive strain of completely polarized state, and both strains are defined with respect to the prototype cubic lattice. Equation (3) directly leads to the following expression:

$$Q_h^{app} = Q_h^{lat} \cdot \left[1 - \frac{\langle P_s^2 \rangle}{P_s^2} \right] , \qquad (4)$$

which relates both electrostrictive coefficients shown in Fig.3.

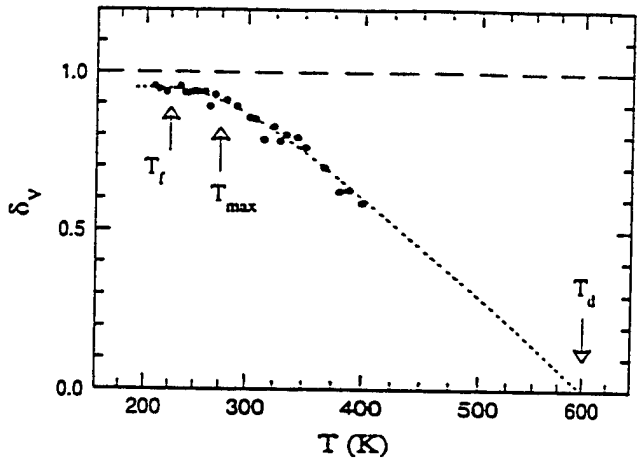

FIGURE 4. Temperature dependence of the volume fraction of the polar regions, δ_V, in PMN. Closed circles correspond to the experimental data and the dotted line shows a possible extrapolation of $\delta_V(T)$ toward high temperatures, where the polar regions appear at $T_d \approx 600$ K. Also shown are the temperature of the dielectric permittivity maximum, T_{max}, corresponding to the radio-frequency interval. Hz - MHz, and the freezing temperature, $T_f = 220$ K.

In Eq.(4), $\sqrt{\langle P_s^2 \rangle}$ is the root mean squared local spontaneous polarization of PMN. Taking into account that at a given temperature, the absolute value of the local spontaneous polarization of the polar regions most likely is equal to the macroscopic polarization, P_s, in the homogeneously polarized state at E_m, one can write: $\langle P_s^2 \rangle = \delta_V \cdot P_s^2$, where δ_V is the volume fraction of the polar regions in the crystal. Therefore, the expression in the brackets in Eq.(4) is equal to: $[1 - \delta_V]$.

Based on the above argument, from the data shown in Fig.3, we can find the volume fraction of the polar regions in PMN using: $\delta_V = 1 - \left[Q_h^{app} / Q_h^{int} \right]$. The obtained temperature dependence of δ_V is plotted in Fig.4. As one can see, within the temperature interval investigated, δ_V first increases upon cooling from 400 K to 250 K, and then saturates around the freezing temperature $T_f = 220$ K [21]. It is this increase in the volume fraction of the polar regions in the material which causes the decrease in the electrostrictive coefficient, Q_h^{app}, of PMN at temperatures below T_d. Fig.3. Also, it is worth noting that the data shown in Fig.4 brings new evidence about the absolute values of the volume fraction of the polar regions in PMN. So far, the only estimate which was used in the literature, especially in the works devoted to the theoretical description and modeling of the polarization response of relaxors, was that reported by Mathan *et al.* [3]. From the profile analysis of the X-ray diffraction data for PMN recorded at 5 K, Mathan *et al.* obtained that δ_V is approximately equal to 20%. Clearly, this estimate is very different from the data obtained in the present study. As one can see from the plot in Fig.4, below the freezing temperature the volume fraction of the polar regions is close to unity, and at temperatures around T_{max} it is equal to $\delta_V \approx 90\%$.

Furthermore, the above picture of the temperature evolution of δ_V can be correlated with the results of the quasielastic neutron scattering study of PMN by Vakhrushev *et al.* [22]. That study showed that the correlation length of the polarization fluctuations monotonically increased upon cooling, and at temperatures around $T_f = 220$ K it reached the saturation value equal to 20 nm. The saturation of the correlation length actually implied the stabilization of the average size of the polar regions. Similar behavior can be seen in Fig.4 for $\delta_V(T)$, where it first increases upon cooling and then saturates at temperatures around $T_f = 220$ K.

If only small electric field is applied to the sample, the total polarization and strain response of the material originates from different mechanisms, which were discussed in the *Introduction*. For the volumetric strain, we can divide these mechanisms into those which contribute to the volume change of the crystal [crystal lattice response, (d), and phase switching, (c)], and those which do not involve the volume change [domain wall motion, (b), or reorientation of the polar regions, (a)]. It is apparent that if these two groups of mechanisms coexist, one can write the following expression, [11]:

$$Q_h^{app} \cdot [P_v + P_i]^2 = Q_h^{lat} \cdot P_v^2 , \qquad (5)$$

where P_v is the polarization coming from mechanisms involving the volume change, and P_i is the induced polarization which does not produce the volume strain. From Eq.(5), one can obtain that the relative contribution from the crystal lattice, P_v to the total induced polarization, $P_v + P_i$, is given by $\sqrt{Q_h^{app}/Q_h^{lat}}$. Using this expression and the data shown in Fig.3, one can estimate that at temperatures around $T_{max} \approx 270$ K, the contribution from the crystal lattice is about 30 % of the total polarization induced in PMN.

CONCLUSIONS

In the present work, we investigated the volumetric electrostrictive coefficient, Q_h, PMN relaxor using a high-resolution neutron powder diffraction and a conventional strain measurements. Using the results of these experiments we: (1) derive the value of Q_h of prototype cubic lattice of PMN, which is equal to $Q_h = (8.3 \pm 1.0) \times 10^{-2}$ (m^4/C^2); (2) find the temperature dependence of the volume fraction, δ_V, of the polar regions in the material, and estimate that at temperatures around the dielectric permittivity maximum, T_{max}, it is equal to $\delta_V \approx 90$ %; (3) estimate the magnitude of the crystal lattice contribution to the polarization response of PMN at temperatures around and below T_{max}.

REFERENCES

1. Burns G. and Dacol F. H., *Solid State Commun.* **48**, 853 (1983).
2. Cross L. E., *Ferroelectrics* **76**, 241 (1987).

3. de Mathan N., *et al.*, *J. Phys.: Condens. Matter* **3**, 8159 (1991).
4. Dorogovtsev S. N. and Yushin N. K., *Ferroelectrics* **112**, 27 (1990).
5. Viehland D. *et al.*, *J. Appl. Phys.* **68**, 2916 (1990).
6. Vugmeister B. E. and Rabitz H., *Ferroelectrics* **201**, 33 (1997).
7. Qian H. and Bursill L. A., *Int. J. Mod. Phys. B* **10**, 2027 (1996).
8. Westphal V., Kleemann W., and Glinchuk M. D., *Phys. Rev. Lett.* **68**, 847 (1992).
9. Glazounov A. E., Tagantsev A. K., and Bell A. J., *Phys. Rev. B* **53**, 11281 (1996).
10. Tagantsev A. K. and Glazounov A. E., *Phys. Rev. B* **57**, 18 (1998).
11. Zhang Q. M. and Zhao J., *Appl. Phys. Lett.* **71**, 1649 (1997).
12. Zhao J., Glazounov A. E., and Zhang Q. M., *Appl. Phys. Lett.*, in press.
13. Sommer R., Yushin N. K., and van der Klink J. J., *Phys. Rev. B* **48**, 13230 (1993).
14. Ye Z.-G. and Schmid H., *Ferroelectrics* **145**, 83 (1993).
15. Bonneau P. *et al.*, *J. Solid State Chem.* **91**, 350 (1991).
16. Arndt H. *et al.*, *Ferroelectrics* **79**, 145 (1988).
17. The electrostrictive coefficients of polycrystalline samples represent the directional average of the single crystal coefficients. Since PMN has a macroscopic cubic symmetry, the average over random orientation of the crystallites in ceramics will yield the following expressions for longitudinal and transverse coefficients [18]: $\overline{Q}_{11} = (3Q_{11} + 2Q_{12} + Q_{44})/5$ and $\overline{Q}_{12} = (Q_{11} + 4Q_{12} - 1/2Q_{44})/5$. where $\overline{Q}_{ij}$ represent the directional average values for ceramics and Q_{ij} are the coefficients of the single crystals. From the above expressions one can see that: $\overline{Q}_{11} + 2\overline{Q}_{12} = Q_{11} + 2Q_{12} = Q_h$.
18. Devonshire A.F., *Philos. Mag.* **42**, 1065 (1951).
19. de Mathan N. *et al.*, *Mater. Res. Bull.* **26**, 1167 (1991).
20. In ferroelectrics, the polarization measured at the tip of the hysteresis loop, at E_m, is equal to $P_s + \varepsilon_{lat} E_m$, where P_s is the spontaneous polarization and ε_{lat} is the dielectric permittivity of the crystal lattice. Since $\varepsilon_{lat} E_m$ is usually much smaller than P_s, we can neglect it.
21. We derive $\delta_V(T)$ from Q_h^{app}, which, we think, also saturates at $T \leq 220$ K, because in this temperature interval the difference between the values of the electrostrictive coefficient measured at different temperatures is comparable to the experimental uncertainty, Fig.2.
22. Vakhrushev S. B. *et al.*, *Ferroelectrics* **90**, 173 (1989).

APPENDIX 8

APPLIED PHYSICS LETTERS VOLUME 72, NUMBER 9 2 MARCH 1998

Neutron diffraction study of electrostrictive coefficients of prototype cubic phase of relaxor ferroelectric $PbMg_{1/3}Nb_{2/3}O_3$

J. Zhao, A. E. Glazounov, and Q. M. Zhang[a)]
Materials Research Laboratory, The Pennsylvania State University, University Park, Pennsylvania 16802

Brian Toby
NIST Center for Neutron Research, National Institute of Standards and Technology, Gaithersburg, Maryland 20899

(Received 20 November 1997; accepted for publication 6 January 1998)

The electrostrictive coefficients of prototype cubic phase of $PbMg_{1/3}Nb_{2/3}O_3$ are studied using a high-resolution neutron powder diffraction experiment. The key idea of the approach is to "eliminate" from the material the inhomogeneity related to the presence of the double-phase mixture "polar regions/nonpolar matrix," and to study two structurally homogeneous states: prototype cubic at temperatures above 600 K and rhombohedral ferroelectric at temperatures below 220 K. The obtained value of volumetric electrostrictive coefficient, $Q_h=(8.3\pm1.0)\times10^{-2}$ (m^4/C^2), is consistent with those of other perovskite ferroelectrics with a prototype cubic phase.
 [S0003-6951(98)03409-3]

In the past two decades, the electrostrictive properties of relaxor ferroelectrics have been intensively studied due to their promising applications in electromechanical actuators.[1] These materials have been found to be very attractive for such applications as they exhibit large strain S under applied electric field E with almost no electromechanical hysteresis,[1] and the sensitivity of strain response, $\partial S/\partial E$, can be tuned by the electric field.[2] In this context, many studies have been devoted to the characterization of the electrostrictive coefficients Q_{ijkl} of these materials, which are defined by:[3]

$$S_{ij}=Q_{ijkl}\,P_k\,P_l, \tag{1}$$

where P_k, P_l and S_{ij} are the components of induced polarization and strain, respectively. Since most relaxors are perovskites and have a prototype cubic structure, only three independent coefficients, Q_{11}, Q_{12} and Q_{44} (in the matrix notations), are required to describe the electrostriction.

One of the problems still remaining in this field is that, despite the large number of the studies, it is not possible to draw a definite conclusion about values of electrostrictive coefficients even for a single composition. For example, according to early works,[1,4] the electrostrictive coefficients of a "classical" relaxor $PbMg_{1/3}Nb_{2/3}O_3$ (PMN) are independent of temperature within a fairly large temperature interval, $T=150-400$ K, whereas other studies[5,6] of the same material showed that its electrostrictive coefficients exhibit substantial change with T in the same temperature range. Moreover, a recent study demonstrated that the temperature dependence of electrostrictive coefficients of PMN can also be altered by the external field from gradual in zero-field-cooling (ZFC) regime to step-like during the field cooling (FC) under large dc bias, where the step-like change in the coefficients occurred below so-called freezing temperature, T_f.[5]

In order to understand the origin of such a different behavior of the electrostrictive coefficients, one should take into account that relaxors are structurally inhomogeneous materials. Microscopically, their structure is divided into small (about 100 Å in size) polar regions which are randomly distributed in the non-polar matrix.[7] In PMN, the polar regions appear at high temperatures, around 600 K, and persist down to 0 K.[7–9] The presence of the polar regions results in that the material response (both electric and elastic) to the applied electric field can originate from different mechanisms: the distortion of the crystal lattice (in polar and non-polar phases), the polar vector reorientation of the polar regions, and the motion of the interphase boundary between the polar regions and the non-polar matrix. It is also possible that several mechanisms coexist. Taking into account that each of the mechanisms can contribute differently to the induced polarization and strain (i.e., giving large polarization but producing very small strain and vice versa),[5] and that they can depend differently upon the applied field, the strain measurements performed with a reference to the structurally inhomogeneous state will have a serious drawback: since the electrostrictive coefficients are calculated as a ratio between the measured values of strain and the square of polarization, e.g., $Q_{11}=S_1/P_1^2$, most likely they will strongly depend upon the electric field magnitude.

The above arguments suggest that in the previous studies, the presence of the polar regions strongly influenced the results and thus did not allow derivation of the "true" electrostrictive coefficients of the prototype cubic phase of relaxors. Therefore, in order to determine these coefficients, one should eliminate from the material the inhomogeneity related to the presence of the double-phase mixture: "polar regions / non-polar matrix." For example, in PMN this could be accomplished by studying the electrostriction at high temperatures, above 600 K. However, at such a high temperature the high electric conduction of the material makes the conventional strain measurements very difficult. On the other hand, the electrostrictive coefficients of prototype cubic phase of

a) Corresponding author; electronic mail: qxz1@psu.edu

PMN can be determined microscopically, i.e., from the change of the lattice constants related to the structural phase transition into the ferroelectric state induced during FC below T_f. In this method, two experiments must be performed, where the lattice parameters of PMN are measured in the FC and ZFC regimes. However, it should be stressed that because of the existence of the polar regions which introduce an additional strain in the cubic lattice of PMN[8,10] one cannot use as a reference the lattice parameters measured directly in the ZFC experiment at temperatures below 600 K. Therefore, in order to determine the lattice parameters of the prototype cubic phase at temperatures below 600 K, one should adopt the approach employed in Refs. 8 and 9, i.e., at $T<600$ K, the parameters of the prototype cubic phase can be found from the extrapolation of the experimentally measured lattice constants at temperatures above 600 K, which should change linearly according to the normal thermal expansion of the lattice. The comparison of the lattice parameters of the rhombohedral ferroelectric state[11,12] with the extrapolated values of the cubic lattice thus will give the electrostrictive strain related to the structural phase transition.

In this letter, we report the experimental result on the electrostrictive coefficients based on the latter approach. In this experiment, the lattice parameters of PMN were investigated over a wide temperature interval, from 100 to 1050 K using high-resolution neutron powder diffraction. The low temperatures were required to study the ferroelectric state induced in PMN during FC below $T_f=220$ K,[11,13] whereas the high temperature interval (600–1050 K) was important to obtain reliable data on the prototype cubic phase to be extrapolated to low temperatures. The choice of neutron diffraction relied on the fact that neutrons have a larger penetration depth compared to conventional x-rays, thus allowing us to study the bulk properties of the material.

In this experiment, neutron powder diffraction data were collected using the BT-1 high-resolution diffractometer at the NIST Center for Neutron Research reactor, NBSR. The instrument has 32 detectors and offers a choice of two in-pile collimators. A Cu(311) monochromator with a 90° take-off angle, a collimation of 20 min after the monochromator, and 7 min before each detector, were used for this experiment. Depending on the resolution required, in-pile collimation of 7 and 15 min was used for different runs. For the 15 min setting, the optimum instrument resolution is ΔQ[full width at half maximum (FWHM)]$=0.013$ Å^{-1}, while for the 7 min setting, the optimum resolution is improved to ΔQ(FWHM)$=0.0098$ Å^{-1}. The data were collected up to $2\theta=170°$. High-resolution data were required in order to detect the phase transformation with a very small lattice distortion in the rhombohedral ferroelectric phase of PMN from the prototype cubic phase, $(90° - \alpha^{rh}) \leq 0.1°$.[14]

In order to be able to apply the electric field in the FC experiment, the samples were prepared in the form of a multilayer sandwich, where 15 ceramic disks, each 2 mm thick with 10 mm diameter, were glued together using a conductive epoxy. The experiment was first conducted in the ZFC regime where the diffraction patterns of PMN were recorded at several temperatures from 1050 to 100 K. Afterwards, the dc field $E = 5$ kV/cm was applied to the same sample at 300 K, then the sample was cooled down (FC regime), and the diffraction patterns were recorded at several temperatures below $T_f=220$ K, where the field induced phase transition was expected in PMN for the electric field larger than the threshold field, $E_{th}=1.7$ kV/cm.[13]

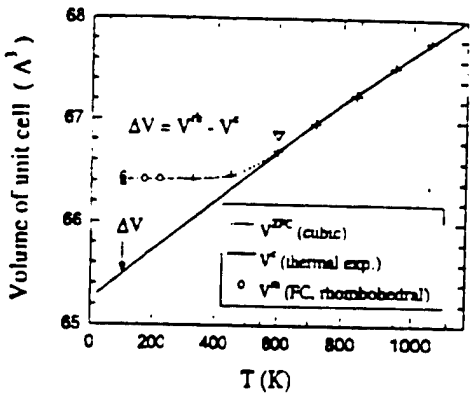

FIG. 1. Temperature dependence of the volume of the unit cell of PMN measured in ZFC (plus signs and the dotted line drawn through them in order to guide the eye) and FC (open circles) regimes. The linear dependence of the unit cell volume on temperature corresponds to the normal thermal expansion of prototype cubic lattice of PMN (solid line). During the FC regime, PMN is in the ferroelectric state with a rhombohedral structure at $T<220$ K (open circles). ΔV denotes the volume change in the crystal lattice during the phase transition to the ferroelectric state. The standard uncertainty of the evaluation of the unit cell volume is about 20% of the size of the data points.

The results of both ZFC and FC experiments are in good agreement with similar experiments performed by other research groups. For ZFC, the crystal lattice of PMN is cubic in the whole studied temperature interval,[7,10] whereas for FC using $E = 5$ kV/cm the crystal structure is rhombohedral at temperatures below 220 K.[12,14] The transformation of the crystal structure from cubic to rhombohedral at $T \leq 220$ K was evidenced, for example, by splitting in the (hhh) reflection into (hhh) and $(h\bar{h}\bar{h})$ under applied field. In both cases, unit cell parameters, a^c (for cubic), and a^{rh} and α^{rh} (for rhombohedral), were determined using the structural refinement procedure based on the Le Bail adaptation[15] of the Rietveld method. Finally, using the lattice parameters of PMN, two electrostrictive coefficients: Q_{44} (which is related to the angular distortion of the lattice) and $Q_h = Q_{11} - 2Q_{12}$ (which describes the change of the volume of the unit cell during the phase transition), were calculated.[16]

Figure 1 presents the temperature dependence of the volume of the unit cell, V, of PMN for both ZFC and FC experiments, and also illustrates the approach which we used to calculate the volume strain of the crystal lattice related to the phase transition. In the plot, open circles show the volume V^{rh} of the unit cell of rhombohedral crystal lattice corresponding to the ferroelectric state induced in PMN at $T \leq 220$ K by the dc field $E = 5$ kV/cm. Pluses and the dotted line connecting them correspond to the ZFC regime, $V^{ZFC}(T)$, with the cubic structure. Taking into account that no polar regions exist in the material above $T_0=600$ K, the linear variation of V^{ZFC} in the high-temperature interval is the normal thermal expansion of the prototype cubic lattice of PMN, $[V^c(T) - V^c(T_0)] \propto \beta_V (T - T_0)$, where β_V is the volumetric thermal expansion coefficient and V^c is the vol-

TABLE I. Electrostrictive coefficients Q_{11} and Q_{12} of prototype cubic lattice of PMN relaxor calculated from the results of the structural study of PMN using high-resolution neutron powder diffraction.

T (K)	100	170	220
Q_{11} (10^{-2} m^4/C^2)	8.2±1.0	8.1±1.0	8.5±1.0
Q_{12} (10^{-2} m^4/C^2)	0.7±0.1	0.7±0.1	0.6±0.1

ume of the unit cell of the prototype cubic lattice. Below 600 K, $V^{ZFC}(T)$ deviates from the linear dependence due to the appearance of polar regions in PMN which introduce an additional strain in host cubic lattice, which is equal to $Q_h \langle P_s^2 \rangle / 3$, where $\sqrt{\langle P_s^2 \rangle}$ is the root mean squared local spontaneous polarization.[8,9]

In order to find Q_h from the data in Fig. 1, the volumetric strain related to the structural phase transformation was calculated as $\Delta V/V^c$, where $\Delta V = V^{ob} - V^c$, Fig. 1. Below 220 K, the volume V^c of the prototype cubic phase was found by the extrapolation of the high-temperature linear dependence down to low temperatures, as shown in Fig. 1 with the solid line. The volumetric electrostrictive coefficient, Q_h, was determined from the equation:

$$Q_h = \frac{1}{P_s^2} \frac{V^{ob} - V^c}{V^c}. \tag{2}$$

where P_s is the macroscopic spontaneous polarization. The P_s was evaluated from saturated polarization hysteresis loops measured on PMN single crystal samples along ⟨111⟩ direction using the ac field of 30 kV/cm amplitude (which is much larger than the threshold field E_{th}[13]). For the temperature equal to 100, 170 and 220 K, the magnitude of spontaneous polarization was equal to 0.42, 0.38 and 0.35 C/m^2, respectively. Another electrostrictive coefficient, Q_{44}, was calculated using the following expression:

$$Q_{44} = \frac{1}{P_s^2} \left[\frac{\pi}{2} - \alpha^{ob} \right], \tag{3}$$

where the rhombohedral distortion of the lattice ($\pi/2 - \alpha^{ob}$) is now given in radians. The results are summarized in Table I. From that table, it can be seen that within the error of experiment, both coefficients remain temperature independent in the studied temperature interval of more than 100 K. This result is in agreement with the conventional wisdom that the electrostrictive coefficients coupling electric and elastic properties of the crystal lattice should be "proper" material constants, i.e., should be temperature independent.

The obtained results find support in the other data available in the literature. In a previous work,[5] the electrostrictive coefficient Q_h of PMN was measured using a conventional technique, i.e., strain as a function of the applied field. Under similar experimental conditions (FC regime, temperature range below T_f, the structurally homogeneous state in PMN is the normal ferroelectric state induced by large enough dc bias)[11,13] the obtained value was equal to: $Q_h = (6.0 \pm 0.5) \cdot 10^{-2}$ (m^4/C^2), which was also independent of temperature at $T \leq T_f$.[5] This result is close to the average value $Q_h = (8.3 \pm 1.0) \times 10^{-2}$ (m^4/C^2) derived from the present structural study of PMN. Apparently, Q_h derived here is about an order of magnitude higher than those found in many early studies.[1,3,4] The reason behind this is the existence of polar regions in the material, the response of which to the external electric field does not generate volume change, as has been discussed in an early publication.[5]

TABLE II. Comparison of electrostrictive coefficients Q_h of the crystal lattice strain of several perovskite ferroelectrics.

Composition	Q_h (10^{-2} m^4/C^2)
PMN	8.3±1.0
$BaTiO_3$	2.0
$PbTiO_3$	3.7
$SrTiO_3$	4.7
$KTaO_3$	5.2

Table II compares Q_h of several perovskite ferroelectrics[3] including the new value for PMN. As one can clearly see, the Q_h of PMN nicely fits the values of the electrostrictive coefficients describing the strain of the prototype cubic lattice of other perovskites.

Work at Penn State University was supported by the Office of Naval Research.

[1] K. Uchino, S. Nomura, L. E. Cross, R. E. Newnham, and S. J. Jang, J. Mater. Sci. 16, 569 (1981).
[2] J. Zhao, Q. M. Zhang, N. Kim, and T. Shrout, Jpn. J. Appl. Phys., Part 1 34, 5658 (1995).
[3] V. Sundar and R. E. Newnham, Ferroelectrics 135, 431 (1992).
[4] J. Kuwata, K. Uchino, and S. Nomura, Jpn. J. Appl. Phys. 19, 2099 (1980).
[5] Q. M. Zhang and J. Zhao, Appl. Phys. Lett. 71, 1649 (1997).
[6] G. Schmidt, G. Borchhardt, J. von Cieminsky, D. Grutzmann, E. Purinsch, and V. A. Isupov, Ferroelectrics 42, 3 (1982).
[7] N. de Mathan, E. Husson, C. Calvarin, J. Gavarri, A. Hewat, and A. Morell, J. Phys.: Condens. Matter 3, 8159 (1991).
[8] L. E. Cross, Ferroelectrics 76, 241 (1987).
[9] G. Burns and F. H. Dacol, Solid State Commun. 48, 853 (1983).
[10] P. Bonneau, P. Garnier, G. Calvarin, E. Husson, J. Gavarri, A. Hewat, and A. Morell, J. Solid State Chem. 91, 350 (1991).
[11] Z.-G. Ye and H. Schmid, Ferroelectrics 145, 83 (1993).
[12] H. Arndt, F. Sauerbier, G. Schmidt, and L. A. Shebanov, Ferroelectrics 79, 145 (1988).
[13] R. Sommer, N. K. Yushin, and J. J. van der Klink, Phys. Rev. B 48, 13230 (1993).
[14] N. de Mathan, E. Husson, G. Calvarin, and A. Morell, Mater. Res. Bull. 26, 1167 (1991).
[15] A. Le Bail, H. Duroy, and J. L. Fourquet, Mater. Res. Bull. 23, 447 (1988).
[16] For the phase transition from cubic to rhombohedral phase, electrostrictive coefficients Q_{11} and Q_{12} cannot be determined separately using only the data on the lattice parameters which allow only determination of their combination, $Q_{11} + 2Q_{12}$. Independent evaluation of Q_{11} and Q_{12} requires additional experiment.

APPENDIX 9

Ferroelectrics (accepted September 1997).

ELECTRIC FIELD INDUCED ANISOTROPY IN ELECTROSTRICTIVE $Pb(Mg_{1/3}Nb_{2/3})O_3$ - $PbTiO_3$ CRYSTALS

Seung-Eek Park and Thomas R. Shrout

Materials Research Laboratory, The Pennsylvania State University, University Park, PA 16801

Paul Bridenbaugh, Jason Rottenberg and Gabriel M. Loiacono

Crystal Associates, 15 Industrial Park, Waldwick, NJ 07463

Abstract

The electrostrictive behavior in single crystals of $Pb(Mg_{1/3}Nb_{2/3})O_3$ (PMN) and $0.93Pb(Mg_{1/3}Nb_{2/3})O_3$ - $0.07PbTiO_3$ (PMN-7%PT) was investigated as a function of crystallographic direction. The pseudocubic nature of these materials became highly anisotropic at relatively high electric fields. The observed anisotropy was believed to be associated with an electric field induced rhombohedral symmetry. Strain values were found to be larger for <001> oriented crystals though larger polarization values were measured in <111> oriented crystals, a consequence of larger electrostrictive coefficients (Qij). The electrostrictive coefficient Qij of the induced phase was found to be independent of composition. Though the crystals exhibited a high degree of anisotropy, no apparent improvement in induced polarization or strain was found when compared with polycrystalline counterparts.

Keywords : Relaxor ferroelectrics, single crystal, anisotropy. (77.65.-j, 77.90.+K)

$Pb(Mg_{1/3}Nb_{2/3})O_3$ (PMN) is a prototypical relaxor ferroelectric exhibiting a diffuse phase transition and large frequency dispersion with dielectric maximum at T_{max} ~ -7°C (1 kHz).[1] In contrast to normal ferroelectrics such as $PbTiO_3$ (PT), the dielectric maxima does not correspond with a phase transition. Neither macroscopic structural distortion nor optical anisotropy is detectable even at temperatures significantly below T_{max} . This macroscopic isotropy is often referred to as the "glassy state [2]" or "cubically stabilized perovskite [3]", a consequence of a "freezing" of polarization fluctuations. The phase transition into the long-range ordered ferroelectric phase, however, can be induced by an E-field.[1] The most direct evidence of an E-field induced phase transition was in-situ XRD studies reported in reference [4,5], where rhombohedral peak splitting occurred at the expense of fundamental cubic perovskite peaks. In the case of PMN single crystals, the initial phase induced from the relaxor state was found to be rhombohedral, regardless of the E-field direction with respect to the crystallographic orientation. [6,7]

The diffuse dielectric maxima around room temperature and subsequently large dielectric constant of PMN based relaxor ferroelectric materials and correspondingly large electrostrictive strain dependence on polarization with hysteresis-free behavior are attractive for actuator applications.[8] At room temperature, low-field polarization/strain behavior of PMN and PMN-PT with low PT content (< 15%) is isotropic. The isotropic electrostrictive Q_{11} coefficients for PMN and PMN-PT crystals are presented in table 1. In case of PMN-PT ceramics, electrostrictive Qij coefficients are dependent upon PT content as depicted in table 1.

The objective of this work was to investigate the polarization and strain behavior for PMN and PMN-7%PT crystals as a function of crystallographic orientation. It will be shown that

electrostrictive strain values of <001> oriented crystals are smaller or at most equal to those for <111> oriented crystal at low fields, becoming larger at high E-fields (>50kV/cm). This strain behavior will be discussed in relation to the symmetry of an E-field induced phase, and to the domain configuration which is associated with the induced ferroelectric phase.

Crystals of PMN and their solid solution with PT were grown using the high temperature flux technique. Raw powders were weighed with a desired molar ratio with B_2O_3 and excess Pb_3O_4 as a flux. The mixed powders were loaded into a Platinum crucible, which was placed in an alumina crucible sealed with an alumina lid and alumina cement to minimize PbO volatilization. The crucible and powder were placed in a tube furnace and held at soak temperatures (1100 to 1200°C), followed by slow cooling (1 to 5°C/hr). The crucible was then furnace-cooled to room temperature. Hot HNO_3 was used to separate the crystals out of the rest of the melt. Typically, crystal size ranged from 3 to 20 mm. Further details on the flux growth technique of these crystals can be found in ref. [9,10].

Individual crystals were oriented along their pseudocubic <001> and the <111> axes using a Laue back reflection camera. For electrical characterization, samples were prepared by polishing with silicon carbide and alumina polishing powders to achieve flat and parallel surfaces onto which gold electrodes were sputtered. The dielectric properties were determined with multifrequency LCR meters (Hewlett Packard 4274A and 4275A) in conjunction with a computer controlled temperature chamber (Delta Design Inc., Model MK 2300) over the frequency range of 100Hz, 1kHz, 10kHz and 100kHz. High-field measurements included polarization and strain hysteresis using a modified Sawyer-Tower circuit and linear variable differential transducer (LVDT) driven by a lock-in amplifier (Stanford Research Systems, Model

SR830). Electric fields as high as ~120 kV/cm were applied using an amplified sine wave form at 0.2 Hz. using a Trek 609C-6 high voltage DC amplifier. During testing the samples were submerged in Fluorinert (FC-40, 3M, St. Paul. MN), an insulating liquid, to prevent arcing.

Figure 1 presents dielectric constant/loss vs. temperature curves (cooling, no bias) for a PMN crystal. As shown, a frequency dispersion accompanies a diffuse phase transition, with $T_{max} \sim -5$ °C (1 KHz). The dielectric constants (K) ~ 16000 (1 kHz) was determined for both <111> and <001> oriented crystals at room temperature. Polarization and strain behavior is plotted as a function of E-field in figure 2. As anticipated for pseudocubic PMN crystals. polarization, strain values. and electrostrictive coefficients (Q_{ij}) were independent of crystallographic orientation at low fields (<5kV/cm). From <001> oriented PMN crystals a Q_{11} value of 1.0×10^{-2} m^4C^{-2} was measured, significantly smaller than that reported by Uchino et al. [11]. An apparent anisotropy in electrical properties was observed at increased E-fields, as shown in figure 2. Polarization values, which had been crystallographically identical at low fields, exhibited differences starting at E ~ 5kV/cm. As shown in figure 2(a) and presented in table 1, polarization levels for <111> oriented crystals were larger than <001> oriented crystals, in agreement with previous observations [6,7]. However, higher strain levels were accompanied by lower polarization values for the <001> oriented crystals at E > ~50kV/cm, shown in figure 2(b). Higher strain values along with less polarization must also be a result of E-field induced anisotropy in Q_{11} values. Figure 3 presents strain (X) vs. P^2 curves for both <111> and <001> oriented crystals, where Q_{11} values can be directly calculated from the slope of the curves. As can be seen in figure 3, the slope ($Q_{11} \sim 1.0 \times 10^{-2}$ m^4C^{-2}) at low fields continuously increases from $P^2 = \sim 70$ $\mu C^2/cm^4$ (E=~7kV/cm) and saturates to a different value at high fields (at high polarization values) due to

a E-field induced phase transition. In figure 3, Q_{11} values of the induced phase(s) are presented as a function of crystallographic orientation. A Q_{11} (3.4×10^{-2} m^4C^{-2}) value for the <001> oriented crystals was found to be larger than the <111> oriented crystal (1.5×10^{-2} m^4C^{-2}). Since the E-field induced phase is expected to be rhombohedral with <111> being the polar direction [6], an applied E-field along <001> results in a tendency for the polarization direction to shift in the direction of the E-field, resulting in more lattice distortion and consequently higher values in both strain and Qij. It is also expected that the E-field induced phase in <001> oriented crystals must result in domain configuration with the ferroelectric domains possessing four possible polar directions - <111>, <-111>, <1-11>, <-1-11>, i.e. an engineered domain state.

With the addition of 7mole% PT, the induced anisotropy occurred at lower E-fields and polarization values were found to increase, as presented in figure 5 and table 1, respectively. The <111> oriented crystals were superior to the <001> orientation with induced strain values at low fields (< ~40kV/cm), explained by higher polarization levels of <111> oriented crystals However, induced anisotropy resulted in higher strain values for the <001> oriented crystal at high fields (>40kV/cm), in spite of smaller polarization values.

Table 1 summarizes polarization and electrostrictive coefficients of PMN and PMN-7%PT crystals as a function of crystallographic orientation and their polycrystalline counter parts, as well. In contrast to previously reported data for electrostrictive PMN-PT ceramics [8], electrostrictive coefficient of PMN-PT crystals were found to be independent of composition, especially for the induced ferroelectric phase. The compositional dependence of Q_{ij} [8] in electrostrictive PMN-PT ceramics may explained by a level of E-field necessary to induce the

relaxor-ferroelectric phase transition. Increased PT content may result in increased anisotropy and subsequently increased Qij.

It is important to note that electrostrictive PMN-PT crystals are not superior to their polycrystalline counterparts as shown in figure 5. Though maximum levels are limited by the dielectric breakdown strength, polarization and strain values of ceramics fall between <111> and <001> oriented crystals.

Using direct investigation of E-field induced polarization and strain as a function of crystallographic orientation for electrostrictive PMN-PT crystals, it could be concluded that higher strain values with lower polarization levels for <001> oriented crystals was a result of the E-field induced anisotropy. Electrostrictive coefficients Q_{11} (3.4×10^{-2} m^4C^{-2}) for <001> oriented crystals was found to be larger than that of <111> oriented crystals ($Q_{11} \sim 1 \times 10^{-2}$ m^4C^{-2}), for the induced phases at high fields, being independent of composition. In spite of the induced anisotropy, strain levels obtained from electrostrictive PMN-PT crystals were only comparable to those of polycrystalline counterparts.

Authors would like to acknowledge that this research has been supported by Office of Naval Research. The authors would like to thank Shi-Fang Liu and Hua Lei for their helps with crystal growing and sample preparation, respectively, and L. E. Cross and S.-J. Jang for their helpful suggestions.

Reference

1. G. A. Smolensky, "Physical Phenomena in Ferroelectrics with Diffused Phase Transition," *Journal of Physical Society of Japan*, 28, suppl. 26 (1970).
2. D. Viehland, S. J. Jang, L. E. Cross, and M. Wuttig, " Deviation from Curie-Weiss Behavior in Relaxor Ferroelectrics," *Physical Review B*, 46, 8003 (1992).
3. G. Schmidt, "Diffuse Ferroelectric Phase Transitions in Cubically Stabilized Perovskite," *Phase Transitions*, 20, 127 (1990).
4. H. Arndt, F. Sauerbier, and G. Schumidt, "Field-induced Phase Transition in $Pb(Mg_{1/3}Nb_{2/3})O_3$ Single Crystals," *Ferroelectrics*, 79, 145 (1988).
5. G. Calvarin, E. Husson, and Z. G. Ye, "X-ray Study of the Electric Field-Induced Phase Transition in Single Crystal $Pb(Mg_{1/3}Nb_{2/3})O_3$," *Ferroelectrics*, 165, 349 (1995).
6. G. Schumidt, H. Arndt, J. V. Cieminski, T. Petzsche, H.-J. Voigt, and N. N. Krainik, "Field-induced Phase Transition in Lead Magneium Niobate," *Kristall und Technik*, 15 [12], 1415 (1980).
7. G. Schumidt, G. Borchhardt, J. V. Cieminski, D. Grutzmann, E. Purinsch, and V. A. Isupov, "Electromechanical Properties of Ferroelectrics with Diffuse Phase Transition," *Ferroelectrics*, 42, 3 (1982).
8. S. J. Jang, K. Uchino, S. Nomura, and L. E. Cross, "Electrostrictive Behavior of Lead Magnesium Niobate Based Ceramics Dielectrics," *Ferroelectrics*, 27, 31 (1980).
9. M. L. Mulvihill, S. -E. Park, G. Risch, Z. Li, K. Uchino, T. R. Shrout, "The Role of Processing Variables in the Flux Growth of Lead Zinc Niobate-Lead Titanate Relaxor Ferroelectric Single Crystals," *Japanese Journal of Applied Physics*, 35 [7], 51, (1996).

10. S. -E. Park, M. L. Mulvihill, G. Risch, and T. R. Shrout, "The Effect of Growth Condition on Dielectric Properties of $Pb(Zn_{1/3}Nb_{2/3})O_3$ Crystal," *Japanese Journal of Applied Physics*, Pt. 1, 36 [3], (1997).

11. K. Uchino, S. Nomura, L. E. Cross, S.J. Jang, and R. E. Newnham, "Electrostrictive Effect in Lead Magnesium Niobate Single Crystals," *Journal of Applied Physics*, 51, 1142 (1980).

Table 1 Polarization and electrostrictive coefficient (Q_{11}) of PMN and PMN-7%PT ceramics and single crystals as a function of orientation.

Composition		Orient-ation	Ps ($\mu C/cm^2$)	Q_{11} (low field*, $\times 10^{-2} m^2 C^{-4}$))	Q_{11} (high field, $\times 10^{-2} m^2 C^{-4}$))	Ref.
PMN	Single Crystal	111	28	0.9	1.5 (>30kV/cm)	this work
		001	17	1.0	3.4 (>30kV/cm)	
		001	15[a]	2.5[b]	-	[a]6,[b]11
	Ceramics		20	1.1 (<25kV/cm)		1
PMN-7%PT	Single Crystal	111	34	0.9	1.5 (>10kV/cm)	this work
		001	22	0.9	3.4 (>10kV/cm)	
	Ceramics		24	2.0 (<25kV/cm)		1, this work

* Low Fields : < 5 kV/cm.

[a] at the temperature ~ -6.5°C

Figure Caption

Figure 1 Dielectric constant and loss as a function of temperature for PMN crystal at various measuring frequencies (0.1, 1, 10, and 100 kHz)

Figure 2 Electric field dependence of the induced polarization (a) and longitudinal strain (b) for PMN crystals oriented along <111> and <001> directions.

Figure 3 Longitudinal strain as a function of polarization squared for PMN crystals oriented along <111> and <001> directions.

Figure 4 Electric field dependence of the induced polarization (a) and longitudinal strain (b) for PMN-7%PT ceramics and single crystals oriented along <111> and <001> directions.

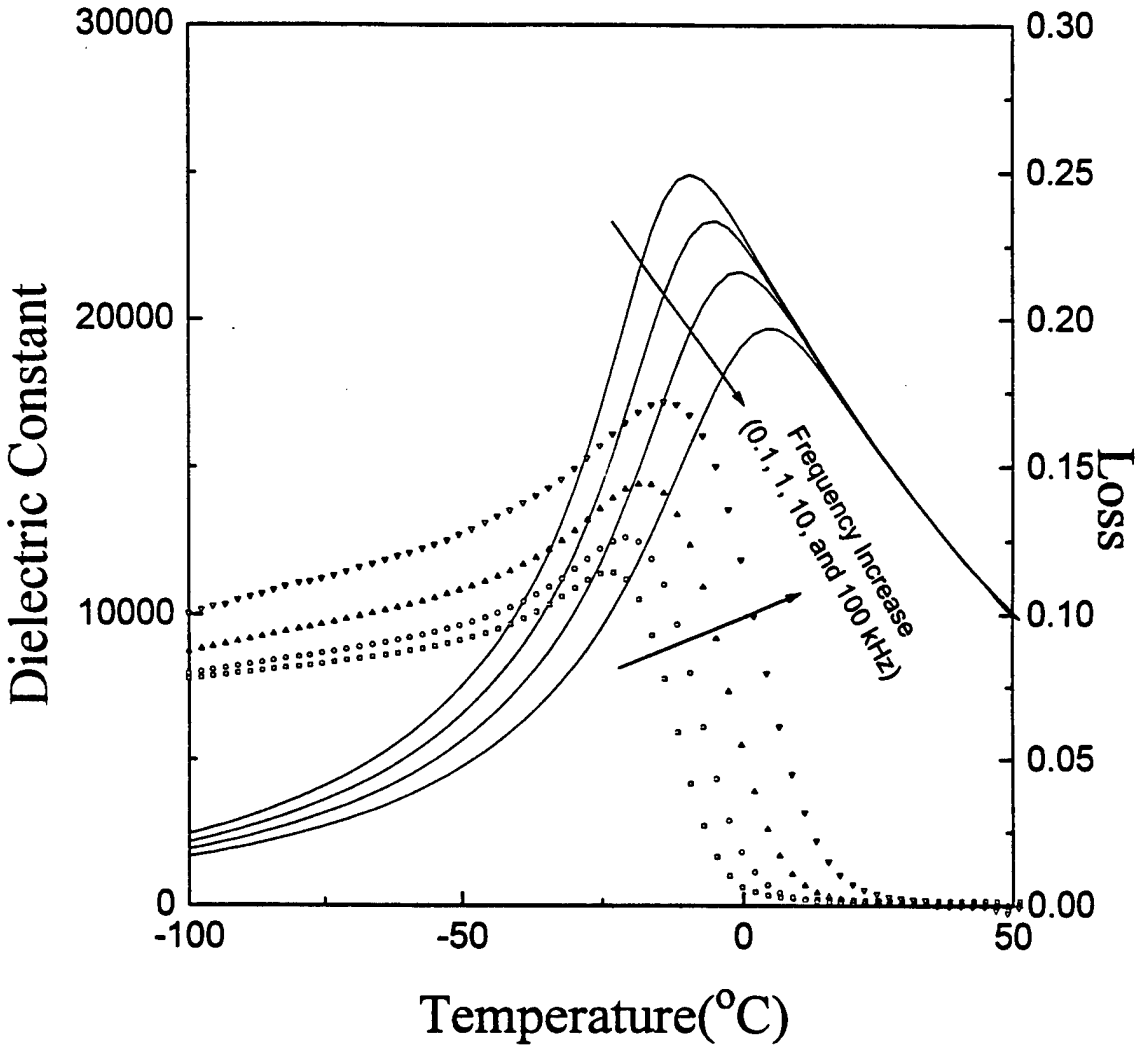

94 S.-E. Park et. al.

Figure 1 Dielectric constant and loss as a function of temperature for PMN crystal at various measuring frequencies (0.1, 1, 10, and 100 kHz)

L1643

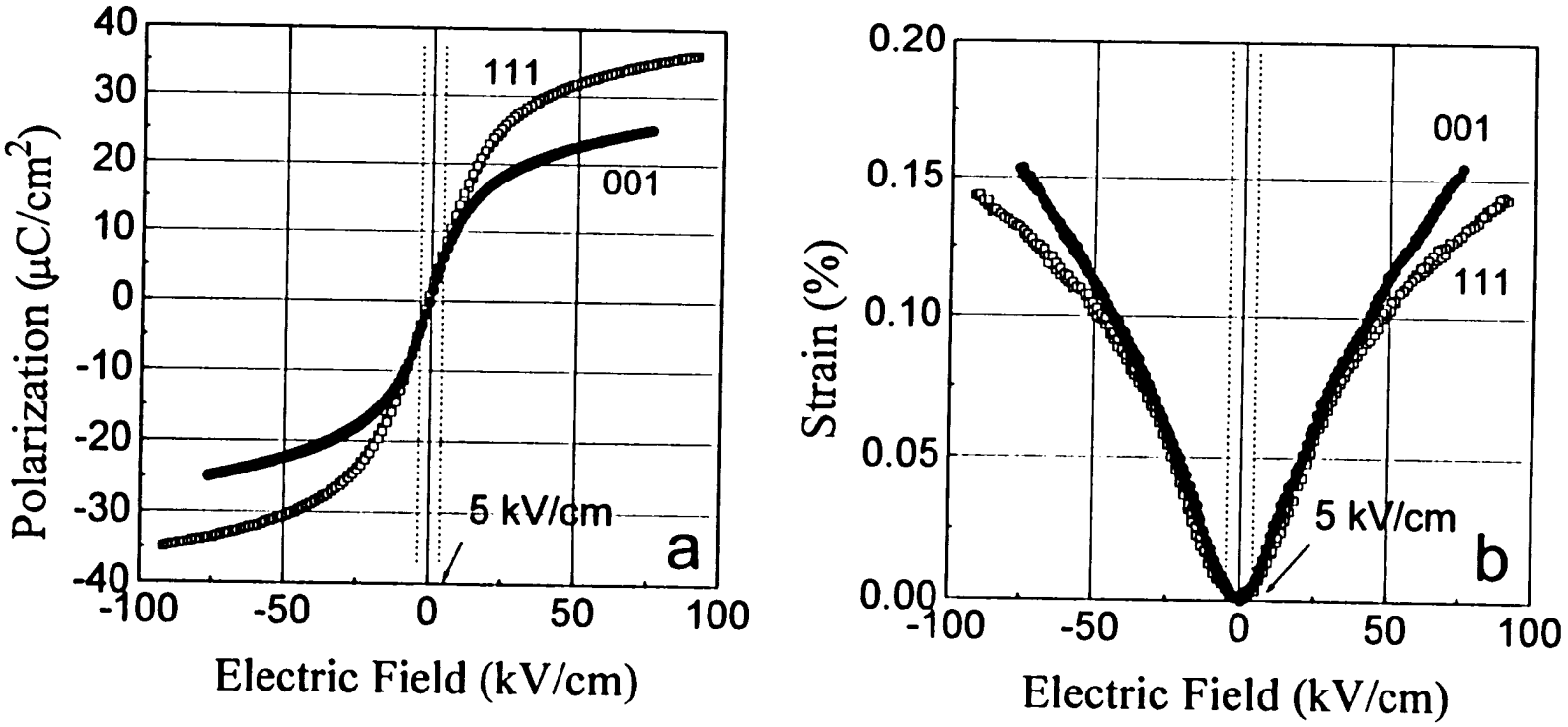

S.-E. Park et al.

Figure 2 Electric field dependence of the induced polarization (a) and longitudinal strain (b) for PMN crystals oriented along <111> and <001> directions.

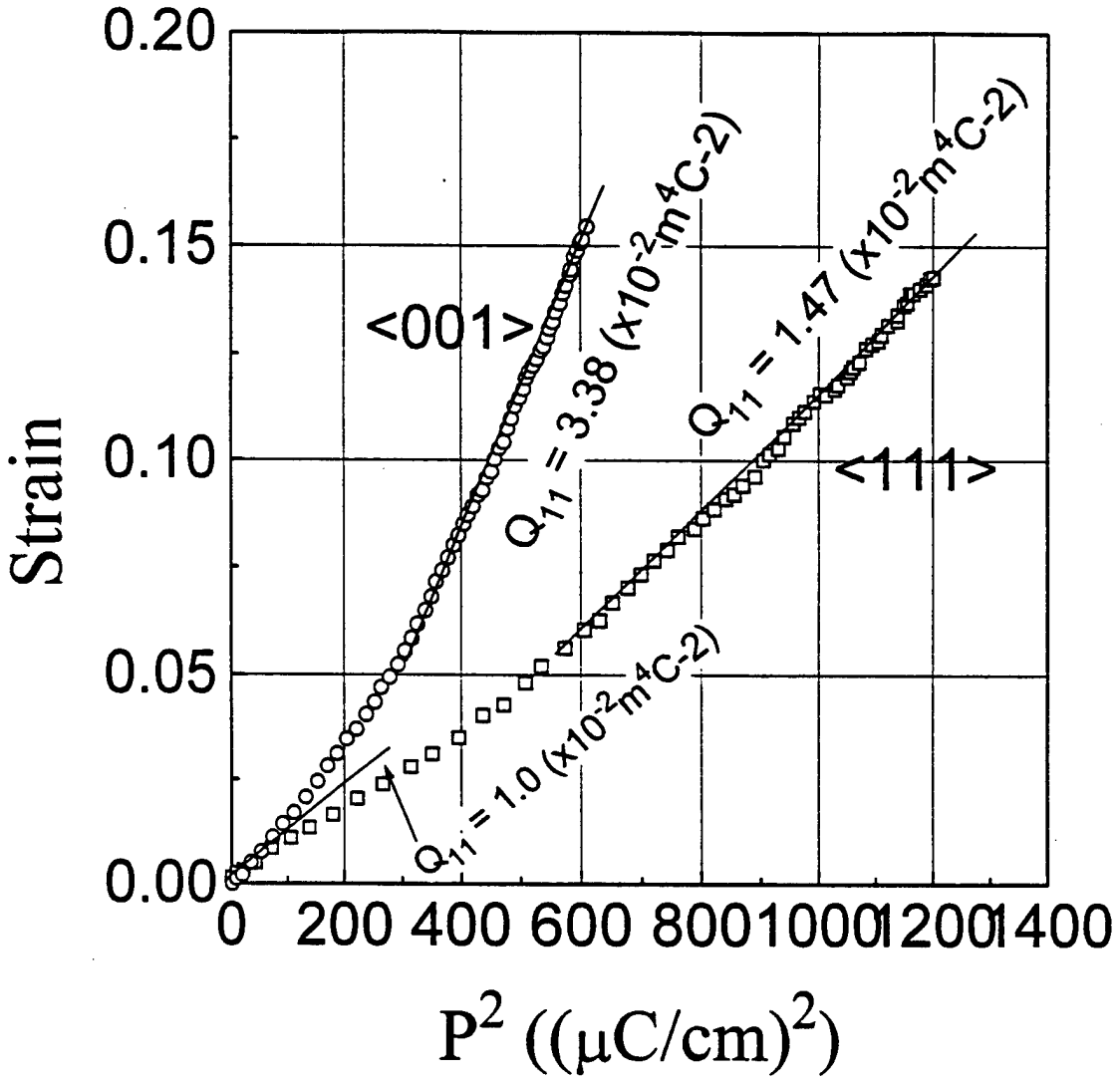

S.-E. Park et al.

Figure 3 Longitudinal strain as a function of polarization squared for PMN crystals oriented along <111> and <001> direction.

L-1043

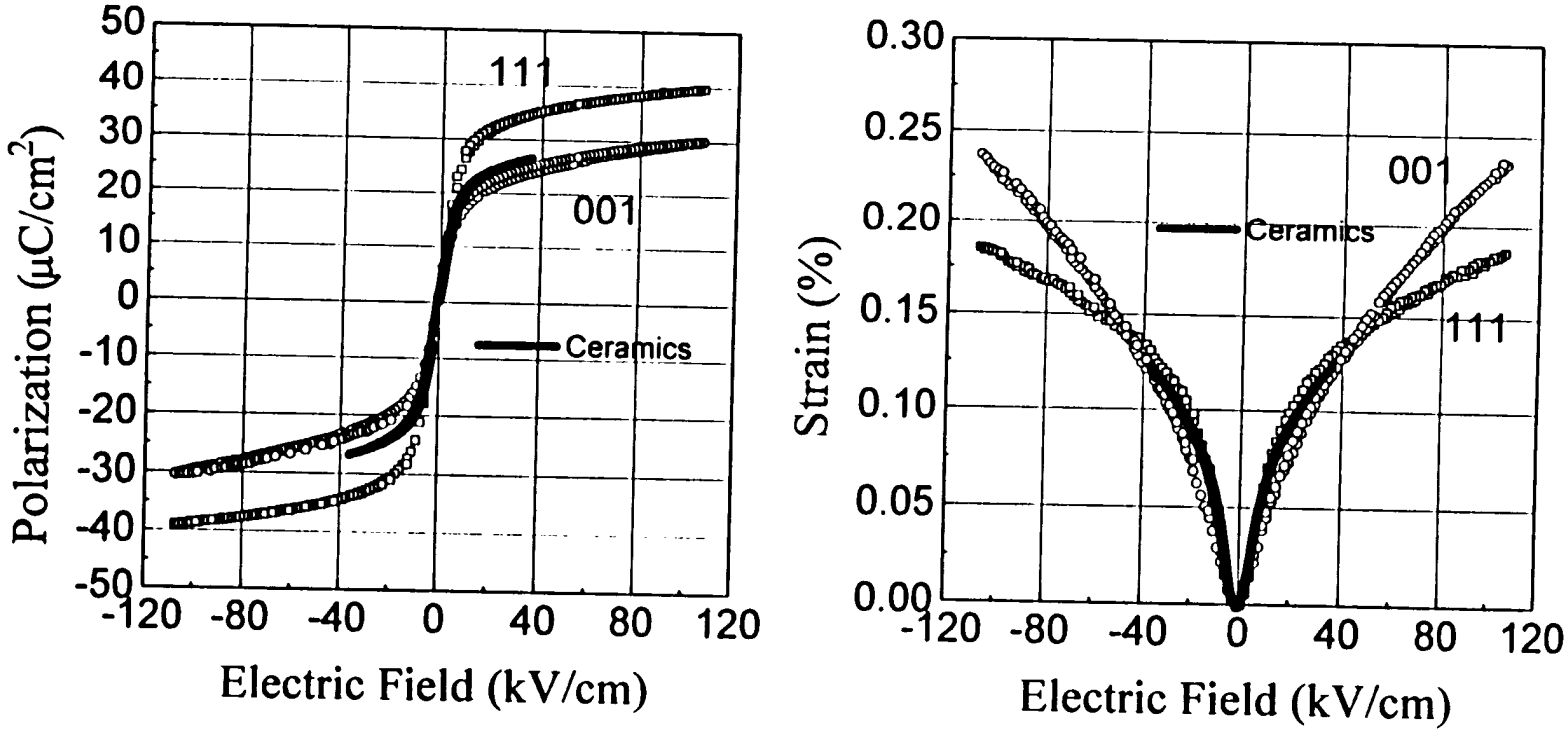

S.-E. Park et al.

Figure 4 Electric field dependence of the induced polarization (a) and longitudinal strain (b) for PMN-7%PT ceramics and crystals oriented along <111> and <001> directions.

APPENDIX 10

Diffuse X-Ray Scattering Study of Lead Magnesium Niobate Single Crystals

H. You

Argonne National Laboratory, Materials Science Division, 9700 South Cass Avenue, Argonne, Illinois 60439

Q. M. Zhang

Materials Research Laboratory, The Penn State University, University Park, Pennsylvania 16802

(Received 25 April 1997)

Single crystals of lead magnesium niobate, $PbMg_{1/3}Nb_{2/3}O_3$, were studied with x-ray scattering measurements at temperatures between 10 and 350 K. The diffuse scattering around odd-integer Bragg reflections ($H + K + L$ = odd) has a significant anisotropic component with ledges along $\langle 110 \rangle$ directions. We show that the transverse optic (ferro distortion) modes whose polarizations are along $\langle 1\bar{1}0 \rangle$ directions are soft and responsible for the observed diffuse scattering. Upon cooling, these modes undergo a freezing process with q-dependent freezing temperatures. Below the lowest freezing temperature ($T \lesssim 190$ K) the diffuse scattering follows $1/q^2$ law, indicating an elastically distorted, static structure. [S0031-9007(97)04551-1]

PACS numbers: 77.80.Bh, 61.10.Eq, 64.70.Kb, 77.84.Dy

Relaxor ferroelectrics belong to a special class of ferroelectric materials which exhibit a diffuse dielectric response to external fields with frequency-dependent, broad dielectric maxima. In addition, their low-temperature structures cooled under zero field show no long-range ferroelectric order even at near 0 K [1]. Among them, lead magnesium niobate, $Pb[Mg_{1/3}Nb_{2/3}O_3]$ (PMN), is considered as a model system and has been most extensively studied in recent years, in an attempt to elucidate its peculiar transition behavior. Although significant progress has been made over the last decade, some aspects of its nature remain unclear and often controversial. In particular, with respect to the low-temperature ferroelectric structure, two alternative models were previously suggested: (i) the presence of microscopic ferroelectric domains whose polarizations are frustrated by local random fields at low temperature [2], or (ii) the glassy nature of interactions between ferroelectric dipoles [3]. More recently, in pressure-dependent studies of a related relaxor material, lanthanum-modified lead zirconate-titanate, it was suggested that the glasslike behavior is related to the freezing of the soft mode [4]. These proposed models, which are extremely interesting but largely based on indirect evidence, motivated us to perform x-ray scattering studies of PMN.

The PMN has a cubic perovskite structure where the A site is occupied by Pb^{+2}, and the B site (surrounded by an oxygen octahedra) is randomly occupied by Mg and Nb $[Mg^{+2}_{1/3}Nb^{+5}_{2/3}O^{-2}_3]$ (MN). Unlike ordinary cubic perovskites, the positions of both sublattices are substantially displaced along symmetry directions as much as 9% [5], which is suggested to be the result of short-ranged ferroelectric ordering. In addition, there present randomly embedded microdomains with a doubled unit cell [6,7]. From the structure refinement, we find that the unit cell doubling of microdomains [superlattice reflections at $(H + 0.5K + 0.5L + 0.5)$] in the crystal is largely due to a 1:1 compositional ordering of Nb and Mg ($P\bar{4}3m$ supercell) but their positions are significantly disordered [8]. The size (~100 Å and volume fraction ($\lesssim$1000 Å apart) of the microdomains are probably limited due to the charge imbalance due to the Mg and Nb 1:1 compositional ordering [6,8]. The objective of this Letter is, based on these existing results, to elucidate the structural origin of the large displacements [5] and the role of the ordered microdomains on the freezing of the displacements, thereby to provide a structural basis for the *relaxor* behavior of this material.

Single crystals of PMN were grown by the flux solution technique. They were light yellow in color with a cubic morphology. The crystal used in this experiment was oriented and cut into an approximately rectangular plate of $2 \times \frac{1}{4} \times \frac{1}{4}$ mm^3 with the largest face parallel to a (001) plane. The cut surfaces were mechanically flat but deliberately unpolished in order to avoid surface scattering. However, the samples were carefully annealed in oxygen flow to heal the possible damage done during the mechanical cutting. Prior to this study, the dielectric response of the specimen was measured and the results were previously reported [7]. The samples exhibit a well-defined, diffuse phase transition with the dielectric relaxation observed in typical PMN materials. The x-ray measurements were performed with a 12 kW rotating anode x-ray generator. Targets of Cu K_α and Mo K_α were used in our study. Bent graphite monochromators were used to focus the x-ray beam to 1×2 mm^2 at the sample position. Some x-ray measurements were reproduced with a higher instrumental resolution at the X6B beam line of the National Synchrotron Light Source. The temperature of the sample was controlled with a Displex cryostat.

As shown in Fig. 1(a), the integrated intensities for most reflections *decrease* substantially as temperature decreases

 0031-9007/97/79(20)/3950(4)$10.00

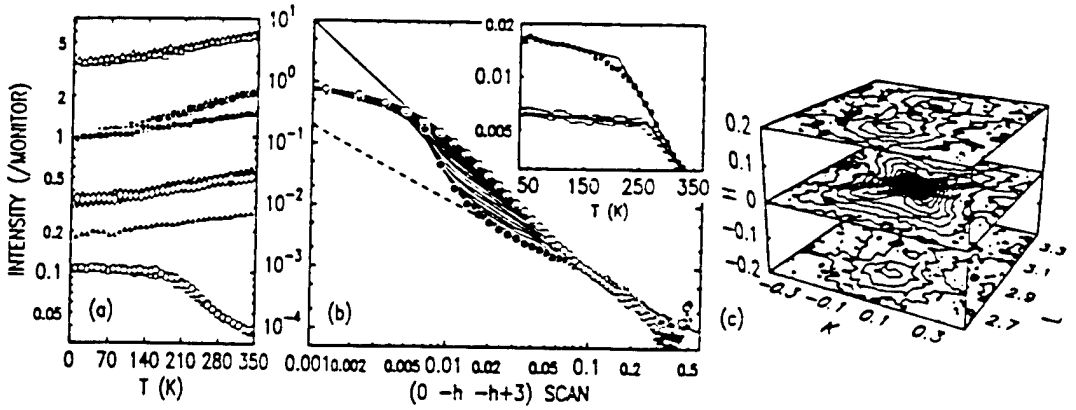

FIG. 1. (a) Temperature-dependent intensity of selected Bragg reflections. Diamonds, filled squares, down triangles, up triangles, filled circles, open triangles, and open circles are for (333), (022), (111), (033), (011), (002), and (003), respectively. (b) X-ray diffuse scattering near (003) Bragg reflections and its temperature dependence. The solid and dashed lines are the linear fits to the open and solid circles at $h = 0.01$. As an inset, intensities at $h = 0.01$ (squares) and $h = 0.04$ (line) vs temperature are shown. (c) Isointensity contour plots around (003) reflection.

while their widths remain unchanged (not shown). This is opposite to the usual effect of the Debye-Waller factor, or in other words, the system *disorders* as temperature decreases. Contrary to most reflections, however, intensity of (003) significantly increases and its width broadens upon cooling from 350 to 190 K, near the freezing temperature previously reported [2,3]. As will become clear below, the exceptional behavior of the (003) is due to its small structure factor and the diffuse scattering near every odd integer reflection in the presence of ferroelectric distortion of the lattices [9]. As the static disorder increases, the (003) intensity becomes so small that the diffuse scattering dominates the measured reflection profiles [8]. This allows us to measure more accurately the diffuse scattering around it. In addition, the diffuse scattering near (003) is considerably larger than that near (001) due to the Q^2 factor as discussed below and the diffuse scattering due to nonferrodistortions near it is not as strong as near (005). For these reasons and because it is along the high symmetry direction, the (003) reflection and its neighbor is the most favorable place for the diffuse scattering study of the ferrodistortion mode [10].

X-ray diffuse scattering per unit volume of a sample at a point in the reciprocal space, Q, due to a single Fourier component of wave vector $\mathbf{q} = \mathbf{Q} - \mathbf{G}$ (G is a crystal momentum and $q < G$) and mode j can be expressed as,

$$I(\mathbf{Q}) = \frac{Q^2}{q^2} X_{\mathbf{q},j} |\hat{\mathbf{Q}} \cdot \boldsymbol{\epsilon}_{\mathbf{q},j}|^2. \quad (1)$$

For a static modulation, $X_{\mathbf{q},j} = |\mathcal{U}_{\mathbf{q},j}|^2$ with an amplitude and a polarization, $\mathcal{U}_{\mathbf{q},j}$ and $\boldsymbol{\epsilon}_{\mathbf{q},j}$, respectively, which are determined by the elastic response of the crystal to the specific imperfection in the lattice for the static case [11,12]. For a phonon mode, $X_{\mathbf{q},j} = \frac{2kTa^2}{\rho\omega_j^2(\mathbf{q})}$ with the mass density ρ at a high-temperature limit [13]. In either case, every mode in general contributes to the diffuse scattering. However, when only one specific mode has a dominant contribution to the diffuse scattering because of either exceptionally small sound velocity for the corresponding phonon mode [14] or in the presence of a *soft mode* [15], the nature of the corresponding mode can be learned from the diffuse scattering measurements otherwise obtainable only by neutron scattering experiments. In particular, temperature-dependent diffuse scattering measurements were used to study the soft modes in ferroelectric materials [16]. Note that $\mathcal{U}_{\mathbf{q},j}$ is independent of q [11,12] for small q which is a general result derived from the equation of elastic equilibrium *independent* of the details of the crystal. Therefore, the $1/q^2$ form is the prime signature of static and *elastic* response of the crystal in the presence of impurities or defects, known as Huang scattering [12].

In Fig. 1(c), the diffuse scattering around (003) is shown as a set of isointensity contours. The diffuse scattering intensity shows a significant anisotropy around (003) reflection with the maxima along four [101] and four [011] directions. A close examination of Eq. (1) and the diffuse scattering yields a qualitative but illuminating picture about the nature of lattice distortion responsible for the anisotropy. First, it suggests that the ⟨110⟩ type phonon modes along the Γ-N direction are soft and dominant contributors to the diffuse scattering ($\mathbf{q} \parallel \langle 110 \rangle$). Second, the *absence* of the diffuse scattering along four [110] directions additionally suggests that the polarization is pure transverse and $\boldsymbol{\epsilon}_{[110]} \parallel [1\bar{1}0]$ since $\hat{\mathbf{Q}} \cdot \boldsymbol{\epsilon}_{\mathbf{q},j} = 0$ and $\hat{\mathbf{Q}} \simeq (001)$ [10].

In order to test the qualitative observation, we examined the diffuse scattering near several other Bragg reflections. We show in Fig. 2 contour plots of diffuse scattering (solid lines) at room temperature near three Bragg reflections and calculated contour plots (dashed contours). In the lower left panel the positions of the contour plots are shown as open squares. Each contour represents tripling of the intensity and the calculations were made by assuming that the phonon modes are softest

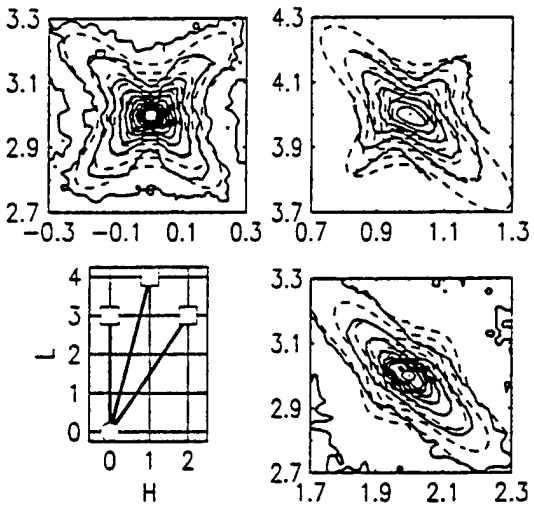

FIG. 2. Contour plots of x-ray diffuse scattering around three reflections indicated as open squares at the lower left panel.

along Γ-N with a finite width of 0.5 rad. As we can see, the calculated contours agree well with the measured contours [17], confirming that the simple transverse modes along ⟨110⟩ are indeed responsible for the anisotropic diffuse scattering. Here we showed data around only three reflections in the h-l zone but the anisotropic diffuse scattering is observable near every odd integer reflection ($H - K - L$ = odd) [9] and the contour shapes can be similarly explained. The distortion amplitude, $\mathcal{U}_{q,j}$, of the center-of-mass conserving optic mode (ferroelectric distortion) is nearly zero at the even integer Bragg reflections due to the canceling of the structure factor [9]. Therefore, the absence of such anisotropic diffuse scattering around even integer reflections is additional evidence that the anisotropic diffuse scattering comes indeed from the ferroelectric distortion.

As temperature is varied, we do not observe qualitative changes in the contour shapes shown in Fig. 2. However, the intensity of the diffuse scattering does change with temperature and, furthermore, this temperature dependent behavior is also strongly q dependent as shown in the main panel of Fig. 1(b). Here, the intensities along one of the ridges measured at the temperatures between 10 K (open circles) and 350 K (solid circles) are shown in a log-log plot as solid curves between the open and solid circles. In addition, a straight solid line of $I = h^{-2}$ (Huang scattering) and a dashed line of $I = h^{-1.3}$ (best linear fit to the high-temperature, large-h diffuse scattering) are shown to guide the eye. In essence, the diffuse scattering intensity at room temperature shows no simple functional form while that at 10 K shows a $1/q^2$ form except for the instrumental rounding near $h = 0$. This $1/q^2$ dependency is consistent with the above-discussed static and elastic distortion modes. There are two things to notice in this figure: (1) apparent absence of the Bragg peak and (2) the increase of the diffuse scattering for $0.007 < h < 0.06$ as temperature decreases. The intensity at 350 K shows a rapid decrease near $h = 0.005$ indicating the presence of a weak (003) Bragg reflection but the diffuse scattering continues from $h = 0.005$ to the zone boundary. As temperature decreases, the diffuse scattering near the zone boundary (short wavelength distortion) decreases while the diffuse scattering near the Bragg peak (long wavelength distortion) increases. Below ~190 K, however, the Bragg peak can no longer be separated from the diffuse scattering and the diffuse scattering precisely follows the $1/q^2$ form until it reaches the rounding at $h = 0.005$ due to the instrumental resolution. (The small overshoot near $h = 0.01$ is due to the Q^2 factor and the peak at $h = 0.5$ is a $\lambda/2$ of the graphite monochromator.)

While the structure of the 1:1 ordered microdomains is nearly isomorphic with that of the host crystal, therefore with little mechanical stress expected, the charge imbalance within them (~0.5 e^- per unit cell) should significantly distort the lattices within and around them by pulling the Pb site and pushing the MN site. Under these radial electric fields, the softest mode will respond most strongly resulting in the qualitatively similar anisotropic diffuse scattering. The amplitude of the ferrodistortion should have a maximum at the boundary of the ordered domain but gradually decrease as the distance from the ordered domain increases in order to satisfy the equation of elastic equilibrium evidenced by $1/q^2$ form. In addition, the polarizations may reorient in order to minimize the strain energy, which cannot be easily accommodated by various combinations of the discussed ⟨110⟩ modes, under the radial electric field. Such reorientation is not evident within the data presented here but the significant temperature effect found in the high-resolution radial and transverse scans through (003) [10] provide a possibility that such reorientation may indeed exist. Then, immediately around an ordered microdomain, there should form a strong radially symmetric distortion field with polarizations pointing towards the ordered microdomain. The radial distortion field weakens, however, as the distance from the ordered domain increases and eventually overlap with the distortion fields emanating from other ordered microdomains around it. Therefore, in the middle region (several hundreds of angstroms in size and most volume fractions belong to this region) sufficiently away from the ordered microdomains, the ferrodistortions must be *frustrated* under zero-field cooling. Under field cooling, of course, a large ferroelectric domain can be established in the middle region, such as the recently observed rhombohedral distortion upon ⟨111⟩ poling [18] by an appropriate combination of the ⟨110⟩ transverse modes. Within this scenario, our picture of low-temperature structure is closer to the model of the ferroelectric domains frustrated by random fields [2] than the model of glassy dipoles [3].

A closer examination of the temperature-dependent intensity at each h value reveals that the modes at different h freeze at different temperatures. For example, $I_{0.01}$ (squares) and $I_{0.04}$ (solid lines) vs temperature are shown

as an inset in Fig. 1(b). The intensities $h = 0.01$ and $h = 0.04$ increase rapidly on cooling but *saturate* at two different temperatures. The saturation temperatures were ~200 and ~260 K, respectively, estimated from the intersections of two solid straight lines as shown in the figure. The solid lines show that the two modes *freeze* to static distortions at the respective temperatures. Over all, the long-wavelength phonons freeze at lower temperatures than short-wavelength ones do. This shows a competition between the above-mentioned static distortions and the phonon excitation along the dispersion curve. This competition offers a basis for another possible model for relaxor ferroelectrics in addition to the previously studied models of inhomogeneous polar regions or transition temperatures [19].

In conclusion, we show that pure transverse soft phonon modes along ⟨110⟩ directions are present and freeze gradually within the temperature range from ~260 K for short-wavelength phonons to ~190 K for long-wavelength phonons. Contrary to ordinary ferroelectrics where a condensation of *a* soft mode at T_c results in an abrupt phase transition, the observed branch of soft modes in PMN is electrostatically pinned by the randomly located microdomains and freezes gradually with q-dependent freezing temperatures. Our picture of PMN, namely, soft modes interacting with the pinning centers of microdomains and their q-dependent freezing, may provide a microscopic physical basis for the observed relaxor behavior of PMN.

We thank Professor J. Toulouse for prividing us Ref. [6], Professor R. Colella for bringing our attention to Ref. [15], and Dr. P. Lee for his assistance during X6B measurements. The work at Argonne National Laboratory was supported by DOE under Contract W-31-109-ENG-38 and the work at Penn State University was supported by the Office of Naval Research.

[1] L.E. Cross, Ferroelectrics **76**, 241 (1987); D. Viehland, S. Jang, L.E. Cross, and M. Wuttig, Philos. Mag. B **64**, 335 (1991); M.E. Lines and A.M. Glass, *Principles and Applications of Ferroelectrics and Related Materials*, (Clarendon Press, Oxford, 1977).

[2] V. Westphal, W. Kleemann, and M.D. Glinchuk, Phys. Rev. Lett. **68**, 847 (1992).

[3] E.V. Colla, E.Yu. Koroleva, N.M. Okuneva, and S.B. Vakhrushev, Phys. Rev. Lett. **74**, 1681 (1995).

[4] G.A. Samara, Phys. Rev. Lett. **77**, 314 (1996).

[5] N. de Mathan, E. Husson, G. Calvarin, J.R. Gavarri, A.W. Hewat, and A. Morell, J. Phys. Condens. Matter **3**, S159 (1991); P. Bonneau, P. Garnier, and G. Calvarin, E. Husson, J.R. Gavarri, A.W. Hewat, and A. Merell, J. Solid State Chem. **91**, 350 (1991).

[6] J. Chen, Ph.D. dissertation, Lehigh University, 1991.

[7] Q.M. Zhang, H. You, M.L. Mulvihill, and S.J. Jang, Solid State Commun. **97**, 693 (1996).

[8] H. You (unpublished).

[9] The first order diffuse scattering *amplitude* of a lattice distortion [11], whether it is due to thermal fluctuation or impurity-induced static disorder, can be written as $A_1(\mathbf{Q}) = i\mathbf{Q} \cdot \sum_n \bar{\mathbf{u}}_n e^{i\mathbf{Q}\cdot\mathbf{a}_n}$, by defining $\bar{\mathbf{u}}_n = \sum_m$, where $\mathbf{u}_{m,n}$ is the deviation of the mth sublattice in the nth unit cell from its equilibrium position $(\mathbf{a}_n + \mathbf{b}_{m,n})$. For an optic mode of PMN where the center of masses of unit cells are undistorted, $\bar{u} = u_{\mathrm{Pb}} f_{\mathrm{Pb}} + u_{\mathrm{MN}} f_{\mathrm{MN}} e^{i\pi(H-K-L)}$ and we expect little diffuse scattering for $H + K - L =$ even ($\bar{u} \simeq 0$) while there is significant diffuse scattering for $H + K + L =$ odd ($\bar{u} = 2u_P f_P$) since the scattering factor is proportional to the atomic mass.

[10] S. Vakhrushev, A. Naberesznov, S.K. Sinha, Y.-P. Feng, and T. Egami, J. Phys. Chem. Solids **57**, 1517 (1996); this high-resolution x-ray study along radial and transverse directions of (003) is unrelated to our discussion because the soft modes of our discussion must have zero diffuse-scattering intensity in their scans as is clear from Eq. (1).

[11] H. Ekstein, Phys. Rev. **68**, 120 (1945).

[12] K. Huang, Proc. R. Soc. A **190**, 102 (1947).

[13] For example, see Appendix N of N.W. Ashcroft and N.D. Mermin, *Solid State Physics* (Sunders College, Philadelphia, 1976).

[14] H. Cole and B.E. Warren, J. Appl. Phys. **23**, 335 (1952).

[15] R. Comes, M. Lambert, and A. Guinier, Acta Crystallogr. Sect. A **26**, 244 (1970).

[16] R.J. Nelmes, R.O. Piltz, W.F. Kuhs, Z. Tun, and R. Restori, Ferroelectrics **108**, 165 (1990); N. Takesue, M. Maglione, and H. Chen, Phys. Rev. B **51**, 6696 (1995).

[17] The apparent distortion in the data [seen clearly in the diffuse scattering around (401) reflections] is due to the skewed resolution envelope during x-ray measurements. The calculations were not adjusted for it in order to show clearly the actual symmetry.

[18] G. Calvarin, E. Husson, and Z.G. Ye, Ferroelectrics **165**, 349 (1995).

[19] A.J. Bell, J. Phys. Condens. Matter **5**, 8773 (1993); A.E. Glazounov, A.J. Bell, and A.K. Tagantsev, *ibid.* **7**, 4145 (1995).

APPENDIX 11

Journal of Materials Research (submitted 1998).

The Influence of the External Stress on the Electromechanical Response of Electrostrictive $0.9Pb(Mg_{1/3}Nb_{2/3})O_3$-$0.1PbTiO_3$ in the DC Electrical Field Biased State

J. Zhao, Volkmar Mueller, and Q. M. Zhang*

Materials Research Laboratory and Electrical Engineering Department

The Pennsylvania State University, University Park, PA 16802

Abstract:

The influence of uniaxial compressive stress T_3, in parallel with the applied electrical field, on the electromechanical parameters of $0.9Pb(Mg_{1/3}Nb_{2/3})O_3$-$0.1PbTiO_3$ ceramic in the DC electrical field biased state and at temperatures near the dielectric constant maximum T_m was investigated. It was found that, in general, T_3 reduces the dielectric constant and polarization level which results in a reduction of the piezoelectric coefficient with stress. However, the compliance of the material does not show much change with stress. As a consequence, the coupling factor k_{33} is also reduced with stress. On the other hand, the existence of the local micro-polar region in the material causes anomalous changes in these properties when the material is subjected to a high electric field, which induced a macro-polar state. The transformation of this macro-polar state back to a micro-polar state under stress involves a large volume strain and results in an enhancement of the hydrostatic piezoelectric response.

* Corresponding author

I. Introduction

Lead magnesium niobate-lead titanate (PMN-PT) based electrostrictive materials exhibit many attractive features such as high dielectric constant, high electrical and elastic energy density, low hysteresis, for actuator and transducer applications. In these applications, the materials are often subjected to high external stresses due to a prestress or high external load. In order to properly use the materials under different external conditions it is necessary to understand how the electromechanical properties are influenced by those conditions.

In PMN-PT used in the electrostrictive regions (at temperatures near or above the dielectric constant maximum T_m), the material is composed of two phases: micro-polar regions embedded in a non-polar matrix.[1,2] And as has been demonstrated in a recent study, the polarization response, and hence the dielectric and electric field induced strain behaviors, at temperatures near T_m are mainly controlled by the response of the micro-polar regions, rather than by the so called "intrinsic" contribution from the change of the unit cell dimension and polarization level.[2,3] This is somewhat similar to the another widely used electromechanical material, the piezoceramic lead zirconate titanate (PZT), where the material properties are largely controlled by the macro-domain configuration and the movements of the domain boundaries.[4] One difference between the two systems is that in PMN-PT the response of the micro-polar region exhibits only weak hysteresis while in PZT, large irreversibility occurs when external fields cause depoling of the piezoceramic.[5] The influence of external stresses on the response of micro-polar region is still unclear at this stage.

In this paper, we report the results of an experimental investigation on the effect of uniaxial compressive stress (T_3), which is parallel to the applied electric field direction (defined as the 3-direction), on various electromechanical parameters of PMN-PT with the composition of 10% PT (0.9PMN-0.1PT). As has been demonstrated by many early studies, for electrostrictive applications at near room temperature, the composition of PMN-PT is near 0.9PMN-0.1PT whose weak field dielectric constant is presented in figure 1.[6-8] In addition, by applying a DC bias electric field to the material, an effective piezoelectric state can be induced, as shown

schematically in figure 2. For an electrostrictive material such as the one investigated here, the material is often operated in the field biased state. In this investigation, therefore, all the parameters are characterized also under different DC electric bias fields to simulate this operation mode.

II. Experimental

All the specimens used in this investigation were made by the mixed oxide method following the columbite B-site precursor method.[9] Most of the specimens were sintered at a temperature of 1250 °C for 2 -- 6 hours followed by annealing in an oxygen rich atmosphere at 900 °C for 6 -- 24 hours. The typical dielectric constant of the specimens is shown in figure 1.

In this investigation, the uniaxial stress applied to the specimens is provided by an apparatus developed recently which has been described in an early publication.[5] Making use of this apparatus, the effective piezoelectric coefficient, the elastic compliance, and the dielectric constant in the DC electric field biased state can be characterized under well defined boundary conditions.

In this apparatus, the strain response was measured by a strain gauge (KYOWA KFR-02-120-C1-11). In the DC electric field biased state, the strain response of the specimen is described by[10]

$$S_3 = d_{33}E_3 + s_{33}^E T_3 \quad \text{and} \quad S_1 = d_{31}E_3 + s_{13}^E T_3 .$$

Hence, in the DC electric field biased state, a weak AC electric field E_{ac} (<100 V/cm) induces AC strains S_3 and S_1 (under constant stress condition), parallel and perpendicular to E_{ac} respectively, from which the piezoelectric coefficients d_{33} ($=S_3/E_{ac}$) and d_{31} ($=S_1/E_{ac}$) can be determined (see figure 2). In analogy, by measuring the strains S_3 and S_1 induced by a weak AC stress field T_{ac} (about 0.1 MPa) under constant electric field condition, the elastic compliance s_{33}^E and s_{13}^E can be determined. In this investigation, the strain was acquired at a frequency of 10 Hz. In order to improve the signal-to-noise ratio, the voltage signal from the strain gauge amplifier was measured by a Lock-in amplifier. Further more, to ensure that T_3 was uniformly applied to the

specimen two strain gauges attached to opposite faces of the specimen were utilized. Adjustment was made before the data acquisition so that the strain readings from the two strain gauges were the same within 5%. From repeated measurements, it was found that this adjustment was not very crucial to the determination of piezoelectric coefficients. However, for the elastic compliance, any non-uniformity in T_3 can result in a large error. Hence, the error in the piezoelectric coefficient determined is within 5% while in the elastic compliance it is about 10%.

The dielectric constant was determined using either a multi-frequency LCR meter (HP model 4192A), or a calibrated small resistor in series with the specimen. In the later method, the voltage across the resistor, which is directly proportional to the current flowing through the specimen, was measured using a Lock-in amplifier. From the data, the complex dielectric constant can be determined. The frequency range for the dielectric constant measurement is from 10 Hz to 1 MHz. The polarization level at each electric bias field and DC stress state was measured by a Saywer-Tower circuit.

Since the material is operated at a temperature near the dielectric constant maximum T_m where there is a large change in the dielectric constant (see figure 1) and the polarization level in the field biased state, it is necessary to characterize the electromechanical parameters over a temperature region about T_m. In this investigation, three temperatures were chosen: 25 °C ($<T_m$), 50 °C (near above T_m) and 80 °C ($>T_m$).

III. The Dielectric Responses

Presented in figure 3 is the dielectric constant acquired at 25 °C, which is below the dielectric constant maximum (T_m=37 °C at 1 kHz). Without DC electric bias fields, the data in figure 3 shows that the dielectric constant decreases as the compressive stress T_3 increases, a trend generally expected for a dielectric material with a positive electrostrictive coefficient Q_{11}.[11,12] On the other hand, at high DC bias fields, for instance at 5 kV/cm, an increase of the dielectric constant with the compressive stress was observed. And in the pressure range investigated, a dielectric maximum was observed at near 60 MPa, which seems to be inconsistent with

conventional electrostrictive behavior. This could be understood from the fact that because of the existence of micro-polar regions, a high DC bias field can induce a macro-polar state in the material. As the compressive stress increases, which tends to reduce the macro-polarization level in the material, a "transformation" of the macro-polar domain state to micro-polar state occurs, resulting in the observed broad dielectric constant anomaly.

It is well known that for a dielectric material, the change of the dielectric constant K with external stress can be a result of the electrostrictive coupling in the material. In fact, for many non-ferroelectric material, the electrostrictive coefficient can be determined conveniently from the slope of 1/K vs. the applied stress T.[11,12] However, for a ferroelectric based electrostrictive material such as PMN-PT, the change in the dielectric constant can also be a result of the changes in the local polarization state as has been pointed out in an early publication (shifting of the local curie temperatures).[12] Moreover, the polarization response near T_m is mainly from the reorientation process of the micro-polar regions to the external electric field. These so called "extrinsic" contributions to the dielectric response can be affected by external stress. As a consequence, the 1/K vs. T_3 relation even for the data without DC electric field exhibits a strong non-linear behavior and the slope of the curve is far below Q_{11} measured directly from the strain-polarization relationship.

For the data at temperatures above the dielectric constant maximum, the dielectric constants all show monotonic decrease with the compressive stress for the DC bias fields investigated (up to 5 kV/cm) although at 50 °C, the dielectric constant under 5 kV/cm DC electric bias field exhibits a plateau at $T_3 < 50$ MPa, which is presented in figure 4. The existence of this plateau is reminiscent of the transformation of the material from a macro-polar state to a micro-polar state, analogous to that observed at 25 °C. Due to the existence of the micro-polar regions, even for the data at 80 °C (shown in figure 5), the slope of the dielectric stiffness vs. stress is still far below that determined by the electrostrictive coefficient even though in the stress range investigated, the curve of 1/K vs. T_3 exhibits a nearly linear relationship. In addition, the slope

of the curve decreases as the DC bias field increases, a signiture of increased ferroelectric activity in the material when subjected to high electric fields.

At 25 °C and 50 °C, the dielectric data exhibit a strong frequency dispersion. For that reason the data were collected at frequencies from 10 Hz to above 100 kHz to probe the influence of this dispersion by the applied stress T_3. Apparently, the external stress T_3 reduces the frequency dispersion significantly and accompanying this reduction in the frequency dispersion the dielectric loss is also reduced. The results reveal that the compressive stress T_3 reduces the response of the micro-polar regions and hence the degree of the relaxor behavior in the material. The data at 80 °C was acquired at 1 kHz only because of a very weak frequency dispersion at the temperature.

IV. The Elastic Compliance as a Function of the Compressive Stress at Different Bias Fields

Elastic compliances s_{33}^E and s_{13}^E were characterized as a function of compressive stress at different electric bias fields and temperatures are presented in figures 6 and 7 respectively. The general features revealed from the data are: (i) the elastic compliance increases with DC bias fields and hence, the polarization level in the material; (ii) the compliance exhibits a slight decrease with the compressive stress; (iii) the compliance decreases with temperature for the three temperatures measured. For the data at 25 °C under 5 kV/cm, an anomaly is observed which is apparently related to the phase transformation from a macro-polar state to a micro-polar state as been discussed in the dielectric data. In the temperature and stress range investigated, the ratio of $-s_{13}^E/s_{33}^E$ remains near 1/3.

In an early investigation by Cao and Evans,[13] it was found that in soft PZT, Poisson's ratio can reach near 0.5 when there is a stress depoling of the samples which is a direct consequence of the domain reorientation during the depoling process. If there is a significant contribution from the reorientation of the micro-polar regions to the elastic process in the material, one would expect the similar results since this process will not generate volume strain. Therefore the

relatively small ratio of $-s_{13}^E/s_{33}^E$ implies that the reorientation process of micro-polar regions which is responsible for the large dielectric constant at near T_m is not contributing significantly to the elastic process. Indeed, there is only a very weak elastic compliance peak at temperatures near T_m.[14]

V. The Effective Piezoelectric Responses in DC Field Biased States

The effective piezoelectric coefficients d_{33} and d_{31} in the electric field biased state were characterized and are presented in figures 8 and 9. Analogous to the dielectric constant and elastic compliance data, a broad peak of d_{33} at the bias field of 5 kV/cm data was observed. In addition, there is also a weak peak at 3 kV/cm, while at 1 kV/cm d_{33} decreases monotonically with the stress. As pointed out earlier, this anomalous behavior observed at 3 kV/cm and 5 kV/cm bias fields is associated with the phase transformation in the material in the DC field biased state from a macro-polar state to a micro-polar state. The peak is much less pronounced in the data of d_{31}. At higher temperatures, both d_{33} and d_{31} exhibit a monotonic decrease with the compressive stress. The decrease of d_{33} and d_{31} with the compressive stress at higher temperatures is a result of the reduction of the polarization level P_3 and the dielectric constant K at the DC field biased state with the stress. In fact, the ratio of d_{33} (or d_{31}) to P_3*K, which is directly proportional to the effective electrostrictive coefficients of the ceramic sample, does not show marked change with stress.

Based on d_{33} and d_{31} data, the hydrostatic piezoelectric coefficient d_h ($d_h = d_{33} + 2\ d_{31}$) in the DC field biased state is evaluated and presented in figure 10. One of the interesting features of the data in figure 10 is that a very pronounced peak in d_h is observed at 25 °C under a 5 kV/cm bias field. For the data at higher temperatures, a weaker but clear peak is observed under 5 kV/cm bias field. This is in sharp contrast to the dielectric, elastic compliance, and piezoelectric d_{33} and d_{31} coefficients where the peak associated with the anomaly is much weaker. As has been pointed out, the anomaly is due to the transformation from a macro-polar state to a micro-polar

state due to the applied stress. The result reveals that this transformation involves a large volume change which yields a large change in d_h in the broad transition region.

In a recent study of the electrostrictive coefficients of prototype cubic phase of PMN, it was found that the hydrostatic electrostrictive coefficient is at about 0.08 m^2/C^4.[3] This value is more than 10 times higher than that determined directly from a field induced strain measurement.[2] The difference between the two results lies in the fact that at temperatures near T_m, the material has a high population of micro-polar regions and the reorientation of these polar regions does not generate volume change. Consequently, the Q_h measured from the volume strain-polarization relationship at temperatures near T_m has a much smaller value than the intrinsic Q_h value of the material. (Q_h for the prototype cubic phase of 0.9PMN-0.1PT is nearly the same as that of PMN.) In this paper, this low value of Q_h measured from field induced volume strain S_v at temperatures near T_m is named as the apparent Q_h (Q_h^a) of the material to distinguish it from the intrinsic Q_h which is determined from the change in the lattice constant of the unit cell due to the change in polarization.

For 0.9PMN-0.1PT, $Q_h^a = 0.006\ m^4/C^2$ at room temperature without external field. From the electrostrictive relation $S_v = Q_h^a P^2$, where P is the total polarization response in the sample, and also $S_v = Q_h P_v^2$, where P_v is the polarization response which generates volume strain, the ratio $\frac{P_v}{P} = \sqrt{\frac{Q_h^a}{Q_h}}$ can be determined. For PMN-PT at near T_m, this ratio is about 0.27, which implies that about 70% of the weak field polarization response in 0.9PMN-0.1PT at temperatures near T_m is due to the reorientation of the micro-polar regions, which does not generate the volume change of the material.

This observation raises an interesting issue on how to improve the hydrostatic response of the material, which is important for many underwater applications. By reducing the polarization response related to the micro-polar region reorientation, even if this may not increase d_h in case that P_v in the material does not change (from the electrostrictive relation, $d_h = 2\ Q_h * P_v * \Delta P_v$ in the field biased state), the reduction of the dielectric constant will improve the hydrostatic figure of

merit $d_h g_h$ since g_h is equal to d_h/K. $d_h g_h$ for the samples investigated is presented in figure 11. As can be seen from the figure, in spite of the fact that the material possesses a relatively high d_h (> 400 pm/V, about 10 times higher than that of PZT piezoceramics), the relatively high dielectric constant due to the micro-polar region reorientation results in a figure of merit which is only about 20 times higher than that of PZT piezoceramics and is nearly the same as that of the piezo-polymer PVDF.[15]

VI. The Electromechanical Coupling Factor k_{33} Under Uniaxial Stress T_3

From the data presented in the preceding sections, the electromechanical coupling factor k_{33}, defined as $k_{33}^2 = \frac{d_{33}^2}{K\varepsilon_0 s_{33}^E}$ where ε_0 is the vacuum permittivity, can be derived.[10] The data thus derived is presented in figure 12. Apparently, at high DC bias electric fields and without external stress, k_{33} of 0.9PMN-0.1PT at temperatures near T_m is near that of soft PZT, i.e., above 0.7. A disappointing fact of this material is that k_{33} drops quite significantly as the material is subjected to external compressive stress. This seems inevitable from the data presented in the preceding sections since the reduction of the piezoelectric coefficients with stress is due to the reduction in both the dielectric constant and the polarization level in the field biased state while the elastic compliance does not show a marked reduction with stress. As a result, k_{33} is reduced with stress. In order to improve the material performance with stress, one may need to develop materials with a broader dielectric peak so that the reduction of the polarization and dielectric constant with stress can be reduced.

VII. Summary

The influence of the uniaxial compressive stress on the electromechanical behavior of 0.9PMN-0.1PT under DC bias electric fields at temperatures near T_m was investigated. The results reveal that the compressive stress T_3 reduces the responses of the micro-polar regions which result in a decrease in the dielectric constant, the dielectric dispersion and dielectric loss,

and the effective piezoelectric coefficients. The results also show that the response of the micro-polar regions does not contribute to the elastic process significantly as compared with the dielectric process. Hence, the elastic compliance does not exhibit a marked change with stress and the ratio of $-s_{13}^E/s_{33}^E$ remains near 1/3. By combining the data of the piezoelectric coefficient, the dielectric constant, and elastic compliance, the longitudinal electromechanical coupling factor k_{33} was derived which decreases with the compressive stress T_3.

For electrostrictive PMN-PT at temperatures near T_m, the material can be converted into a macro-polar state by applying a high DC electric field. Compressive stress will force the material back into a micro-polar state and the experimental results reveals that there is a broad transformation region between the two states instead of a smooth process. This transformation involves a change in part of the material between a rhombohedral phase and a cubic phase which involves a large volume strain as revealed by a pronounced peak in the hydrostatic piezoelectric coefficient d_h. This phenomenon could be used to enhance the hydrostatic piezoelectric response of the material if the bias stress level is properly adjusted. On the other hand, for a given external prestress level, the material composition may be adjusted so that this transformation will occur at the given stress.

This work was supported by the Office of Naval Research.

References:

[1] L. Eric Cross, "Relaxor ferroelectrics," *Ferroelectrics*, vol. 76, pp. 241-267 (1987).

[2] Q. M. Zhang and J. Zhao, "Polarization response in lead magnesium niobate based relaxor ferroelectrics," *Appl. Phy. Lett..*, vol. 71, no. 12, pp. 1649-1651, (1997).

[3] J. Zhao, A. E. Glazounov and Q. M. Zhang, "Neutron diffraction study of electrostrictive coefficients of prototype cubic phase of relaxor ferroelectric $PbMg_{1/3}Nb_{2/3}O_3$," Appl. Phys. Lett. in press (1998).

[4] Q. M. Zhang, H. Wang, N. Kim, and L. E. Cross. "Direct Evaluation of Domain Wall and Intrinsic Contributions to the Dielectric and Piezoelectric Response and Their Temperature Dependence of PZT ceramics," J. Appl. Phys. 75, 454 (1994).

[5] Q. M. Zhang, Jianzhong Zhao, K. Uchino and Jiehui Zheng, " Change of the weak- field properties of $Pb(ZrTi)O_3$ piezoceramics with compressive uniaxial stresses and its links to the effect of dopants on the stability of the polarizations in the materials," *J. Mater. Res.*, vol. 12, No. 1, pp. 226-234 (1997).

[6] J. Zhao, Q. M. Zhang, N. Kim and T. Shrout, "Electromechanical properties of relaxor ferroelectric lead magnesium niobate titanate ceramic," *Jpn. J. Appl. Phys.*, vol. 34, no. 10, pp. 5658-5663, (1995).

[7] Steven M. Pilgrim, Mona Massuda, Jackie D. Prodey and Andrew P. Ritter, "Electromechanical properties of some $Pb(Mg_{1/3}Nb_{2/3})O_3$ - $PbTiO_3$ - $(Ba,Sr)TiO_3$ ceramics: I," *J. Am. Ceram. Soc.*, vol.75, no.7, pp. 1964-1969 (1992).

[8] Craig L. Hom, Steven M. Pilgrim, Natarajan Shankar, Keith Bridger, Mona Massuda, and Stephen R. Winzer, "Calculation of quasi - static electromechanical coupling coefficients for electrostrictive ceramic materials," *IEEE Trans. Ultrason., Freq. Cont.*, vol. 41, no. 4, pp. 542-551 (1994).

[9] S. L. Swartz and T. R. Shrout, "Fabrication of perovskite lead magnesium niobate," *Mater. Res. bull.*, vol. 17, pp. 1245-1250 (1982).

[10] *IEEE standard on piezoelectricity*, IEEE, Ultrason., Ferroelect., and Freq. Contr. Soc., ANSI/IEEE Std 176-1897 (1987).

[11] V. Sundar and R. E. Newnham, " Electrostriction and polarization," Ferroelectrics, vol. 135, pp. 431-446 (1992).

[12] Q. M. Zhang, W. Y. Pan, S. J. Jang and L. E. Cross, " The pressure dependence of the dielectric response and its relation to the electrostriction," *Ferroelectrics*, vol. 88, pp. 147-154 (1988).

[13] Hengchu Cao and Anthony G. Evans, "Nonlinear deformation of ferroelectric ceramics," *J. Am. Ceram. Soc.*, vol. 76, no. 4, 890-896 (1993).

[14] Dwight D. Viehland, "The glassy behavior of relaxor ferroelectrics," Ph.D. Thesis, The Pennsylvania State University (1991).

[15] Hong Wang, " Electromechanical effects in polymeric materials," Ph.D. Thesis, The Pennsylvania State University (1994).

Figure captions:

Figure 1. The dielectric constant K and dielectric loss D as a function of temperature for 0.9PMN-0.1PT under stress free condition. The measuring frequency is 0.1 kHz, 1 kHz, and 10 kHz.

Figure 2. Schematic drwaing of the polarization P and strain S responses of 0.9PMN-0.1PT in the DC electric field biased state where the effective dielectric constant is defined as P_{ac}/E_{ac} and the effective piezoelectric coefficient as S_{ac}/E_{ac}, respectively. S_{ac} can be S_1 and S_3 and E is the electric field.

Figure 3. The dielectric constant K and dielectric loss D as a function of the compressive stress T_3 measured at 25 °C and different DC bias electric fields (indicated in each figures). The measuring frequency of the data: 10 Hz (filled triangles), 0.1 kHz (open circles), 1 kHz (black dots), 10 kHz (crosses), 100 kHz (open triangles), and 1 MHz (pluses).

Figure 4. The dielectric constant and dielectric loss as a function of the compressive T_3 measured at 50 °C. The measuring frequency: 10 Hz (filled triangles), 0.1 kHz (open circles), 1 kHz (black dots), 10 kHz (crosses), 100 kHz (open triangles), and 1 MHz (pluses).

Figure 5. The dielectric constant as a function of the compressive T_3 at 80 °C, 1 kHz, and under different DC bias fields. The dielectric constant at this temperature exhibits very little dispersion.

Figure 6. The elastic compliance s_{33}^E as a function of the compressive T_3 at different temperatures and DC electric bias fields: 1 kV/cm (open squares), 3 kV/cm (open circles), and 5 kV/cm (dots).

Figure 7. The elastic compliance s_{13}^E as a function of the compressive T_3 at different temperatures and DC electric bias fields: zero bias (crosses), 1 kV/cm (open squares), 3 kV/cm (open circles), and 5 kV/cm (dots).

Figure 8. The effective piezoelectric coefficient d_{33} at the DC field biased states as a function of the compressive T_3 at different temperatures and DC electric bias fields.

Figure 9. The effective piezoelectric coefficient d_{31} at the DC field biased states as a function of the compressive T_3 at different temperatures and DC electric bias fields.

Figure 10. The effective hydrostatic piezoelectric coefficient d_h at the DC field biased states as a function of the compressive T_3 at different temperatures and DC electric bias fields.

Figure 11. The hydrostatic figure of merit $d_h g_h$ at the DC field biased states as a function of the compressive T_3 at different temperatures and DC electric bias fields.

Figure 12. The electromechanical coupling factor k_{33} (calculated at 10 Hz) as a function of the compressive T_3 at different temperatures and DC electric bias fields.

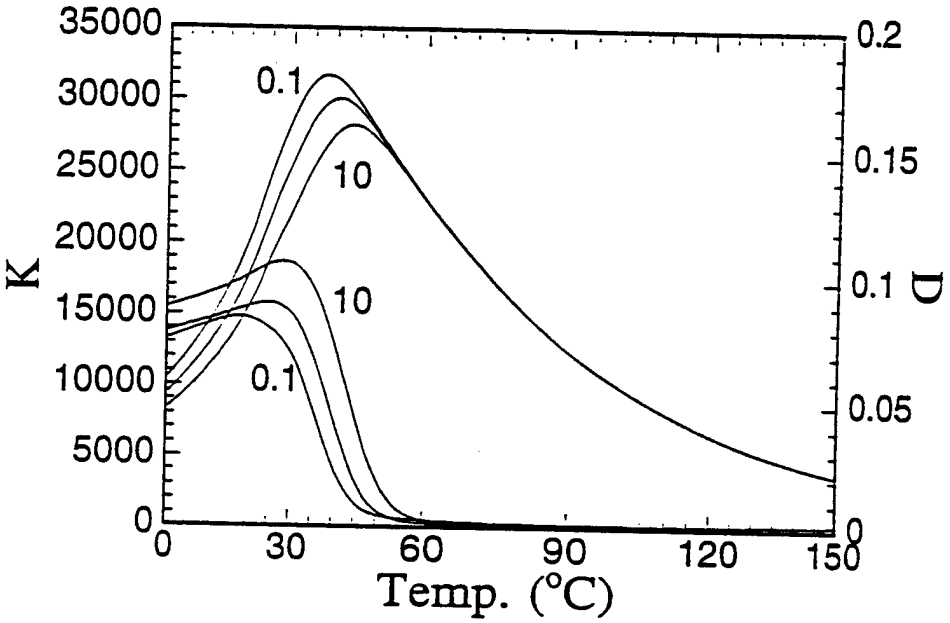
35000
30000
25000
20000
15000
10000
5000
0
K
0.2
0.15
0.1
0.05
0
D
0.1
10
10
0.1
0
30
60
90
120
150
Temp. (°C)

F. 1

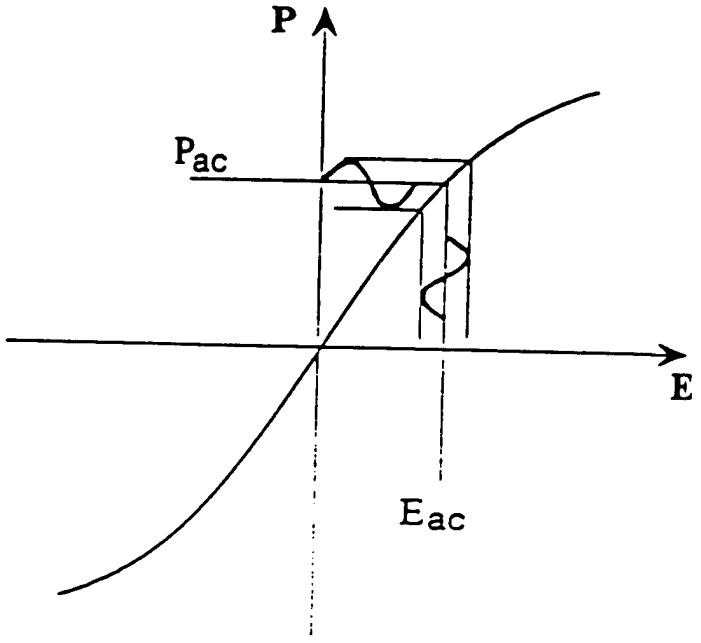
P
Pac
E
Eac

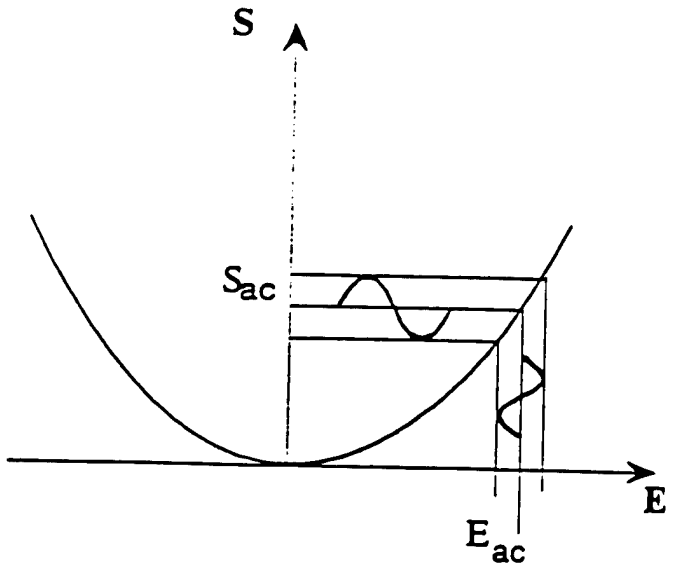
S
Sac
E
Eac

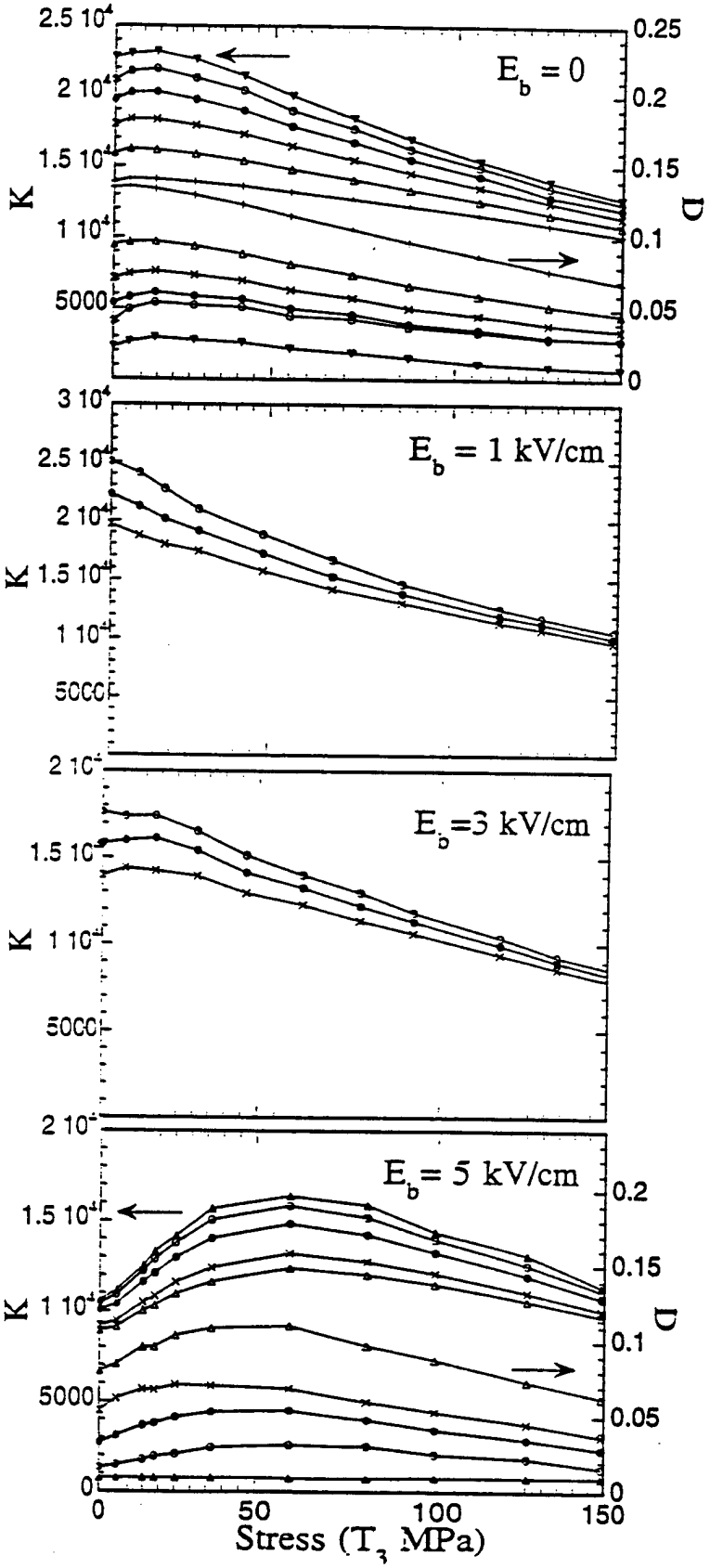
$E_b = 0$
$E_b = 1$ kV/cm
$E_b = 3$ kV/cm
$E_b = 5$ kV/cm
K
D
Stress (T_3 MPa)
0
50
100
150
2.5 10⁴
2 10⁴
1.5 10⁴
1 10⁴
5000
3 10⁴
0.25
0.2
0.15
0.1
0.05

Fig 2

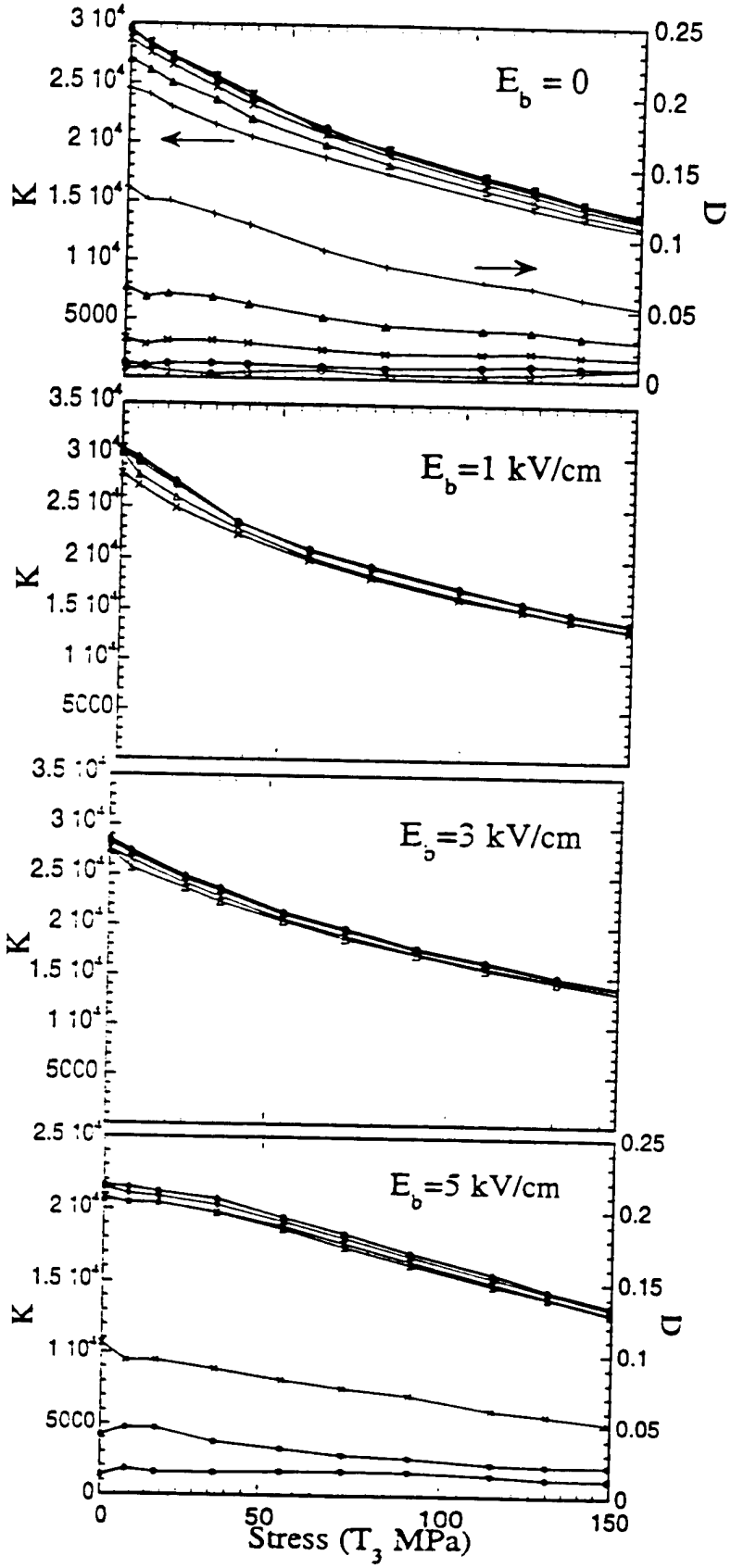
$E_b = 0$
E_b=1 kV/cm
E_b=3 kV/cm
E_b=5 kV/cm
K
D
Stress (T_3 MPa)
3 10^4
2.5 10^4
2 10^4
1.5 10^4
1 10^4
5000
0
0.25
0.2
0.15
0.1
0.05
50
100
150

Fig. 4

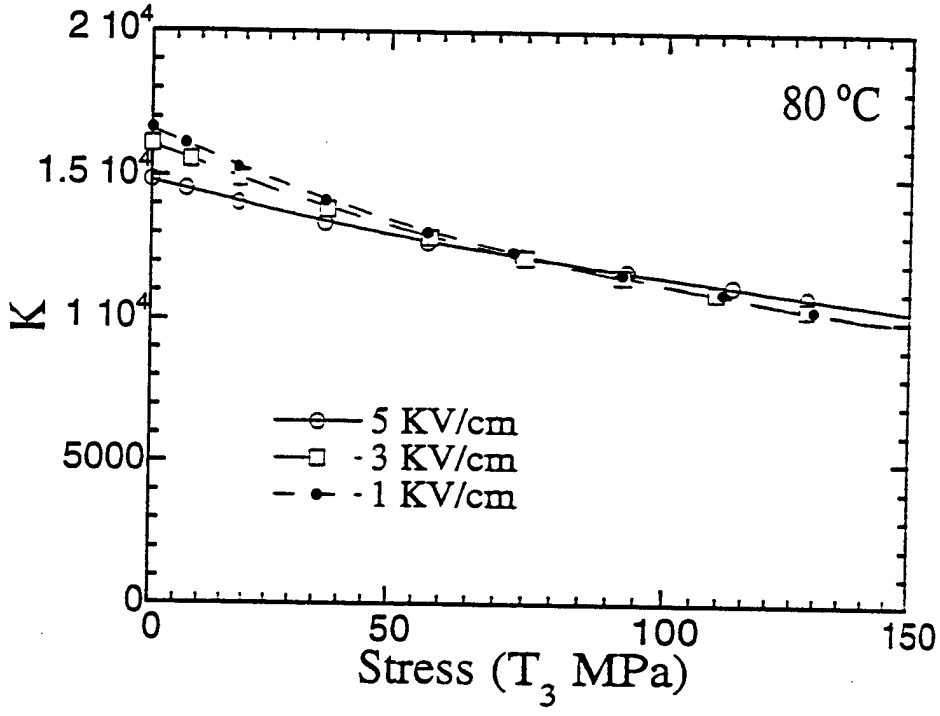
2 10^4
1.5 10^4
1 10^4
5000
0
K
80 °C
5 KV/cm
-3 KV/cm
-1 KV/cm
0
50
100
150
Stress (T3 MPa)

Fig. 5

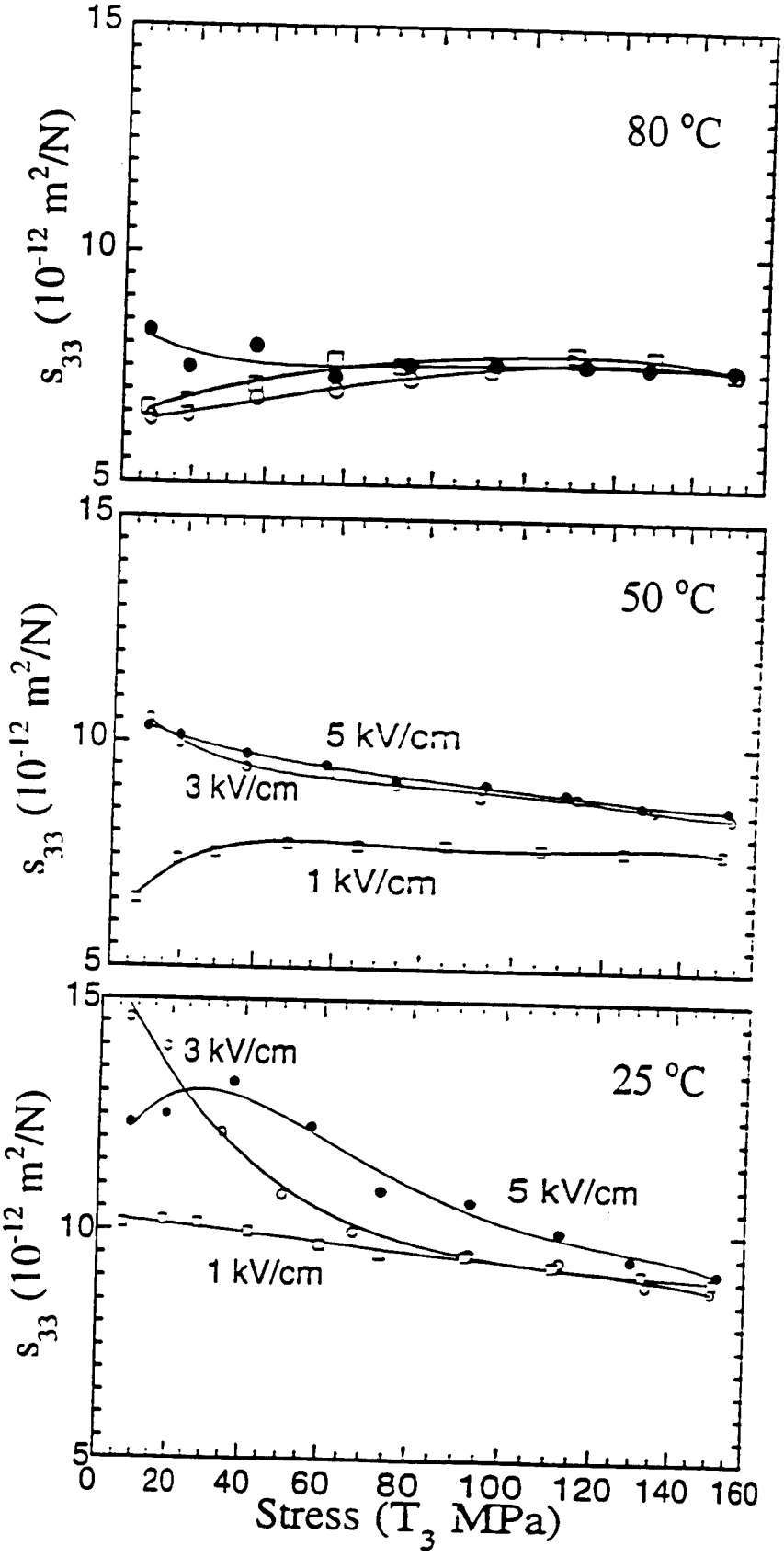
80 °C
50 °C
25 °C
5 kV/cm
3 kV/cm
1 kV/cm
s_{33} (10^{-12} m^2/N)
Stress (T_3 MPa)
15
10
5
0
20
40
60
80
100
120
140
160

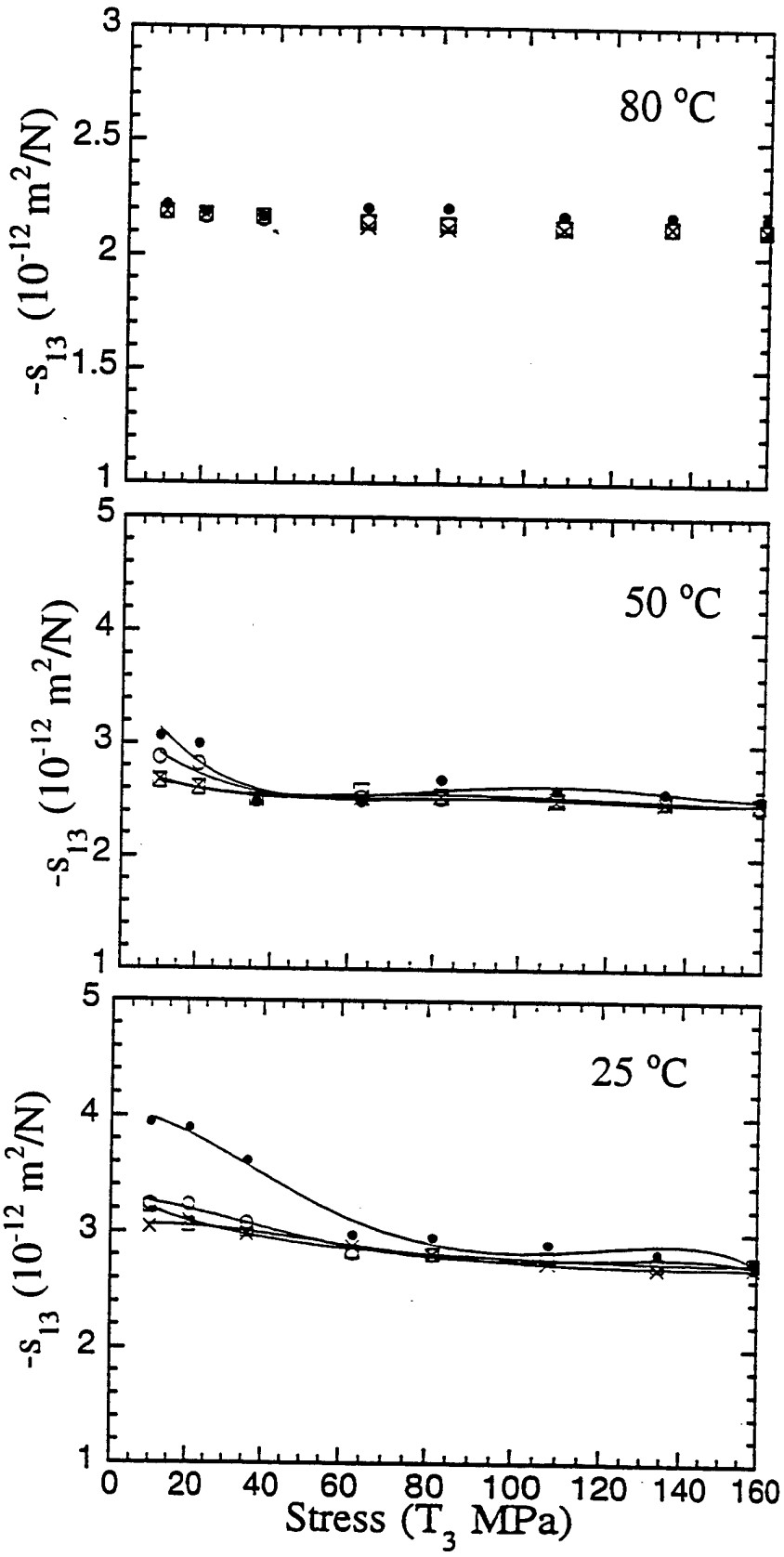
80 °C
50 °C
25 °C
$-s_{13}$ (10^{-12} m^2/N)
Stress (T_3 MPa)
0
20
40
60
80
100
120
140
160
1
1.5
2
2.5
3
4
5

Fig. 7

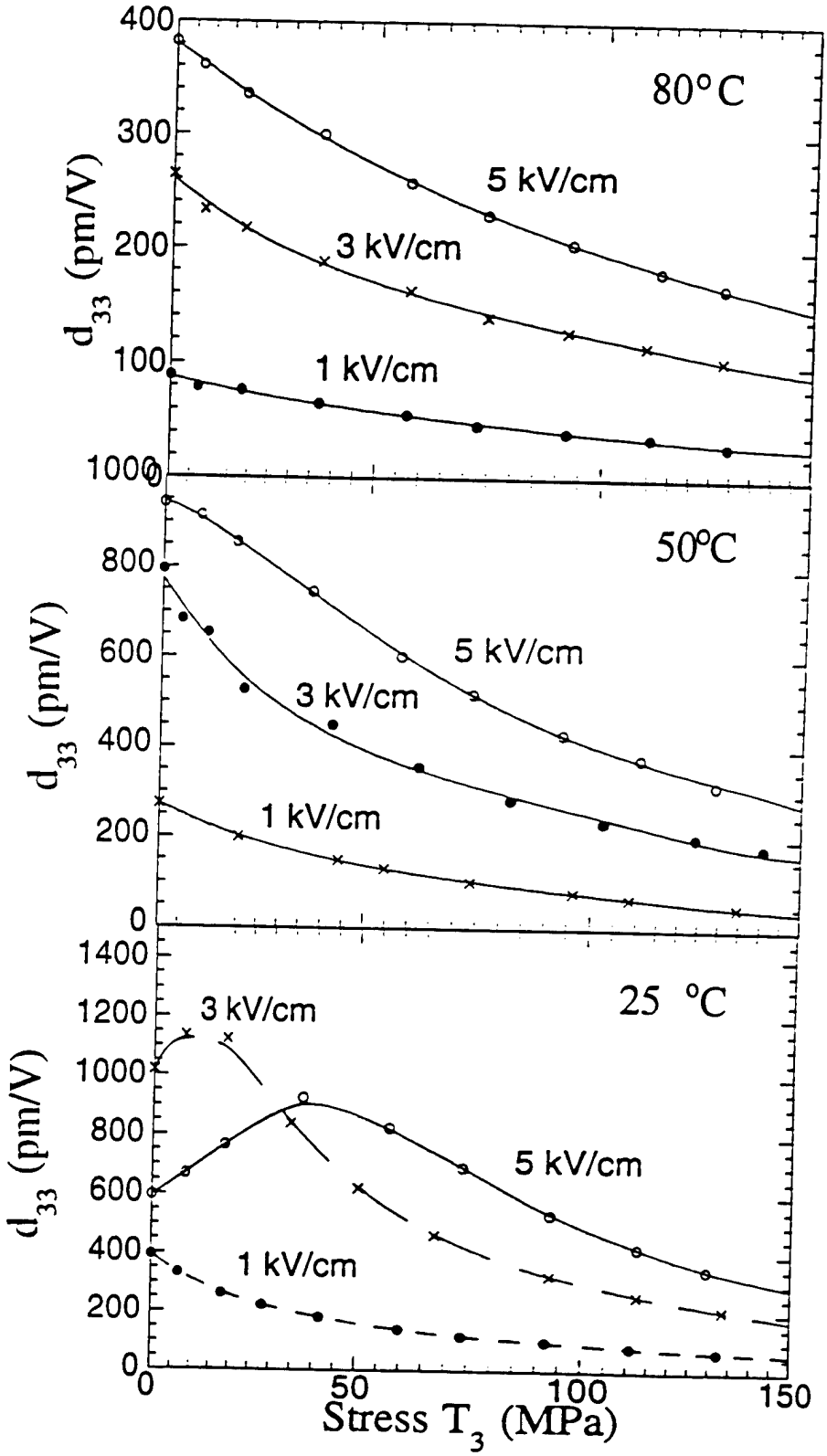
80° C
5 kV/cm
3 kV/cm
1 kV/cm
50°C
5 kV/cm
3 kV/cm
1 kV/cm
25 °C
3 kV/cm
5 kV/cm
1 kV/cm
d33 (pm/V)
Stress T3 (MPa)
0
50
100
150
200
400
600
800
1000
1200
1400
300

Fig. 5

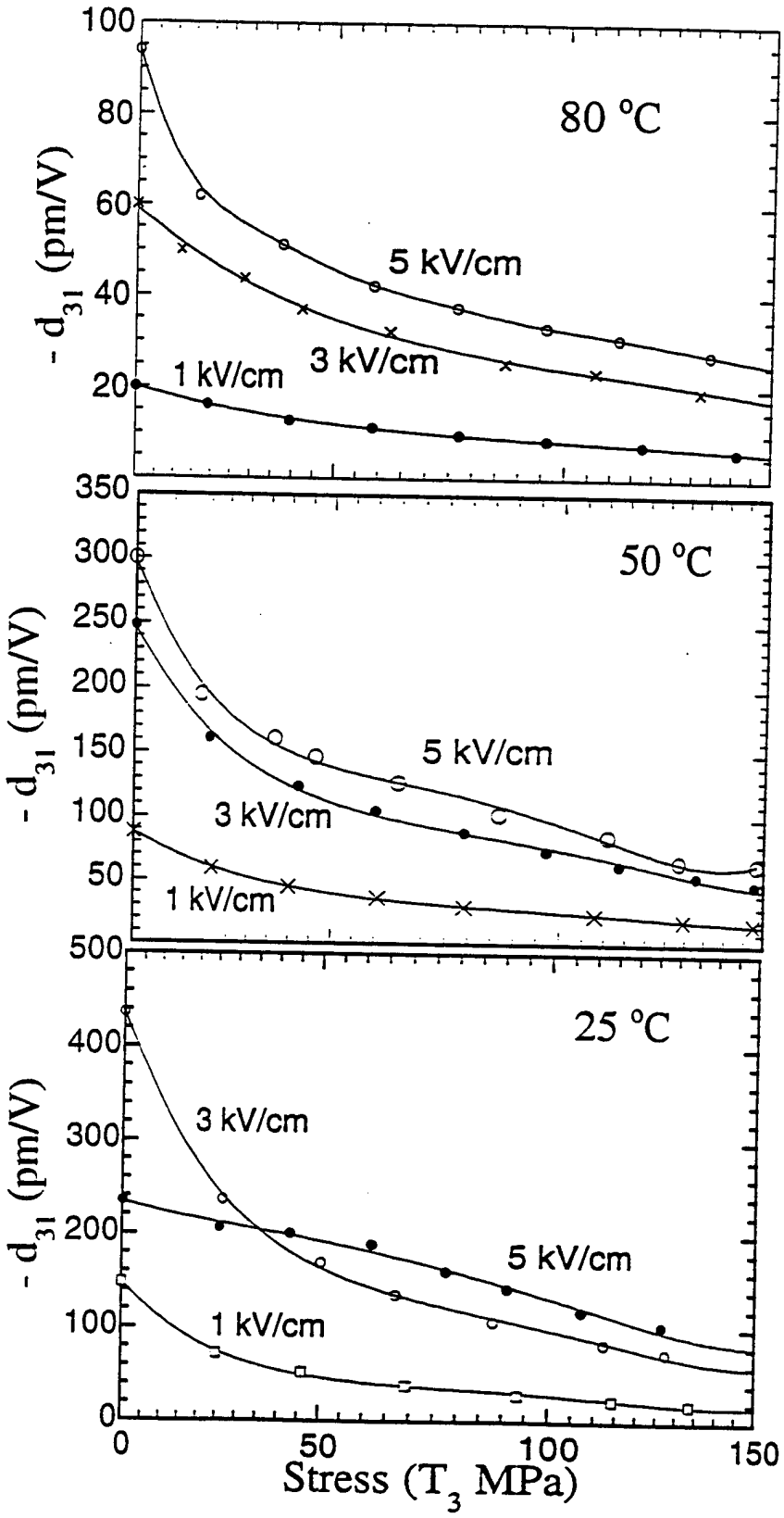
80 °C
5 kV/cm
3 kV/cm
1 kV/cm
50 °C
5 kV/cm
3 kV/cm
1 kV/cm
25 °C
3 kV/cm
5 kV/cm
1 kV/cm
- d31 (pm/V)
Stress (T3 MPa)
0
50
100
150

Fig 9

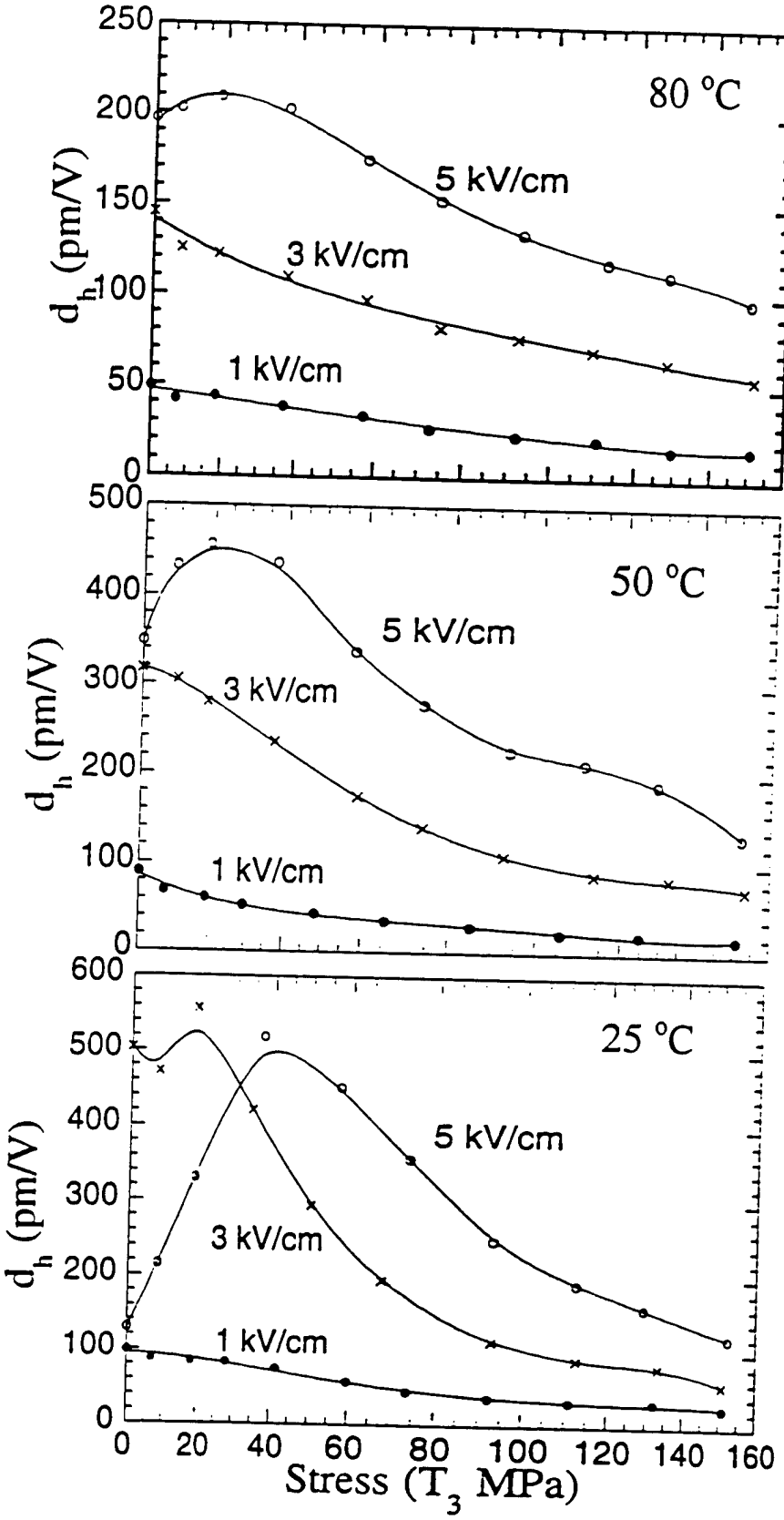
80 °C
5 kV/cm
3 kV/cm
1 kV/cm
d_h (pm/V)
50 °C
25 °C
Stress (T_3 MPa)

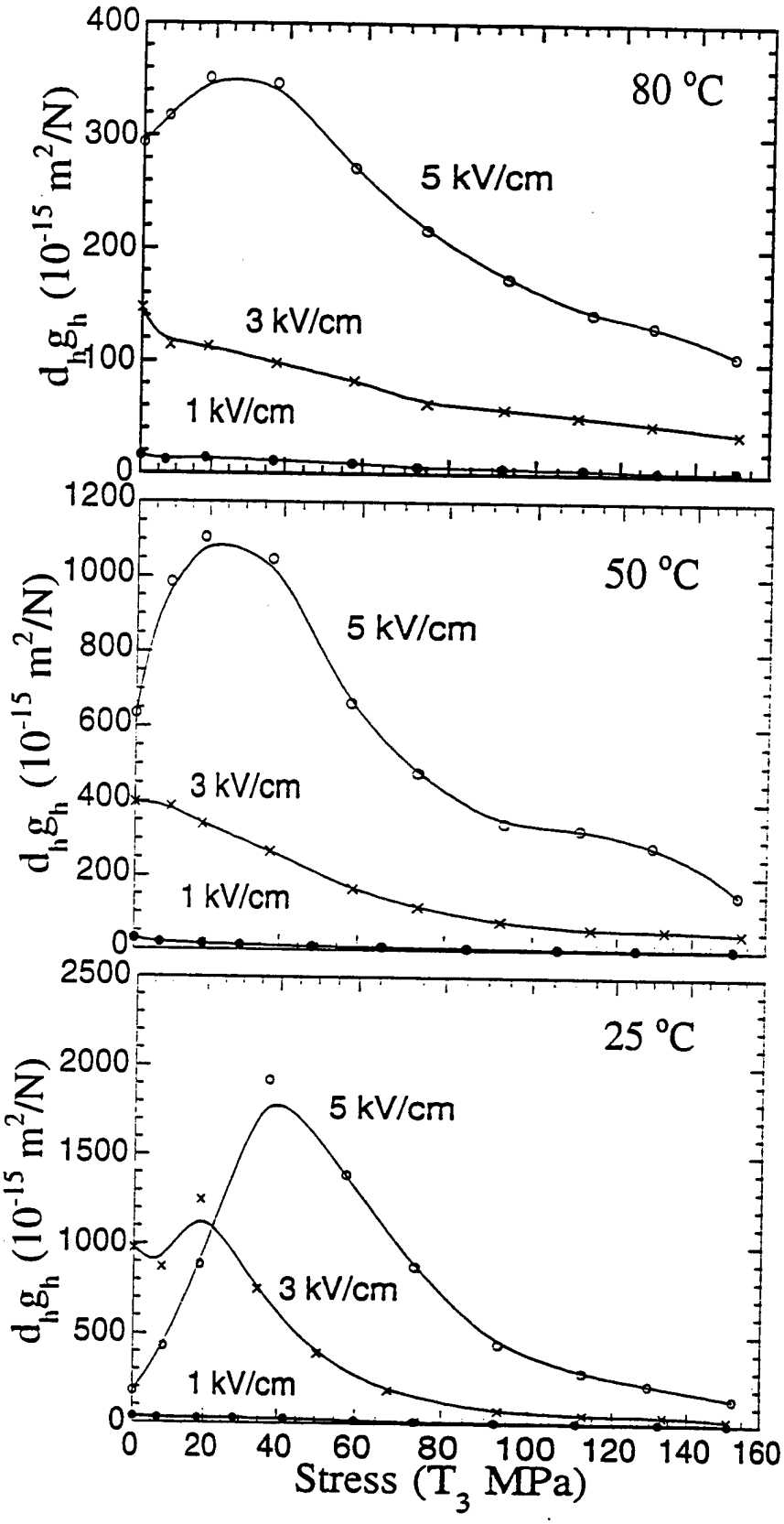
80 °C
5 kV/cm
3 kV/cm
1 kV/cm
50 °C
5 kV/cm
3 kV/cm
1 kV/cm
25 °C
5 kV/cm
3 kV/cm
1 kV/cm
$d_h g_h$ (10^{-15} m^2/N)
Stress (T_3 MPa)
0
100
200
300
400
600
800
1000
1200
500
1500
2000
2500
20
40
60
80
120
140
160

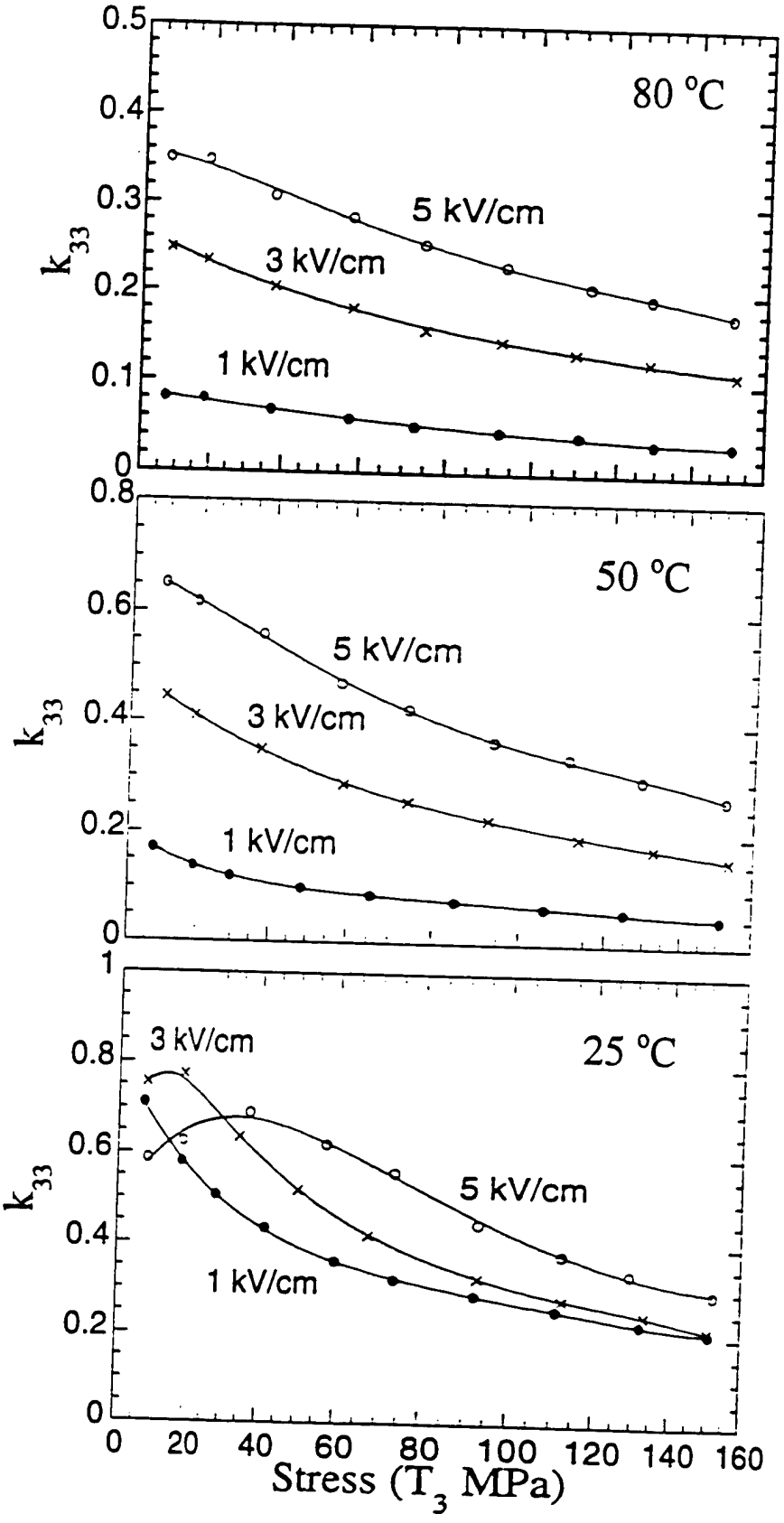
80 °C
5 kV/cm
3 kV/cm
1 kV/cm
50 °C
5 kV/cm
3 kV/cm
1 kV/cm
25 °C
3 kV/cm
5 kV/cm
1 kV/cm
k_{33}
Stress (T_3 MPa)